Characterization of polarization sensitive neurons of the central complex in the brain of the desert locust *(Schistocerca gregaria*)

Charakterisierung von polarisationssensitiven Neuronen des Zentralkomplexes im Gehirn der Wüstenheuschrecke (*Schistocerca gregaria*)

Dissertation zur Erlangung des
Doktorgrades der Naturwissenschaften
(Dr. rer. nat.)

dem Fachbereich Biologie
der Philipps-Universität Marburg
vorgelegt von
Stanley Heinze
aus Großröhrsdorf
Marburg/Lahn, 2009

Vom Fachbereich Biologie der Philipps-Universität Marburg
als Dissertation am 21.04.2009 angenommen.

Erstgutachter: Prof. Dr. Uwe Homberg
Zweitgutachter: Prof. Dr. Monika Stengl

Tag der mündlichen Prüfung am: 30.04.2009

Contents

Erklärung: Eigene Beiträge und veröffentlichte Teile der Arbeit

Laut §8, Absatz 3 der Promotionsordnung der Philipps-Universität Marburg (Fassung vom 28.4.1993) müssen bei den Teilen der Dissertation, die aus gemeinsamer Forschungsarbeit entstanden sind, „die individuellen Leistungen des Doktoranden deutlich abgrenzbar und bewertbar sein." Dies betrifft die Kapitel 1-5, und soll im Folgenden detailliert erläutert werden.

Kapitel 1: Neuroarchitecture of the Central Complex of the Desert Locust: Intrinsic and Columnar Neurons

- Durchführung aller Farbstoffinjektionen für Fluoreszenz-Wholemount Aufbereitung, sowie ca. zwei Drittel der Farbstoffinjektionen für Aufbereitung mittels DAB-Methode.
- Anfertigung aller immuncytochemischen Mehrfachmarkierungen, aller dreidimensionaler Rekonstruktionen, sowie 92% aller Zeichnungen (24 von 26).
- Entwicklung der Methode zur Rehydrierung von fluoreszenzmarkierten Wholemountpräparaten zum Zweck der gezielten Mehrfachmarkierung von injizierten Neuronen.
- Etablierung einer Methode zur Anfertigung von Dickschnitten zur gezielten Rekonstruktion des Zentralkomplexes mittels Fluoreszenz-Dreifachmarkierungen.
- Anfertigung aller Abbildungen und Tabellen.
- Anfertigung des Manuskriptes und layout der fertigen Abbildungen in Zusammenarbeit (Korrektur) mit Prof. Dr. Uwe Homberg.
- Dieses Kapitel wurde in der vorliegenden Form im Journal of Comparative Neurology veröffentlicht. (Heinze, S., Homberg, U. (2008) Neuroarchitecture of the Central Complex of the Desert Locust: Intrinsic and Columnar Neurons. J Comp Neurol 511:454–478.

Kapitel 2: Maplike representation of celestial *E*-vector Orientations in the brain of an insect.

- Durchführung von 68% (25 von 37) der präsentierten intrazellulären Ableitungen (darunter 17 von 18 TB1 Neuronen).
- Auswertung und statistische Analyse aller Daten.
- Anfertigung aller zweidimensionalen Rekonstruktionen.
- Durchführung aller immuncytochemischen Doppelmarkierungen.
- Anfertigung aller Abbildungen.

- Anfertigung des Manuskriptes und layout der fertigen Abbildungen in Zusammenarbeit (Korrektur) mit Prof. Dr. Uwe Homberg.
- Dieses Kapitel wurde in der vorliegenden Form im Journal Science veröffentlicht. (Heinze, S., Homberg, U. (2007) Maplike representation of celestial E-vector Orientations in the brain of an insect. Science 315:995-997.)

Kapitel 3: Linking the input to the output - New sets of neurons complement the polarization vision network in the locust central complex

- Durchführung von 82% (37 von 45) der präsentierten elektrophysiologischen Experimente.
- Planung und Leitung der Konstruktion des elektrophysiologischen Arbeitsstandes, mit dem circa 20% der Experimente durchgeführt wurden.
- Auswertung und statistische Analyse aller Daten.
- Anfertigung von allen gezeigten Rekonstruktionen, sowie histochemische Aufbereitung der fluoreszenzmarkierten Präparate mittels konfokaler Mikroskopie.
- Anfertigung aller Abbildungen.
- Anfertigung des Manuskriptes sowie layout der fertigen Abbildungen in Zusammenarbeit (Korrektur) mit Prof. Dr. Uwe Homberg.
- Dieses Kapitel wurde in der vorliegenden Form am 21.01.2009 bei Journal of Neuroscience eingereicht.

Kapitel 4: Transformation of polarized light information in the central complex of the locust

- Durchführung von 70% (80 von 114) der präsentierten elektrophysiologischen Experimente.
- Weiterentwicklung der Reizapparatur zur Applikation von monokularen Stimuli.
- Entwicklung der Analysemethoden zur Auswertung der Tuningbreite von POL-Zellen und Anfertigen eines automatischen Skriptes in MatLab zu diesem Zweck.
- Auswertung aller Daten.
- Planung und Durchführung aller statistischen Analysen.
- Anfertigung aller Abbildungen, inklusive aller Rekonstruktionen injizierter Neuronen.
- Anfertigung des Manuskripts sowie layout der fertigen Abbildungen in Zusammenarbeit (Korrektur) mit Prof. Dr. Uwe Homberg.
- Dieses Kapitel wird in der vorliegenden Form in Kürze bei Journal of Neuroscience eingereicht.

Kapitel 5: Integration of multiple visual information in neurons of the locust central complex

- Planung, Durchführung und Auswertung aller Experimente
- Planung und Entwicklung der Versuchsapparatur in Zusammenarbeit mit der Feinmechanik- und Elektronikwerkstatt der Universität Marburg.
- Programmierung aller Stimulations- und Auswertungsskripte für Reizung mit unpolarisiertem Licht mittels der Software MatLab.
- Anfertigen aller Abbildungen.
- Anfertigung des Manuskripts in Zusammenarbeit (Korrektur) mit Prof. Dr. Uwe Homberg.

Die Abfassung der Dissertation in englischer Sprache wurde vom Dekan des Fachbereichs Biologie am 12.01.2009 genehmigt.

Zusammenfassung

Viele Tiere orientieren sich mit Hilfe eines Himmelskompasses. Dabei dient neben der Sonne, dem auffälligsten Merkmal, auch das durch Streuung an Luftmolekülen entstehende polarisierte Licht als wichtiger Faktor. Die Schwingungsrichtung (*E*-Vektor) des gestreuten, polarisierten Lichtes ist abhängig vom Stand der Sonne, wobei die Ausrichtung der *E*-Vektoren tangential an konzentrischen Kreisen um die Sonne erfolgt. In einem Winkel 90° zur Sonne ist der Polarisationsgrad des Himmelslichtes am größten; Licht direkt aus Richtung der Sonne dagegen ist unpolarisiert (Horváth und Varjú, 2004). Durch diese Abhängigkeiten kann der solare Meridian direkt aus der Orientierung der *E*-Vektoren in einem kleinen Ausschnitt blauen Himmels errechnet werden. Dass linear polarisiertes Licht auch ohne Blick auf die Sonne als Navigationsgrundlage genügt, konnte durch zahlreiche Verhaltensexperimente für Bienen und Ameisen gezeigt werden (Wehner, 1984). Orientierungsreaktionen auf polarisiertes Licht wurden darüber hinaus für Grillen (Brunner and Labhart, 1987), Fliegen (von Philipsborn and Labhart, 1990) und Heuschrecken (Mappes und Homberg, 2004) unter Laborbedingungen nachgewiesen. Von diesen erwiesen sich insbesondere Wüstenheuschrecken (*Schistocerca gregaria*) als besonders geeignet für elektrophysiologische Untersuchungen zur Charakterisierung der neuronalen Prozesse, die der Wahrnehmung von polarisiertem Licht und den gezeigten Verhaltensreaktionen zu Grunde liegen.

Zur Detektion von polarisiertem Licht besitzen Heuschrecken wie viele weitere Insekten eine spezialisierte Region im Komplexauge, die so genannte dorsale Randregion (engl. dorsal rim area, DRA). Diese nach oben gerichteten Augenregionen besitzen Photorezeptoren, die hoch spezialisiert sind für die Wahrnehmung von polarisiertem Licht (Homberg und Paech, 2002). Aus dieser Region projizieren die Axone der Photorezeptoren in ebenfalls spezialisierte Areale der Lamina und der Medulla, den ersten beiden visuellen Verarbeitungszentren des Insektengehirns (Abb. 1A). Von diesen Regionen verschalten Neurone in Teile der Lobula (drittes optische Neuropil) sowie den anterioren optischen Tuberkel (Homberg, 2004). Mehrere Neuronentypen dieses kleinen Gebiets im Protocerebrum konnten außerordentlich detailliert untersucht werden (Pfeiffer, 2006). Generell konnte gezeigt werden, dass Neurone der Polarisationssehbahn auf rotierende, von dorsal präsentierte *E*-Vektoren mit einer tonischen Modulation ihrer Aktionspotentialfrequenz reagieren und dabei so genannte Gegenpoleigenschaften besitzen. Das heißt, sie werden von einer bestimmten *E*-Vektor Orientierung maximal aktiviert (Φ_{max}-Wert) und von der *E*-Vektor Orientierung senkrecht zu Φ_{max} maximal inhibiert. Neurone des anterioren optischen Tuberkels verschalten zu spezialisierten Regionen der lateralen akzessorischen Loben (LAL), dem lateralen Dreieck und der medianen Olive (Abb. 1B). Von hier erhalten tangentiale Zellen des Zentralkomplexes ihre Eingangssignale und projizieren ihrerseits zur unteren Einheit des Zentralkörpers (Vitzthum et al., 2002; Träger et al., 2008). Im Zentralkomplex konnten drei weitere Neuronentypen identifiziert werden, die ebenfalls auf polarisiertes Licht reagieren (Vitzthum et al., 2002).

Da somit der Endpunkt der bekannten Polarisationssehbahn im Zentralkomplex zu finden ist, scheint diese Struktur von entscheidender Bedeutung für die Himmelskompassnavigation der Heuschrecke zu sein. Der Zentralkomplex ist eine Gruppe von Neuropilen im Zentrum des Heuschreckengehirns. Er besteht aus vier eng miteinander verbundenen Arealen: Protozerebralbrücke (PB), obere und untere Einheit des Zentralkörpers (engl. upper and lower unit of the central body, CBU, CBL), sowie den paarigen Noduli. Charakteristisch ist der regelmäßige strukturelle Aufbau aus 16 vertikalen Kolumnen, sowie mehreren horizontalen Schichten in CBU und CBL. Welche Funktionalität dieser komplexe Aufbau besitzt, ist unbekannt. Insgesamt konnten dem Zentralkomplex Rollen bei der Steuerung von Lokomotion (Strauss, 2002a), visuellem Gedächtnis (Liu et al., 2006), sowie bei sensorischer Verarbeitung von visuellen (insbesondere polarisiertes Licht) und mechanosensorischen Reizen zugeordnet werden. Aufgrund dieser sowohl motorischen als auch sensorischen Funktionsaspekte, insbesondere aber aufgrund der Translationsinvarianz der geschilderten Gedächtnisinhalte, stellte Strauss (2002b) die Hypothese auf, dass die kolumnäre Struktur des Zentralkomplexes das neuronale Substrat für eine sensorische Repräa-

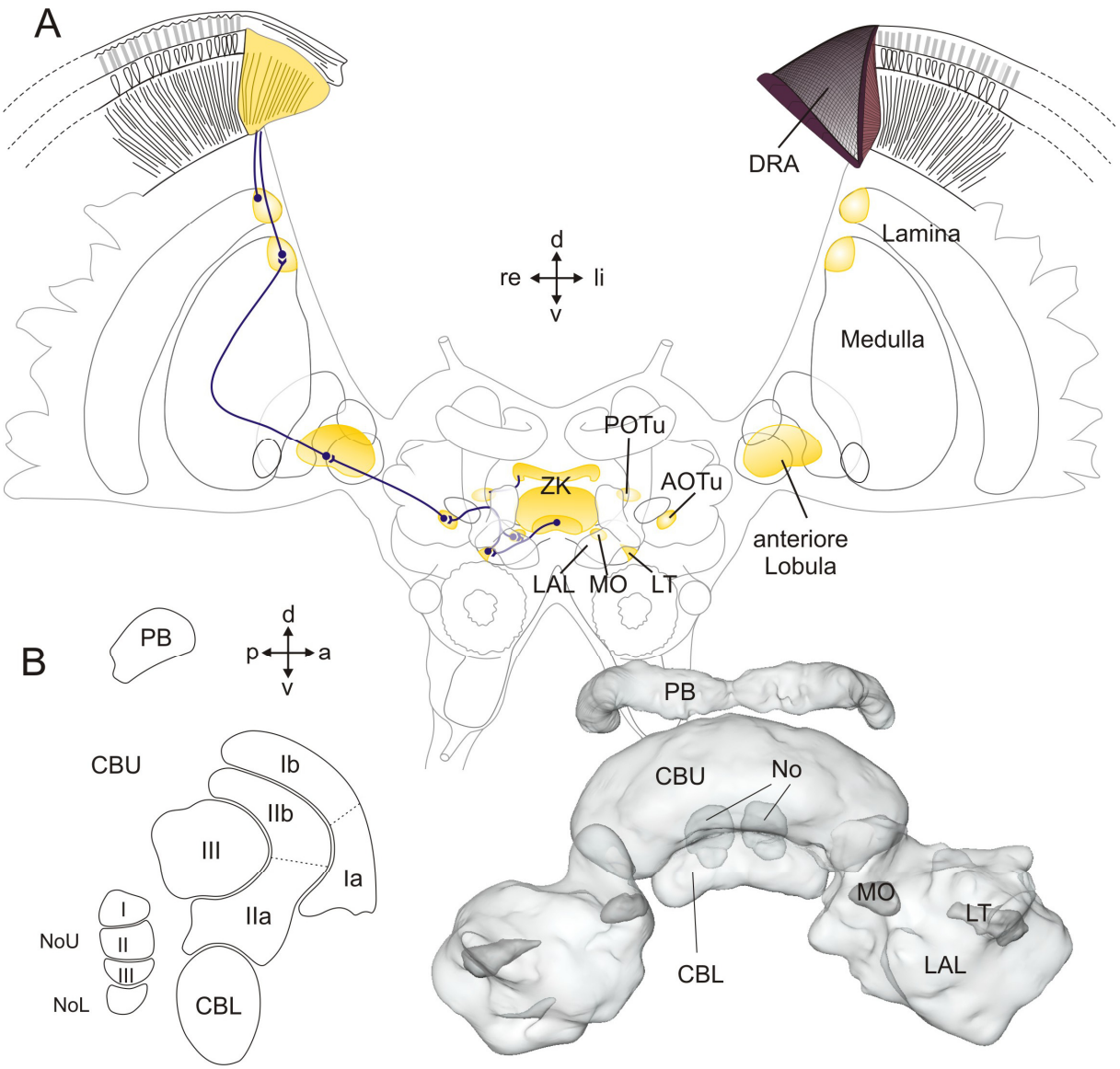

Abb.1 Polarisationssehbahn und Übersicht über die Anatomie des Zentralkomplexes der Wüstenheuschrecke. A. Darstellung der Polarisationssehbahn (blau) von den dorsalen Randregionen der Komplexaugen (DRA) bis zum Zentralkomplex (ZK) in schematischer Frontalansicht des Heuschreckengehirns. Areale, die bei der Verarbeitung von polarisiertem Licht eine Rolle spielen, sind in gelb hervorgehoben. B. rechts: Dreidimensionale Rekonstruktion des Zentralkomplexes und der lateralen akzessorischen Loben (LAL) aus frontaler Sicht. Links: Schematische Darstellung der Schichtung des Zentralkomplexes aus saggitaler Ansicht. PB, Protozerebralbrücke; CBU, obere Einheit des Zentralkörpers; CBL, untere Einheit des Zentralkörpers; MO, mediane Olive; LT, laterales Dreieck; NoU, obere Einheit der Noduli; NoL, untere Einheit der Noduli; POTu, posteriorer optischer Tuberkel; AOTu, anteriorer optischer Tuberkel; d, dorsal; v, ventral; a, anterior; p, posterior; li, links; re, rechts.

sentation des Azimuts um das Tier darstellt, auf deren Grundlage die Generierung von motorischen Planungssignalen stattfindet.

Die Erkenntnis, dass einige Neurone des Zentralkomplexes sensitiv für polarisiertes Licht sind, eröffnete die Möglichkeit, der genannten Hypothese mittels einfach zu kontrollierender, zugleich aber nachweislich für das Verhalten relevanter Stimuli (rotierende *E*-Vektoren) nachzugehen.

In der vorliegenden Arbeit wurde dies mittels elektrophysiologischer Methoden untersucht. Hierzu wurden intrazelluläre Ableitungen aus Neuronen dem Zentralkomplex, insbesondere der Protozerebralbrücke etabliert (Abb. 1B), die kombiniert wurden mit Farbstoffinjektionen in die abgeleiteten Zellen. Dies ermöglichte neben der Untersuchung der physiologischen Antworten eines Neurons auf die gezeigten Reize stets auch die Analyse der anatomischen Charakteristika der abgeleiteten Zellen. Die anatomischen Untersu-

chungen wurden des Weiteren kombiniert mit immuncytochemischen Färbemethoden, einerseits zum Nachweis von in den abgeleiteten Neuronen vorhandenen neuroaktiven Substanzen, sowie zur genauen Lokalisation von Verzweigungsgebieten.

Die vorliegende Arbeit gliedert sich in fünf Kapitel, deren Inhalt im Folgenden kurz beschrieben werden soll.

Kapitel 1: Neuroarchitecture of the Central Complex of the Desert Locust: Intrinsic and Columnar Neurons

In diesem Kapitel wurden die Neuronentypen des Zentralkomplexes in einer rein anatomischen Arbeit dokumentiert. Da es eine nahezu unüberschaubare Vielfalt von Neuronentypen in diesem Areal gibt, habe ich mich hier zunächst auf Zellen beschränkt, die alle unter dem in *Drosophila* geprägten Begriff Kleinfeldneurone zusammen zu fassen sind. Dies umfasst kolumnäre Zellen, die einzelne Kolumnen der PB und/oder des Zentralkörpers mit den LALs oder den Noduli verbinden, sowie die pontinen Zellen, die in zwei kolumnären Bereichen der CBU verzweigen.

Um Verzweigungsgebiete von Neuronen miteinander vergleichen zu können, wurden zunächst dreidimensionale Rekonstruktionen der einzelnen Bestandteile des Zentralkomplexes und des LALs angefertigt. Hierbei wurden zum ersten Mal alle Schichten der CBU, sowie alle Untereinheiten der Noduli und der LALs vollständig rekonstruiert. Die dabei entwickelte Methodik umfasst immuncytochemische Markierungen des Synapsenproteins Synapsin sowie des biogenen Amins Serotonin, kombiniert mit konfokaler Mikroskopie und dreidimensionaler volumetrischer Rekonstruktion. Die Reproduzierbarkeit dieses Ablaufes erlaubt es in Zukunft, auf dessen Grundlage einen auf vielen individuellen Präparaten beruhenden Standard-Zentralkomplex zu errechnen.

Durch Analyse von mit Farbstoff markierten Neuronen konnten insgesamt 21 verschiedene Typen von kolumnären Zellen, drei Typen von pontinen Zellen und eine amakrine Zelle mit ihren Verzweigungsmustern, Projektionsschemata und Faserverläufen beschrieben werden. Die meisten Neurontypen waren Teil von isomorphen Neuronensystemen, bestehend aus jeweils 16 individuellen Zellen desselben Typs, die sich in den innervierten Kolumnen unterschieden. Diese heterolateralen Projektionsmuster waren in nahezu allen Fällen zelltypspezifisch und erlauben Rückschlüsse auf den Informationsfluss im Zentralkomplex. Weiterhin konnten aufgrund der Feinstruktur der neuronalen Endigungen für die meisten Zelltypen wahrscheinliche Eingangs- und Ausgangsregionen ermittelt werden. Allgemein ließ sich schlussfolgern, dass alle beschriebenen Neuronen entweder intrinsische Zellen des Zentralkomplexes sind, oder aber Ausgangsneurone darstellen. Der neuronale Eingang in diese Region muss folglich über die hier nicht beschriebenen Tangentialneuronen erfolgen. Weiterhin konnte kein direkter neuronaler Kontakt zwischen der CBU und der CBL nachgewiesen werden. Zellen aus den beiden Untereinheiten des Zentralkörpers projizieren entsprechend auch zu nicht überlappenden Bereichen des LALs. Damit finden sich im Zentralkomplex zwei getrennte Schaltkreise, die ausschließlich über die PB in indirektem Kontakt miteinander stehen. Die Untereinheiten der Noduli verhalten sich entsprechend; die untere Einheit der Noduli steht mit der CBL, die obere dagegen mit der CBU in Verbindung.

Als erste umfassende Beschreibung der neuronalen Zusammensetzung des Zentralkomplexes der Wüstenheuschrecke erlaubt diese Studie den Vergleich zu *Drosophila*, dem einzigen Insekt, dessen Zentralkomplex-Neurone in vergleichbarer Weise beschrieben wurden (Hanesch et al., 1989). Somit können Schlüsselkomponenten des neuronalen Netzwerkes im Zentralkomplex leichter identifiziert werden und so die Grundlage schaffen für eine Fokussierung und leichtere Interpretation von funktionalen Studien.

Kapitel 2: Maplike Representation of celestial *E*-vectors in the brain of an insect.

Nachdem im ersten Kapitel die neuronalen Komponenten des Zentralkomplexes eingehend untersucht worden sind, habe ich in Kapitel 3 die physiologischen Antworten von kolumnären Neuronen der PB auf polarisierte Lichtreize systematisch analysiert. Dabei wurde von 37 Neuronen aus unterschiedlichen Kolumnen der PB intrazellulär abgeleitet, während die Heuschrecke aus dorsaler Richtung mit einem rotierenden Polarisationsfilter stimuliert wurde. Im Anschluss an die Ableitung wurden die Neurone mit einem Farbstoff injiziert, so dass der jeweilige Zelltyp, sowie die innervierte Kolumne festgestellt werden konnte.

Wie bereits bekannt (Vitzthum et al., 2002), führte die Stimulation mit dorsal rotierenden *E*-Vektoren für die analysierten kolumnären Neurone zu einer typischen Gegenpolantwort, bei der eine eindeutige Vorzugsrichtung (Φ_{max}-Wert) nachweisbar war, die mittels zirkulärer Statistik objektiv berechnet werden konnte (Pfeiffer et al., 2005). Neben den bereits bekannten kolumnären Neuronen, wurde in dieser Arbeit ein bislang unbekannter Neuronentyp physiologisch beschrieben (TB1-Neurone, n = 18). Diese Zellen, deren Morphologie in Kapitel 2 eingehend analysiert wurde, stellen einen Typ von tangentialen Zellen dar, der darüber hinaus kolumnäre Verzweigungsdomänen besitzt, die zum Teil varikos (wahrscheinlich präsynaptisch) und zum Teil fein (wahrscheinlich postsynaptisch) sind. Interessanterweise zeigte sich, dass die Φ_{max}-Werte dieser Neurone mit der anatomischen Position der varikosen Verzweigungsdomänen entlang der PB korrelieren. Das bedeutet, dass eine Zelle, die in einer bestimmten Kolumne der PB ihre varikosen Verzweigungen hat, einen spezifischen Φ_{max}-Wert besitzt. Dieser Φ_{max}-Wert ändert sich systematisch um ca. 26° zwischen zwei Kolumnen. Dabei wird von der gesamten Population dieser Zellen entlang der Breite der PB ein *E*-Vektor-Bereich von 360° abgedeckt. Das heißt, dass jeder mögliche *E*-Vektor genau zweimal repräsentiert ist.

Da TB1-Neurone diese topographische Repräsentation mit ihren potentiellen Ausgangsregionen bilden, und kolumnäre Neurone in den Kolumnen der PB ihren wahrscheinlichen Eingang erhalten, wurden diese Zellen ebenfalls genauer analysiert. Dabei wurde eine ähnliche Abhängigkeit der Φ_{max}-Werte von der Position der Verzweigungsareale in der PB entdeckt. Die gefundene lineare Beziehung deckte unabhängig voneinander für zwei Gruppen von Neuronen einen identischen Bereich von ca. 360° entlang der PB ab (n = 10, sowie n = 9). Dies entsprach ebenfalls den bereits beschriebenen TB1-Neuronen. Allerdings war die Lage der Regressionsgerade vertikal um 90° verschoben. Dies bedeutet, dass in einer Kolumne, in der bei einer bestimmten Stimulussituation eine TB1-Zelle maximale Aktivität zeigt, die dort verzweigenden kolumnären Neurone minimale Aktivität aufwiesen. Dies wurde als Hinweis auf eine inhibitorische Verschaltung interpretiert.

Insgesamt stellt die beschriebene topographische Repräsentation von dorsalen *E*-Vektoren (Polarotopie) eine in mehrerer Hinsicht bedeutsame Entdeckung dar. Aufgrund der direkten Beziehung zwischen zenitalen *E*-Vektoren zum Sonnenstand entspricht die gezeigte Polarotopie einer geordneten Reihe von Kopfrichtungsneuronen, die die Orientierung des Tieres relativ zum solaren Meridian kodieren. Obwohl das Konzept von Kopfrichtungsneuronen aus Vertebraten bereits eingehend bekannt ist, konnte es hier das erste Mal für Invertebraten in modifizierter Form nachgewiesen werden. Das Konzept einer globalen Richtungskodierung impliziert weiterhin, dass der Aktivität der PB-Neurone direkt Information über den Azimut der Sonne entnommen werden kann, d.h. einen internen Kompass darstellen könnte. Schließlich ist die gezeigte Polarotopie die erste funktionale Entsprechung der kolumnären Struktur des Zentralkomplexes und deutet stark auf eine Funktion dieser Struktur als internes Orientierungszentrum hin. Zusammen mit Daten von *Drosophila* (Liu et al., 2006) konnte somit die Hypothese entwickelt werden, dass die Kolumnen des Zentralkomplexes den Azimut des um das Tier befindlichen Raumes repräsentieren, während die Schichten des Zentralkörpers das Vorhandensein von spezifischen, verhaltensrelevanten Aspekten in der Umgebung kodieren, deren Aktivität gemeinsam mit der Richtungsinformation der PB zu motorischen Planungssignalen verarbeitet werden kann.

Kapitel 3: Linking the input to the output - Additional sets of polarization sensitive neurons complement the polarization vision network of the locust central complex.

Die Entdeckung der topografischen Repräsentation von *E*-Vektoren in der PB in Kapitel 2 (Heinze and Homberg, 2007), wirft zwei wesentliche Fragen auf. Einerseits ist bislang unbekannt, wie und mit welchen Neuronen die polarisationssensitiven Eingangszellen der CBL verschaltet werden, um das systematische Tuning in den Kolumnen der PB zu errechnen. Zum Zweiten stellt sich die Frage, in welcher Weise die in der Polarotopie vorhandene Information mit weiteren sensorischen Informationen integriert wird und anschließend zum Steuern von Verhalten genutzt werden kann. Kapitel 3 und 4 befassen sich zunächst mit Aspekten der ersten Frage, bevor in Kapitel 5 erste Versuche aufgezeigt werden, um Antworten auf die zweite Frage zu erhalten.

In Kapitel 3 wurden weitere intrazelluläre Ableitungen durchgeführt, mit dem Ziel, die neuronale Verbindung zwischen den polarisationssensitiven Eingangsneuronen des Zentralkomplexes und den Neuronen der PB zu

identifizieren und zu charakterisieren. Insbesondere konnte von den morphologisch seit langem bekannten CL1 Neuronen 25 mal abgeleitet werden. Dabei besitzt der Untertyp CL1a als einziger Zelltyp des Zentralkomplexes eine geeignete Morphologie, um Informationen von der CBL zur PB zu transferieren. Diese Zellen schließen somit die Lücke in der Polarisationssehbahn zwischen Eingangsneuronen der CBL und den Neuronen der PB. Die Analyse der Φ_{max}-Werte ergab, dass diese Neurone trotz ihrer Morphologie als kolumnäre Zellen nicht Teil der polarotopen *E*-Vektor-Repräsentation sind, was ebenfalls dafür spricht, dass sie eine frühere Stufe im Netzwerk zur Verarbeitung von Polarisationsinformation einnehmen. Weiterhin wurde ein zweiter Typ von tangentialen PB-Neuronen als polarisationssensitiv beschrieben. Diese Zellen unterscheiden sich in ihrem Φ_{max}-Wert von TB1 Neuronen und konnten nur in einer Kolumne jeder Hemisphäre gefunden werden. Letzteres deutet darauf hin, dass sich bestimmte Kolumnen des Zentralkomplexes funktional von den übrigen unterscheiden.

Drei kolumnäre Neuronentypen wurden erstmals physiologisch charakterisiert, die in nur 50% aller Experimente polarisationssensitiv waren. Dies steht im Gegensatz zu allen bisher bekannten polarisationssensitiven Zellen und legt nahe, dass diese Zellen bei Bedarf, möglicherweise in Abhängigkeit vom Verhaltenskontext, zum Netzwerk zur Verarbeitung von polarisiertem Licht hinzugezogen werden können. Zwei dieser konditional polarisationssensitiven Neuronentypen innervieren die Noduli, über die funktional bisher noch nichts bekannt war. Schließlich wurden in dieser Arbeit zwei Typen von Neuronen vorgestellt, die Polarisationsinformation in Richtung motorischer Zentren jenseits des Zentralkomplexes leiten könnten. Diese Zellen erhalten Eingangssignale vom LAL und projizieren entweder zum kontralateralen LAL oder ins posteriore Protocerebrum. In beiden Arealen besitzen Neurone ihre Eingangsregionen, die über die Schlundkonnektive zum Thorax absteigen und direkt an der Ansteuerung von Motorneuronen beteiligt sein können.

Insgesamt konnte mit dieser Arbeit eine wesentliche Lücke der Polarisationssehbahn geschlossen werden. Außerdem konnten weitere Komponenten zum bekannten System hinzugefügt werden, die zum einen auf eine kontextabhängige Modifikation des Zentralkomplex-Netzwerkes hindeuten, und zum anderen einen möglichen Signalweg zur Verschaltung auf motorische Bahnen aufzeigen. Basierend auf diesen zusätzlichen Informationen wurde ein hypothetisches Verschaltungsschema entworfen, das den Fluss der Polarisationsinformation vom Eingang des Zentralkomplexes bis zum wahrscheinlichen Ausgang abdeckt.

Kapitel 4: Transformation of polarized light information in neurons of the locust central complex.

Da das in Kapitel 3 entworfene Verschaltungsschema auf der Morphologie von polarisationssensitiven Neuronen sowie deren Φ_{max}-Werten beruhte, bleibt es zunächst weitgehend hypothetisch. In Kapitel 4 wurde untersucht, wie sich die diversen Typen von polarisationssensitiven Neuronen des Zentralkomplexes physiologisch unterscheiden und inwiefern diese quantitativen Analysen mit dem zuvor propagiertem Netzwerkmodell im Einklang stehen.

Zu diesem Zweck wurden die Reaktionen aller 114 abgeleiteten Neuronen quantifiziert und in Bezug auf Reaktionsstärke, Hintergrundaktivität, Variabilität der Antwortstärke, spontane Variabilität der Hintergrundfrequenz, sowie Breite der *E*-Vektor-Tuningkurven statistisch untersucht. Außerdem wurden weitere Ableitungen vorgenommen, die untersuchten, ob sich die Struktur der rezeptiven Felder zwischen den Zelltypen unterscheidet, und welche der beschriebenen Zellen Informationen von beiden Augen verarbeiten. Letzteres wurde über monokulare Stimulation durch Abdecken entweder der rechten oder der linken DRA realisiert. Die Breite der rezeptiven Felder konnte über einen an ein Perimeter gekoppelten Polarisationsfilter entlang des Meridians quer zur Längsachse des Tieres vermessen werden.

Insgesamt konnte durch diese Analysen gezeigt werden, dass sich die zwölf untersuchten Zelltypen in mehrere Gruppen einteilen lassen. Dabei sind sich morphologisch ähnliche Zellen, sowie Untertypen von Neuronenklassen stets auch physiologisch ähnlich. Die resultierenden Gruppen beinhalten tangentiale Neurone der CBL (TL2 und TL3 Neurone) als Zellen mit dem besten Signal-Rausch-Verhältnis, der geringsten Hintergrundaktivität, sowie der geringsten spontanen Variabilität. Dagegen weisen die an der Polarotopie beteiligten Neurone (TB1, CPU1, und CP1,2 Neurone) eine hohe Hintergrundaktivität, ein relativ schlechtes Signal-Rausch-Verhältnis, sowie hohe polarisationsunabhängige Variabilität auf. Die in Kapitel 4 als Verbindung zwischen CBL und PB eingeführten CL1-Neurone weisen in allen Charakteristika Werte zwi-

schen diesen beiden Extremen auf. Bei Betrachtung der Breite der *E*-Vektor-Tuningkurven fiel auf, dass ein Maximum an Tuningschärfe bei CL1 Neuronen erreicht wurde, dagegen besaßen CPU1- und TB1 Zellen die breitesten Kurven. Alle Daten deuten zusammen genommen darauf hin, dass TL Neurone am Eingang des Zentralkomplexes zu finden sind. In der Nähe des Ausgangs kann man dagegen die Neurone der PB einordnen, die die am wenigsten ausgeprägten *E*-Vektor Antworten besitzen. Dies basiert weitgehend auf der hohen polarisationsunabhängigen Aktivität, die möglicherweise auf zusätzlichen Eingang von anderen sensorischen Modalitäten zurückzuführen ist. Dass CL1 Neurone bei den meisten Parametern zwischen den beiden genannten Gruppen standen, deckt sich mit ihrer anatomischen Position. Alle Neurone außer TL3 Zellen reagieren auf Stimuli von beiden DRAs, integrieren also binokulare Information, und unterscheiden sich darin deutlich von den untersuchten Neuronen des anterioren optischen Tuberkels (Pfeiffer et al., 2005).

Weiter gestützt werden konnte die vorgeschlagene Richtung des Informationsflusses beginnend bei TL-, über CL1-, hin zu TB-, CPU1-, und CP Neuronen, durch die Größe und Orientierung ihrer rezeptiven Felder. So fanden sich in TL2 Neuronen kleinere, ca. 60° breite Sehfelder, deren Zentrum im kontralateralen Gesichtsfeld lag. Dagegen waren die Sehfelder von CL1 Neuronen deutlich größer und im ipsilateralen Gesichtsfeld zentriert. Schließlich fanden sich sehr große, nahezu die gesamte Hemisphäre abdeckende, Zenit-zentrierte rezeptive Felder in TB1-, CPU1- und CP2 Neuronen. Diese Progression erlaubte Rückschlüsse auf die neuronalen Verschaltungen der einzelnen Zelltypen und legt nahe, dass TL2 Neurone ausschließlich auf kontralaterale CL1 Neurone verschalten. Die unilateralen Sehfelder von CL1 Zellen beider Hemisphären können anschließend von TB Zellen zu bilateralsymmetrischen Sehfeldern integriert werden. Die Analyse der Verteilung von Φ_{max}-Werten innerhalb von rezeptiven Feldern deutet darauf hin, dass die Polarotopie in den Zellen der PB eine 360° umfassende Azimut-Kodierung darstellt, und nicht lediglich eine zweifache 180° umfassende *E*-Vektor-Kodierung pro Hemisphäre.

Allgemein decken sich die in diesem Kapitel analysierten physiologischen Daten gut mit dem auf morphologischer Basis entworfenen Modell des polarisationssensitiven Netzwerkes im Zentralkomplex. Der so nahegelegte Informationsfluss reicht von rein sensorischem Eingang in die CBL über ein optimales *E*-Vektor-Tuning in CL1 Neuronen, zu potentiell multimodalen Kopfrichtungszellen in der PB. Von diesen sind CPU1 Neurone morphologisch als Hauptausgangsneurone des Zentralkomplexes geeignet. Ungeklärt ist zwar weiterhin, wie die geordnete *E*-Vektor-Repräsentation in der PB errechnet wird, allerdings scheinen CL1 Neurone und deren potentielle Interaktion mit TB Neuronen das wahrscheinliche neuronale Substrat dieses Vorgangs zu sein.

Kapitel 5: Integration of multiple visual stimuli in neurons of the locust central complex.

Die Kapitel 3 und 4 haben sich damit beschäftigt, wie das polarisationssensitive Netzwerk von Neuronen im Zentralkomplex aufgebaut ist und in welcher Weise *E*-Vektor Informationen dieses Netzwerk durchlaufen und zur Erzeugung der in Kapitel 2 beschriebene Polarotopie beitragen könnten. Zusammen mit den morphologischen Daten aus Kapitel 1 stellte sich dabei heraus, dass bestimmte Neuronen, nämlich CPU1-Zellen, zusammen mit den konditional polarisationssensitiven CPU2 Neuronen, den wahrscheinlichen Ausgang des Zentralkomplexes bilden. Da Ausgangssignale des Zentralkomplexes aller Wahrscheinlichkeit nach entscheidend für die Generierung motorischer Steuersignale sind und neben polarisiertem Licht auch andere sensorische Signale im Zentralkomplex repräsentiert sind (Homberg, 1994; Liu et al., 2006; Ritzmann et al., 2008), sollten diese Ausgangsneurone auf verschiedene verhaltensrelevante Stimuli reagieren. Insbesondere Daten von *Drosophila* (Liu et al., 2006) legen nahe, dass in unterschiedliche Schichten der CBU projizierende tangentiale Neurone für die Erkennung von komplexen visuellen Parametern benötigt werden (Kantenorientierung und Elevation von Balken). Morphologisch wären CPU1- und CPU2 Neurone geeignet, eine bestimmte Azimutposition (kodiert im *E*-Vektor-Tuning der PB) mit in den Schichten der CBU kodierten sonstigen verhaltensrelevanten Sinnesinformationen zu assoziieren. In den Experimenten des Kapitels 5 sollte daher überprüft werden, ob Neurone an unterschiedlichen Stellen des polarisationssensitiven Netzwerkes im Zentralkomplex auf unpolarisierte Stimuli im frontalen Gesichtsfeld der Heuschrecke reagieren.

Zu diesem Zweck wurde eine neue Versuchsapparatur entworfen und gebaut, mit deren Hilfe der Heuschrecke komplexe visuelle Stimuli über einen computergesteuerten CRT-Monitor präsen-

tiert werden konnten. Es wurden verschiedene Stimuli getestet: Kurze Lichtblitze verschiedener Farben (rot, grün, blau, weiß), die den ganzen Monitor einnahmen; weiße Balken verschiedener Orientierungen auf schwarzem Hintergrund, die sich orthogonal zu ihrer Orientierung über den Monitor bewegten; sinusförmige Streifenmuster verschiedener Orientierungen, die sich ebenfalls orthogonal zu ihrer Orientierung bewegten; rotierende Balken (schwarz auf weißem Hintergrund, sowie weiß auf schwarzem Hintergrund); sowie kleine weiße Punkte (Durchmesser: 5.5°) an unterschiedlichen Stellen des Monitors. Da die frontal präsentierten Stimuli selbständig entworfen und programmiert worden sind, und die neuronalen Reaktionen im Zentralkomplex allgemein vergleichsweise schwach ausfielen, wurden die Stimuli zusätzlich an Neuronen getestet, die deutliche Reaktionen zeigen sollten. Dabei handelte es sich um Zellen des optischen Lobus, insbesondere der Lobula.

Insgesamt konnten 26 Neurone aus dem optischen Lobus und dem Zentralkomplex abgeleitet werden. Generell zeigten alle zwölf Neurone des optischen Lobus starke Reaktionen auf frontale, unpolarisierte Lichtreize, wohingegen die Zentralkomplexneurone mit wenigen Ausnahmen schwache oder gar keine Reaktionen zeigten. Die deutlichen Antworten der Zellen des optischen Lobus ließen die Schlussfolgerung zu, dass die verwendeten Stimuli adäquat von Heuschrecken wahrgenommen werden können. Unter diesen Neuronen waren mehrere bewegungssensitive Neurone, zwei Gegenfarbneurone, sowie zwei Zellen, die in ihren Eigenschaften so genannten STDNs (small target detecting neurons) anderer Insekten ähneln. Die meisten dieser Neurone verbanden beide optische Loben oder wiesen Projektionen im posterioren Protocerebrum auf. Da in diesem Areal absteigende Zellen ihre Eingangsregionen besitzen, deutet dies darauf hin, dass insbesondere Bewegungsreize direkt zu den motorischen Zentren des Thorax verschaltet werden, ohne dass der Zentralkomplex an deren unmittelbarer Bearbeitung beteiligt ist. Interessant war weiterhin ein bewegungs- und polarisationssensitives Neuron der Lobula, das zusammen mit Daten von Homberg und Würden (1997) auf ein zweites polarisationssensitives neuronales System hindeutet, das unabhängig vom Kompassnavigationsnetzwerk ist.

Von den 14 abgeleiteten Neuronen des Zentralkomplexes waren zehn polarisationssensitiv. Von diesen entstammten 6 CL1 Neurone, ein CPU1 Neuron, sowie ein TL2 Neuron dem weiter oben beschriebenen polarisationssensitiven Netzwerk. Lediglich eines der CL1 Neurone zeigte eine schwache Inhibition als Antwort auf frontale Lichtreize, wohingegen alle anderen CL1 Zellen keine Reaktionen aufwiesen. Dagegen war bei dem abgeleiteten CPU1 Neuron bei Stimulation mit sich bewegenden Balken eine leichte orientierungssensitive Reaktion vorhanden. Beide Beobachtungen stehen im Einklang mit der zuvor formulierten Hypothese, dass in späten Verarbeitungsstadien des polarisationssensitiven Netzwerkes im Zentralkomplex Reaktionen auf unpolarisierte Lichtreize mit *E*-Vektor Informationen integriert werden. Die vergleichsweise deutliche Reaktion eines TL2 Neurons auf frontale Balkenstimuli ist vorerst nicht zu erklären und zeigt, dass weitere Experimente notwendig sind, bevor endgültige Aussagen über die Verarbeitungswege von Reizantworten auf unpolarisiertes Licht im Zentralkomplex gemacht werden können. Außer den beschriebenen polarisationssensitiven Neuronen konnte von vier konditional polarisationssensitiven Zellen abgeleitet werden (2x CPU2, und je 1x CPU4 und CL2). Dabei unterstreichen die Reaktionen beider CPU2 Neurone auf bewegte Balkenstimuli ihre anatomische Stellung nahe des Zentralkomplex-Ausgangs. Die beiden Neurone mit Projektionen zu den Noduli unterschieden sich in ihrer spektralen Empfindlichkeit und deuten damit auf unterschiedliche visuelle Eingangswege hin.

Zuletzt unterstreichen die Ableitung eines tangentialen Neurons der CBU und dessen starke Antworten auf Bewegungen im lateralen Gesichtsfeld, dass Information über unpolarisiertes Licht tatsächlich über diese Klasse von Neuronen in den Zentralkomplex gelangen kann. Alles in allem deuten die recht schwachen und variablen Antworten, sowie die Existenz von konditional polarisationssensitiven Neuronen darauf hin, dass nur Stimuli im Zentralkomplex repräsentiert werden, die je nach Kontext akut verhaltensrelevant sind. Diese Aspekte der Umwelt könnten mit der Azimutinformation aus polarisiertem Licht integriert werden und so in Signale umgewandelt werden, die der motorischen Steuerung des Tieres dienen.

Literatur

Brunner D, Labhart T (1987) Behavioural evidence for polarization vision in crickets. Physiol Entomol 12:1-10.

Hanesch U, Fischbach KF, Heisenberg M (1989) Neuronal architecture of the central complex in *Drosophila melanogaster*. Cell Tissue Res 257:343-

366.
Heinze S, Homberg U (2007) Maplike representation of celestial E-vector orientations in the brain of an insect. Science 315:995-997.
Homberg U (1994) Flight-correlated activity changes in neurons of the lateral accessory lobes in the brain of the locust *Schistocerca gregaria*. J Comp Physiol A 175:597-610.
Homberg U (2004) In search of the sky compass in the insect brain. Naturwissenschaften 91:199-208.
Homberg U, Paech A (2002) Ultrastructure and orientation of ommatidia in the dorsal rim area of the locust compound eye. Arthropod Struct Dev 30:271-280.
Horváth G, Varjú D (2004) Polarized light in animal vision. Springer, Berlin.
Liu G, Seiler H, Wen A, Zars T, Ito K, Wolf R, Heisenberg M, Liu L (2006) Distinct memory traces for two visual features in the *Drosophila* brain. Nature 439:551-556.
Pfeiffer K, Kinoshita M, Homberg U (2005) Polarization-sensitive and light-sensitive neurons in two parallel pathways passing through the anterior optic tubercle in the locust brain. J Neurophysiol 94:3903-3915.
Pfeiffer K. (2006) Coding of sky-compass information in neurons of the anterior optic tubercle of the desert locust *Schistocerca gregaria*. Dissertation, Philipps-Universität Marburg.
Ritzmann RE, Ridgel AL, Pollack AJ (2008) Multi-unit recording of antennal mechano-sensitive units in the central complex of the cockroach, *Blaberus discoidalis*. J Comp Physiol A 194:341-360.
Strauss R (2002a) The central complex and the genetic dissection of locomotor behaviour. Curr Opin Neurobiol 12:633-638.
Strauss R. (2002b) Die übergeordnete Steuerung des Laufverhaltens durch das Insektengehirn, studiert mit Methoden der *Drosophila*-Neurogenetik. Habilitationsschrift, Universität Würzburg.
Träger U, Wagner R, Bausenwein B, Homberg U (2008) A novel type of microglomerular synaptic complex in the polarization vision pathway of the locust brain. J Comp Neurol 506:288-300.
Vitzthum H, Müller M, Homberg U (2002) Neurons of the central complex of the locust *Schistocerca gregaria* are sensitive to polarized light. J Neurosci 22:1114-1125.
von Philipsborn A, Labhart T (1990) A behavioral study of polarization vision in the fly, *Musca domestica*. J Comp Physiol A 167:737-743.
Wehner R (1984) Astronavigation in Insects. Annu Rev Entomol 29:277-298.

Introduction

Animal navigation

One of the most distinctive features of animals is their ability to move from one place to another to seek favorable environmental conditions. With increasingly complex and long ranging maneuverability the demands on sensory systems and central processing abilities of nervous systems also increased. Animals had to generate motor output adequate to lead them reliably away from harmful situations and into environments that ensured the proximity of food and potential mating partners.

Behavioral responses to stimuli can be classified into the simple, undirected kinesis, the directed telotaxis, and the most elaborate menotaxis. In the first case, activity rate is decreased when favorable conditions are met, thus increasing the likelihood to remain in that situation. Telotactic behavior, e.g. phototaxis, is directed toward the stimulus or 180° away from it. In menotactic behavior, the direction of movement can be freely chosen at any angle to the stimulus and is only achieved in vertebrates, cephalopods and arthropods. Especially demanding forms of orientation behavior are required when animals either migrate over long distances to reach a specific target (monarch butterflies, desert locusts, migrating birds, etc.), or when they have to return to a central place (burrow, hive, etc.) after a foraging trip. In the latter case either path integration or true navigation mechanisms are required. During path integration the animal stores all performed movements (angular and translational) while continuously updating a homing vector, leading the animal directly homewards from any point along their foraging trip (Collett and Collett, 2000). This behavior, well studied in hymenopteran insects (bees, wasps, ants), does not allow the animal to find home when they are passively relocated to unfamiliar terrain. Homing after passive relocation can only be accomplished when true navigation is used (Menzel et al., 2005). Hereby an internal map of landmarks in the environment is stored and combined with directional (compass) information. While attributed exclusively to higher vertebrates for a long time, honey bees and spiny lobsters (*Panulirus argus*) are also likely to possess this 'cognitive' capability (Menzel et al., 2006; Boles and Lohmann, 2003). In the vicinity of the burrow/nest a combination of systematic search strategies and orientation with the help of chemical cues (e.g. odors), location, or structural features of small-scale landmarks is used to reliably find the nest entrance. All types of homing behavior require some form of memory (Collett and Collett, 2002). Especially knowledge about the relation of landmarks to each other and to the nest has to be learned, as demonstrated during orientation flights in honey bees (Menzel et al., 2006). A simplified version of landmark orientation is the so-called snapshot memory, a mechanism proposed for ant navigation, which makes use of a progressing series of images stored along the outgoing path, which have to be matched to the real sensory information to retrace the inward path (Collett, 1992; Durier et al., 2003). For providing a frame of reference during true navigation or long range migration, as well as monitoring angular motion during path integration, the sky and the earth's magnetic field are important orientation cues. Both can be used to obtain information about compass directions, and together with large-scale landmarks, such as mountain ranges and seashores, are likely to provide the basis for long range migrations (Frost and Mouritsen, 2006).

Polarized light and other sky compass cues

For long range migrations as well as for central place foraging in featureless environments, the sky offers the most prominent and reliable orientation cues. During the day, the sun itself stands out as the most obvious one among them. Depending on the season and time of day, the sun is located at a particular position, defined by azimuth and elevation. The continuous changes of these variables over each day throughout the year can be described by the ephemeris function, which by itself depends on the geographic location of the observer. When the date, daytime and ephemeris function are known to the observer, the position of the sun offers precise information about compass directions.

Scattering of sunlight in the upper atmosphere provides additional skylight cues. These include an intensity gradient, a spectral gradient, and a pattern of linearly polarized light, all of which can be described by Rayleigh-scattering (Strutt,

1871). The intensity of skylight depends on the proximity of a particular spot at the sky to the sun, i.e. the amount of scattered light becomes larger with decreasing angle between the sun and the observed spot. Consequently the solar hemisphere of the sky is brighter than the opposite (anti-solar) hemisphere (Coemans et al., 1994, Ugolini et al., 2009). The spectral gradient in the sky is based on the fact that short wavelength light is scattered more effectively than long wavelength light. Hence the ratio of two wavelengths in each point of the sky is a function of its angular distance from the sun (Coemans et al., 1994). Generally, long wavelengths are more dominant in the solar hemisphere, whereas short wavelengths are relatively evenly distributed due to multiple scattering (Coulson, 1988).

At last, Rayleigh-scattering transforms unpolarized sunlight into partly polarized light. In unpolarized light the electric field vectors (*E*-vectors; which together with the magnetic field vector define light as an electromagnetic wave) oscillate with equal probability in all possible orientations, whereas linearly polarized light only possesses one *E*-vector orientation (Wehner, 2001). The amount of linearly polarized light divided by the total amount of light emitted by any light source is called the degree of polarization. The degree of polarization varies with the scattering angle (angle between incoming light and scattered light), and is largest 90° away from the light source. On the other hand, the *E*-vector orientation of scattered light is always perpendicular to the incoming light beam. Both characteristics define the polarization pattern of the blue sky (Horváth and Varjú, 2004). The degree of polarization varies from zero near the position of the sun to a maximum of around 70% at an angle 90° away from the sun, and reaches zero again at the opposite side from the sun (the 'anti-sun'). Hereby the *E*-vector orientations are arranged tangentially to concentric circles around the sun. As this pattern directly depends on the sun's position, it changes correspondingly with the diurnal changes of the solar azimuth and elevation.

In principle, the same phenomena described for the day also apply for the night sky. Hereby the light reflected by the moon is the major light source and produces the same scattering effects as the sun (Horváth and Varjú, 2004), however, several orders if magnitude lower in intensity. Other light sources at night are the planets, the stars and the milky way, which also provide compass information but are more difficult to evaluate at any given time (Wehner, 1984).

Utilisation of polarized light for orientation

In 1923, Felix Santschi observed harvester ants (*Messor barbarus*) in northern Africa on their homeward journey after a foraging trip, and showed conclusively that without visibility of the sun a small fraction of blue sky suffices for correct maintenance of their course. However, only Karl von Frisch (1949) was able to resolve this puzzling observation with behavioral experiments on honey bees (*Apis mellifera*). He showed that the orientation of the *E*-vector of linearly polarized light can serve as source of directional information to insects. Since then, the usage of polarized light information for navigation has been shown also in desert ants *Cataglyphis* (e.g. Wehner, 2003), monarch butterflies (Reppert et al., 2004), and dung beetles (Dacke et al., 2003). The latter animals use the polarization pattern generated by the moon at night to guide them away from a dung source in a straight line. In the laboratory, orientation responses to polarized light have been demonstrated for flies (von Philipsborn and Labhart, 1990), crickets (Brunner and Labhart, 1987), and locusts (Mappes and Homberg, 2004), suggesting that these animals also make use of this skylight feature for orientation in their natural environments.

The polarization vision pathway of the locust brain

The polarization vision system of the desert locust (*Schistocerca gregaria*) has been studied particularly well. Behavioral experiments in this species showed that polarized light is detected with a specialized region of the compound eye, the dorsal rim area (DRA; Mappes and Homberg, 2004). A similar DRA is present in many insect species, which all share several general specializations to increase polarization sensitivity (Labhart and Meyer, 1999). Most importantly, the microvilli of DRA-photoreceptors are highly aligned, and two sets of receptor cells with the same spectral sensitivity possess microvilli arranged orthogonally to one another within each ommatidium. Furthermore, ommatidia have a large acceptance angle for incoming light, due to the lack of screening pigment. Rhabdoms are reduced in length, and the corneae possess several features to scatter light and prevent image formation (Homberg and Paech, 2002). The DRA-ommatidia are directed towards the upper half of the contralateral field of view, but receptive field size of DRA-photoreceptors are not yet known for the locust. However, as zenithal pre-

sentation of polarized light elicits responses in later processing stages, receptive fields must cover a large angle and include the zenith. As in the field cricket, polarization sensitive DRA-photoreceptors are exclusively blue sensitive (Herzmann and Labhart, 1989; Eggers and Gewecke, 1993). Together with antagonistic connections of orthogonally oriented receptors onto later stage neurons, a homochromatic system of polarization analyzers is formed, which is insensitive to changes in absolute intensity or spectral composition of the detected light (Labhart and Meyer, 2002). The DRA-photoreceptors project to dorsal rim areas of the lamina and medulla. Both regions show a simpler, uniform organization compared to the stratified neuroarchitecture of the main lamina/medulla. Dye injections into the dorsal rim medulla revealed neurons projecting to the most ventral layer of the anterior lobe of the lobula and further on to the lower unit of the anterior optic tubercle (AOTu). Additionally, these cells possess one single fiber projecting tangentially through one layer of the medulla (Homberg et al., 2003). The retinotopic organization of the medulla suggests that these neurons receive input from the DRA, as well as from one vertical row of ommatidia of the main compound eye. Unfortunately, nothing is known about the physiology of these cells.

In the AOTu, several types of neuron have been characterized extensively by intracellular recordings (Pfeiffer et al., 2005; Kinoshita et al., 2007; Pfeiffer and Homberg, 2007). LoTu1 and TuTu1 neurons connect the anterior optic tubercles of both hemispheres and LoTu1 have additional branches in the anterior lobula. TuLAL1a and 1b neurons project to two small regions of the lateral accessory lobes (LAL), the lateral triangle (LT; TuLAL1a neurons) and the median olive (MO; TuLAL1b neurons). TuLAL1b neurons possess additional input areas in the anterior lobula. Therefore, two anatomical pathways originate in the anterior lobula and transmit polarized light information in parallel to the LT and MO.

All of these cells respond to dorsally presented, rotating *E*-vectors with tonic modulations of the firing frequency (Pfeiffer et al., 2005). Neurons generally show polarization opponency, i.e. they are tuned to a particular *E*-vector that maximally activates the neuron (Φ_{max}-value), whereas at an *E*-vector 90° different from the Φ_{max}-value the neuron is maximally inhibited. This behavior has been described for the first time in POL1-neurons in the field cricket (Labhart, 1988). The only known exceptions in the locust are LoTu1 neurons, which are tonically activated at all *E*-vector orientations, while the magnitude of activation is modulated during the *E*-vector rotation. Interestingly, these neurons also respond to unpolarized spectral stimuli in an azimuth dependent way (Kinoshita et al., 2007; Pfeiffer and Homberg, 2007). When a colored light spot is rotated around the locust, it elicits activity only at a particular azimuth. Especially in LoTu1 neurons, a prominent green-UV antagonism was revealed. Green light activates the neuron at a particular azimuth, while UV leads to an inhibition (Pfeiffer and Homberg, 2007). The difference between this preferred orientation and the Φ_{max}-value for polarized blue light changed systematically in a day time dependent manner. Modeling these data and comparing them with diurnal changes of *E*-vectors in the proposed receptive fields of the DRAs, suggested that these neurons are suited to compensate for changing *E*-vector information corresponding to changes of solar elevation over the course of day. Also, these cells are able to distinguish the solar from the anti-solar hemisphere and hence to resolve the ambiguity inherent to the symmetrical nature of *E*-vector information.

In the LT and MO, TuLAL1a/b neurons possess characteristic presynaptic endings. Together with postsynaptic endings from tangential neurons of the lower division of the central body (CBL) their cup shaped terminals form so-called microglomeruli (Träger et al., 2008). In addition to these tangential neurons, three types of columnar cells have been described as polarization sensitive (Vitzthum et al., 2002). All of these neurons show polarization opponency and are tuned to Φ_{max}-values covering all possibly occurring *E*-vectors.

Time compensation

As already outlined, the position of the sun, as well as the polarization pattern of the blue sky depends on the time of day. Regarding the sun, the elevation as well as the azimuth varies with daytime. However, only the azimuth of the sun contains compass information, so that variations in the sky polarization pattern due to elevation changes of the sun have to be compensated (Pfeiffer and Homberg, 2007). After this compensation is achieved and the correct solar azimuth is calculated, this information is only usable for deriving compass directions if it is related to daytime once more. Therefore, at some stage during neuronal processing, daytime information has to be integrated with information

about the solar azimuth. How this is achieved, is unknown in any animal.

The insect internal circadian clock has been located in the accessory medulla (aMe), a small neuropil in the optic lobes, in cockroaches, crickets, flies, and beetles (reviewed in Helfrich-Forster et al., 1998). Neurons of the aMe show spontaneous rhythmic activity and are coupled via peptidergic pathways to the rest of the brain (Schneider and Stengl, 2005; Petri et al., 1995). In the locust, the identity of the internal pacemaker has not been verified, but on the basis of anatomical similarities to other insects, the aMe is the most likely candidate as well (Homberg et al., 1991). Interestingly, a neuronal connection has been described from the aMe to the posterior optic tubercle, a small neuropil in the posterior protocerebrum (Homberg et al., 1991, Homberg and Würden, 1997), which is further connected to the protocerebral bridge (PB) of the central complex (Homberg, 1991). Hence anatomically, *E*-vector information and information about daytime could potentially converge in the central complex.

The central complex – neuroanatomy

Because the central complex is the final known processing stage of *E*-vector information, it is likely to play a vital role in sky compass navigation. Its internal neuroarchitecture is most unusual and detailed anatomical knowledge about its structure is likely to be directly important to understand central-complex function. The central complex is a midline spanning group of neuropils, located in the center of the protocerebrum, and consists of four neuropils: the PB, the upper and lower divisions of the central body (CBU, CBL), and the paired noduli (Williams, 1975). This general layout is highly conserved among insects and has been studied in some detail in flies (Strausfeld, 1976; Hanesch et al., 1989), bees (Mobbs, 1985), beetles (Wegerhoff and Breidbach, 1992), and locusts (Williams, 1975; Homberg, 1991; Müller et al., 1997). The central body is tightly interconnected with the ventrally located lateral accessory lobes (LALs) whereas the PB is linked to the posterior optic tubercles near the dorso-posterior face of the brain (Williams, 1975; Homberg, 1991).

Most characteristic to the central complex is its regular, almost crystalline neuroarchitecture. From right to left, all neuropils except the noduli can be divided into 16 vertical columns. These columns are intersected by horizontal layers in the central body. Hereby, the CBU is comprised by three and the CBL by six layers (Homberg, 1991; Müller et al., 1997). Mirroring the central body, the noduli can also be divided into an upper and a lower division, of which the upper division can be further subdivided into three horizontal layers.

This regular matrix is produced by three principle classes of neurons: columnar cells, providing connections between individual columns of central-complex divisions, while projecting either to the LAL or the noduli; tangential cells, connecting complete layers of individual central-complex divisions with diverse regions of the protocerebrum; and pontine cells, which interconnect single CBU-columns on each side of the midline (Hanesch et al., 1989). Columnar neurons are present as isomorphic sets of 16 individual neurons per cell type, i.e. one cell per column (Williams, 1975). As these neurons provide precise interhemispheric connections between the different central-complex divisions, they produce two major chiasmata. The posterior chiasma is located between the CBU and the PB, whereas the anterior chiasma is located anteriorly of the CBL (Williams, 1975; Homberg, 1991). Immunocytochemical labeling of neuropeptides and neurotransmitters revealed numerous different types of columnar, tangential and pontine cells (for reviews see Homberg, 2002; Nässel and Homberg, 2006). In the desert locust, the CBL is particularly well characterized. Here, two different types of columnar cells, and five types of tangential cells have been identified through Golgi-staining and single-cell dye fills (Müller et al., 1997). For the complete central complex, however, an exhaustive attempt to identify all major individual neuron types has only been made in *Drosophila* (Hanesch et al., 1989).

The central complex – function

Despite the fact, that the gross anatomy of the central complex has been described for many decades, very little is known about the function of this brain region. Evidence has been collected largely along two lines. First, the central complex has been suggested to play a role in locomotor control. Structural central-complex mutants in *Drosophila* showed defects in walking speed and leg coordination, as well as in directional control of walking and flight, including abnormal optomotor responses (Bausenwein et al., 1986; Strauss and Heisenberg, 1993; Ilius et al., 1994; Strauss, 2002). In several mutant lines, motivation for locomotor behavior is reduced and the temporal structure of walking bouts is impaired (Strauss and Heisenberg, 1993; Martin et al., 1999). Moreover, lesions in the region of the cen-

tral complex in crickets (Huber, 1960a, Huber, 1960b) caused inhibition of walking and singing behavior, whereas lesions in the cockroach central complex affected turning behavior (Ridgel et al., 2007). The motivation for sound production could be also affected by pharmacological and electrical stimulation experiments in a grasshopper (Wenzel et al., 2005; Hoffmann et al., 2007).

The second line of evidence points towards a role in sensory processing and memory formation in regions of the central complex. Most prominently, intracellular recordings in locusts and crickets have revealed neurons responding strongly to dorsally presented polarized light (Vitzthum et al., 2002; Sakura et al., 2008). Units sensitive to antennal movements and visual stimuli have been found through extracellular recordings from the vicinity of the CBL in cockroaches (Ritzmann et al., 2008). Weak visual responses were also found with intracellular recordings in central-complex neurons of bees (Homberg, 1985). Additionally, some cell types in the locust elicited strong activity changes correlated with wing movement and mechanosensory wind stimuli (Homberg, 1994). In *Drosophila*, recent evidence suggests a role of the fanshaped body (equivalent to the CBU) in memory formation for specific visual features (Liu et al., 2006). The authors showed that memory deficient flies could be rescued by expressing the missing gene in one set of tangential neurons of the fan-shaped body, when tested in an aversive learning paradigm. Surprisingly, the rescue was only effective for a particular set of visual features and not for others (elevation versus edge orientation), dependent on the tested expression line. Additional evidence for memory of behavioral relevant visual features comes from *Drosophila* experiments, in which specific neurons of the ellipsoid body (CBL) were required for memory of a temporarily hidden landmark (Neuser et al., 2008). Altogether, these data suggest a role of the central complex in processing and storage of behavioral relevant sensory information, orientation behavior, and planning of motor command signals.

Scope of this work

As the polarization vision pathway in the locust brain ends in the central complex, and this region has been associated with functions in motor planning and higher order sensory processing, this brain region is likely to play a vital role in sky compass navigation. The major scope of this doctoral thesis was to examine this functional role. Towards this goal, I analyzed the anatomical composition of the locust central complex in sufficient detail to allow for inferences about principles of information flow within this region. This provided the context in which intracellular recordings of polarization-sensitive central-complex neurons could be interpreted. Based on anatomical and physiological properties of the recorded cell types, the role of the central complex in processing of polarized light and the outline of the neuronal network in which this role is achieved was characterized.

References

Bausenwein B, Wolf R, Heisenberg M (1986) Genetic dissection of optomotor behavior in *Drosophila melanogaster* Studies on wild-type and the mutant optomotor-blind. J Neurogen 3:87-109.

Boles LC, Lohmann KJ (2003) True navigation and magnetic maps in spiny lobsters. Nature 421:60-63.

Brunner D, Labhart T (1987) Behavioural evidence for polarization vision in crickets. Physiol Entomol 12:1-10.

Coemans MA, Vos HJJ, Nuboer JF (1994) The relation between celestial colour gradients and the position of the sun, with regard to the sun compass. Vision Res 34:1461-1470.

Collett TS (1992) Landmark learning and guidance in insects. Phil Trans R Soc London Ser B 337:295-303.

Collett TS, Collett M (2000) Path integration in insects. Curr Opin Neurobiol 10:757-762.

Collett TS, Collett M (2002) Memory use in insect visual navigation. Nat Rev Neurosci 3:542-552.

Coulson K (1988) Polarization and intensity of light in the atmosphere. Deepak, Hampton, VA.

Dacke M, Nilsson D, Scholtz CH, Byrne M, Warrant EJ (2003) Animal behaviour: insect orientation to polarized moonlight. Nature 424:433.

Durier V, Graham P, Collett TS (2003) Snapshot memories and landmark guidance in wood ants. Curr Biol 13:1614-1618.

Eggers A, Gewecke M (1993) The dorsal rim area of the compound eye and polarization vision in the desert locust (*Schistocerca gregaria*). In: Sensory systems of arthropods (Wiese K, Gribakin FG, Popov AV, Renninger G, eds), Birkhäuser, Basel, 101-109.

Frost BJ, Mouritsen H (2006) The neural mechanisms of long distance animal navigation. Curr Opin Neurobiol 16:481-488.

Hanesch U, Fischbach KF, Heisenberg M (1989) Neuronal architecture of the central complex in *Drosophila melanogaster*. Cell Tissue Res 257:343-366.

Helfrich-Forster C, Stengl M, Homberg U (1998) Organization of the circadian system in insects. Chronobiol Int 15:567-594.

Herzmann D, Labhart T (1989) Spectral sensitivity and absolute threshold of polarization vision in crickets: a behavioral study. J Comp Physiol A 165:315-319.

Hoffmann K, Wirmer A, Kunst M, Gocht D, Heinrich R (2007) Muscarinic excitation in grasshopper song control circuits is limited by acetylcholine-esterase activity. Zool Sci 24:1028-1035.

Homberg U (1985) Interneurons of the central complex in the bee brain *Apis mellifera*. J Insect Physiol 31:251-264.

Homberg U (1991) Neuroarchitecture of the central complex in the brain of the locust *Schistocerca gregaria* and *S. americana* as revealed by serotonin immunocytochemistry. J Comp Neurol 303:245-254.

Homberg U (1994) Flight-correlated activity changes in neurons of the lateral accessory lobes in the brain of the locust *Schistocerca gregaria*. J Comp Physiol A 175:597-610.

Homberg U (2002) Neurotransmitters and neuropeptides in the brain of the locust. Microsc Res Tech 56:189-209.

Homberg U, Hofer S, Pfeiffer K, Gebhardt S (2003) Organization and neural connections of the anterior optic tubercle in the brain of the locust, *Schistocerca gregaria*. J Comp Neurol 462:415-430.

Homberg U, Paech A (2002) Ultrastructure and orientation of ommatidia in the dorsal rim area of the locust compound eye. Arthropod Struct Dev 30:271-280.

Homberg U, Würden S (1997) Movement-sensitive, polarization-sensitive, and light-sensitive neurons of the medulla and accessory medulla of the locust, *Schistocerca gregaria*. J Comp Neurol 386:329-346.

Homberg U, Würden S, Dircksen H, Rao KR (1991) Comparative anatomy of pigment-dispersing hormone-immunoreactive neurons in the brain of orthopteroid insects. Cell Tissue Res 266:343-357.

Horváth G, Varjú D (2004) Polarized light in animal vision. Springer, Berlin.

Huber F (1960a) Untersuchungen über die Funktion des Zentralnervensystems und insbesondere des Gehirnes bei der Fortbewegung und der Lauterzeugung der Grillen. Z Vgl Physiol 44:60-132.

Huber F (1960b) Experimentelle Untersuchungen zur nervösen Atmungsregulation der Orthopteren (Saltatoria: Gryllidae). Z Vgl Physiol 43:359-391.

Ilius M, Wolf R, Heisenberg M (1994) The central complex of *Drosophila melanogaster* is involved in flight control: studies on mutants and mosaics of the gene ellipsoid body open. J Neurogen 9:189-206.

Kinoshita M, Pfeiffer K, Homberg U (2007) Spectral properties of identified polarized-light sensitive interneurons in the brain of the desert locust *Schistocerca gregaria*. J Exp Biol 210:1350-1361.

Labhart T (1988) Polarization-opponent interneurons in the insect visual system. Nature 331:435-437.

Labhart T, Meyer EP (1999) Detectors for polarized skylight in insects: a survey of ommatidial specializations in the dorsal rim area of the compound eye. Microsc Res Tech 47:368-379.

Liu G, Seiler H, Wen A, Zars T, Ito K, Wolf R, Heisenberg M, Liu L (2006) Distinct memory traces for two visual features in the *Drosophila* brain. Nature 439:551-556.

Mappes M, Homberg U (2004) Behavioral analysis of polarization vision in tethered flying locusts. J Comp Physiol A 190:61-68.

Martin JR, Raabe T, Heisenberg M (1999) Central complex substructures are required for the maintenance of locomotor activity in *Drosophila melanogaster*. J Comp Physiol A 185:277-288.

Menzel R, De Marco RJ, Greggers U (2006) Spatial memory, navigation and dance behaviour in *Apis mellifera*. J Comp Physiol A 192:889-903.

Menzel R, Greggers U, Smith A, Berger S, Brandt R, Brunke S, Bundrock G, Hulse S, Plumpe T, Schaupp F, Schuttler E, Stach S, Stindt J, Stollhoff N, Watzl S (2005) Honey bees navigate according to a map-like spatial memory. Proc Natl Acad Sci U S A 102:3040-3045.

Mobbs PG. 1985. Brain structure. Comprehensive insect physiology biochemistry and pharmacology. Vol.1,.

Müller M, Homberg U, Kuhn A (1997) Neuroarchitecture of the lower division of the central body in the brain of the locust (*Schistocerca gregaria*). Cell Tissue Res 288:159-176.

Nässel DR, Homberg U (2006) Neuropeptides in interneurons of the insect brain. Cell Tissue Res 326:1-24.

Neuser K, Triphan T, Mronz M, Poeck B, Strauss R (2008) Analysis of a spatial orientation memory in *Drosophila*. Nature 453:1244-1247.

Petri B, Stengl M, Wurden S, Homberg U (1995) Immunocytochemical characterization of the accessory medulla in the cockroach *Leucophaea maderae*. Cell Tissue Res 282:3-19.

Pfeiffer K, Homberg U (2007) Coding of azimuthal directions via time-compensated combination of celestial compass cues. Curr Biol 17:960-965.

Pfeiffer K, Kinoshita M, Homberg U (2005) Polarization-sensitive and light-sensitive neurons in two parallel pathways passing through the anterior optic tubercle in the locust brain. J Neurophysiol 94:3903-3915.

Reppert SM, Zhu H, White RH (2004) Polarized light helps monarch butterflies navigate. Curr Biol 14:155-158.

Ridgel AL, Alexander BE, Ritzmann RE (2007) Descending control of turning behavior in the cockroach, *Blaberus discoidalis*. J Comp Physiol A 193:385-402.

Ritzmann RE, Ridgel AL, Pollack AJ (2008) Multi-unit recording of antennal mechano-sensitive units in the central complex of the cockroach, *Blaberus discoidalis*. J Comp Physiol A 194:341-360.

Sakura M, Lambrinos D, Labhart T (2008) Polarized

skylight navigation in insects: model and electrophysiology of e-vector coding by neurons in the central complex. J Neurophysiol 99:667-682.

Santschi F (1923) Messor et autres fourmis paléarctiques. Rev Suisse Zool 30:317-336.

Schneider N, Stengl M (2005) Pigment-dispersing factor and GABA synchronize cells of the isolated circadian clock of the cockroach *Leucophaea maderae*. J Neurosci 25:5138-5147.

Strausfeld NJ (1976) Atlas of an insect brain. New York, Springer.

Strauss R (2002) The central complex and the genetic dissection of locomotor behaviour. Curr Opin Neurobiol 12:633-638.

Strauss R, Heisenberg M (1993) A higher control center of locomotor behavior in the *Drosophila* brain. J Neurosci 13:1852-1861.

Strutt JW (1871) On the light from the sky, its polarization and colour. Philos Mag 41:107-120.

Träger U, Wagner R, Bausenwein B, Homberg U (2008) A novel type of microglomerular synaptic complex in the polarization vision pathway of the locust brain. J Comp Neurol 506:288-300.

Ugolini A, Galanti G, Mercatelli L (2009) Difference in skylight intensity is a new celestial cue for sandhopper orientation (Amphipoda, Talitridae). Animal Behav 77:171-175

Vitzthum H, Müller M, Homberg U (2002) Neurons of the central complex of the locust *Schistocerca gregaria* are sensitive to polarized light. J Neurosci 22:1114-1125.

von Frisch K (1949) Die Polarisation des Himmelslichtes als orientierender Faktor bei den Tänzen der Bienen. Experientia 5:142-148.

Von Philipsborn A, Labhart T (1990) A behavioral study of polarization vision in the fly *Musca domestica*. J Comp Physiol A 167:737-743.

Wegerhoff R, Breidbach O (1992) Structure and development of the larval central complex in a holometabolous insect, the beetle *Tenebrio molitor*. Cell Tissue Res 268:341-358.

Wehner R (1984) Astronavigation in insects. Annu Rev Entomol 29:277-298.

Wehner R (2001) Polarization vision - a uniform sensory capacity? J Exp Biol 204:2589-2596.

Wehner R (2003) Desert ant navigation: how miniature brains solve complex tasks. J Comp Physiol A 189:579-588.

Wenzel B, Kunst M, Gunther C, Ganter GK, Lakes-Harlan R, Elsner N, Heinrich R (2005) Nitric oxide/cyclic guanosine monophosphate signaling in the central complex of the grasshopper brain inhibits singing behavior. J Comp Neurol 488:129-139.

Williams JLD (1975) Anatomical studies of the insect central nervous system: a ground-plan of the midbrain and an introduction to the central complex in the locust, *Schistocerca gregaria* (Orthoptera). J Zool (Lond) 176:67-86.

Neuroarchitecture of the Central Complex of the Desert Locust: Intrinsic and Columnar Neurons

THE JOURNAL OF COMPARATIVE NEUROLOGY 511:454–478 (2008)

Neuroarchitecture of the Central Complex of the Desert Locust: Intrinsic and Columnar Neurons

STANLEY HEINZE AND UWE HOMBERG*
Fachbereich Biologie, Tierphysiologie, Philipps-Universität Marburg,
D-35032 Marburg, Germany

ABSTRACT

The central complex is a group of neuropils in the center of the insect brain. It consists of four major subunits: the upper and lower divisions of the central body (CBU, CBL), the protocerebral bridge (PB), and the paired noduli. A distinctive feature of the central complex is a modular architecture characterized by rows of 16 columns, intersected in the central body by stacks of layers. Evidence from locusts suggests that the central complex plays a major role in sky compass orientation. To understand signal processing in this brain area further, we have analyzed the morphologies of columnar neurons of the central complex of the locust *Schistocerca gregaria*. Intracellular dye fills revealed 21 types of columnar neurons that connect columns of different subunits, three types of pontine neurons linking pairs of columns within the CBU, and one amacrine cell. Most neurons appeared to be part of isomorphic sets with cell type-specific heterolateral projection patterns. Evaluation of arborization areas and neuron polarity suggests that these neurons are either intrinsic to the central complex or provide output to the lateral accessory lobes (LALs) or anterior lip region. No direct connections were found between the CBU and CBL. Instead, neurons of either subdivision were connected with the PB, but projected to non-overlapping regions in the LALs and to different layers of the noduli. This study provides novel insights into the functional organization of the central complex, especially with respect to its likely role in right-left signal matching and decision making. J. Comp. Neurol. 511:454–478, 2008.

Indexing terms: neuroanatomy; insect brain; central body; protocerebral bridge; sky compass navigation; *Schistocerca gregaria*

The central complex is one of the most salient, but also least understood assemblies of neuropils in the insect brain. It is located in the center of the protocerebrum and draws attention by its strikingly regular array of fibers and an almost crystalline general appearance. The central complex consists of four distinct neuropils: the protocerebral bridge (PB), the upper division of the central body (CBU, also termed the fan-shaped body), the lower division of the central body (CBL, also termed the ellipsoid body), and the paired noduli. Although the different neuropils vary in relative size, this general layout is conserved among all pterygote insect species studied (reviewed by Strausfeld, 1976, 1999; Mobbs, 1985; Homberg, 1985, 2008).

Different lines of research have proposed a role of the central complex in sensory signal processing and in the control of various motor programs. Certain neurons with ramifications in the central complex of locusts (Vitzthum et al., 2002; Heinze and Homberg, 2007) and crickets (Sakura et al., 2008) strongly respond to dorsally presented polarized light, a feature of the blue sky, exploited by insects for spatial orientation and navigation. In desert locusts, *E*-vector tuning to polarized light is mapped topographically in the columns of the PB (Heinze and Homberg, 2007), suggesting a compass-like representation of azimuthal space. In the fly *Drosophila*, memory traces for visual object parameters like edge orientation were attributed to specific types of neuron with arboriza-

Grant sponsor: Deutsche Forschungsgemeinschaft; Grant numbers: HO 950/14-3 and 16-2.

*Correspondence to: Uwe Homberg, Fachbereich Biologie, Tierphysiologie, Universität Marburg, D-35032 Marburg, Germany.
E-mail: homberg@staff.uni-marburg.de

Received 30 April 2008; Revised 18 June 2008; Accepted 31 July 2008
DOI 10.1002/cne.21842
Published online in Wiley InterScience (www.interscience.wiley.com).

tions in the CBU and suggest a role of the central complex in object recognition or feature detection (Liu et al., 2006). Additional evidence for a role of the ellipsoid body in spatial working memory during locomotion was recently provided through behavioral orientation experiments in *Drosophila* (Neuser et al., 2008). The authors showed that flies required specific sets of ellipsoid-body neurons to remember the location of a temporarily invisible landmark. Extracellular recordings in cockroaches revealed units responding to mechanosensory stimulation of the antennae as well as to visual stimuli (Ritzmann et al., 2008). Finally, intracellular recordings from central-complex neurons in locusts showed changes in neural activity during stationary flight and suggest that these neurons receive flight-associated mechanosensory input (Homberg, 1994).

A second line of evidence points to a role of the central complex in the control of motor programs. Lesions of the central complex in crickets (Huber, 1960a,b) led to inhibition of walking and acoustic behavior, whereas lesions in cockroaches caused deficits in turning behavior (Ridgel et al., 2007). Electrical and pharmacological stimulation in grasshoppers affected sound production (Wenzel et al., 2005; Hoffmann et al., 2007). Structural central-complex mutants in *Drosophila* showed defects in walking speed, leg coordination, and directional control of walking and flight, including abnormal optomotor responses (Bausenwein et al., 1986; Strauss and Heisenberg, 1993; Ilius et al., 1994; Strauss, 2002). In several of the mutant lines, motivation for locomotor behavior is reduced and the temporal structure of walking bouts is impaired (Strauss and Heisenberg, 1993; Martin et al., 1999). Taken together, these studies point to a key role of the central complex in spatial orientation, motor planning, and goal-directed behaviors.

Further progress in understanding the functional role of the central complex is impeded by lack of anatomical data on its internal organization, its cellular elements, and their connections within the central complex and to surrounding brain areas. In all examined species, including flies (Power, 1943; Strausfeld, 1976; Hanesch et al., 1989), bees (Mobbs, 1985), beetles (Wegerhoff and Breidbach, 1992), and locusts (Williams, 1975; Müller et al., 1997), the central body and the PB consist of rows of 8 or 16 vertical columns, whereas the CBL and CBU, in addition, contain stacks of several horizontal layers.

Details of the neuronal composition of the central complex and the layering of the central body have been revealed by Golgi studies (flies: Strausfeld, 1976; Hanesch et al., 1989; locusts: Müller et al., 1997), single-cell dye injections (bees: Homberg, 1985; locusts: Homberg, 1994; Müller et al., 1997; Vitzthum et al., 2002; Heinze and Homberg, 2007; crickets: Schildberger, 1983; Sakura et al., 2008) and by immunostaining for neuropeptides and transmitters (reviewed by Nässel, 1993; Homberg, 2002; Nässel and Homberg, 2006). These studies showed that three principle classes of neurons constitute the regular neuroarchitecture of the central complex:

1. *Columnar neurons* connect single columns of the PB and/or the central body with the lateral accessory lobes (LAL) or the noduli and occur as isomorphic sets of 16 cells. Columnar neurons provide precise interhemispheric connections and cross the midline in anterior or posterior chiasmata (Williams, 1975; Hanesch et al., 1989). In flies and locusts, their fiber trajectories between the PB and central body are arranged in four characteristic fiber fascicles termed w-, x-, y-, and z-bundles (Williams, 1975; Strausfeld, 1976; Hanesch et al., 1989; Williams and Boyan, 2008).
2. *Tangential neurons* innervate single layers of the CBU, CBL, or PB and provide connections with diverse brain areas (e.g., Strausfeld, 1976; Homberg, 1991; Müller et al., 1997).
3. *Pontine neurons* are intrinsic elements that connect specific columns and layers within the central body (Homberg, 1985; Hanesch et al., 1989).

A comprehensive catalogue of neuronal cell types has so far only been presented for the central complex of *Drosophila* (Hanesch et al., 1989). That study, however, provided little information on connectivity principles in the central-complex network, which requires detailed analysis of the arborization domains of the different cell types in order to identify candidate partners for synaptic connections.

Building upon an earlier anatomical study on the neuronal cell types of the CBL (Müller et al., 1997) we have used Golgi preparations, single-cell dye injections combined with fluorescent neuropil labeling, and digital three-dimensional reconstructions to analyze the arborization patterns of columnar and pontine neurons of the central complex of the locust *Schistocerca gregaria*. This study contributes to the establishment of connectivity patterns and principles of information flow within the central complex, which is essential for a further understanding of the neuronal operations performed by this brain area.

Abbreviations

a	anterior	LT	lateral triangle
aCh	anterior chiasma	med	medial
aL	anterior lip	mL	medial lobe
AU	amacrine neuron of the CBU	MO	median olive
CBL	central body lower division	No	noduli
CBU	central body upper division	NoL	noduli lower division
CL	columnar neuron of the CBL	NoU	noduli upper division
CP	columnar neuron of the PB	p	posterior
CPU	columnar neuron of the PB and CBU	PB	protocerebral bridge
CU	columnar neuron of the CBU	pCh	posterior chiasma
d	dorsal	pG	posterior groove
dS	dorsal shell of the LAL	PoU	pontine neuron of the CBU
IT	isthmus tract	v	ventral
LAL	lateral accessory lobe	vG	ventral groove
lat	lateral	vS	ventral shell of the LAL

MATERIALS AND METHODS

Animal preparation and dye injection

Desert locusts (*Schistocerca gregaria*) were raised in crowded colonies at the Philipps-University of Marburg (28°C, 12L:12D photoperiod). Experiments were performed on adult males and females 1–2 weeks after adult ecdysis. Animals were cold-anesthetized and prepared for electrophysiological recordings as described by Heinze and Homberg (2007). Neurons of the central complex were iontophoretically injected with 4% Neurobiotin (Vector, Burlingame, CA) or with 5% Lucifer Yellow (Sigma, Deisenhofen, Germany) through sharp glass microelectrodes (resistance: 40–150 MΩ). Depolarizing (Neurobiotin) or hyperpolarizing (Lucifer Yellow) current of 1–3 nA was continuously injected for 1–5 minutes. After injection the brain was dissected out of the animal, cleaned from fat and tracheae, and fixed overnight at 4°C in 4% paraformaldehyde in 0.1 M phosphate buffer, pH 7.4 (Lucifer preparations) or in a fixative containing 4% paraformaldehyde, 0.25% glutaraldehyde, 2% saturated picric acid in 0.1 M phosphate buffer (Neurobiotin preparations).

Histology

Fluorescent wholemount preparations. After fixation, Neurobiotin-injected brains were rinsed in 0.1 M phosphate-buffered saline (PBS, 4 × 15 minutes) and incubated with streptavidin-Cy3 conjugate (Dianova, Hamburg, Germany, 1:1,000) for 3 days at 4°C. After rinsing in PBS/0.3% Triton X-100 (PBT) for 2 × 30 minutes, followed by rinses in PBS (3 × 30 minutes) brains were dehydrated in an increasing ethanol series (25%, 50%, 70%, 90%, 95%, and 100%, 15 minutes each), and were transferred to a mixture of methyl salicylate and ethanol (1:1; 15 minutes). After the ethanol was allowed to evaporate, brains were cleared in methyl salicylate for 35 minutes. Finally, the brains were mounted in Permount (Fisher Scientific, Pittsburgh, PA) between two glass cover slides separated by spacing rings to avoid compression.

Wholemounts were scanned with a confocal laser microscope (Leica TCS SP2) equipped with a 10× objective (HC PL APO 10×/0.4 Imm Corr CS; Leica, Bensheim, Germany) to determine the type of stained neuron and its location within the brain. This information was later used for cutting sections, adjusted in thickness to image the stained neuron at higher magnification from one or two of these sections (see below).

Individual preparations were selected for further processing. Mounted brains were incubated in xylene (2–4 hours) to remove the embedding medium. They were rehydrated in a decreasing ethanol series (100–25%, 15 minutes each). After rinsing with PBS they were treated like freshly fixed brains and were processed for peroxidase staining or immunofluorescence.

Peroxidase staining. Peroxidase staining was performed on freshly injected and fixed brains or on rehydrated preparations. Brains were embedded in albumin-gelatin (4.8% gelatin and 12% ovalbumin in demineralized water) and were fixed with 8% formaldehyde in 0.1 M phosphate buffer overnight at 4°C. They were sectioned with a vibrating-blade microtome (VT 1000S; Leica, Wetzlar, Germany) in the frontal plane at 40-μm section thickness, and were subsequently rinsed in 0.1 M phosphate buffer (3 × 15 minutes). Lucifer Yellow-injected brains were treated with an anti-Lucifer Yellow antiserum, raised in rabbit against Lucifer Yellow (Molecular Probes, Eugene, OR), with goat anti-rabbit antiserum and, finally, with a peroxidase antiperoxidase conjugate (Dakopatts, Hamburg, Germany) as described by Homberg and Würden (1997). Specificity of the primary antibody is demonstrated by the fact that only injected neurons showed immunolabeling. Sections of Neurobiotin-injected brains were incubated with streptavidin conjugated to horseradish peroxidase (Amersham Buchler, Braunschweig, Germany) overnight at room temperature (1:200, in PBT). After rinsing in PBS, sections were transferred to 0.05 M Tris-HCl buffer, pH 7.4. The sections were subsequently stained by incubation in 3,3′-diaminobenzidine tetrahydrochloride (0.3 mg/ml) with 0.3% nickel ammonium sulfate in 0.05 M Tris-HCl. The reaction was started by adding 0.015% H_2O_2 and was stopped by rinsing with 0.05 M Tris-HCl after staining intensity had reached a satisfactory level. Sections were mounted on chrome alum/gelatin-coated glass slides, dehydrated in ethanol, cleared in xylene, and embedded in Entellan (Merck, Darmstadt, Germany).

Immunofluorescence. Selected rehydrated preparations were used for immunofluorescent colabeling with antibodies against synapsin and serotonin. The anti-synapsin antibody (SYNORF1, kindly supplied by E. Buchner, Würzburg, Germany) was a monoclonal antibody raised in mouse against fusion proteins consisting of glutathione-S-transferase and the *Drosophila* SYN1 protein (Klagges et al., 1996). The specificity of the antibody has been characterized by Klagges et al. (1996). It labels synaptic neuropil as demonstrated in *Drosophila* (Klagges et al., 1996), honeybees (Brandt et al., 2005), and locusts (Leitinger et al., 2004; Kurylas et al., 2008). The anti-serotonin antiserum (Diasorin, Dietzenbach, Germany) was raised in rabbit against paraformaldehyde-coupled conjugates of bovine serum albumin and 5-hydroxytryptamine. In the locust central complex, the staining pattern obtained with this antiserum was indistinguishable from that of the anti-serotonin immunostaining reported by Homberg (1991). For the latter, liquid-phase preadsorption of the diluted antiserum with 10 mM serotonin creatinine sulfate or 20 μM of the putative antigen 6-hydroxy-tetrahydro-β-carboline (Schipper and Tilders, 1983) abolished all immunostaining (Homberg, 1991).

For double and triple fluorescent staining, brains were embedded in albumin-gelatin and fixed overnight in 8% formaldehyde (in PBS). Judged from imaging of the preparations as wholemounts, one or two thick (140-μm) frontal sections were cut with the vibrating-blade microtome, which ideally contained the complete neuron. Sections were rinsed in PBS (4 × 15 minutes) and were preincubated with 5% normal goat serum (NGS; in PBT, 5 hours). Primary antibodies were applied together with streptavidin-Cy3 (1:1,000) for 5 days at 4°C (anti-synapsin 1:50, anti-serotonin 1:20,000 in PBT with 1% NGS). After rinsing (6 × 20 minutes in PBT), the secondary antibodies goat anti-mouse-Cy5 and goat anti-rabbit-Cy2 (Dianova, Hamburg, Germany; 1:300, in PBT with 1% NGS) were applied together with streptavidin-Cy3. The sections were rinsed in PBT (6 × 20 minutes), dehydrated in an increasing ethanol series, transferred to methyl salicylate/ethanol (1:1; 5 minutes), and cleared for 20 minutes in methyl salicylate. The sections were embedded in Permount between two coverslips by using spacers to avoid compression.

Bodian staining. General neuropil staining was achieved with Bodian's silver-proteinate technique (Greg-

The Journal of Comparative Neurology

ory, 1980). Dissected brains were fixed in a mixture of 10% formalin, 5% glacial acetic acid, and 85% ethanol (3–4 hours), dehydrated, and embedded in Paraplast Plus (Sigma). After the brains were sectioned at a thickness of 10 μm, they were stained according to the Bodian-protargol procedure (Gregory, 1980). Briefly, the deparaffinized sections were incubated in 2% aqueous Argent Proteinate solution (Prolabo, Paris, France) for 16–20 hours at 60°C. The solution contained 7.5 g copper mesh/250 ml solution. Reduction, gold toning, and differentiation were performed as described (Gregory, 1980). Sections were finally dehydrated and mounted in Entellan.

Golgi impregnations. A combination of the Golgi-Colonnier method (Colonnier, 1964) and Golgi-rapid method (Strausfeld, 1980) was used according to Müller et al. (1997). Locust brains were dissected out of the head capsule in an aqueous solution of 2.5% potassium dichromate and 1.3% sucrose (PDS). After 5 days of incubation with 4 parts PDS/1 part 0.25% glutaraldehyde at 4°C, brains were washed several times with PDS, and incubated at 4°C with 9 parts PDS/1 part 1% osmium tetroxide for 5 days. After rinsing, brains were immersed in an aqueous solution of 0.75% silver nitrate (24 hours, 4°C), and finally rinsed in distilled water, dehydrated, and embedded in Epon (Serva, Heidelberg, Germany). Sections were cut at a thickness of 30 μm with a sliding microtome (Reichert-Jung, Wien, Austria) and were finally coverslipped in Epon.

Data evaluation

Peroxidase staining and Golgi impregnation. Dye-injected/peroxidase-labeled neurons and Golgi-impregnated cells were reconstructed with a camera-lucida attachment to a Leitz compound microscope equipped with a 40× objective. Drawings were scanned, and contrast was optimized with Adobe Photoshop CS2 software (Adobe Systems, San Jose, CA). Drawings of neuropil outlines from the individual preparations were used to produce an adequate projection onto a three-dimensional reconstruction of the central complex.

Fluorescent preparations. Neurons labeled with streptavidin-Cy3 were scanned with a confocal microscope (Leica TCS SP2) by using a 40× objective (HCX PL Apo 40×/1.25 Oil) and a z-resolution of 0.5 μm. The three channels (Cy2, Cy3, and Cy5) were sequentially scanned in a frame-by-frame manner, at excitation wavelengths of 488, 543, and 633 nm, respectively. For each neuron several image stacks had to be scanned from different sides and regions of the same section owing to the limited focal distance and area covered by the objective. Image stacks were merged to a single file with Amira 4.1.2 (Visage Imaging, Berlin, Germany). Visualization of neurons was achieved by maximal projections of confocal data, by presentation of single optical slices, or by a threshold-based volume-rendering algorithm in Amira 4.1.2. Maximal projection views and single optical slices were optimized for brightness and contrast with Adobe Photoshop. In some cases, maximal projections of confocal data were merged into a single file covering the whole neuron. Color inversion and removal of background were used to create a camera-lucida-like presentation.

Neuropil reconstructions. Reconstructions of neuropils from fluorescent preparations were achieved through manual segmentation in Amira 4.1.2 and were based on anti-synapsin labeling or on a combination of anti-synapsin and anti-serotonin labeling (in the case of CBU subcompartments). Confocal scans with a 20× objective were sufficient for reconstructions of all neuropils except the noduli subcompartments (scanned with a 40× objective). In this way multiple sections of the neuropil of interest were labeled in the x-, y-, and z-planes. This scaffold was then used as a reference to create a label field containing the whole neuropil volume. Due to the limited processing power of available computers, data had to be downsampled to a voxel size of 1 μm^3 in some cases. The label field obtained was used afterwards to create a smooth, volumetric surface, which could be visualized simultaneously with the neuron data. The nomenclature of central-complex subdivisions follows Williams (1972) and Homberg (1991). Orientations are indicated with respect to the body axis.

RESULTS

Organization of the locust central complex

The gross organization of the locust central complex was analyzed through anti-synapsin immunostaining combined with anti-serotonin immunolabeling. Four major neuropils were identified as parts of the central complex: the protocerebral bridge (PB), the upper division of the central body (CBU), the lower division of the central body (CBL), and the paired noduli (Fig. 1). Two adjacent structures, the paired lateral accessory lobes (LALs) and the anterior lip, are closely attached to the central complex frontally (anterior lip; Fig. 1F–I) and laterally (LALs; Fig. 2C–F).

The CBU is an arched neuropil between the anterior lip and the dorsoposterior PB (Fig. 1A–C). It is subdivided into three layers (Fig. 1), termed I, II, and III, from anterior to posterior (Homberg, 1991). Based on distinct serotonin immunostaining, Homberg (1991) introduced further subdivisions of CBU layers I and II into dorsal sublayers Ia and IIa and ventral sublayers Ib and IIb, which provide a useful coordinate system for locating individual areas in the CBU. Anti-synapsin staining differentiates between layer I and the combined layers II and III, which were difficult to distinguish in most preparations (Fig. 1B). Layer I covers the anterior side of the CBU and wraps spherically around the lateral and dorsal sides of the underlying layer II. Layer II extends laterally, dorsally, and ventrally around layer III and provides most of the ventral face of the CBU. Its posterior-ventral side faces the fiber complex of the posterior groove (Fig. 1C,H). Layer III is the smallest and most posterior layer of the upper division. It has an elongated, bean-like shape and shows intense serotonin immunostaining (Fig. 1B,C). The CBU is further compartmentalized into vertical columnar domains. This compartmentation is mainly caused by regularly spaced fiber bundles, most prominently the posterior vertical fiber bundles in layers II and III (Figs. 1B, 2B) and the anterior vertical bundles at the boundary of layer I and II, which all lack anti-synapsin labeling.

The CBL lies anteriorly to the posterior groove and ventrally from layer II of the upper division. It has a compact, bean-shaped structure and a stratified appearance with anti-synapsin staining (Fig. 1B). The arrangement of six layers in the CBL has been described by Müller et al. (1997).

The paired noduli are separated from the CBU by the posterior groove, which is free of anti-synapsin labeling

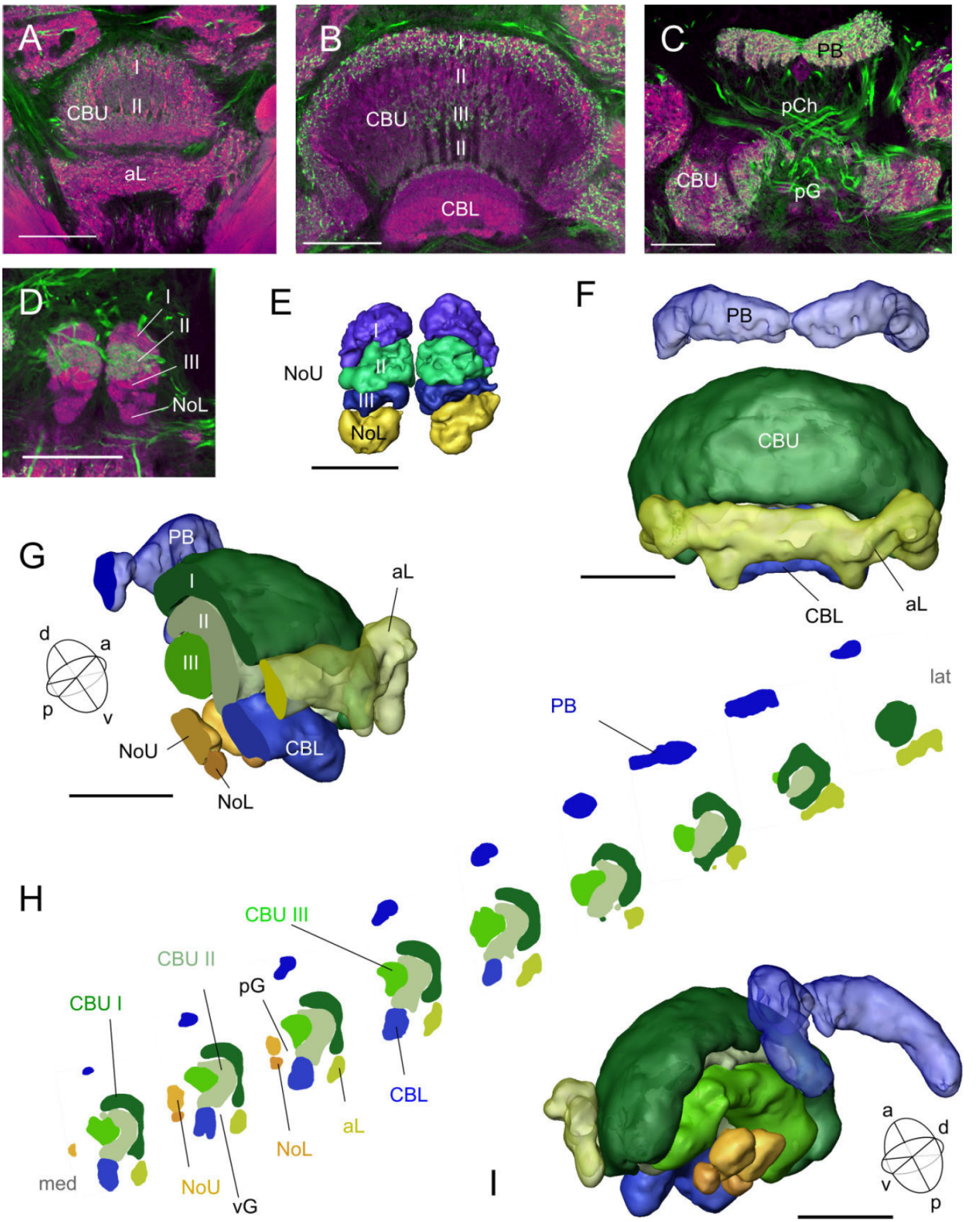

Fig. 1. Organization of the central complex and anterior lip neuropil of the desert locust. **A–C:** Single optical sections (frontal plane, thickness 1 μm) from confocal image stacks showing anti-synapsin staining (magenta) and anti-serotonin staining (green) at different levels through the central complex (A, most anterior). Three layers labeled I–III can be distinguished in the upper division of the central body (CBU). **D:** Frontal section through the noduli (single optical section) showing synapsin- (magenta) and serotonin immunostaining (green). Numbers indicate layers I–III of the upper unit of the noduli. **E:** Three-dimensional reconstruction of the noduli. **F:** Three-dimensional reconstruction of the central complex and anterior lip neuropil, frontal view. **G:** Oblique view (anterior-ventral) of the central complex. A sagittal cut reveals the layered organization of the CBU. **H:** Series of sagittal sections from medial to lateral through the central complex/anterior lip, obtained from the three-dimensional reconstruction in F, G, and I. **I:** Oblique view (posterior-dorsal) of the central complex emphasizing the shape of the protocerebral bridge. For abbreviations, see list. Scale bar = 100 μm in A–D,F,G,I; 50 μm in E.

The Journal of Comparative Neurology

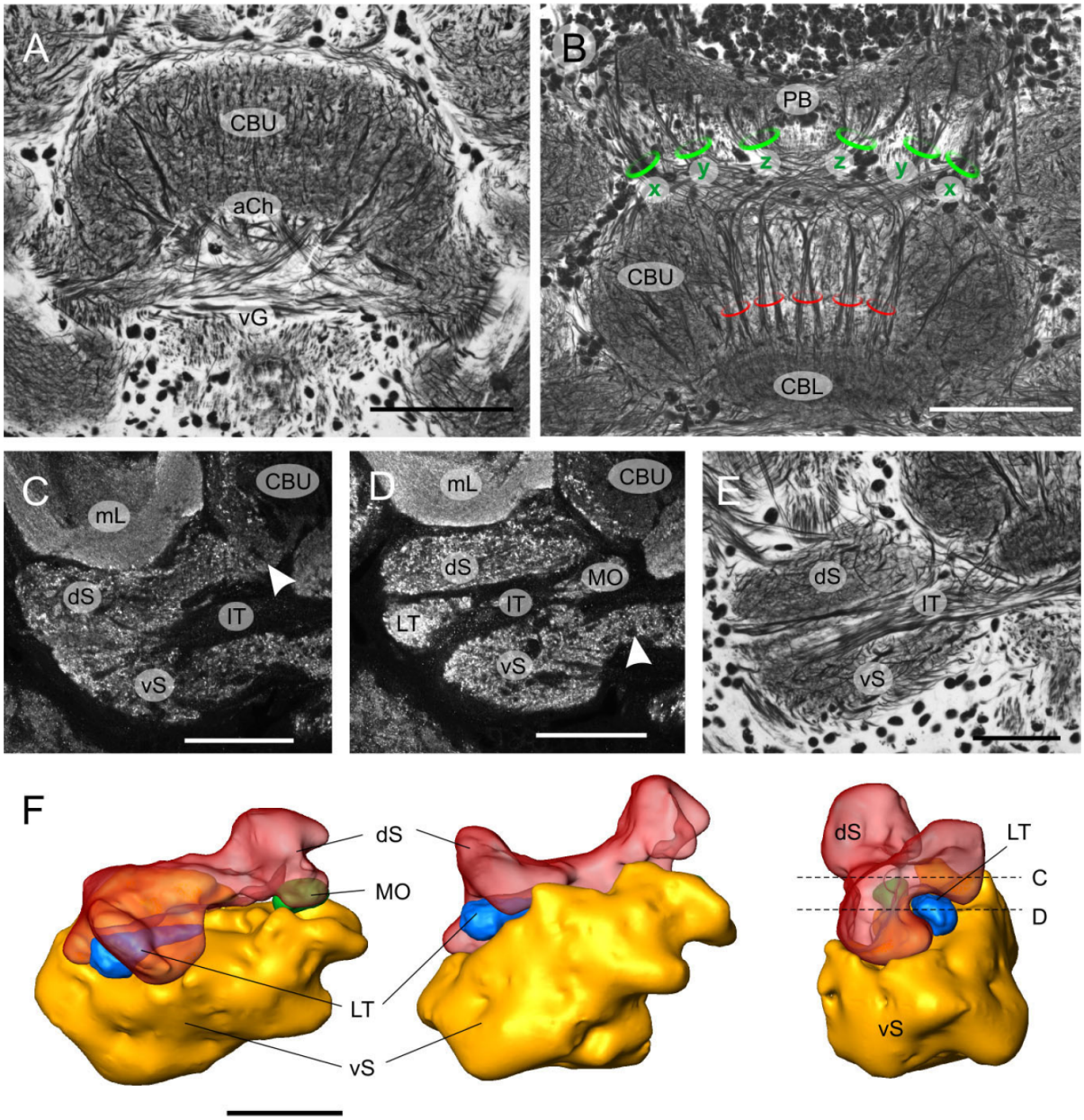

Fig. 2. Organization of the central complex and lateral accessory lobe. **A:** Bodian-stained frontal section (10 μm) showing the anterior chiasma and the ventral groove of the central body. **B:** Superposition image from five Bodian-stained frontal sections of posterior parts of the central complex. The posterior vertical bundles (red circles) and the x-, y-, and z-bundles connecting the PB with the central body (green circles) are highlighted. **C,D:** Single optical sections (frontal plane, thickness 1 μm) from a synapsin-labeled preparation, showing the neuropil compartmentation of the lateral accessory lobe (LAL) at two levels (as indicated in F). Arrowheads point to neuropil isthmi connecting the LAL with layer I of the upper division of the central body (C), and with the median accessory lobe (D). **E:** Bodian-stained frontal section (10 μm) showing the isthmus tract (IT) connecting the LAL with the central body. **F:** Three-dimensional reconstruction of the subunits of the LAL based on synapsin labeling. From left to right: frontal view, ventral view, lateral view. Dashed lines in the lateral view indicate planes of sections shown in C and D. For abbreviations, see list. Scale bar = 100 μm in A–F.

(Fig. 1C). They lie on either side of the midline, just posteriorly from layer III. The noduli are subdivided into upper and lower units, with the upper units being further divided into three layers (I to III, dorsal to ventral). All divisions can be clearly seen with anti-synapsin staining and are even more pronounced with anti-serotonin double

The Journal of Comparative Neurology

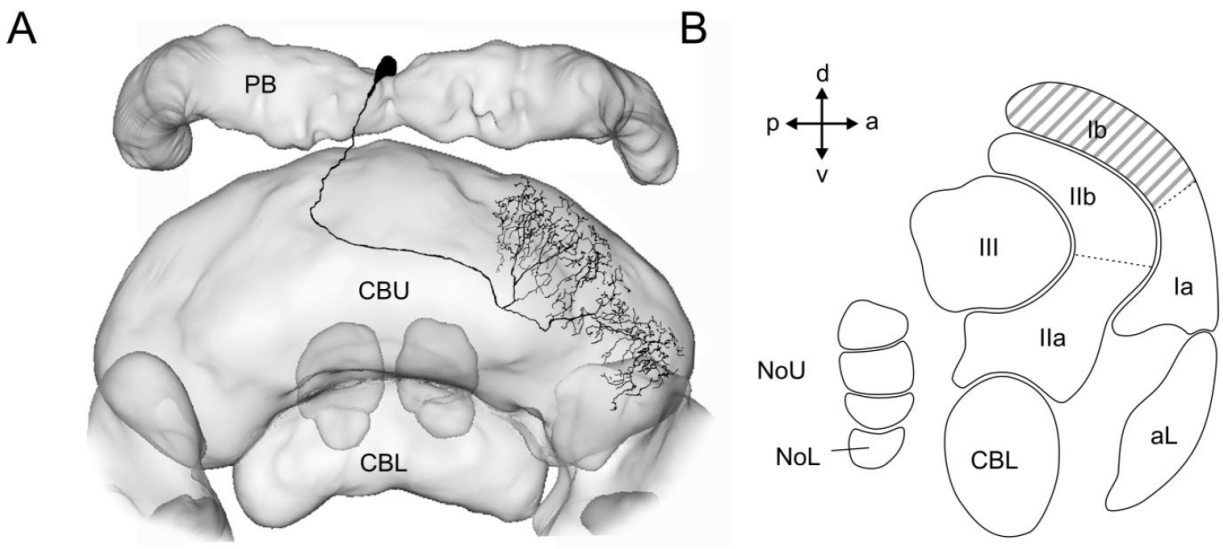

Fig. 3. Morphology of an amacrine neuron of the upper division of the central body. **A:** Camera lucida reconstruction of a Neurobiotin-injected amacrine neuron, projected onto a three-dimensional reconstruction of the central complex. **B:** Schematic sagittal view of the central complex. Hatched area indicates the location of terminal arborizations of the neuron in A. For abbreviations, see list.

labeling, as serotonin immunostaining is confined to layer II of the upper units of the noduli (Fig. 1D,E).

The PB lies dorsally and posteriorly from the CBU and is surrounded dorsoposteriorly by cell bodies of the pars intercerebralis (Figs. 1F–H, 2B). Its anterior face occupies the same frontal plane as the posterior face of the CBU. The PB has a sausage-like shape with ends bent posterioventrally (Fig. 1I). Fibers of tangential neurons connect both PB hemispheres and lead to its continuous appearance across the brain midline. The PB, the central body, and the noduli are connected with each other and with the LALs through regular right-left fiber trajectories crossing the brain midline. These occur in the posterior chiasma between the PB and the central body (Fig. 1C), in the anterior chiasma of the ventral groove fiber complex between the central body and the LALs (Fig. 2A), and in the posterior groove between the CBL and the noduli (Fig. 1C). Four characteristic fiber tracts, the w-, x-, y-, and z-bundles (from lateral to median) connect the PB with the central body in each hemisphere. The x-, y-, and z- bundles are located at the same frontal level as the horizontal part of the PB (Fig. 2B), whereas the w-bundles leave the PB near its lateral ends. Useful landmarks for identification of the different bundles are the inner antenno-cerebral tracts, which vertically intersect between the x- and y-bundles, and the median ocellar nerve root, which is located between the two z-bundles (Williams, 1975).

Fiber connections between the central body and the LALs consist of several fascicles in a bundle of fibers collectively termed the isthmus tract. The isthmus tract is free of anti-synapsin immunostaining and is accompanied by an isthmus of neuropil between the CBU and the LAL (Fig. 2C–E). The LALs themselves are subdivided into four compartments, the dorsal shell, the ventral shell, the medial olive, and the lateral triangle (Fig. 2C–F). A second structure closely connected with the central complex is the anterior lip (Fig. 1). This elongated neuropil spans the brain midline dorsal to the medial lobes of the mushroom bodies. Anti-synapsin staining shows no subcompartments of the anterior lip. At its lateral edges the anterior lip merges into neuropil connecting the LALs with anterior regions of the CBU. A ventral groove of fibers, which lack synapsin immunostaining, separates the anterior lip from the CBU and CBL (Figs. 1H, 2A).

Intrinsic neurons of the central body

Amacrine neuron. An anaxonal, amacrine neuron was encountered only once (Fig. 3). Its soma is located in the anterior pars intercerebralis, just anteriorly from the PB. A thin primary neurite enters the CBU posteriorly via the ipsilateral z-bundle. It follows the anterior boundary of CBU-layer III across the midline and gives rise to four main branches that penetrate layer II in a fan-like arrangement. Fine processes with mixed endings terminate in layer I but are restricted to dorsal areas (layer Ib). They cover the width of the lateral half of one CBU hemisphere, i.e., about four columns. No subcompartments of the arborization tree were observed.

Pontine neurons. Pontine neurons connect pairs of columns across the brain midline. They were only found in the CBU. The two domains of arborization are in the same layer or in different layers and have a constant columnar distance of roughly eight columns. The arborization domains do not strictly follow columnar boundaries. The arborization trees are generally centered on a single column and extend laterally to both sides, covering a total area of two to three columns. In most cases, the distal arborization tree appeared to be slightly broader. Assuming a total number of 16 neurons per cell type (or multiples thereof), all pontine neurons follow the same interhemispheric connectivity scheme (Fig. 4F), whereas some variations between cell types are present with regard to the

The Journal of Comparative Neurology

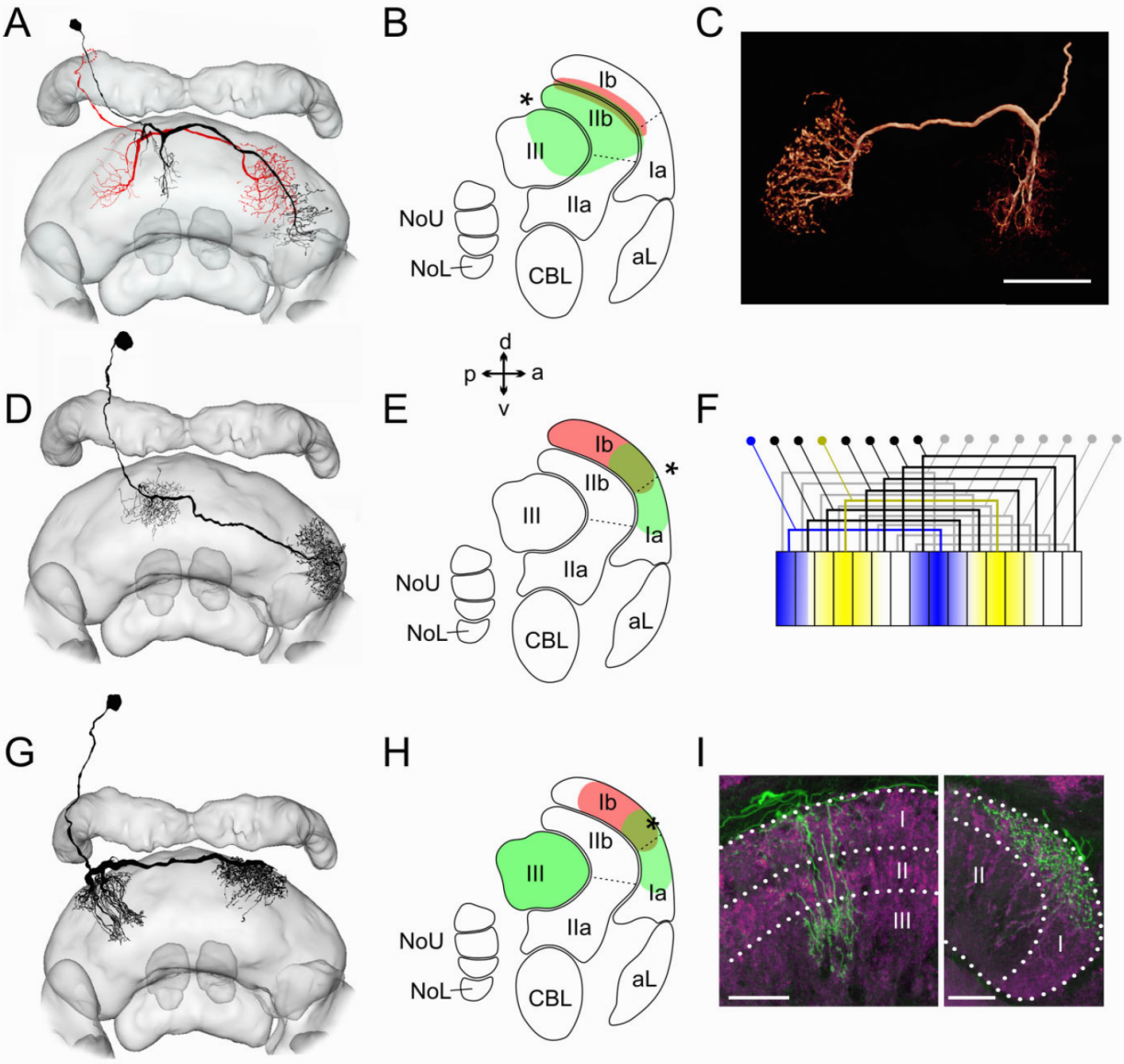

Fig. 4. Morphology of pontine neurons of the upper division of the central body. **A,D,G:** Camera lucida reconstructions of PoU1- (A), PoU2- (D), and PoU3-type (G) pontine neurons projected onto a three-dimensional reconstruction of the central complex. **B,E,H:** Sagittal diagrams of the central body indicating the layers innervated by the different types of pontine neuron (B: PoU1, E: PoU2, H: PoU3). Potentially postsynaptic (fine) arborizations are shown in green and potentially presynaptic (varicose) endings in red. Asterisks indicate sites of the midline-crossing neurites. **C:** Frontal view of a three-dimensional reconstruction (volume rendering) from a confocal image stack of a Neurobiotin-injected PoU1 neuron. Ipsi- and contralateral arborizations have strikingly different terminal fiber specializations. **F:** Proposed connectivity scheme of pontine neurons assuming one neuron per column. Two individual neurons are highlighted in yellow and blue. **I:** Details of arborization trees of a PoU3 neuron (green) with synapsin-labeling (magenta); single optical sections (frontal plane) of the ipsilateral (left) and contralateral projections (right). Numbers indicate CBU layers. For abbreviations, see list. Scale bar = 50 μm in C; 40 μm in I.

lateral extension of arborizations. Terminals of smooth appearance are in the ipsilateral hemisphere and mostly varicose endings on the contralateral side. Somata are located in the anterior pars intercerebralis with the primary neurite passing the PB anteriorly (Fig. 4D) or laterally (Fig. 4G). Three types of pontine neuron could be distinguished with regard to the invaded layers and the course of the main midline-crossing neurite.

PoU1 neurons were encountered most frequently (n = 11) and were examined in most detail (Fig. 4A–C). They form a system of isomorphic cells regularly spaced over the 16 CBU columns, as revealed by citrulline immuno-

staining (Theresa Siegl, unpublished data) and NADPH-diaphorase staining (Kurylas et al., 2005). Midline-crossing of axonal fibers occurs in the posterior chiasma. Ipsilaterally, one or two main branches give rise to numerous fine arborizations extending anteroventrally. Within their lateral range they invade layer III (except the posteriormost areas) and cover most of layer IIb (Fig. 4B). Very fine branches also extend into layer Ib, but are concentrated at the boundary between layer Ib and IIb. Contralateral arborizations are varicose (Fig. 4C). The main neurite typically makes a curve ventrally into layer III. From here side branches extend upward to terminals that are strictly concentrated along the boundary between layers Ib and IIb, but do not extend to the surface of layer I, as demonstrated through serotonin double-immunostaining (not shown).

In contrast to PoU1 neurons, the midline crossing neurites of PoU2 pontine cells (n = 6) run along the anterior and dorsal face of the CBU, and all terminals are restricted to layer I (Fig. 4D,E). Laterally, the arborizations extend to two to three columns as in PoU1 cells. Contralateral endings are very dense and have a heavily beaded appearance, whereas ipsilateral endings are fine and mostly faintly stained. Owing to the lack of three-dimensional data and the limited number of impaled cells, the exact location of terminals within layer I could not be examined thoroughly. A double staining with a PoU1 cell did not reveal a clear overlap in projection areas, and thus PoU2 pontine cells seem to arborize in more anteroventral parts of layer I. PoU2 neurons likely correspond to the second set of pontine cells labeled through NADPH-diaphorase staining by Kurylas et al. (2005) and are possibly a subset of 48 crustacean cardioactive peptide (CCAP)-immunoreactive pontine neurons reported by Dircksen and Homberg (1995).

Five neurons of a third type of pontine cell were impaled and termed PoU3 neurons (Fig. 4G–I). Their main neurites cross the midline along the anterior-dorsal face of the upper division, like PoU2 neurons, but the invaded CBU layers clearly differ. Fine endings are concentrated in layer Ib. From here, thin branches protrude through layer II and give rise to a second set of terminals in layer III. On the contralateral side, strongly varicose endings are present in layer Ib. In some preparations, these endings are considerably wider than in the other pontine cell types and cover a range of up to four columns (Fig. 4I).

Columnar neurons of the CBU

Fifteen distinct types of columnar neuron with arborizations in the CBU were encountered. They were classified into four groups, according to their projection areas outside the CBU. All cells had cell bodies in the pars intercerebralis and connected distinct columns of the CBU with one or two of the adjacent neuropils (PB, LAL, noduli, anterior lip), but none of the cell types had ramifications in the CBL.

PB-CBU-LAL connections. Three types of neuron, CPU1a, CPU1b, and CPU2, were filled most frequently, which was likely due to their large fiber diameters. All of these cell types have somata in the anterior pars intercerebralis and connect the PB and CBU to the LAL. Their primary neurites pass the PB anteriorly and give rise to smooth arborizations in single columns of the PB and in restricted areas of the CBU (Figs. 5, 6). Axonal projections with large varicose arborizations are confined to the ventral shell of the LAL (Figs. 5C,E,F, 6B,C). This pronounced polarity was obvious in all cells filled.

Three subtypes of CPU1 neurons were distinguished that collectively correspond to CC III neurons of Williams (1972). CPU1a neurons (n = 19) connect single columns of the ipsilateral hemisphere of the PB with the contralateral LAL (Fig. 5A,B). The main neurite leaves the PB on the anterior side, runs through the posterior chiasma, and enters the CBU dorsally. Three-dimensional reconstructions combined with serotonin immunostaining revealed large arborization trees with smooth terminals that extend through all layers of the CBU. The density and number of fiber processes is not evenly distributed, but declines ventrally, and only a few terminals extend to the ventral part of layer II and to layer III. The width of the CBU arborizations comprises about two columns. The position of innervated CBU columns is correlated with the position of the innervated PB column and follows the connectivity scheme presented in Figure 5B. Unfortunately, we were not able to fill in CPU1a neurons in the two lateralmost columns of the PB. Therefore, the connectivities of CPU1a neurons of these columns—if they exist—are hypothetical, in particular, the ipsilateral projections of the CBU1a neurons of the lateralmost columns. The exact position of midline crossing depends on the innervated columns and occurs in the anterior chiasma for cells innervating ipsilateral CBU columns and in the posterior chiasma for contralateral columns. In most preparations, the main neurite runs along the anterior face of the CBU, penetrates the anterior face between layer Ia and the anterior lip, and enters the ventral groove. In five neurons and independently from the innervated column, the main neurite followed a more posterior course close to the posterior vertical bundles. From the ventral groove, the axon joins the isthmus tract into the LAL, where it finally branches.

Several differences distinguish CPU1b neurons (n = 9) from CPU1a cells (Fig. 5A). First, all arborization areas are contralateral to the soma; hence these neurons provide a connection between the PB and LAL of the same hemisphere. Second, the arborization trees in the CBU are considerably wider than those of CPU1a neurons, covering at least half of the CBU hemisphere throughout all layers (Fig. 5C, right). Third, the number of terminals in the LAL appears to be larger compared with CPU1a cells (Fig. 5F). Finally, only neurons with arborizations in PB columns R7/L7 were encountered (Fig. 5D). A double staining of two CPU1b neurons in the same preparation showed arborizations covering almost the entire hemisphere of the CBU. PB arborizations of both neurons seemed to overlap in column 7, but could not be traced with certainty to the main neurite. The main neurite of CPU1b neurons runs through the contralateral z-bundle, and then follows the frontolateral surface of the CBU without crossing the midline.

The third type of CPU1 neuron (CPU1c, n = 6) closely resembles CPU1a neurons, but has a much narrower arborization domain in the CBU, which only covers the width of a single column (Fig. 5A). Neurons of this type were found in columns 5, 6, and 7 of the PB and innervated ipsilateral CBU columns near the midline (6, 7, and 8, respectively), before sending an axon to the contralateral ventral shell of the LAL. This connectivity between columns of the PB and CBU differs markedly from that of CPU1a neurons (Fig. 5B). However, the limited number of

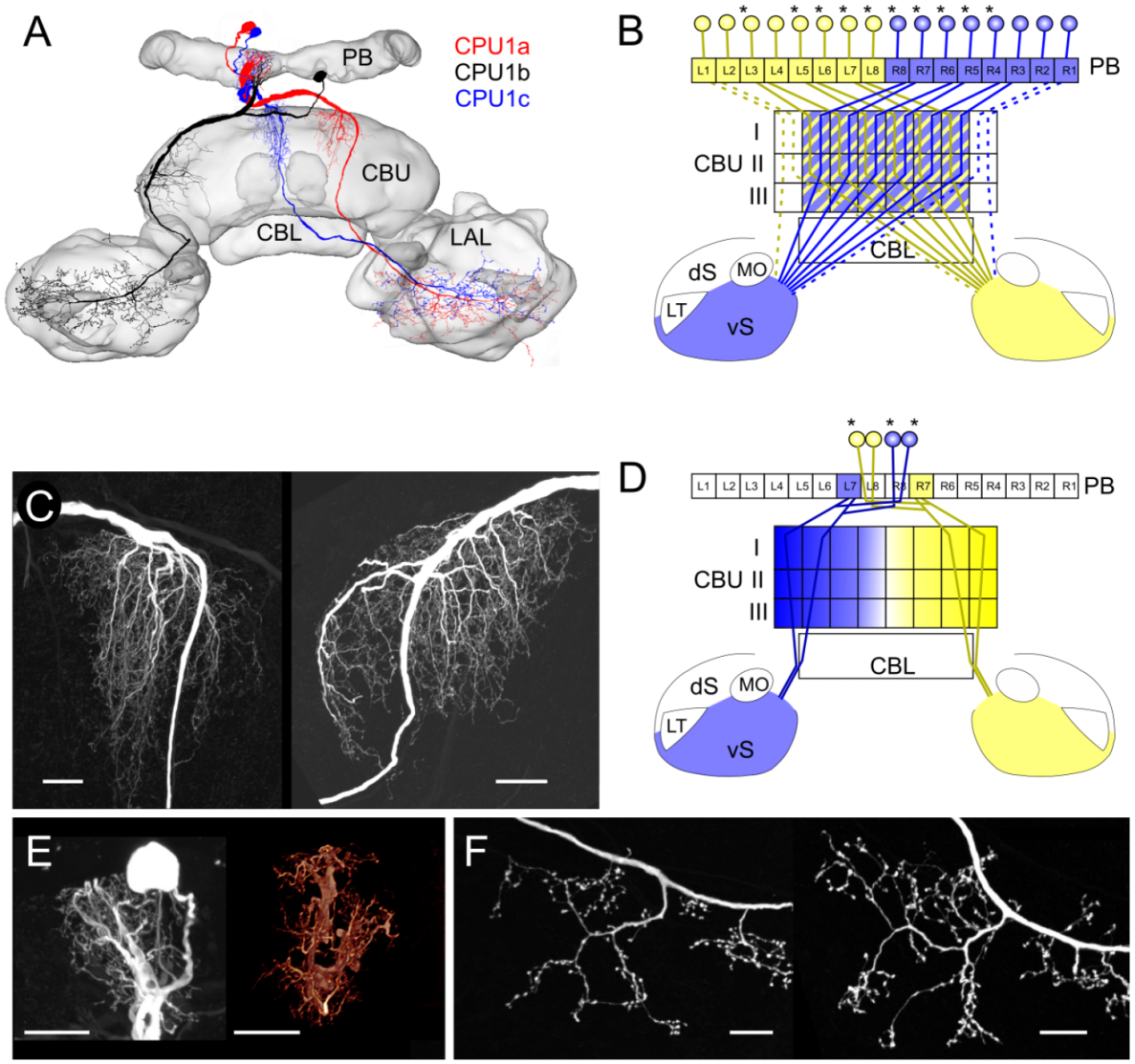

Fig. 5. Morphology of CPU1 neurons. **A:** Camera lucida reconstruction of a CPU1a (red), a CPU1b (black), and a CPU1c neuron (blue), projected onto a three-dimensional reconstruction of the central complex. **B:** Proposed connectivity scheme of CPU1a neurons. Asterisks point to neurons that were encountered at least once. **C:** Arborizations in the upper division of the central body. Maximal projections of confocal image stacks (frontal plane) of a Neurobiotin-injected CPU1a neuron (left) and CPU1b neuron (right). **D:** Proposed connectivity scheme of CPU1b neurons. Only neurons with ramifications in columns R7 and L7 were found. **E:** Arborizations in the protocerebral bridge. Maximal projection of confocal image stack of a CPU1a arborization tree (left) and frontal view of three-dimensional image (volume rendering) of a CPU1b arborization tree obtained from confocal data (right). **F:** Maximal projections of confocal image stacks of arborizations in the lateral accessory lobe (CPU1a left, CPU1b right). For abbreviations, see list. Scale bar = 20 μm in C–F.

stained cells did not allow us to extrapolate the complete connectivity scheme of this cell type. With respect to innervated CBU layers, polarity of the cell, course of the main neurite, and location of the soma, CPU1c neurons appear identical to CPU1a neurons.

CPU2 neurons (n = 17; CC II neurons of Williams, 1972) form an isomorphic set of 16 neurons and connect columns of the ipsilateral PB and CBU to both LALs (Fig. 6). Arborizations in the CBU extend through all layers, cover a width of two to three columns, and are of similar appearance to those of CPU1 neurons (Fig. 6B). Double staining of CPU1 and CPU2 neurons showed overlapping projection areas in the ventral shell of the LAL. An important difference between CPU1 and CPU2 neurons is the projection scheme between the PB and CBU. CPU2 neurons innervate identical columns in the CBU and the PB (Fig. 6D), but with substantial lateral overlap of arborizations of neurons of adjacent columns. As in most

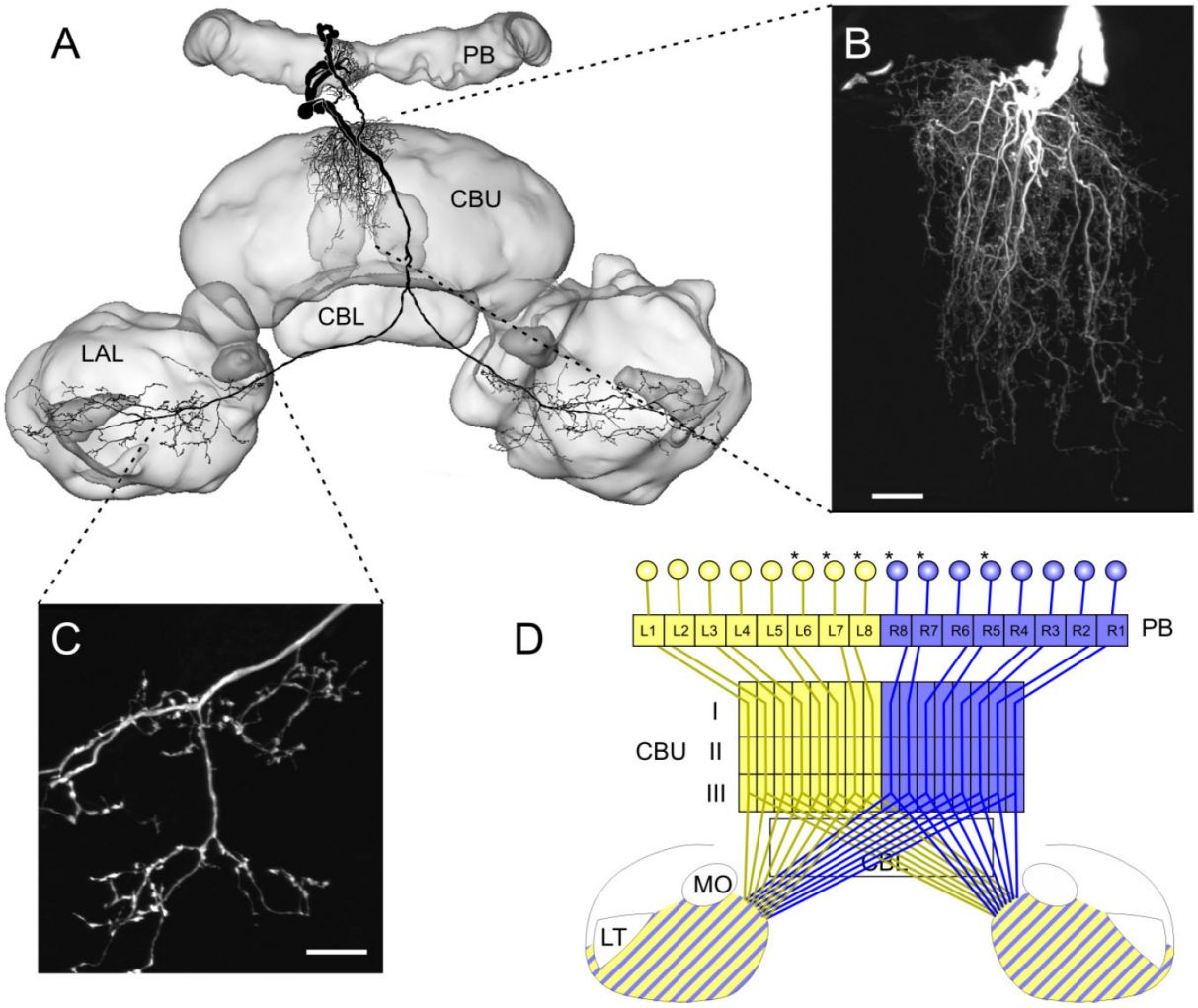

Fig. 6. Morphology of CPU2 neurons. **A:** Camera lucida reconstruction of a CPU2 neuron, projected onto a three-dimensional model of the central complex. **B:** Maximal projection of confocal images from arborizations in the upper division of the central body. **C:** Maximal projection of confocal data from varicose arborizations in the left lateral accessory lobe. **D:** Proposed arborization scheme for CPU2 neurons. Asterisks point to neurons stained at least once. For abbreviations, see list. Scale bar = 20 μm in B,C.

CPU1 cells, the main neurite does not enter the CBU but runs along the dorsal and anterior face of the CBU toward the point of bifurcation in the ventral groove. From the ventral groove the axon collaterals join the isthmus tracts on either side.

PB-CBU connections. A neuron connecting the PB to the CBU, termed a CPU3 neuron, was found in one preparation only (Fig. 7). It provides a connection of a single PB column (R6) with columns L3/4 in layer III of the CBU. The soma is located about 40 μm posteriorly from the PB in the pars intercerebralis, and hence the primary neurite enters the PB from the posterior direction. Arborizations in the PB appeared less varicose than those in the CBU, but were superimposed by terminals from other neurons, so no definite statement about their lateral extension and structure can be made at this point. The neurite connecting the two projection areas leaves the PB at its posterior side, follows the y-bundle into the posterior chiasma, and enters layer III of the CBU via the posterior groove. The arborization tree in the CBU has a width of around one-eighth of the total width of layer III and thus covers an area of two columns. Three-dimensional reconstruction showed that within these columns the complete cross section of layer III is filled with a loose mesh of large varicosities (Fig. 7B,C).

PB-CBU-No connections. Two major groups of neurons, termed CPU4 and CPU5, each consist of three distinct subtypes of columnar neuron connecting the CBU with different layers of the upper units of the noduli.

The morphology of an isomorphic set of CPU4 neurons has been established through immunostaining by using antisera against serotonin (Homberg, 1991) and Dip-

The Journal of Comparative Neurology

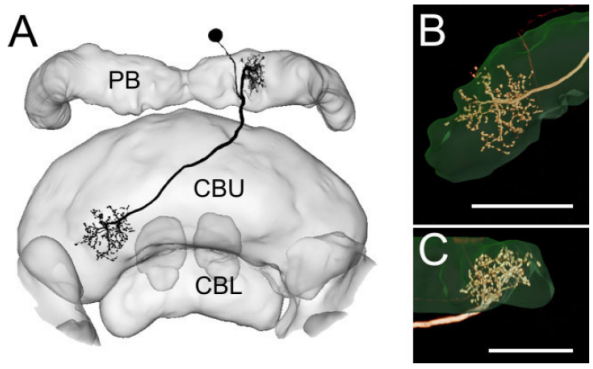

Fig. 7. Morphology of a CPU3 neuron. **A:** Maximal projection of merged confocal image stacks (posterior view, frontal plane) projected onto a three-dimensional model of the central complex. Arborizations in the protocerebral bridge are restricted to column R6, whereas columns L3/4 in layer III of the upper division of the central body are innervated. **B,C:** Three-dimensional visualization of confocal image data showing central-body arborizations of the neuron illustrated in A (posterior view in B, dorsal view in C). Reconstruction of the central-body layer III is shown in green (based on anti-synapsin staining). For abbreviations, see list. Scale bar = 50 μm in B,C.

allatostatin (Vitzthum et al., 1996) and through histochemical labeling for NADPH-diaphorase (Kurylas et al., 2005). All three studies showed systems of columnar neurons with cell bodies in the pars intercerebralis and ramifications in the PB, in layer III of the CBU, and in layers of the upper division of the noduli. Single cell fills and Golgi impregnations reveal three distinct subtypes, termed CPU4a (n = 1), which projects to nodulus layer I, CPU4b (n = 2), which innervates nodulus layer II, and CPU4c (n = 4), projecting to nodulus layer III (Fig. 8). Double labeling experiments confirm that the nodulus layer II projections (type CPU4b) are serotonin-immunoreactive (Fig. 8E,F), whereas the nodulus layer III projections (type CPU4c) are distinct from the latter and probably correspond to the NADPH-diaphorase-positive neurons. All CPU4 neurons have somata in the posterior pars intercerebralis. Their primary neurites pass the PB posteriorly and give rise to their main neurites just ventrally from the PB. Endings in the PB are of a smooth appearance and are restricted to single columns. After the main neurite leaves the PB it projects through the posterior chiasma and passes the midline (in case of contralateral CBU projections). It then runs through layer III of the CBU and bends into the posterior groove toward the contralateral nodulus. In case of ipsilateral CBU projections, midline crossing occurs in the posterior groove before the axon enters the nodulus. Unlike in the PB, arborizations in the CBU are varicose. They are concentrated in layer III, but a few extensions into layer II may occur occasionally (observed in CPU4c neurons). Arborizations in the CBU cover a width of about two columns, without showing clear lateral boundaries. All endings of these cells in the noduli have a varicose appearance.

CPU5a-c neurons (n = 9) were stained only in mass fills or as fragments in a total of five preparations. They connect the PB with layer II of the CBU and with dorsal layers of the noduli (Fig. 9). The three subtypes differ with regard to the nodulus layer they invade (Fig. 9D). Somata could be identified in two cases in the pars intercerebralis. Arborizations in the PB are of a smooth appearance and cover single columns. The main neurite crosses the midline in the posterior chiasma and enters the CBU posteriorly. From a major branching point in layer III, several smaller projections extend anteriorly into layer II, whereas one large fiber projects through the posterior groove toward the contralateral nodulus (Fig. 9A–C). Endings in layer II are varicose and extend throughout two to four columnar domains, and the number of terminals appears to increase toward the dorsal edge. In the noduli, arborizations are dense and of fine appearance. The neurons invade the uppermost layer I (CPU5a, n = 3), the median layer II (CPU5b, n = 4), or both of these layers (CPU5c, n = 2; Fig. 9A–D).

Columnar neurons without PB connections. Three types of columnar neuron lack arborizations in the PB. Two types connect columns of the CBU with specific areas in the LAL, whereas one type of neuron connects the CBU with the anterior lip.

CU1 neurons (n = 5) link the CBU with the anterior lip (Fig. 10A). These neurons have small somata in the pars intercerebralis and are of a generally fine, slender appearance with small neurite diameters. Their primary neurites pass the PB anteriorly and enter the CBU dorsally. They run via the anterior vertical bundles along the border between layer I and II, and leave the CBU ventrally as they enter the anterior lip from the posterior direction. Within the CBU, these neurons send fine processes anteriorly into layer Ib, covering an area of one to two columns. In the anterior lip, the neurons have bilateral arborizations of a finely beaded appearance. Terminals arise from a horizontally running fiber covering large areas of the anterior lip.

In contrast, CU2 neurons (n = 4) connect areas in layer I of the CBU (one to two columns wide) with the anterior dorsal shell of the contralateral LAL (Fig. 10B). Their cell bodies are located in the pars intercerebralis. Thin primary neurites bypass the PB just anteriorly, and enter the CBU dorsally. Main fibers follow a similar but slightly more anterior path through the CBU than those of CL1 neurons, pass through the ventral groove, and join the isthmus tract to the contralateral LAL. Arborizations in the LAL have varicose endings and arise from four to five branches given off at regular intervals from the main neurite. These endings are distributed in the dorsal shell ranging from the boundary to the CBU to as far lateral as the lateral triangle. Terminals in the CBU form a dense mesh of fibers with a generally smooth appearance, although some mixed endings cannot be ruled out. Two subtypes of CU2 neurons can be distinguished based on the location of their CBU projections. CU2a neurons innervate more dorsal areas of layer I, whereas endings of CU2b cells are concentrated in layer Ia (Fig. 10B). Individual neurons with innervations of ipsilateral or contralateral CBU columns were encountered. Although all of the innervated columns were clustered around the midline, we suggest that each of the subtypes forms a set of 16 isomorphic cells connecting all columns of the CBU to the dorsal shell of the contralateral LAL (Fig. 10D).

In addition to several fragmentary stainings, complete CU3 neurons were found in a double impalement of only a single preparation (Fig. 10E). It showed a pair of identical cells connecting an area of the contralateral CBU to both anterior dorsal shells of the LALs. The small somata are

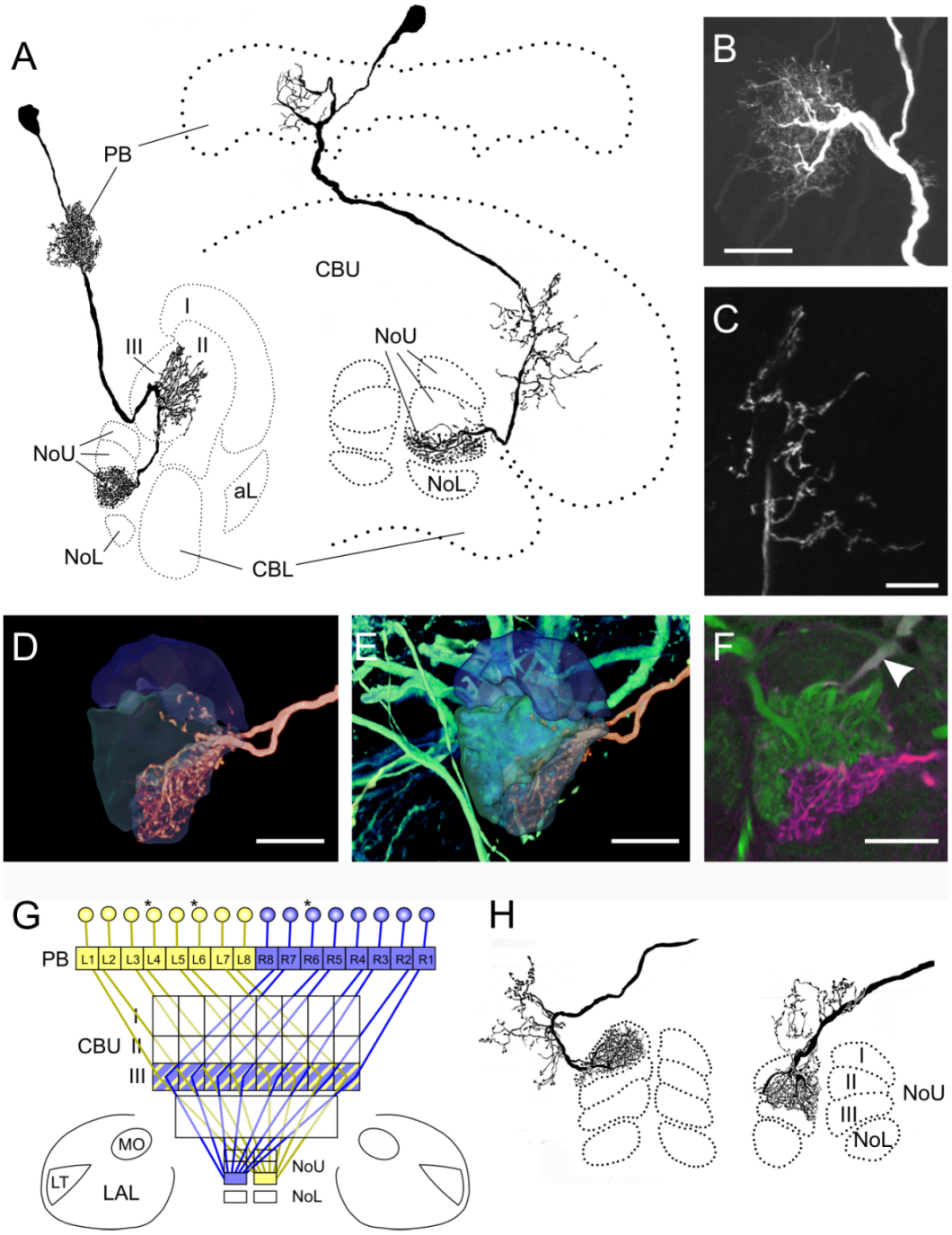

Fig. 8. Morphology of CPU4 neurons. **A:** Sagittal reconstruction of a Golgi-stained CPU4c neuron (left) and frontal camera lucida reconstruction of a neuron of the same type (right). **B,C:** Maximal projections (frontal plane) of confocal image stacks of CPU4c neuron projections in the protocerebral bridge (fine, B) and in the upper division of the central body (varicose, C). **D,E:** Three-dimensional visualization of the arborization tree in a nodulus (CPU4c neuron), together with the reconstruction of anti-synapsin-labeled subcompartments of the upper unit of the innervated nodulus. In E, serotonin-immunoreactive projections of CPU4b cells are shown in green and illustrate the non-overlapping arborizations of the two subtypes in the upper unit of the nodulus. **F:** Single optical slice showing serotonin-immunoreactive projections (green) and two Neurobiotin-injected CPU4 neurons (red) in a nodulus. The strongly stained neuron (magenta) is a CPU4c neuron, whereas the weakly stained, serotonin-colabeled neuron (arrowhead) is a CPU4b neuron. **G:** Connectivity scheme of CPU4 neurons (illustrated for the CPU4c subtype), based on immunocytochemical data (Vitzthum et al., 1996) and individually filled cells (asterisks). The two other subtypes only differ with regard to the innervated layer of the NoU. **H:** Frontal camera lucida reconstructions of arborizations in the CBU and noduli of Golgi-stained CPU4 neurons, emphasizing the different NoU layers innervated by CPU4a neurons (left) and CPU4b neurons (right) as opposed to CPU4c neurons (shown in A–G). For abbreviations, see list. Scale bar = 20 μm in B–F.

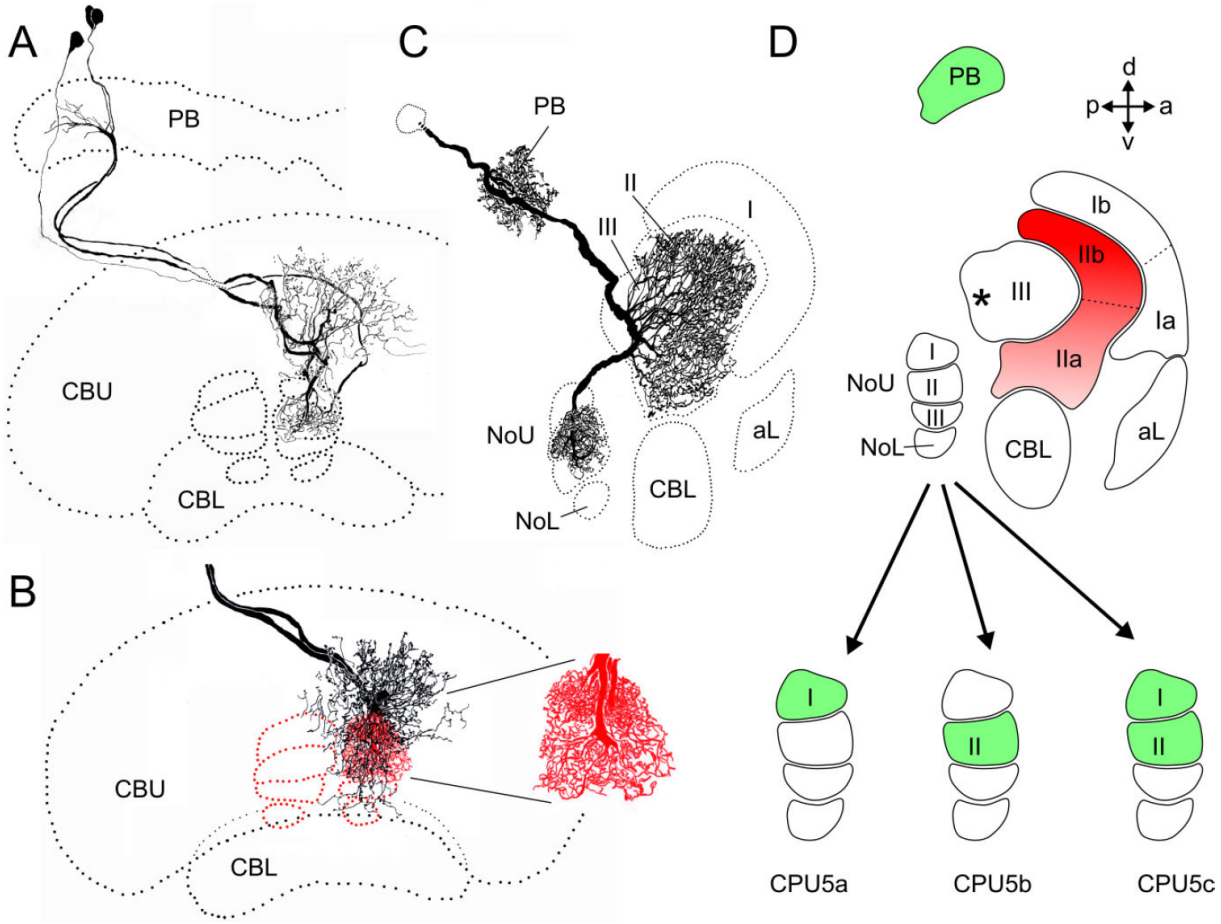

Fig. 9. Morphology of CPU5 neurons. **A:** Camera lucida reconstruction of two CPU5b neurons (with an unidentified third neuron superimposed). The neurons innervate a single column of the protocerebral bridge (fine arborizations) and project to layer II of the upper division of the central body (CBU, varicose arborizations) and further to layer II of the upper division of the contralateral nodulus (NoU, fine arborizations). **B:** Partial reconstruction of a double impalement of a CPU5a and a CPU5c neuron. These cells differ with regard to the innervated NoU layer, shown in the enlargement. CPU5a neurons innervate the uppermost NoU layer I, whereas CPU5c neurons innervate NoU layers I and II. **C:** Sagittal camera lucida reconstruction of a Golgi-impregnated CPU5b neuron, revealing that endings in the CBU are restricted to layer II. **D:** Schematic sagittal view illustrating arborization areas of CPU5 neurons. Fine (potentially postsynaptic) endings are shown in green and varicose (potentially presynaptic) endings in red. The three subtypes of CPU5 neurons are distinguished by the location of their noduli innervations (CPU5a–c). Asterisk indicates the location of the main branching point in CBU layer III. For abbreviations, see list.

located in the pars intercerebralis and send primary neurites to the CBU along a path similar to that of CU2 neurons. Within dorsal regions of layers I and II of the CBU, an area corresponding to about four columns is filled with fine arborizations. Axonal fibers leave the CBU ventrally and bifurcate in the ventral groove into an ipsilateral and a contralateral branch. In the LAL, the anteriormost parts of the dorsal shells that extend laterally and medially around the medial lobes of the mushroom bodies are filled with fibers terminating in small varicosities.

Columnar neurons of the CBL

Two types of columnar neuron, termed CL1 and CL2 neurons, have been identified by Müller et al. (1997). We present additional details of the branching patterns of these neurons and provide evidence for the presence of three subtypes of CL1 neurons, termed CL1a, CL1b, and CL1c.

PB-CBL-(LAL) connections. Owing to their large axon diameters, CL1 neurons (= CCI neurons of Williams, 1975) were filled most frequently (n = 64, including 34 stained cells in Müller et al., 1997). CL1 neurons connect single columns of the PB with single columns in the CBL. Their main neurites traverse the CBU in the posterior vertical bundles, which are characteristically arranged like the staves of a fan as they pass through layer III of the CBU (Fig. 2B). Three subtypes of CL1 neurons were distinguished. CL1a neurons were encountered most frequently (n = 59). They have small, spheroidal cell bodies in the anterior pars intercerebralis. A very thin primary

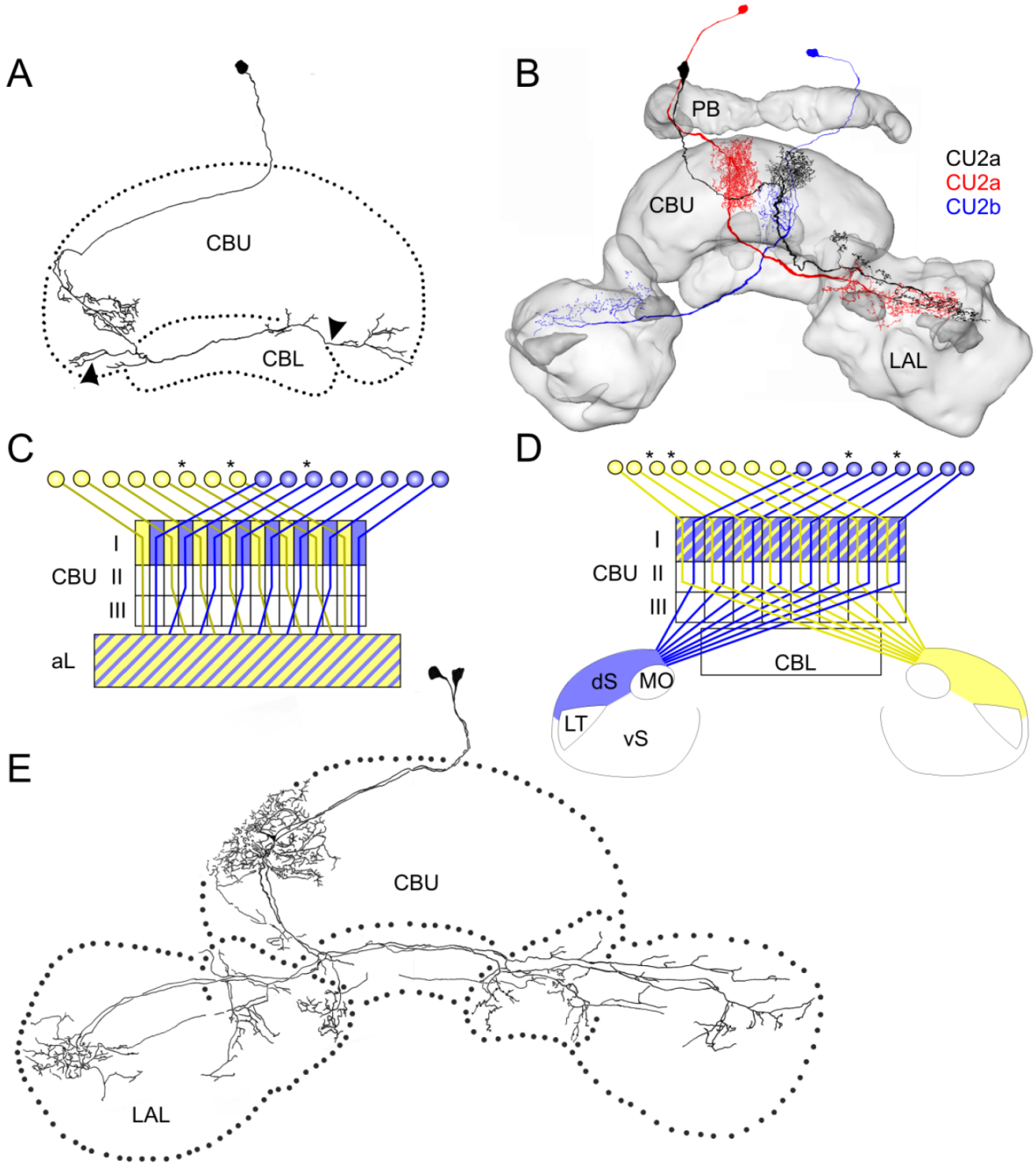

Fig. 10. Columnar neurons without arborizations in the PB. A,B,E: Camera lucida reconstructions (frontal plane) of Neurobiotin-injected CU neurons. **A:** Reconstruction of a CU1 cell. Arrowheads indicate arborizations in the anterior lip, anterior to the central body. Their finely beaded appearance is only visible at higher magnification. Arborizations in the upper division of the central body (CBU) originate from the main neurite in the anterior vertical bundles at the border of layers I and II and protrude anteriorly into layer Ib. **B:** CU2a (red and black) and CU2b neurons (blue) are projected onto a three-dimensional reconstruction of the central complex. They connect parts of layer I of the CBU to the dorsal shell of the contralateral lateral accessory lobe (LAL). **C,D:** Proposed connectivity schemes for CU1 neurons (C, modified from Vitzthum et al., 1996) and CU2 neurons (D, based on individually stained neurons). Asterisks indicate neurons that have been found at least once. **E:** Double impalement of CU3 neurons, connecting dorsal parts of CBU layer I and II to anterior regions of the dorsal shell of the LAL. For abbreviations, see list.

The Journal of Comparative Neurology

neurite passes the PB anteriorly, gives off side branches into the PB, and connects to the main neurite. The main neurite runs through the posterior chiasma, enters the CBU posteriorly, and crosses layer III as part of the posterior vertical bundles before innervating the CBL from its dorsal rim. Just before the major branching occurs within the CBL, a small axon separates from the main neurite and joins the isthmus tract to the lateral triangle of the contralateral LAL (Fig. 11A). Midline crossing occurs in the posterior chiasma (neurons with contralateral CBL projections) or in the ventral groove (neurons with ipsilateral CBL projections). CL1a neurons form an isomorphic set of 16 cells. Columns of the right and left hemispheres of the PB are connected topographically to alternating columns of the CBL so that each hemisphere of the PB is projected onto the complete width of the CBL (Fig. 11B). The endings in the PB and in the lateral triangle have a varicose appearance (Fig. 11G,J). Arborization trees in the CBL instead have a center-surround organization and consist of a central core with bleb-like endings and a peripheral zone with smooth terminals (Fig. 11C–F). The bleb-like endings are confined to a single column and extend through all major layers. The smooth endings in the periphery are concentrated in layer 2; they are much wider and cover three to four columns. As a result, neighboring CL1a neurons show extensive overlap in their smooth arborizations in the CBL, but nearly no overlap of their varicose endings. Arborizations of all CL1a neurons in the lateral triangle are restricted to small subareas, but so far we are unable to find any correspondence between the location of these endings and the innervated columns in the CBL or PB.

A second and a third subtype of CL1 neurons, termed CL1b (n = 3) and CL1c (n = 2), was only found in preparations with many stained neurons and in Golgi impregnations. Hence no individual cell could be traced with absolute certainty due to partly superimposed arborizations from other neurons or incomplete staining. CL1b and c neurons resemble CL1a neurons with regard to the location of their cell bodies, the course of the main neurite, and the areas of arborization in the PB and CBL. However, several differences were apparent. First, neuron polarity as seen in CL1a neurons appears to be reversed in CL1b/c neurons, so that smooth endings are found in the PB (Fig. 11H) and only varicose endings in the CBL (Fig. 11I). No substructure in the CBL arborizations is obvious, and endings are not restricted to a specific layer. However, in dorsal layers 1 and 2, as well as in the ventralmost layer 6, arborizations are substantially wider than in the remaining layers, where they are tightly restricted to a single column. Second, an axon to the lateral triangle is only present in CL1b neurons, but is lacking in CL1c (Fig. 11A). Finally, the somata of CL1b/c neurons are typically about twice as large as those of CL1a neurons, have a more angular shape, and give rise to a much thicker primary neurite. Three of the five stained CL1b/c neurons were found as colabeling of one CL1a together with a CL1b or CL1c cell with arborizations in identical columns, suggesting that all three subtypes of CL1 cells follow the same connectivity scheme.

PB-CBL-No connections. Columnar neurons with arborizations in the PB, CBL, and noduli were first described by Müller et al. (1997) and were termed CL2 neurons (Fig. 12; n = 15, including 9 cells from Müller et al., 1997). Three-dimensional analyses of high-resolution confocal image stacks revealed further details on the structure of endings and the connectivity scheme. Cell bodies of CL2 neurons in the pars intercerebralis give rise to small primary neurites that pass anteriorly around the PB and send off processes into the bridge. From the ventral side of the PB, a main neurite runs through the posterior chiasma (for contralateral CBL projections), passes in one of the posterior vertical bundles through layer III of the CBU, and enters the posterior groove. The fiber bifurcates; one branch is sent to the CBL and the other to the contralateral nodulus (Fig. 12A,C). Midline crossing for CL2 neurons with ipsilateral CBL projections occurs in the posterior groove. Within the PB, a dense mesh of smooth endings is formed, which fills the entire cross section of a single column (Fig. 12E). In the CBL, terminals have a clearly beaded appearance and cover a width of slightly more than one column (Fig. 12A,C). Arborizations in the CBL are confined to a single layer, probably layer 2. Endings in the noduli are fine and form a very dense mesh of arborizations, which is (with one exception of some dorsally protruding fibers) confined to the lower unit (Fig. 12C,D).

Judged from a double impalement, at least two identical neurons are present in each column of the PB. From individually filled cells covering six out of eight PB columns, a connectivity scheme can be extrapolated, which, despite similarities, differs in detail from the system of CL1 neurons (Müller et al., 1997). Each hemisphere of the PB projects onto the whole width of the CBL, as in CL1 neurons. In contrast to CL1 neurons, however, the innermost PB column (R8/L8) is connected to the outermost contralateral CBL column (L1/R1). The following PB columns project to every other CBL column, so that the outermost PB column (R1/L1) is connected with the second outer ipsilateral CBL column (R2/L2; Fig. 12B). In CL1 neurons, in contrast, the innermost PB column (R8/L8) is connected to the second outer contralateral CBL column (L2/R2), with all other connections differing accordingly (Fig. 11B).

Columnar neurons without central body arborizations

Two types of neuron directly connect the PB with different regions in the contralateral LAL (Fig. 13). No arborizations were detected in the central body in any of the fills, and both cells likely form isomorphic sets of 16 neurons each.

CP1 neurons (n = 7) have arborizations in single columns of the PB and project to the contralateral median olive (Fig. 13A; Vitzthum et al., 2002). Their cell bodies are located in the pars intercerebralis. The main neurite runs along the anterior face of the central body, crosses the midline in the ventral groove, and continues to the median olive. In the median olive a dense mesh of beaded endings extends through the entire structure. Arborizations in the PB fill one column with dense smooth processes.

CP2 neurons (n = 7) are similar to CP1 neurons, but project to the lateral triangle (Fig. 13B; Vitzthum et al., 2002). Their main neurites also follow the anterior edge of the CBU (with one exception running in the posterior vertical bundle), but cross the midline in the posterior chiasma. Within the PB, CP2 cells form a dense mesh of arborizations confined to a single column (with occasional extensions into neighboring columns). In peroxidase-stained preparations these endings have a generally smooth appearance, whereas high-resolution confocal

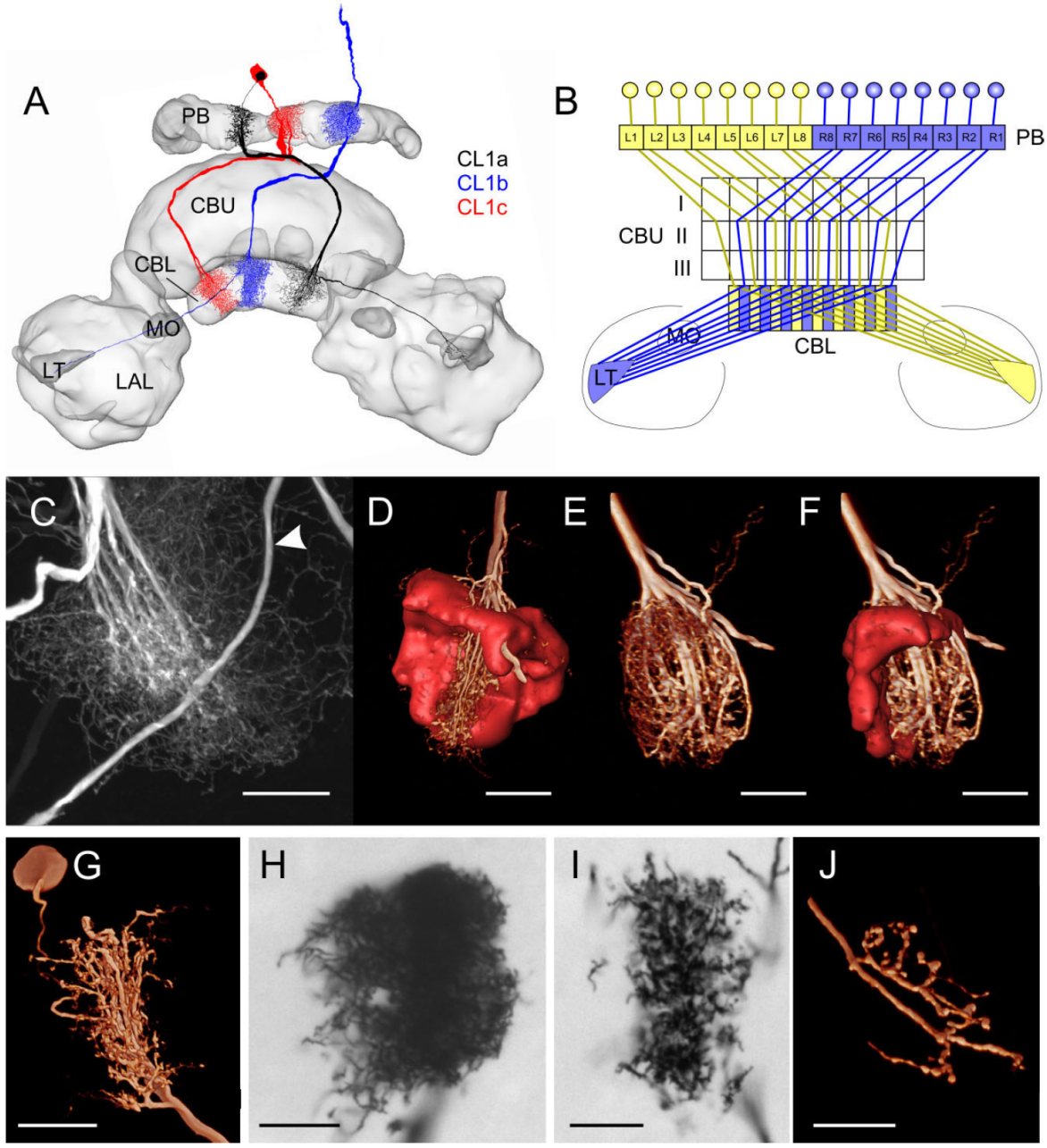

Fig. 11. Morphology of three types of CL1 neurons. **A:** Camera lucida reconstructions (frontal plane) of a CL1a neuron (black), a CL1b neuron (blue), and a CL1c neuron (red). Note the difference in size and shape of the somata between the CL1a and CL1c cell. Arborizations in the lateral triangle as well as the soma were not stained in the CL1b neuron (Golgi impregnation). **B:** Connectivity scheme of CL1a/b neurons. At least one CL1a neuron has been stained in each column of the protocerebral bridge (PB). C,D: Frontal views of arborizations of CL1a neurons in the lower division of the central body (CBL). **C:** Maximal projection of a confocal image stack. A dense cluster of varicosities in the center of the arborization tree is surrounded by a tangle of very fine processes. The main neurite of a CPU2 neuron passes along the frontal surface of the CBL (arrowhead). **D:** Three-dimensional visualization of another CL1a cell. The fine fibers are occluded by an opaque envelope (red) to reveal the well-defined width of the varicose arborizations. **E,F:** Three-dimensional lateral views of the CBL arborizations shown in D. Fine endings in F are covered with an opaque envelope. **G:** Three-dimensional visualizations of PB arborizations of a CL1a neuron illustrating thick, varicose endings (posterior view). **H,I:** Details of a CL1b neuron (Golgi staining, anterior views). Microscopic images reveal a dense cluster of fine endings in the PB (H) and varicose arborizations in the CBL (I). **J:** Three-dimensional anterior view of varicose endings in the lateral triangle of a CL1a neuron. For abbreviations, see list. Scale bar = 20 μm in C–J.

The Journal of Comparative Neurology

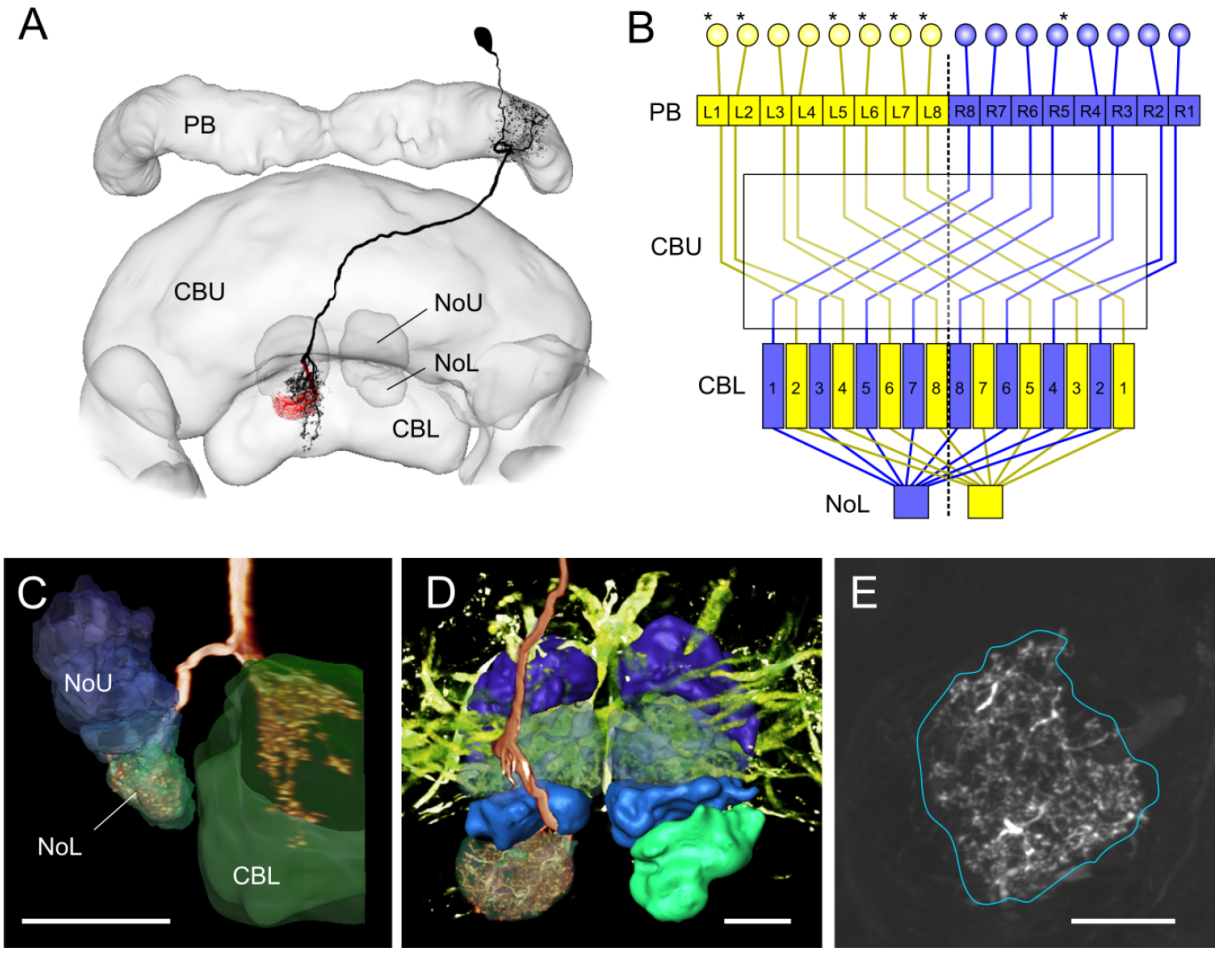

Fig. 12. Morphology of CL2 neurons. **A:** Maximal projection from multiple merged confocal image stacks, projected onto a three-dimensional reconstruction of the central complex. **B:** Proposed connectivity scheme of CL2 neurons. Asterisks indicate neurons that were encountered at least once. C–E: Details of the neuron shown in A. **C:** Lateral view of a three-dimensional visualization of arborizations in the lower unit of a nodulus (NoL) and in the lower division of the central body (CBL) together with surface reconstructions of the innervated neuropils. Arborizations in the CBL are restricted to a region likely corresponding to layer 2. **D:** Frontal view of a three-dimensional reconstruction of CL2 arborizations in a nodulus together with serotonin-immunolabeled fibers and surface reconstructions of both noduli. CBL projections have been removed for clarity. **E:** Maximal projection (frontal plane) of a confocal image stack of fine endings in the protocerebral bridge. Neuropil dimensions are outlined based on synapsin labeling. For abbreviations, see list. Scale bar = 50 μm in C; 20 μm in D,E.

analysis showed small beaded endings (Fig. 13E). In the LAL, endings are clearly varicose, and invade the whole lateral triangle. In most cases, arborizations are not confined to the lateral triangle proper, but also invade the surrounding tract area and the adjacent neuropil of the LAL; occasionally, a small neurite even projects back to the median olive (Fig. 13F).

DISCUSSION

The central complex is a group of neuropils with unique modular architecture in the insect brain. An internal organization into linear rows of 16 columns appears to be present in all species studied (Homberg, 2008), and until recently (Heinze and Homberg, 2007) the functional significance of this columnar organization has been completely obscure. The analysis of arborization patterns of pontine and columnar neurons in the desert locust has been preceded by only one study of similar detail in the fruit fly (Hanesch et al., 1989). Our data provide an essential basis for an understanding of information flow through the central complex, of principles of internal signal processing, and of the identification of target areas of central-complex neurons in the brain. In this study we have identified and characterized an amacrine neuron, three types of pontine neuron, and 21 types of columnar neuron of the locust central complex. Most of these cell types appear to consist of isomorphic sets of neurons with at least one element per column. The patterns of columnar connections of these

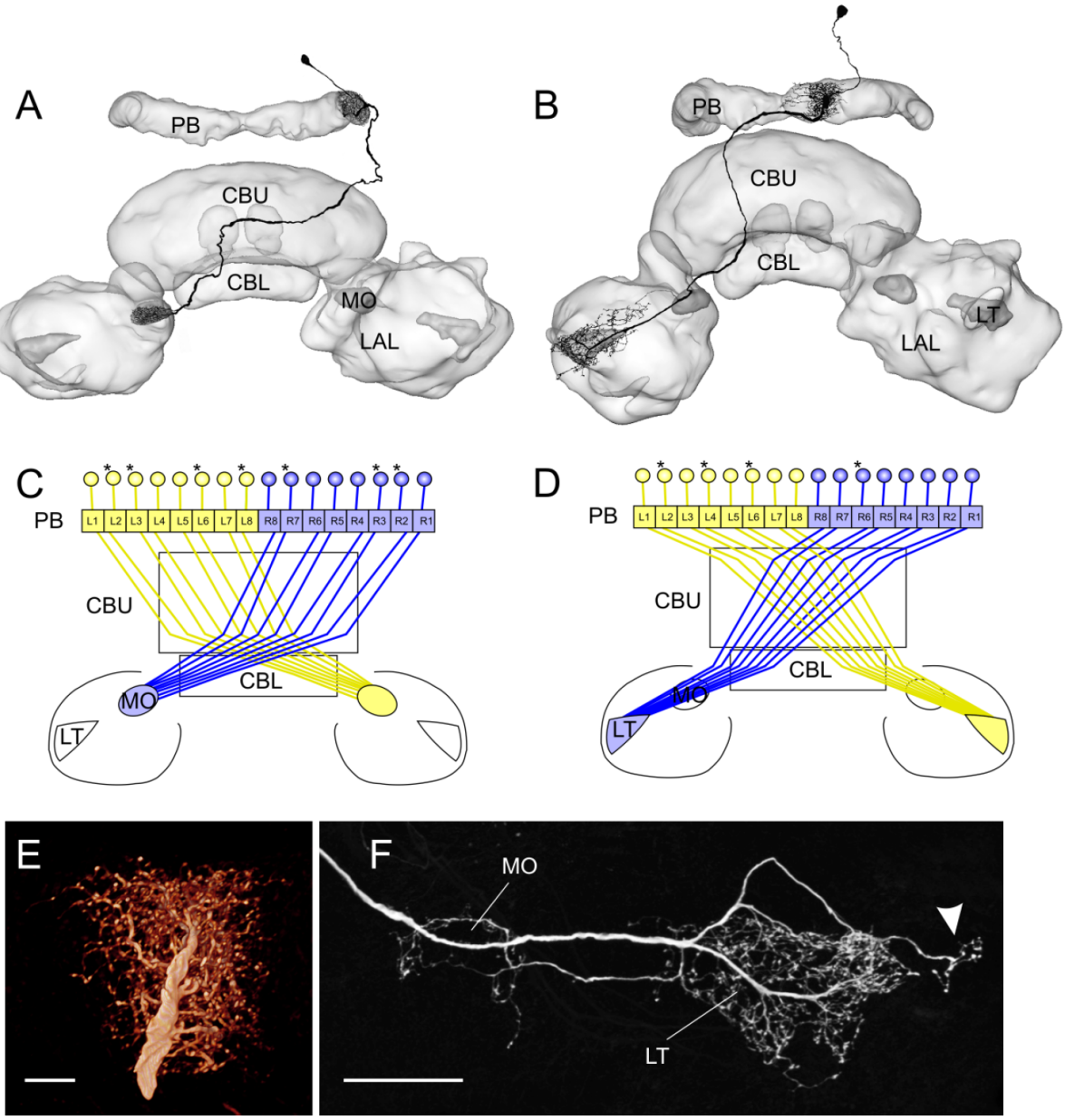

Fig. 13. Columnar neurons without central-body arborizations. **A,B:** Camera lucida reconstructions of a CP1 (A) and a CP2 neuron (B) projected onto a three-dimensional reconstruction of the central complex. **C,D:** Connectivity schemes of CP1 (C) and CP2 neurons (D). Neurons highlighted by asterisks were found at least once. **E:** Frontal view of a three-dimensional visualization of projections in the protocerebral bridge of a CP2 neuron. **F:** Frontal maximal projection of a confocal image stack, showing the projections of a CP2 neuron to the lateral triangle. Single fibers extend beyond the boundaries of the lateral triangle (arrowhead) or project back to the median olive. For abbreviations, see list. Scale bar = 10 μm in E; 40 μm in F.

cell types have important implications for functional considerations.

Arborization domains in the central complex

The columnar organization of the locust PB is pronounced. This is consistent with studies of other insects (Hanesch et al., 1989; Wegerhoff et al., 1996), which have described the PB as a cylindrical neuropil comprised of a linear array of columns (termed glomeruli in flies). All cell types had arborizations largely confined to single PB columns with only marginal extensions to neighboring columns. Nevertheless, in double staining of neurons innervating adjacent columns, the separation of terminal

The Journal of Comparative Neurology

branches was difficult, suggesting that some overlap does occur.

In the CBU, boundaries between layers were generally better respected by the arborization domains of individual neurons than boundaries between adjacent columns. The best and perhaps only cases of unicolumnar innervations of the CBU are CU1 and CPU1c neurons, with arborizations in layer I (CU1) and layers I–III (CPU1c) of the CBU. In all other cell types, arborization areas covered at least two CBU columns. Consequently, lateral overlap of arborizations may be as high as 80%, as in CPU2 neurons (Fig. 6). Whereas pontine neurons had CBU arborizations centered in single columns with lateral overlap to the adjacent columns, many types of columnar neurons had arborization domains matching the width of two adjacent columns. In these cell types, arborizations from neurons of the right and left hemispheres of the bridge coincided in identical domains of the CBU covering roughly two columns, thereby reducing the number of columns from 16 in the bridge to 8 in the CBU. Column reduction was not found in CPU1c, CPU2, and CU1 neurons, or in the pontine neurons. These cell types had exclusive or major arborizations in CBU layer I and did not show heterolateral connections between the PB and the CBU. An eightfold columnar organization of the CBU has been described in a variety of other insect species, including crickets (Dietl, 1876; Panov, 1959; Schildberger, 1983), cockroaches (Strausfeld, 1999), a beetle (Wegerhoff and Breidbach, 1992), an ant (Goll, 1967), and the fly *Drosophila* (Hanesch et al., 1989). Therefore, superposition of arborizations of columnar neurons from the right and left hemispheres of the PB, and thus reduction from 16 PB to 8 CBU columns, may be a common principle in the organization of certain CBU layers across insects.

Although anti-synapsin staining for synaptic neuropil did not reveal clear evidence for a columnar organization of the CBU, it strongly supported its layered organization. The number of layers differs between three in the locust (Homberg, 1991) and six in flies (Strausfeld, 1976; Hanesch et al., 1989). However, these figures may not be directly comparable, as identification of layers has been achieved through different methods (immunostaining in the locust, silver staining in flies). Layer I of the locust CBU was most distinct, and its boundary to layer II was clearly defined by the 16 anterior vertical bundles. In contrast, the boundary between layer II and III was hardly visible in anti-synapsin staining. This is partly reflected in the arborization domains of the stained cell types. Neurons with ramifications restricted to layer I were common and include the amacrine cell, two types of pontine cells (PoU2 and PoU3), and three types of columnar neuron (CU1, CU2a, and CU2b). Only a few cell types had arborization trees restricted to layer II (CPU5a–c) or layer III (PoU3, CPU3). Arborizations consistently crossing the boundary between layers II and III occurred in subtypes of CPU4 neurons and in PoU1 cells, and crossing between layer I and II was also present in PoU1-type pontine cells. The cell types of the CBU with largest fiber diameters (CPU1a–c, CPU2) had arborization trees extending through all CBU layers, with the density of terminals declining from dorsal to ventral and from anterior to posterior, independent of layers. Most neurons did not invade a particular layer completely within their columnar range, but were restricted to certain parts.

These domains did not necessarily correspond to the sublayers (Ia, Ib, IIa, IIb) that had been introduced on the basis of serotonin immunostaining (Homberg, 1991), but were cell-type specific. As a result, layer boundaries are somewhat blurred, depending on how many neurons with non-layer-matching ramifications exist. Nevertheless, the definition of layers and sublayers based on serotonin immunostaining provides a good orientation cue within the CBU, and double labeling of single-cell preparations for serotonin immunostaining has been highly valuable for determination of neuronal projection areas.

The CBL is strongly layered in anti-synapsin staining, but again, a columnar organization was not obvious. This agrees with findings by Müller et al. (1997) based on Bodian staining. Two of the four types of columnar neuron presented here have columnar projections that are wider than single columns and hence show considerable lateral overlap (CL1c and CL2). CL1a/b neurons, instead, had unicolumnar arborizations in most layers except one (likely layer two), where endings covered an area of three to four columns. Thus, these neurons contribute to both layers and columns in the CBL. Müller et al. (1997) did not distinguish between CL1 subtypes; they also reported virtually no overlap in most layers but extended lateral ramifications of these cells in dorsal layers (1, 2) and layer 6. These characteristics can now be attributed to CL1b neurons.

The noduli are divided into four horizontal layers that were unambiguously identified with anti-synapsin staining. This compartmentation was well respected by all cell types and virtually no overlap occurred between the projections to different layers. The layered organization and division into two subunits of the locust noduli have already been described by Williams (1972), but no study of other species has been sufficiently elaborated to allow detailed comparisons. In *Drosophila*, the noduli are particularly large; they consist of two subunits of about equal size, arranged in a layered fashion (Hanesch et al., 1989).

Connectivity patterns

Topography. Several principles of connectivity patterns emerge, when we consider how the substructures of the central complex and lateral accessory lobes are connected by the different types of neurons (Table 1). Most prominently, we did not find direct connections between the CBU and the CBL. Instead, these subdivisions appear to be completely separate systems, connected in parallel to the protocerebral bridge. In concert with this finding, the lower units of the noduli were exclusively connected with the CBL and the upper units with the CBU. Finally, the anterior lip and the ventral and dorsal shells of the LAL were only connected to the CBU, whereas the lateral triangle and median olive were exclusively linked to the CBL. The observation that neural pathways through the CBU and CBL are distinct and only connected in parallel to the protocerebral bridge is supported by earlier work on the locust (Williams, 1972), but is in contrast to findings in flies. Hanesch et al. (1989) reported three types of columnar neuron having arborizations in both the fan-shaped body and the ellipsoid body of *Drosophila*. Direct links between both subdivisions have also been reported for *Musca* (Strausfeld, 1976).

Although all layers of the upper unit of the noduli are connected to CBU layer III, only the upper two layers (noduli layers I and II) are connected to CBU layer II,

TABLE 1. Types of Amacrine, Pontine, and Columnar Neurons of the Locust Central Complex, the Substructures They Connect, Their Neuroactive Substances as Judged by Immunostaining, and Possible Homologues in *Drosophila*

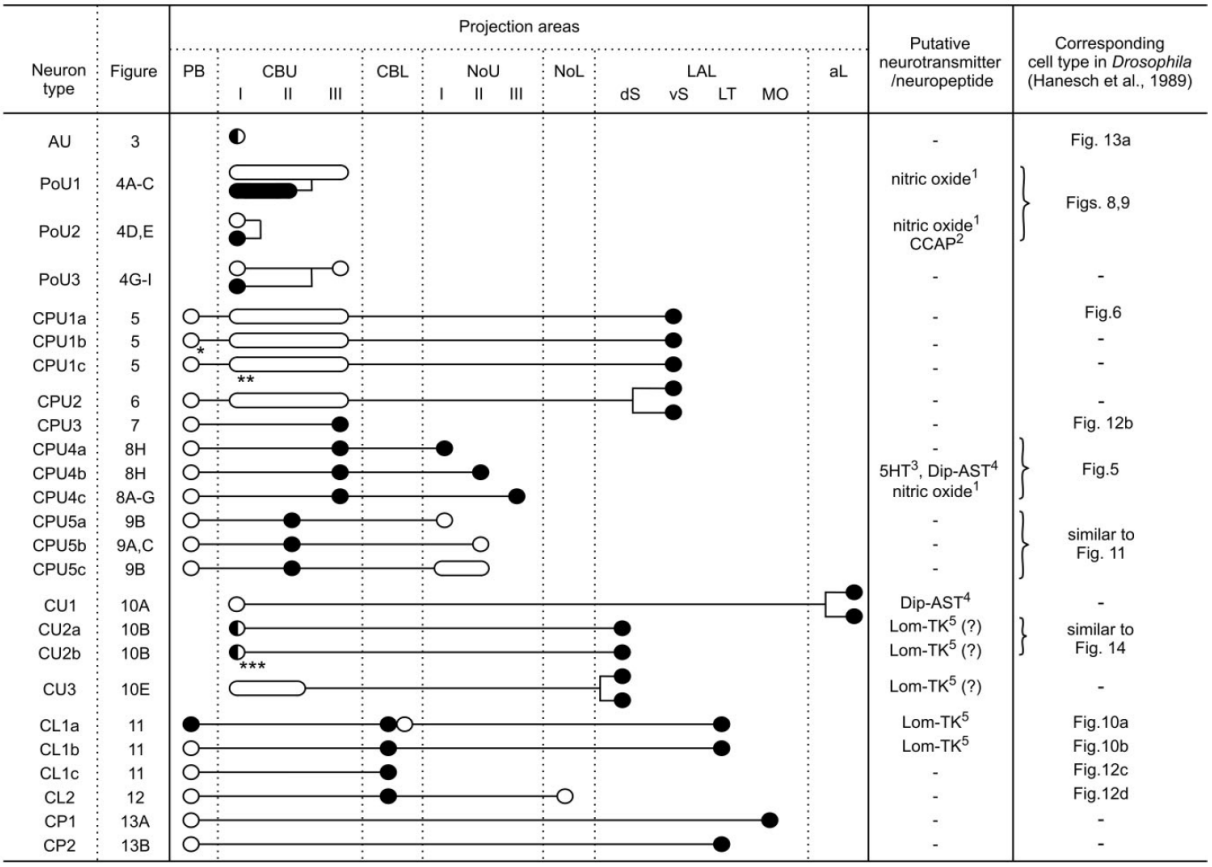

Neuron type	Figure	Putative neurotransmitter /neuropeptide	Corresponding cell type in *Drosophila* (Hanesch et al., 1989)
AU	3	-	Fig. 13a
PoU1	4A-C	nitric oxide[1]	Figs. 8,9
PoU2	4D,E	nitric oxide[1] CCAP[2]	Figs. 8,9
PoU3	4G-I	-	-
CPU1a	5	-	Fig.6
CPU1b	5	-	-
CPU1c	5	-	-
CPU2	6	-	-
CPU3	7	-	Fig. 12b
CPU4a	8H	-	Fig.5
CPU4b	8H	5HT[3], Dip-AST[4]	Fig.5
CPU4c	8A-G	nitric oxide[1]	Fig.5
CPU5a	9B	-	similar to Fig. 11
CPU5b	9A,C	-	similar to Fig. 11
CPU5c	9B	-	similar to Fig. 11
CU1	10A	Dip-AST[4]	-
CU2a	10B	Lom-TK[5] (?)	similar to Fig. 14
CU2b	10B	Lom-TK[5] (?)	similar to Fig. 14
CU3	10E	Lom-TK[5] (?)	-
CL1a	11	Lom-TK[5]	Fig.10a
CL1b	11	Lom-TK[5]	Fig.10b
CL1c	11	-	Fig.12c
CL2	12	-	Fig.12d
CP1	13A	-	-
CP2	13B	-	-

Open circles, smooth arborizations; closed circles, varicose or bleb-like arborizations; mixed circles, mixed specializations. PB, protocerebral bridge; CBU (I–III), layers I–III of the upper division of the central body; CBL, lower division of the central body; NoU (I–III), layers I–III of the upper division of the noduli; NoL, lower division of the noduli; LAL, lateral accessory lobe; LT, lateral triangle; MO, median olive; CCAP, crustacean cardioactive peptide; Dip-AST, *Diploptera puncta* allatostatin; 5HT, serotonin; Lom-TK, *Locusta migratoria* tachykinin.
[1]Kurylas et al., 2005.
[2]Dircksen and Homberg, 1995.
[3]Homberg, 1991.
[4]Vizthum et al., 1996.
[5]Vizthum and Homberg, 1998.
*Contralateral arborization tree.
**Connectivity scheme and width of arborization tree differs from CPU1a cells.
***Arborization tree restricted to layer 1a.

whereas CBU layer I is not connected to the noduli at all. Together with the exclusive connections between the lower units of the noduli and the CBL, these data suggest roughly topological connections of the different layers of the noduli with the layers and subunits of the central body. The noduli, therefore, appear to be secondary, non-columnar processing units in parallel to the central body.

Polarity of neurons. Polarity of neurons was inferred from the appearance of their endings. Varicose and bleb-like terminals were regarded as presynaptic and fine endings as postsynaptic. Although more solid conclusions about neuronal polarity require ultrastructural analyses, even the distinction between both types of terminal specializations was not always clear. Intracellularly filled neurons and Golgi-stained neurons of the same type had occasionally different appearances in terminal regions of fine branches (Müller et al., 1997), possibly due to restricted abilities of different dyes to reach into fine processes or to swelling or shrinking artifacts during the different tissue processing procedures.

The largest columnar neurons of the central complex (CPU1a–c, CPU2) had smooth arborizations in the PB and in all layers of the CBU and projected to overlapping areas in the ventral shell of the LAL. These neurons were unique in these features, showed pronounced polarity, and are, therefore, likely to serve as major outputs from the central complex to the ventral shells of the LALs. CPU1-like neurons have also been found in *Drosophila* (Hanesch et al., 1989), in the honeybee (Homberg, 1985), and in the meal beetle *Tenebrio* (Wegerhoff et al., 1996), and argue for a conserved output pathway from the central complex to the LAL. Another possible output pathway from the

CBU is provided by CU2a-, CU2b-, and CU3-type columnar neurons connecting layer I with the dorsal shell of the LAL, but without ramifications in the PB. This again corresponds with data from *Drosophila*, in which all neurons that send fibers outside the central complex exclusively projected to the LAL and had only varicose terminals in this region (Hanesch et al., 1989). When considering possible input into the CBU from the PB, only layers II and III receive projections with bleb-like endings (CPU4/5). In addition, dorsal layers of the noduli may provide input to CBU layer II via CPU5 neurons. Interestingly, the proposed direction of information flow within the CBU through pontine neurons is mainly from layer III to layer I. CU1 neurons connecting layer I of the CBU to the anterior lip might provide another possible output from the central complex.

Direct connections from the PB to the LAL served the lateral triangle and the medial olive of the LAL, suggesting that these neurons provide feedback to input areas of the central complex (Homberg et al., 2003; Pfeiffer et al., 2005). Whereas CL2 neurons provided input to the CBL from the PB and to the lower division of the noduli, CL1a/b/c neurons might mediate complex bidirectional information flow between the CBL and the PB, in addition to a minor output to the lateral triangle. The sole output from the CBL might be provided via CL1a neurons (Table 1), which points to extensive signal convergence in the CBL. However, their possible postsynaptic endings were present in only one layer of the CBL, which raises the question about the postsynaptic elements in the other layers.

In summary, neurons with columnar arborization domains are either intrinsic elements of the central complex or candidate output neurons, which target the LALs and the anterior lip as output areas. None of the neurons presented appeared to provide input into the central complex. Our data, therefore, support earlier suggestions by Hanesch et al. (1989) and Homberg (2004) that columnar neurons are the principal output elements of the central complex, whereas the second major category of neurons, tangential neurons, may provide input signals.

Right-left connectivity patterns. All the cells presented are likely part of isomorphic sets of neurons, consisting of 16 individual cells (or multiples thereof), with the possible exception of CPU1b neurons, which appeared to occur only in columns R7 and L7 with two individual neurons each. Immunocytochemical studies provided evidence for at least seven isomorphic sets of columnar neurons and two sets of pontine cells (Homberg, 1991; Dircksen and Homberg, 1995; Vitzthum et al., 1996; Vitzthum and Homberg, 1998; Kurylas et al., 2005).

In the CBL, CL1 and CL2 neurons constitute two similar but nevertheless distinct connectivity schemes between columns of the PB and CBL. In both cell types, each hemisphere of the PB was projected onto the complete width of the CBL, meaning that neighboring CBL columns connected to columns R8/L1, R7/L2, etc. However, the innervated CBL columns were exactly inverted in CL2 neurons compared with CL1 neurons. Hence the lateralmost column of the PB is linked to the lateralmost ipsilateral column of the CBL in CL1 cells, but to the second-lateralmost column in CL2 neurons. Both connectivity schemes are supported by detailed analysis of the locust w-bundle projections (Williams, 1972). Whether corresponding neurons in *Drosophila* (Hanesch et al., 1989) and bees (only CL1-like cells; Homberg, 1985) follow the same connectivity schemes as in locusts remains to be determined.

At least six isomorphic sets of columnar neurons connected the PB to the CBU (CPU1a, CPU1c, CPU2, CPU4a/b/c, and likely CPU5a/b/c). Three of these (CPU4a/b/c) followed a connectivity scheme very similar to that of CL1 neurons. In *Drosophila*, the vertical fiber system, like the CPU4 neurons, connects the PB to the CBU and the noduli (Hanesch et al., 1989), but unlike in the locust, no crossing-over occurs between the PB and the CBU in *Drosophila*. Individual examples of this type of neuron have also been shown in *Musca* by Strausfeld (1976), but the connectivity scheme in *Musca* has not been resolved. CPU1a, CPU1c, and CPU2 neurons were unique in their connectivity schemes. CPU1a neurons connected columns of the PB and CBU in a pattern strikingly similar to that of the horizontal fiber system of *Drosophila* (Hanesch et al., 1989). CPU2 neurons, instead, connected corresponding columns in the PB and CBU, whereas CPU1c neurons differed from both of these neurons, but the limited number of stained cells did not allow us to extrapolate a complete connectivity scheme. Overall, each type of neuron seems to follow a unique connectivity pattern, which can presently not be related to known functions of these cells in an obvious way.

Finally, the 16 columns of the PB may not be completely equal with regard to number of neurons and connectivity patterns. Support for this notion is largely based on CPU1a/b neurons, with CPU1b neurons only existing in columns R7/L7, and CPU1a neurons possibly connecting the lateralmost columns of the PB to the ipsilateral LAL instead of the contralateral one. These examples illustrate that one has to be cautious when extrapolating isomorphic sets of neurons from few examples of individually filled cells.

Species-specific differences

In addition to locusts, the central complex has been studied in some detail in (*D. melanogaster* (Hanesch et al., 1989), *M. domestica* (Strausfeld, 1976), the honeybee *A. mellifera* (Homberg, 1985), and the meal beetle *Tenebrio molitor* (Wegerhoff et al., 1996). In all of these species, the overall organization of the central complex is highly similar. In the most detailed study to date, Hanesch et al. (1989) described 20 small-field neurons in the central complex of *Drosophila*. These included 17 types of columnar neuron, two types of pontine neuron, and one type of amacrine neuron. In the present study we presented 21 types of columnar neuron, three types of pontine cell, and one amacrine cell. A comparison between the fly and the locust shows not only the same general classes of neurons in both species (Table 1) but also strikingly similar numbers of cell types in each class. This is all the more remarkable, as both studies were carried out with different methods, Golgi impregnations in the fly versus intracellular dye injections in the locust.

Despite these similarities, differences are found at the level of single cell types. Hence not all cell types had their respective counterparts in both studies (Table 1). Corresponding with the anatomical specialization of the CBL in flies (circular arrangement of columns), most differences in neuronal cell types are associated with this structure. Three times as many columnar neurons were associated with the ellipsoid body in the fly as with the CBL in the

The Journal of Comparative Neurology

locust, and all types found in the locust were also present in *Drosophila*. Besides our observation that no neurons link the CBL directly to the CBU, locusts also lack neurons connecting two distant parts of the ellipsoid body (CBL) with the PB, or neurons exclusively linking the noduli to the ellipsoid body (CBL), as shown in *Drosophila* (Hanesch et al., 1989). Differences between the assumed locust-*Drosophila* counterparts (Table 1) concern details such that the *Drosophila* CL1-like neurons project to the ventral bodies and not to the lateral triangles, and CL2-like cells to the ipsilateral nodulus rather than to the contralateral one.

Within the CBU, comparison between species is more difficult, as the present study is the first to report in detail on the innervated layers, and definition of neuronal subtypes was often based on this information. Nevertheless, most of the locust CBU neurons have been found in *Drosophila* as well (CPU1a, CPU3, CPU4, and cells similar to CPU5; Table 1). Some differences are still apparent: CBU arborizations of CPU1 and CPU3 neurons were only varicose in the locust, but the corresponding type in *Drosophila* was reported with mixed terminals. The three subtypes of CPU5 neurons corresponded to a set of cells that were only partly similar. These cells lack PB arborizations in *Drosophila* and appear to differ with regard to the invaded CBU layer. A cell type similar to CU2 neurons was also described by Hanesch et al. (1989), but the fly neurons projected to the lateral triangle rather than to the LAL (Table 1).

The only type of neuron not found in *Drosophila* were all types of neurons with bifurcating axons (CPU2, CU1, and CU3), and both types of cells directly linking the PB to the LAL (CP1/2). These neurons, therefore, might be specializations of the locust, a secondary loss in *Drosophila*, or they were not stained in the Golgi preparations. In the larger fly *Musca*, also using Golgi impregnations, bifurcating columnar neurons were reported by Strausfeld (1976), which might suggest that similar cell types are present in *Drosophila* as well. Finally, pontine neurons of similar appearance were found by Hanesch et al. (1989) in *Drosophila* as well as by Homberg (1985) in bees. One type of pontine neuron, which connected adjacent columns of the CBU, was only found in *Drosophila*.

How many neurons comprise the central complex?

Based on embryological and immunohistochemical data, the central complex of the desert locust is comprised of roughly 3,600 small-field neurons (60 sets of 16 neurons) and an unknown number of tangential neurons. One way to estimate the proportion of neurons we might have missed is a comparison with embryonic data on the locust central complex. Williams et al. (2005) showed that neurons from each of the w-, x-, y-, and z-bundles can be traced to single protocerebral neuroblasts. Estimating that each neuroblast divides up to 60 times (Williams and Boyan, 2008), this results in a total upper estimate of 100–120 cells per bundle and, thus, 50–60 neurons per column. On a first account this number is considerable higher than the 25 types of neurons per column in the present study. However, when we consider immunocytochemical studies, it becomes clear that many types of neurons are represented by more than one individual cell per column. Several sets of columnar/pontine neurons in the locust have been described by using antisera against the neurotransmitter candidates serotonin (Homberg, 1991), CCAP (Dircksen and Homberg, 1995), Dip-allatostatin (Vitzthum et al., 1996), Lom-TK (Vitzthum and Homberg, 1998), and a histochemical staining for NADPH-diaphorase indicating the presence of nitric oxide (Kurylas et al., 2005; Table 1).

A group of about 60 serotonin-immunoreactive cells (S1 in Homberg, 1991) closely resembles CPU4 neurons. These neurons selectively invade NoU layer II (CPU4b) and are distinct from CPU4c cells projecting to NoU layer III (Fig. 8). A subset of about 48 of these cells showed Dip-allatostatin immunostaining (Vitzthum et al., 1996). CPU4c neurons, instead, are likely to correspond to a group of 48 cells labeled for NADPH-diaphorase (Kurylas et al., 2005). Together, at least eight sets of CPU4 cells appear to exist: four CPU4b, containing serotonin and, in a subset, Dip-allatostatin; three CPU4c, containing NADPH-diaphorase, and at least one set of CPU4a. Another set of cells (ASC1), stained by using Dip-allatostatin antisera, resembles CU1 neurons. However, arborizations in the PB that have been attributed to these cells by Vitzthum et al. (1996), could not be unambiguously confirmed in more recent preparations in our laboratory. Endings in the PB are not present in CU1 cells, but cannot be completely excluded in several fragmentary stainings.

Altogether, the set of ASC1 cells consists of 12 fibers per bundle, corresponding to 6 fibers per column. Four sets of columnar cells were also found with Lom-TK immunostaining (Vitzthum and Homberg, 1998). Two of these (16 cells each) roughly match the morphologies of CL1a/b neurons, with one system having large somata and one having small somata. However, all of these cells have axons to the lateral triangle, and one system has considerably smaller axon diameters than any of the three neuron types reported here. Considering this, it appears likely that there are at least four sets of these neurons. This number matches with the 64 CCI neurons described by Williams (1975), which correspond to CL1-like cells. The other two systems of Lom-TK-immunoreactive cell types could not be reconstructed completely and are hence difficult to compare with individual neuron morphologies. Arborizations were found in the PB, in layers I and II of the CBU, and in the dorsal shell of the LAL. Eight large and 16 small somata were described in the pars intercerebralis. Thus, some of these cells possibly correspond to neurons of the CU class, whereas the Lom-TK-immunoreactive arborizations in the PB might belong to an unidentified type of cell.

Together with the observation in double labelings of two CPU5a- and two CL2 cells per column, a minimum number of 33 columnar neurons should occur in each column of the PB except R7 and L7. These two columns contain two additional CPU1b neurons each, raising the number of columnar fibers to 35. In addition, we found three types of pontine cells and one amacrine cell of the CBU, which also arise from somata in the pars intercerebralis. The number of pontine cells can be partly extrapolated from CCAP and NADPH-diaphorase staining. About 48 neurons with arborizations in layer I and anterior neurites stain with CCAP antisera and are likely to correspond to type 2 pontine cells. A potentially overlapping set of about 45 cells (layer I and II, anterior and posterior neurites) are labeled for NADPH-diaphorase. Thus, at least one set of PoU1 and PoU3 cells and three sets of PoU2 cells exist. Hence, a total number of 39 (or 41 in R7 and L7) neurons

per column can be extrapolated from the present data. Additionally, Williams (1972) found neurons in the w-bundle that innervate the upper noduli division without central-body arborizations, as well as neurons with small axon diameter, which end in neighboring columns of the CBL. Neither of these cell types has been found in the present study.

Comparing our total number of 39–41 cells per column with the rough estimate of the upper limit of 60 neurons per column, it becomes clear that we might know at least about two-thirds of all small field neurons of the locust central complex. The missing cells could be multiples of known types of cells and if not, are likely to have small diameters, as our method of intracellular staining is biased toward large neurons.

Sensory processing and functional role of the central complex

Most neurons described here were filled during intracellular recordings intended to characterize visual response properties, in particular responses to polarized light. Accordingly, data on the physiology of these neurons are biased toward their role in visual processing. Most of the neurons with small neurites have not been recorded directly, but have been colabeled with recorded neurons.

No functional data exist for CPU3 and CPU5 neurons, all CU neurons, and the amacrine cell. A neuron similar to CU1 showed increased activity during manipulation of the forewing and during flight, suggesting proprioreceptive input and a possible role in flight control (Homberg, 1994). All remaining cell types responded at least weakly to visual stimuli. CPU1a, CPU1b, CPU1c, CPU2, CL1, CP1, and CP2 neurons responded to changing *E*-vector orientations during zenithal stimulation with a rotating polarization filter (Vitzthum et al., 2002; Heinze and Homberg, 2007; Heinze and Homberg, in preparation). In CPU1a, CPU1b, and CP neurons the *E*-vector tuning corresponded with the position of the arborization tree in the PB. As a result, a compass-like arrangement of zenithal *E*-vector orientations covering roughly 180° is represented in the eight columns of each hemisphere of the PB. Because zenithal *E*-vectors provide direct information on the sun's azimuth, activity in these systems of neuron provides direct information on the position of the sun along the horizon relative to the locust's head orientation (Heinze and Homberg, 2007). Most of the remaining cell types (pontine cells and CL2 neurons) responded weakly, but not consistently, to polarized light, as well as to unpolarized light flashes (unpublished data). Variable responses were found for CL2 neurons, including flight-associated excitation (Müller, 1997), responses to polarized and unpolarized light (Heinze, unpublished data), and no visual responses (Müller, 1997), pointing toward a context-dependent recruitment of these neurons. Strong phasic light responses on top of weaker tonic responses were shown for a single PoU1 cell (Müller, 1997), whereas another PoU1 and a PoU3 neuron responded weakly to polarized light (unpublished data). In bees, weak visual and mechanosensory responses were reported for CPU1-like, CL1-like, and pontine neurons (Homberg, 1985).

Overall, the reported neurons clearly have a role in higher order visual processing. At least some neurons appear to process mechanosensory stimuli, perhaps in an azimuth-related fashion. In *Drosophila* a role of tangential neurons in the memory for visual object parameters and in spatial orientation memory has been reported (Liu et al., 2006; Neuser et al., 2008). These sensory aspects of central-complex functions are easily reconciled with the proposed role of the central complex in motor coordination (Strausfeld, 1999; Strauss, 2002), and, together with the topographic representation of azimuthal space underlying the columnar organization of the locust PB (Heinze and Homberg, 2007), point to a key role of the central complex in spatial orientation and motor planning. How the establishment of azimuthal maps, integration of multimodal sensory information, and a possible sensory motor transition is achieved on a cellular level is unknown. The catalogue of neurons in the central complex presented in this study provides first insights into possible patterns of information flow and candidate synaptic partners based on overlapping arborization areas.

ACKNOWLEDGMENTS

We thank Dr. Erich Buchner for supplying anti-synapsin antibodies, Sascha Gotthardt for providing the reconstructions of Figures 10A and E, Dr. Les Williams for insightful discussions, Basil el Jundi for assistance with Amira, and Stephan Gebhardt, Sascha Gotthardt, Harm Vitzthum, and Monika Müller for dye-filled neurons.

LITERATURE CITED

Bausenwein B, Wolf R, Heisenberg M. 1986. Genetic dissection of optomotor behavior in *Drosophila melanogaster* studies on wild-type and the mutant *optomotor-blind*^{H31}. J Neurogenet 3:87–109.

Brandt R, Rohlfing T, Rybak J, Krofczik S, Maye A, Westerhoff M, Hege H, Menzel R. 2005. Three-dimensional average-shape atlas of the honeybee brain and its applications. J Comp Neurol 492:1–19.

Colonnier M. 1964. The tangential organization of the visual cortex. J Anat 98:327–344.

Dietl MJ. 1876. Die Organisation des Arthropodengehirns. Z Wiss Zool 27:488–517.

Dircksen H, Homberg U. 1995. Crustacean cardioactive peptide-immunoreactive neurons innervating brain neuropils, retrocerebral complex and stomatogastric nervous system of the locust, *Locusta migratoria*. Cell Tissue Res 279:495–515.

Goll W. 1967. Strukturuntersuchungen am Gehirn von *Formica*. Z Morphol Ökol Tiere 59:143–210.

Gregory GE. 1980. The Bodian protargol technique. In: Strausfeld NJ, Miller TA, editors. Neuroanatomical techniques. New York: Springer. p 75–95.

Hanesch U, Fischbach KF, Heisenberg M. 1989. Neuronal architecture of the central complex in *Drosophila melanogaster*. Cell Tissue Res 257: 343–366.

Heinze S, Homberg U. 2007. Maplike representation of celestial E-vector orientations in the brain of an insect. Science 315:995–997.

Hoffmann K, Wirmer A, Kunst M, Gocht D, Heinrich R. 2007. Muscarinic excitation in grasshopper song control circuits is limited by acetylcholinesterase activity. Zool Sci 24:1028–1035.

Homberg U. 1985. Interneurons of the central complex in the bee brain *Apis mellifera*. J Insect Physiol 31:251–264.

Homberg U. 1991. Neuroarchitecture of the central complex in the brain of the locust *Schistocerca gregaria* and *S. americana* as revealed by serotonin immunocytochemistry. J Comp Neurol 303:245–254.

Homberg U. 1994. Flight-correlated activity changes in neurons of the lateral accessory lobes in the brain of the locust *Schistocerca gregaria*. J Comp Physiol A 175:597–610.

Homberg U. 2002. Neurotransmitters and neuropeptides in the brain of the locust. Microsc Res Techn 56:189–209.

Homberg U. 2004. In search of the sky compass in the insect brain. Naturwissenschaften 91:199–208.

Homberg U. 2008. Evolution of the central complex in the arthropod brain with respect to the visual system. Arthropod Struct Dev 37:347–362.

Homberg U, Würden S. 1997. Movement-sensitive, polarization-sensitive, and light-sensitive neurons of the medulla and accessory medulla of the locust, *Schistocerca gregaria*. J Comp Neurol 386:329–346.

Homberg U, Hofer S, Pfeiffer K, Gebhardt S. 2003. Organization and neural connections of the anterior optic tubercle in the brain of the locust, *Schistocerca gregaria*. J Comp Neurol 462:415–430.

Huber F. 1960a. Experimentelle Untersuchungen zur nervösen Atmungsregulation der Orthopteren (Saltatoria: Gryllidae). Z Vgl Physiol 43: 359–391.

Huber F. 1960b. Untersuchungen über die Funktion des Zentralnervensystems und insbesondere des Gehirnes bei der Fortbewegung und der Lauterzeugung der Grillen. Z Vgl Physiol 44:60–132.

Ilius M, Wolf R, Heisenberg M. 1994. The central complex of *Drosophila melanogaster* is involved in flight control: studies on mutants and mosaics of the gene ellipsoid body open. J Neurogenet 9:189–206.

Klagges BR, Heimbeck G, Godenschwege TA, Hofbauer A, Pflugfelder GO, Reifegerste R, Reisch D, Schaupp M, Buchner S, Buchner E. 1996. Invertebrate synapsins: a single gene codes for several isoforms in *Drosophila*. J Neurosci 16:3154–3165.

Kurylas AE, Ott SR, Schachtner J, Elphick MR, Williams L, Homberg U. 2005. Localization of nitric oxide synthase in the central complex and surrounding midbrain neuropils of the locust *Schistocerca gregaria*. J Comp Neurol 484:206–223.

Kurylas AE, Rohlfing T, Krofczik S, Jenett A, Homberg U. 2008. Standardized atlas of the brain of the desert locust, *Schistocerca gregaria*. Cell Tissue Res 333:125–145.

Leitinger G, Pabst MA, Rind FC, Simmons PJ. 2004. Differential expression of synapsin in visual neurons of the locust *Schistocerca gregaria*. J Comp Neurol 480:89–100.

Liu G, Seiler H, Wen A, Zars T, Ito K, Wolf R, Heisenberg M, Liu L. 2006. Distinct memory traces for two visual features in the *Drosophila* brain. Nature 439:551–556.

Martin JR, Raabe T, Heisenberg M. 1999. Central complex substructures are required for the maintenance of locomotor activity in *Drosophila melanogaster*. J Comp Physiol A 185:277–288.

Mobbs PG. 1985. Brain structure. In: Kerkut GA, Gilbert LI, editors. Comprehensive insect physiology biochemistry and pharmacology, vol. 5. Nervous system: structure and motor function. Oxford: Pergamon, p 299–370.

Müller M. 1997. Anatomische und funktionelle Charakterisierung der unteren Einheit des Zentralkörpers im Gehirn der Heuschrecke *Schistocerca gregaria*. PhD Thesis, University of Regensburg, Germany.

Müller M, Homberg U, Kühn A. 1997. Neuroarchitecture of the lower division of the central body in the brain of the locust (*Schistocerca gregaria*). Cell Tissue Res 288:159–176.

Nässel DR. 1993. Neuropeptides in the insect brain: a review. Cell Tissue Res 273:1–29.

Nässel DR, Homberg U. 2006. Neuropeptides in interneurons of the insect brain. Cell Tissue Res 326:1–24.

Neuser K, Triphan T, Mronz M, Poeck B, Strauss R. 2008. Analysis of a spatial orientation memory in *Drosophila*. Nature 453:1244–1247.

Panov AA. 1959. Structure of the insect brain at successive stages of postembryonic development. II. The central body. Entomol Rev 38: 276–284.

Pfeiffer K, Kinoshita M, Homberg U. 2005. Polarization-sensitive and light-sensitive neurons in two parallel pathways passing through the anterior optic tubercle in the locust brain. J Neurophysiol 94:3903–3915.

Power ME. 1943. The brain of *Drosophila melanogaster*. J Morphol 72:517–559.

Ridgel AL, Alexander BE, Ritzmann RE. 2007. Descending control of turning behavior in the cockroach, *Blaberus discoidalis*. J Comp Physiol A 193:385–402.

Ritzmann RE, Ridgel AL, Pollack AJ. 2008. Multi-unit recording of antennal mechano-sensitive units in the central complex of the cockroach, *Blaberus discoidalis*. J Comp Physiol A 194:341–60.

Sakura M, Lambrinos D, Labhart T. 2008. Polarized skylight navigation in insects: model and electrophysiology of e-vector coding by neurons in the central complex. J Neurophysiol 99:667–682.

Schildberger K. 1983. Local interneurons associated with the mushroom bodies and the central body in the brain of *Acheta domesticus*. Cell Tissue Res 230:573–586.

Schipper J, Tilders FJ. 1983. A new technique for studying specificity of immunocytochemical procedures: specificity of serotonin immunostaining. J Histochem Cytochem 31:12–18.

Strausfeld NJ. 1976. Atlas of an insect brain. New York: Springer.

Strausfeld NJ. 1980. The Golgi method: its application to the insect nervous system and the phenomenon of stochastic impregnation. In: Strausfeld NJ, Miller TA, editors. Neuroanatomical techniques. New York: Springer. p 131–203.

Strausfeld NJ. 1999. A brain region in insects that supervises walking. Prog Brain Res 123:273–284.

Strauss R. 2002. The central complex and the genetic dissection of locomotor behaviour. Curr Opin Neurobiol 12:633–638.

Strauss R, Heisenberg M. 1993. A higher control center of locomotor behavior in the *Drosophila* brain. J Neurosci 13:1852–1861.

Vitzthum H, Homberg U. 1998. Immunocytochemical demonstration of locustatachykinin-related peptides in the central complex of the locust brain. J Comp Neurol 390:455–469.

Vitzthum H, Homberg U, Agricola H. 1996. Distribution of Dip-allatostatin I-like immunoreactivity in the brain of the locust *Schistocerca gregaria* with detailed analysis of immunostaining in the central complex. J Comp Neurol 369:419–437.

Vitzthum H, Müller M, Homberg U. 2002. Neurons of the central complex of the locust *Schistocerca gregaria* are sensitive to polarized light. J Neurosci 22:1114–1125.

Wegerhoff R, Breidbach O. 1992. Structure and development of the larval central complex in a holometabolous insect, the beetle *Tenebrio molitor*. Cell Tissue Res 268:341–358.

Wegerhoff R, Breidbach O, Lobemeier M. 1996. Development of locustatachykinin immunopositive neurons in the central complex of the beetle *Tenebrio molitor*. J Comp Neurol 375:157–166.

Wenzel B, Kunst M, Günther C, Ganter GK, Lakes-Harlan R, Elsner N, Heinrich R. 2005. Nitric oxide/cyclic guanosine monophosphate signaling in the central complex of the grasshopper brain inhibits singing behavior. J Comp Neurol 488:129–139.

Williams JLD. 1972. Some observations on the neuronal organization of the supra-oesophageal ganglion in *Schistocerca gregaria* Forskål with particular reference to the central complex. PhD Thesis, University of Wales.

Williams JLD. 1975. Anatomical studies of the insect central nervous system: a ground-plan of the midbrain and an introduction to the central complex in the locust, *Schistocerca gregaria* (Orthoptera). J Zool Lond 176:67–86.

Williams JLD, Boyan GS. 2008. Building the central complex of the grasshopper *Schistocerca gregaria*: axons pioneering the w, x, y, z tracts project onto the primary commissural fascicle of the brain. Arthropod Struct Dev 37:129–140.

Williams JLD, Güntner M, Boyan GS. 2005. Building the central complex of the grasshopper *Schistocerca gregaria*: temporal topology organizes the neuroarchitecture of the w, x, y, z tracts. Arthropod Struct Devel 34:97–110.

Maplike representation of celestial E-vector Orientations in the brain of an insect

8. G. Giannone *et al.*, *Cell* **116**, 431 (2004).
9. N. Watanabe, T. J. Mitchison, *Science* **295**, 1083 (2002).
10. G. Danuser, R. Oldenbourg, *Biophys. J.* **79**, 191 (2000).
11. T. M. Svitkina *et al.*, *J. Cell Biol.* **160**, 409 (2003).
12. A. Mallavarapu, T. Mitchison, *J. Cell Biol.* **146**, 1097 (1999).
13. J. A. Theriot, T. J. Mitchison, L. G. Tilney, D. A. Portnoy, *Nature* **357**, 257 (1992).
14. G. H. Patterson, J. Lippincott-Schwartz, *Science* **297**, 1873 (2002).
15. Materials and methods are available as supporting material on *Science* Online.
16. T. Nishizaka, Q. Shi, M. P. Sheetz, *Proc. Natl. Acad. Sci. U.S.A.* **97**, 692 (2000).
17. C. G. Galbraith, K. M. Yamada, M. P. Sheetz, *J. Cell Biol.* **159**, 695 (2002).
18. W. B. Kiosses, S. J. Shattil, N. Pampori, M. A. Schwartz, *Nat. Cell Biol.* **3**, 316 (2001).
19. D. P. Felsenfeld, P. L. Schwartzberg, A. Venegas, R. Tse, M. P. Sheetz, *Nat. Cell Biol.* **1**, 200 (1999).
20. N. A. Medeiros, D. T. Burnette, P. Forscher, *Nat. Cell Biol.* **8**, 215 (2006).
21. A. Horwitz, K. Duggan, C. Buck, M. C. Beckerle, K. Burridge, *Nature* **320**, 531 (1986).
22. J. A. DePasquale, C. S. Izzard, *J. Cell Biol.* **113**, 1351 (1991).
23. C. A. Otey, F. M. Pavalko, K. Burridge, *J. Cell Biol.* **111**, 721 (1990).
24. D. M. Suter, P. Forscher, *J. Cell Biol.* **155**, 427 (2001).
25. D. Bentley, A. Toroian-Raymond, *Nature* **323**, 712 (1986).
26. D. Choquet, D. P. Felsenfeld, M. P. Sheetz, *Cell* **88**, 39 (1997).
27. T. P. Loisel, R. Boujemaa, D. Pantaloni, M. F. Carlier, *Nature* **401**, 613 (1999).

28. We thank C. Smith and T. Reese for suggestions on the experiments and manuscript and M. Sheetz for use of optical trap data collected by C.G.G. while in his laboratory. For use of the laser scanning microscopes, we thank the National Institute of Neurological Disorders and Stroke (NINDS) Light Imaging Facility for the LSM 510 (VIS/405) and Carl Zeiss, Inc., for the LSM 5 LIVE and LSM 5 DUO. We also thank Z. Iwinski for confocal software; E. Shumsky, R. Engelmann, and S. Tille for assistance; G. Patterson and J. Lippincott-Schwartz for PaGFP and discussions; and M. Hoffman for assistance with reverse transcription–polymerase chain reaction studies. Reagents provided by R. Tsien (mRFP), J. Wehland (EGFP-VASP), and S. Yamada (human foreskin fibroblasts). Support provided by the intramural research programs of NINDS and National Institute of Dental and Craniofacial Research, NIH.

Supporting Online Material

www.sciencemag.org/cgi/content/full/315/5814/992/DC1
Materials and Methods
Figs. S1 to S5
References
Movies S1 to S4

2 November 2006; accepted 5 January 2007
10.1126/science.1137904

Maplike Representation of Celestial *E*-Vector Orientations in the Brain of an Insect

Stanley Heinze and Uwe Homberg*

For many insects, the polarization pattern of the blue sky serves as a compass cue for spatial navigation. *E*-vector orientations are detected by photoreceptors in a dorsal rim area of the eye. Polarized-light signals from both eyes are finally integrated in the central complex, a brain area consisting of two subunits, the protocerebral bridge and the central body. Here we show that a topographic representation of zenithal *E*-vector orientations underlies the columnar organization of the protocerebral bridge in a locust. The maplike arrangement is highly suited to signal head orientation under the open sky.

Many animals, including birds, fishes, cephalopods, and arthropods, share the ability to perceive linearly polarized light (*1*, *2*). The plane of polarization (*E*-vector) varies systematically across the blue sky and depends on the Sun's position. For a variety of insects this pattern has been shown to guide spatial orientation (*2*). In locusts, polarotactic orientation depends on a specialized part of the compound eye, the dorsal rim area (*3*), and involves several central processing stages, including the central complex (*4*–*7*). The central complex (CC) is a group of neuropils spanning the midline of the insect brain. Substructures are the protocerebral bridge (PB) and the upper and lower divisions of the central body. An outstanding anatomical feature of the CC is its regular and highly sophisticated internal neuroarchitecture (*8*–*10*). In simplified terms, it consists of stacks of arrays, each composed of a linear arrangement of 16 columns with topographic interhemispheric connections between columns both within and between different arrays. Hypotheses on the functional roles of the CC range from a control center for motor coordination (*11*) to a recently demonstrated involvement in visual pattern learning and recognition (*12*). In the locust, several cell types of the CC are sensitive to the orientation of zenithal *E*-vectors (*5*), but the correspondence of cell morphology and *E*-vector tuning has remained obscure. In this study, we have used intracellular recordings combined with dye injections to analyze *E*-vector tuning in CC neurons of the locust with columnar arborization domains.

Two major classes of polarization-sensitive (POL) neurons were encountered regularly when we recorded from CC neurons: (i) a particular type of tangential neuron of the PB and (ii) several types of columnar neurons. Tangential neurons of the PB, termed here TB1 neurons, have not been described previously in the locust or any other insect. A total number of 18 of these cells were analyzed. Their morphology was revealed by iontophoretic tracer injection, histological processing, and camera lucida reconstruction (*13*). TB1 neurons provide a connection between a posterior brain region, the posterior optic tubercle, and the PB (Fig. 1, A and B). Each TB1 neuron had two domains of varicose and, thus, putatively presynaptic arborizations confined to a single column in each hemisphere of the PB. When PB columns are numbered as L1 (lateralmost column in the left hemisphere of the PB) to L8 (most medial column in the left hemisphere) and, accordingly, from R1 to R8 in the right hemisphere of the bridge, TB1 neurons with varicose ramifications in columns R1/L8, R2/L7, R4/L5, R5/L4, R6/L3, and R7/L2 were encountered. Varicose processes were always eight columns apart, with processes ipsilaterally in one of the four outer columns and contralaterally in one of the four inner columns (Fig. 1E). The columns neighboring those with varicose processes were free of ramifications, and six to eight other columns were invaded with fine, smooth arborizations. Furthermore, all TB1 neurons had varicose arborizations in the posterior optic tubercle, a brain area connected to a small neuropil in the optic lobe, the accessory medulla (*14*).

The pattern of varicose arborizations in the PB corresponded to physiological properties of the TB1 neurons. For intracellular recordings, the animals were fixed in the recording setup and stimulated from the zenith with a rotating *E*-vector. Recordings were obtained from their main neurite in the PB. Each TB1 neuron showed polarization opponency, i.e., *E*-vector orientations leading to an increase in spiking activity (excitation) were oriented perpendicularly to *E*-vectors, leading to a decrease in spiking activity (inhibition) (Fig. 1, C and D). The *E*-vector tuning (*E*-vector orientation resulting in maximum excitation, Φ_{max}) was determined for each neuron by circular statistics [Rayleigh test (*15*)]. *E*-vector tuning of TB1 neurons showed a linear relation to the position of their varicose ramifications in the PB (Fig. 1F). Thereby, a range of Φ_{max} tunings of 182° ± 71° extends through the eight columns of each hemisphere of the PB and, thus, corresponds to the whole range of possibly occurring *E*-vector orientations.

Because the *E*-vector map in the PB corresponds with the proposed output regions of the TB1 neurons, we asked whether candidate postsynaptic neurons show a similar representation of *E*-vector tuning. Columnar neurons have ar-

Animal Physiology, Department of Biology, Philipps University, 35032 Marburg, Germany.

*To whom correspondence should be addressed. E-mail: homberg@staff.uni-marburg.de

REPORTS

borizations in single columns of the PB and send axonal projections to an area outside the CC, the lateral accessory lobe (LAL). Several cell types have additional arborizations in distinct columns of the central body. Three types of these neurons are polarization-sensitive (Fig. 2). We evaluated the data from 19 recordings from these cell types, termed CPU1, CP1, and CP2 neurons. CPU1 neurons have smooth endings in single columns of the PB, in columns of the dorsalmost layer I of the upper division of the central body (CBU), and an axonal fiber with varicose endings in the LAL (Fig. 2A). Each neuron connects a single column of the PB with two neighboring columns of the CBU, following a wiring scheme described for *Drosophila* (*9*) (Fig. 2G). All CPU1 neurons (10 recordings) showed polarization opponency and background spiking activity of 20 to 40 Hz. Comparison of the innervated columns in the PB and Φ_{max} tuning again revealed a spatial representation of *E*-vector orientations across the PB, which covered a range of 228° ± 73° through the 8 PB columns in one brain hemisphere (Fig. 2I). The slope of the regression lines of TB1 and CPU1 neurons did not differ significantly [$P = 0.32$, analysis of covariance (*16*)], indicating that the tuning range through the 16 columns of the bridge matched for both cell types. However, the CPU1 map was shifted by 101° (equivalent to −79°) relative to the map of TB1 neurons (significantly different elevation of regression lines, $P < 0.0001$).

The remaining two types of columnar neurons, CP1 and CP2 neurons, also connected the PB with the LAL (Fig. 2, B, C, and H), but lacked arborizations in the central body. Within the LAL, projections were confined to either of two subcompartments, the median olive (CP1) or the lateral triangle (CP2). Both types of neuron had smooth arborizations in the PB and varicose endings in the LAL. In all recordings ($n = 9$), CP1 and CP2 neurons showed polarization opponency, but had lower background activity (3 to 15 Hz) than CPU1 and TB1 neurons. As for CPU1 and TB1 neurons, regression analysis of pooled data from CP1 and CP2 neurons revealed a linear correlation between the innervated column in the PB and the *E*-vector tuning of the neurons (Fig. 2J). The linear regression for CP1 and CP2 covered a range of 206° ± 76° over one hemisphere (eight columns) of the PB and was not significantly different from the linear regression for CPU1 neurons (slope: $P = 0.4777$, elevation: $P = 0.3525$). It was, however, phase-shifted by 111° (equivalent to −69°) against the map of TB1 neurons.

The present study shows, independently for three different cell types, that a map of zenithal *E*-vector orientations underlies the columnar organization of the locust PB. This spatial representation adds a level of complexity to sensory processing in the insect brain, hitherto thought to be achieved only in vertebrates. In most neurons at least half-maximal activation occurred over an *E*-vector orientation range of about 60°, implying considerable overlap for neighboring columns and the necessity of a population code for retrieving exact information from the firing rates of these cells (*17*).

Under the open sky, the activity in the POL neurons described here is directly related to the directional orientation of the locust's head, provided that additional mechanisms (color coding, intensity coding) allow the animal to distinguish the solar from the antisolar hemisphere of the sky. Color-coding properties suited to fulfill this requirement have been demonstrated recently for POL neurons at an input stage to the CC, the anterior optic tubercle (*18*). Neurons encoding head direction have been intensely studied in mammals (*19*, *20*). An important difference of the locust polarization analyzers in the CC is their global nature of signaling. The neurons fire according to zenithal *E*-vectors, which provide information about the Sun's azimuth and, therefore, these neurons behave like an internal 180° compass. In rats, in contrast, head-direction cells are recalibrated to visual landmarks in each new environment and are apparently not arranged topographically (*21*, *22*).

Although some progress has been made in analyzing the wiring principles from which computational maps arise in vertebrates (*23*, *24*), the simple brains of locusts offer the opportunity to address this question at the level of single identified neurons. Within the PB, the spatial maps of tangential and columnar neurons are out of phase by about 90°. If TB1 neurons are directly connected to the columnar neurons, a phase shift of 90° might most easily result from inhibitory connections of TB1 neurons to the dendritic

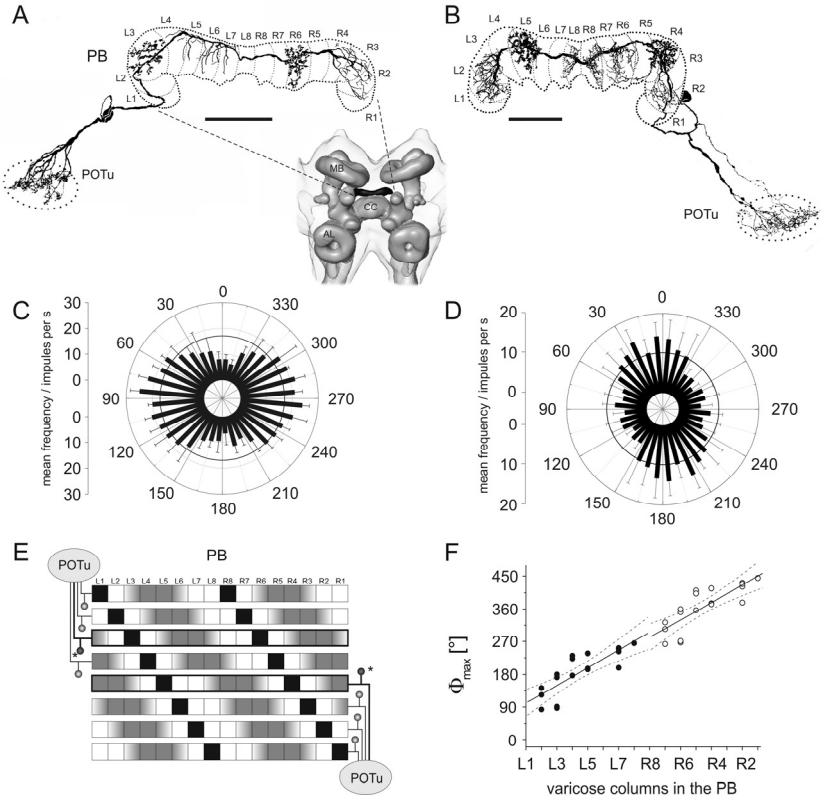

Fig. 1. Morphological and physiological properties of TB1 neurons. (**A** and **B**) Frontal reconstructions of two TB1 neurons; inset shows frontal view of the locust midbrain. Scale bars, 100 μm. (**C** and **D**) Circular plots of mean firing rate during *E*-vector rotations for the neuron in (A) [(C)] and (B) [(D)] ($n = 4$, bin width 10°; error bars: SD). Solid lines indicate background activity. (**E**) Wiring scheme of the TB1 neuron system. Each line represents one TB1 neuron in the PB (black squares: columns with varicose arborizations; gray squares: columns with smooth arborizations; white squares: columns without arborizations). Asterisks indicate TB1 neurons shown in (A) and (B). (**F**) Correlation between location of varicose columns in the PB and *E*-vector tuning (Φ_{max}) of TB1 neurons ($n = 18$). Because each neuron has varicose arborizations in single columns in the right and left PB hemisphere, Φ_{max} values were plotted twice for the right hemisphere (open circles) and the left hemisphere (filled circles). Linear regression shows significant correlation ($r = 0.81$, SD = 35.8°, $P < 0.0001$, two-tailed t test, $y = 24.2x + 77.0$). Also shown are 95% confidence bands (*13*). AL, antennal lobe; CC, central complex; MB, mushroom body; PB, protocerebral bridge; POTu, posterior optic tubercle.

trees of columnar neurons. Double-labeling experiments showed that serotonin and a Dip-allatostatin–related neuropeptide are present in TB1 neurons (fig. S5). For both substances, inhibitory effects have been demonstrated in other systems (*25*, *26*). Whereas azimuthal space is linearly represented in the columns of the PB, the wiring of CPU1 neurons should result in a superposition of the two 180° representations of the PB in the CBU, but with a lateral shift of about 50° (fig. S3). The functional consequences of this shift are presently unknown. If the *E*-vector tunings of corresponding CPU1 neurons in each of the eight double columns of the CBU are merged, the azimuth representation would be reduced to only about 156° of frontal space.

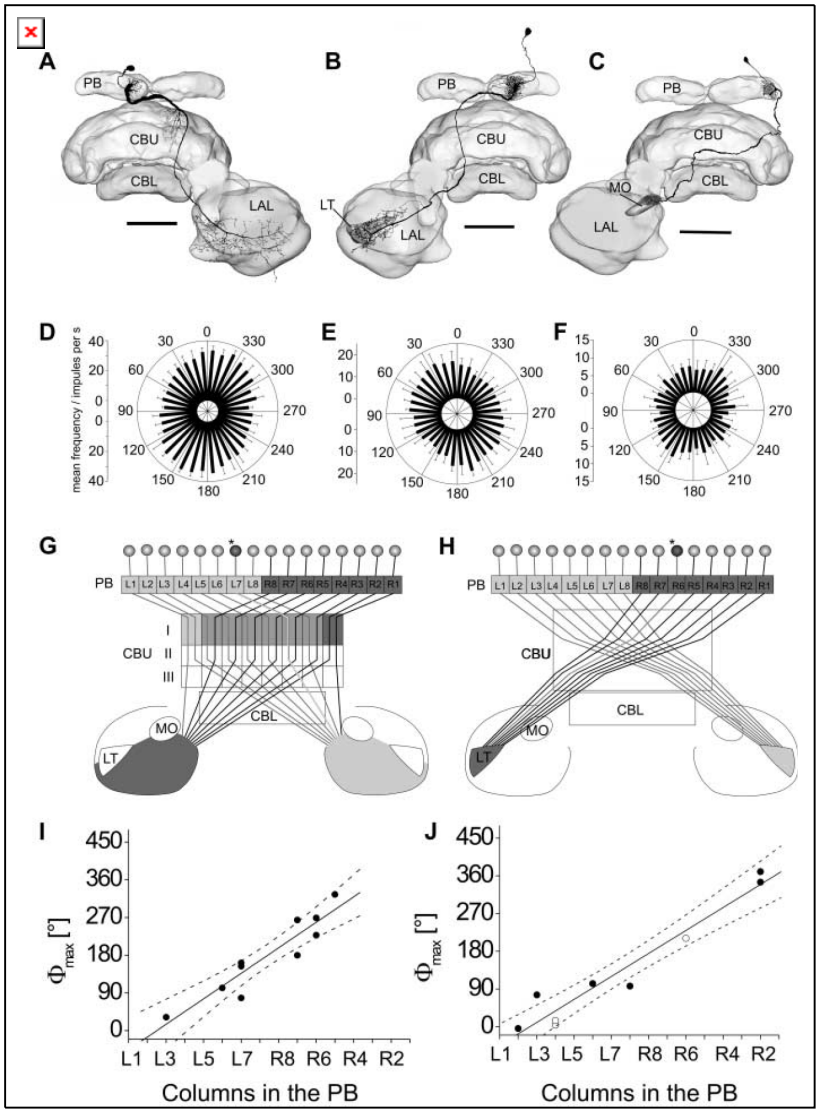

Fig. 2. Morphology and physiology of columnar neurons. (**A** to **C**) Camera lucida drawings of a CPU1 neuron (A), CP2 neuron (B), and CP1 neuron (C) projected onto three-dimensional reconstructions of the central complex. Scale bars, 100 μm. (**D** to **F**) Circular plots of mean firing rate during *E*-vector rotations for the neurons shown in (A) to (C) (n = 4, bin width 10°; error bars: SD). (**G** and **H**) Wiring schemes of the CPU1 neuron system and the CP2 neuron system. Asterisks indicate the CPU1 neuron shown in (A) [(G)] and the CP2 neuron shown in (B) [(H)]. The CP1 neuron system (not shown) projects to the MO but is otherwise identical to the CP2 system. (**I** and **J**) Linear correlation between the location of the columnar arborization domain in the PB and the *E*-vector tuning (Φ_{max}) of columnar neurons. (I) CPU1 neurons (r = 0.93, SD = 36.5°, P = 0.0001, two-tailed t test, $y = 30.4x - 76.2$). Midline crossing occurs at 182°. (J) CP1 neurons (open circles) and CP2 neurons (filled circles) have been combined for statistical analysis (r = 0.97, SD = 38.0°, $P < 0.0001$, two-tailed t test, $y = 27.4x - 61.8$). Midline crossing occurs at 171°. Confidence bands are shown at 95%. CBL, CBU, lower and upper divisions of the central body; LAL, lateral accessory lobe; LT, lateral triangle; MO, median olive; PB, protocerebral bridge.

On the basis of the data presented here and a recent paper by Liu *et al.* (*12*), a coherent functional role for the CC is emerging. In *Drosophila*, tangential neurons innervating specific layers of the central body are essential for recognizing features of visual objects (elevation in the panorama; contour orientation). Columnar neurons, like the CPU1 neurons, are ideal candidates to associate these visual features with information on their azimuthal direction (fig. S4). Liu *et al.* (*12*) already hypothesized that the width of the CBU represents azimuthal space. This is strongly supported by our data, but this representation may differ between cell types and CC substructures as pointed out above.

References and Notes

1. R. Wehner, *J. Exp. Biol.* **204**, 2589 (2001).
2. G. Horváth, D. Varjú, *Polarized Light in Animal Vision: Polarization Patterns in Nature* (Springer, Berlin, 2004).
3. M. Mappes, U. Homberg, *J. Comp. Physiol. A* **190**, 61 (2004).
4. M. Mappes, U. Homberg, *J. Comp. Physiol. A* **193**, 43 (2007).
5. H. Vitzthum, M. Müller, U. Homberg, *J. Neurosci.* **22**, 1114 (2002).
6. U. Homberg, S. Hofer, K. Pfeiffer, S. Gebhardt, *J. Comp. Neurol.* **462**, 415 (2003).
7. K. Pfeiffer, M. Kinoshita, U. Homberg, *J. Neurophysiol.* **94**, 3903 (2005).
8. J. L. D. Williams, *J. Zool. London* **176**, 67 (1975).
9. U. Hanesch, K. F. Fischbach, M. Heisenberg, *Cell Tissue Res.* **257**, 343 (1989).
10. M. Müller, U. Homberg, A. Kühn, *Cell Tissue Res.* **288**, 159 (1997).
11. R. Strauss, *Curr. Opin. Neurobiol.* **12**, 633 (2002).
12. G. Liu *et al.*, *Nature* **439**, 551 (2006).
13. Material and methods are available as supporting material on *Science* Online.
14. U. Homberg, S. Würden, *J. Comp. Neurol.* **386**, 329 (1997).
15. E. Batschelet, *Circular Statistics in Biology* (Academic Press, London, 1981).
16. J. Zar, *Biostatistical Analysis* (Prentice-Hall, Englewood Cliffs, NJ, 1999).
17. E. I. Knudsen, S. du Lac, S. Esterly, *Annu. Rev. Neurosci.* **10**, 41 (1987).
18. K. Pfeiffer, M. Kinoshita, U. Homberg, *Proceedings of the 6th Meeting of the German Neuroscience Society* (www.neuroanatomie.uni-goettingen.de/neurobio_archiv/2005/pdf/Proceedings-Goettingen2005.pdf), p. 218.
19. P. E. Sharp, H. T. Blair, J. Cho, *Trends Neurosci.* **24**, 289 (2001).
20. J. S. Taube, J. P. Bassett, *Cereb. Cortex* **13**, 1162 (2003).
21. F. Sargolini *et al.*, *Science* **312**, 758 (2006).
22. H. Mittelstaedt, *Biol. Cybern.* **83**, 261 (2000).
23. H. J. Chisum, D. Fitzpatrick, *Neural Netw.* **17**, 681 (2004).
24. F. Mooser, W. H. Bosking, D. Fitzpatrick, *Nat. Neurosci.* **7**, 872 (2004).
25. W. Blenau, A. Baumann, *Arch. Insect Biochem. Physiol.* **48**, 13 (2001).
26. E. M. Tan *et al.*, *Neuron* **51**, 157 (2006).
27. We thank S. Gebhardt, S. Gotthardt, K. Pfeiffer, and H. Vitzthum for contributing physiological data; K. Pfeiffer for help with data evaluation; A. Kurylas for providing three-dimensional reconstructions of brain structures; and E. Buchner for providing the antibody to synapsin. This work was supported by the Deutsche Forschungsgemeinschaft (grants HO 950/14-3 and HO 950/16-1).

Supporting Online Material

www.sciencemag.org/cgi/content/full/315/5814/995/DC1
Material and Methods
Figs. S1 to S5
References

25 September 2006; accepted 4 January 2007
10.1126/science.1135531

www.sciencemag.org/cgi/content/full/315/5814/995/DC1

Supporting Online Material for

Maplike Representation of Celestial *E*-Vector Orientations in the Brain of an Insect

Stanley Heinze and Uwe Homberg*

*To whom correspondence should be addressed. E-mail: homberg@staff.uni-marburg.de

Published 16 February 2007, *Science* **315**, 995 (2007)
DOI: 10.1126/science.1135531

This PDF file includes:

Science **Supporting online material**

Map-like representation of celestial *E*-vector orientations in the brain of an insect

Stanley Heinze & Uwe Homberg

Animal Physiology, Department of Biology, Philipps University, 35032 Marburg, Germany

Contents

Material and Methods

Animals.

Experiments were performed on 37 adult desert locusts (*Schistocerca gregaria*) of both sexes from a crowded laboratory colony. Locusts were waxed to a holder as described (S1). After removal of the legs and wings, the head was opened frontally and the brain was exposed. The brain was supported from posterior with a small metal platform that also served as indifferent electrode. To allow penetration of the recording electrode, the neurilem was mechanically removed. During recording the brain was constantly bathed in locust saline (S2).

2

Visual stimuli.

Visual stimuli were produced by passing light from a xenon arc (XBO 150 W) through a standard glass light guide and a rotating polarizer. Stimuli were presented from the zenith, had an irradiance of 94 μW/m², and appeared at an angular size of 2.7°. For testing polarization sensitivity the polarizer was rotated through 360° (in one experiment 180°) in both directions with an angular velocity of 21°/s.

Electrophysiology.

Microelectrodes (resistance: 60 – 150 MΩ) were drawn from borosilicate capillaries. Their tips were filled with 4% Neurobiotin in 1 M KCl and backed up with 1 M KCl. Signals were amplified (10x) with a custom-built amplifier, sampled at 25 kHz with a Digidata 1322A, and stored on a personal computer using pClamp9. After recording, Neurobiotin was injected iontophoretically into the recorded neuron with a constant depolarizing current (3 nA, 1 - 2 min).

Histology.

After recording, brains were dissected out of the animals, fixed over night at 4° C, and incubated for three days with Cy3-conjugated Streptavidin at a concentration of 1:1000. Brains were dehydrated in ethanol, cleared in methylsalicylate, and mounted in Permount between coverslides. For detailed analysis, preparations were rehydrated in a decreasing ethanol series, embedded in albumin/gelatine, sectioned at 40 μm with a vibrating blade microtome, and incubated with Streptavidin conjugated with horseradish peroxidase (1:200), followed by staining with 3,3'-diaminobenzidine tetrahydrochloride (DAB) as described by Vitzthum et al. (S3). DAB-stained neurons were reconstructed using a light microscope with camera lucida attachment. Three-dimensional reconstructions of the locust brain were performed with Amira3.1. Image stacks were obtained using a confocal microscope. Detailed images of the central complex were scanned from thick slice preparations (200 μm, 20x objective) immunolabelled with anti-synapsin (kindly provided by E. Buchner, University of Würzburg, Germany). Whole brain reconstructions were

obtained from wholemount preparations (10x objective) immunolabelled with anti-synapsin. For visualization of neuronal ramifications, 3D-reconstructions and camera lucida reconstructions were projected onto each other.

Evaluation of morphologies.

To determine the identity of innervated columns, we evaluated the boundaries of the PB with differential interference contrast optics (DAB-stained preparations), anti-synapsin-staining (Cy3-fluorescent preparations with anti-synapsin counterstaining), or unspecific background staining. As neighboring columns are not separated by visible structures, their individual identity was inferred from the location of the brain midline, the overall length of the PB, and the exit sites of major axonal tracts projecting from the PB to the CBU.

Data analysis.

Spike trains were analysed with custom-designed scripts in Spike2-software. Relative times of action potentials were evaluated with a threshold-based detection algorithm. During stimulation with the rotating polarizer, each spike was assigned to its corresponding *E*-vector angle. Neurons were regarded as polarization-sensitive if the distribution of these *E*-vector angles differed significantly from randomness (Rayleigh test for axial data (S4); $\alpha = 0.05$, software Oriana 2.0). The mean vector of the distribution was defined as the preferred *E*-vector orientation (Φ_{max}) of that neuron.

E-vector orientations (Φ_{max}-values) are bidirectional axial data with a periodicity of 180° and can, therefore, be plotted from 0°-180° or from 180°-360°. In a first step of analysis of the spatial representation of *E*-vector tuning of columnar neurons we consequently plotted each Φ_{max}-value twice, as x (ranging from 0°-180°) and as x+180° (ranging from 180°-360°) against their columnar arborization domains (Fig. S1). This led to three approximately linear and parallel bands of data points and, thus, suggests a linear correlation between Φ_{max}-values and columnar arborization domains throughout the 16 columns of the PB. For a statistical analysis of the data, Φ_{max}-values from neurons with arborizations in the left hemisphere were, therefore, plotted in the range from 0°-180° and

4

Φ_{max}-values from neurons with arborizations in the right hemisphere in the range from 180°-360°.

As TB1-neurons have one varicose columnar arborization domain in each hemisphere of the PB, only the data covering one hemisphere were evaluated statistically. Because of the morphology of these neurons (varicose columns are strictly 8 columns apart from each other) data points for the second hemisphere of the bridge are identical to those of the first one. Hence the 180°-shift for the right hemisphere in Fig. 1F has been performed to provide easier comprehensiveness and the same format as used in Fig. 2. Analysis of linear correlation between the columnar arborization domains of the neurons and their Φ_{max}-values was performed with the linear fit tool in Origin 6.0. It calculated the correlation coefficient r, the 95% confidence bands and performed a two-tailed t-test. The confidence bands indicate that at an α-level of 0.05 the mean y-values (here Φ_{max}) for any given x-value (here columns or relative distance) lie within the confidence bands. The correlation was rated significantly different from 0 if the p-value of the t-test was below the significance level of 0.05. The resulting regression line was used to calculate the *E*-vector range of one PB hemisphere and the intersection point with the brain midline. Phase-shifts between different functions were determined at the intersection with the brain midline. Doubled standard deviations are indicated as errors of the *E*-vector-range for each regression function.

The residues of each linear regression were tested for normality with the Shapiro-Wilk-Test (performed with XLSTAT 2006 Version 2006.2). The test is regarded as the most reliable test for non-normality for small to medium sample sizes (S5). No significant indications of non-normality could be found for any neuron type (p-values: TB1: 0.262, CPU1: 0.140, CP: 0.903). Regression lines of different neuron types were compared using GraphPadPrism4.0. The resulting (two-tailed) p-values were derived from a method equivalent to ANCOVA analysis as described (S6). The slopes and intercepts of two regression lines were rated significantly different if p-values were below 0.05.

To test for the reliability of column identification, we evaluated the position of the arborizations with a second method. We measured the distance of arborization centers from the midline (summed distance in XY- and Z-direction) and normalized these distances

5

for the total length of the PB. These values were plotted with respect to the left end of the PB (left end, 0; midline, 0.5; right end, 1; shown in Fig. S2). Comparison with the columnar plots (Figs. 1, 2) show that both methods provide virtually identical results. For comparison of the slopes of the linear regressions with those in Figs. 1 and 2, slope values of Fig. S2 have to be divided by 15, because x-values in Figs 1 and 2 range from 1-16.

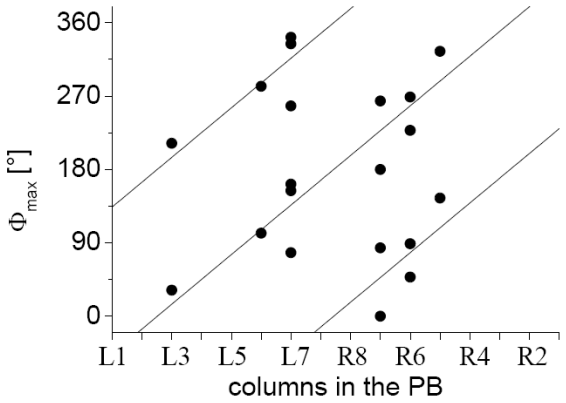

Fig. S1. Correlation between Φ_{max}–values and columnar arborizations of CPU1-neurons. Each data point is plotted twice, first in the range of 0°-180° and second in the range of 180°-360°, as described in the supplementary methods. Superimposed on the data is the linear regression line obtained from one complete dataset plus the corresponding lines shifted by ±180° (equation: y = 30.4x – 76.2).

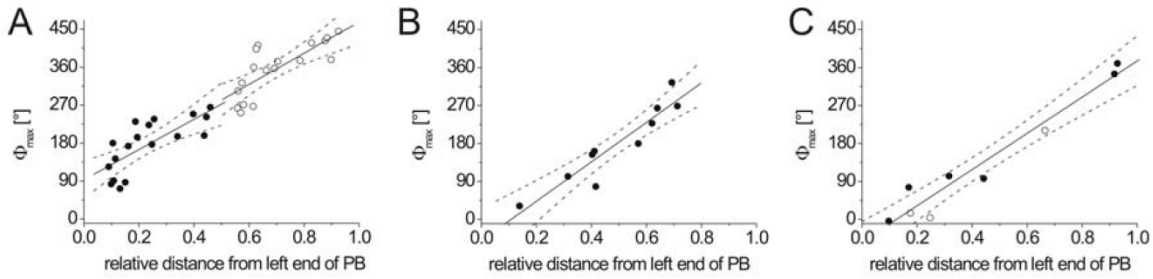

Fig. S2. Linear correlations between *E*-vector tuning (Φ_{max}) and relative distance of columnar arborization from the left end of the protocerebral bridge. **(A)** TB1-neurons. Details for left hemisphere: r = 0.75, SD = 42.7°, p < 0.001, two-tailed t-test, y = 358.9x + 93.0. Right hemisphere: r = 0.77, SD = 40.7, p < 0.001, y = 369.6x + 97.4. **(B)** CPU1-neurons: r = 0.93, SD = 35.2, p < 0.0001, y = 468x - 50.7. Midline crossing occurs at 183.3°. **(C)** CP-neurons (filled circles, CP1-neurons; open circles, CP2-neurons): r = 0.97, SD = 35.3, p < 0.0001, y = 429.8x - 53.8. Midline crossing occurs at 161.1°. Confidence bands are shown at 95%.

6

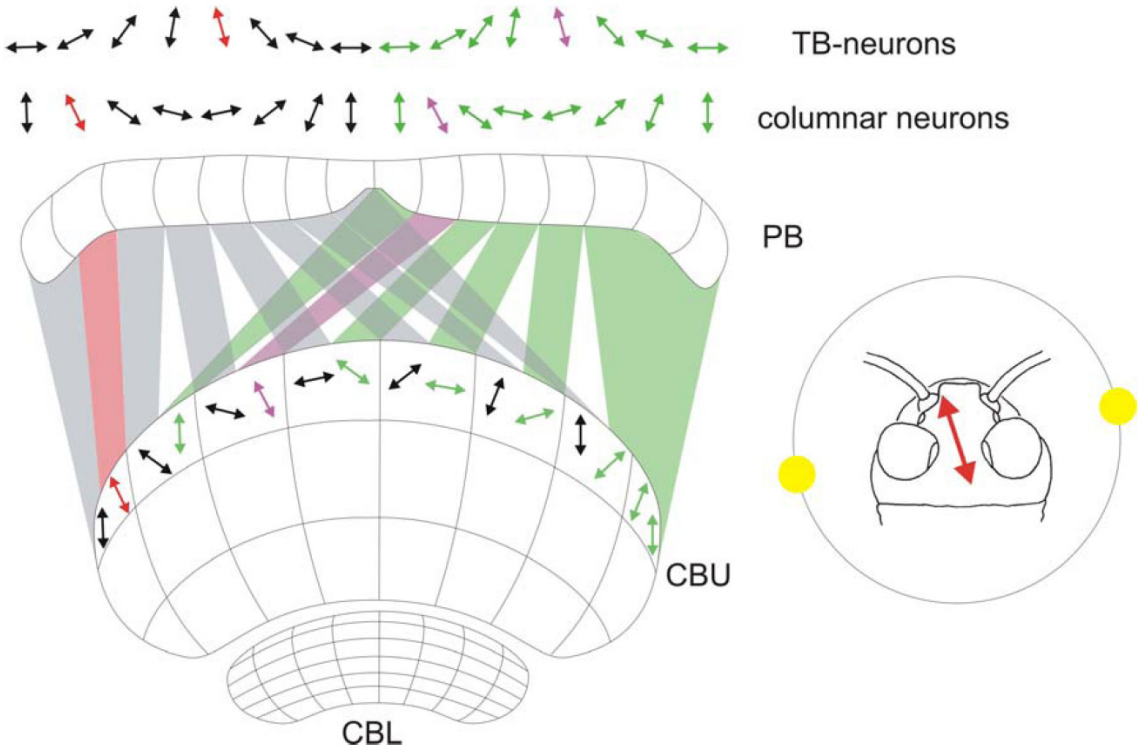

Fig. S3. Summary of the main findings of the paper. *E*-vector orientations of polarized light, shown to the animal from the zenith, are represented in a topographical manner within the columns of the protocerebral bridge (PB). Neurons with ramifications in a particular column respond maximally to a certain *E*-vector. Over the range of the PB each possibly ocurring *E*-vector is represented twice, with neighboring columns differing by an angle of approximately 26°. The maps of TB-neurons and columnar neurons are out of phase by about 90°, which means that at any given stimulus situation the column with maximal activity for TB1-neurons corresponds to the column with minimal activity for columnar neurons. The columnar map is projected onto the upper unit of the central body (CBU) by columnar CPU1-neurons. Here the twofold representation of the PB is superimposed and shifted laterally by about 50°. When the locust is stimulated with a certain *E*-vector (right side), it follows that activity is highest in the highlighted (red and violet) columns of the central complex. This enables the animal to determine the direction it faces relative to the sun, as long as the solar and antisolar side of the sky can be determined by other means.

7

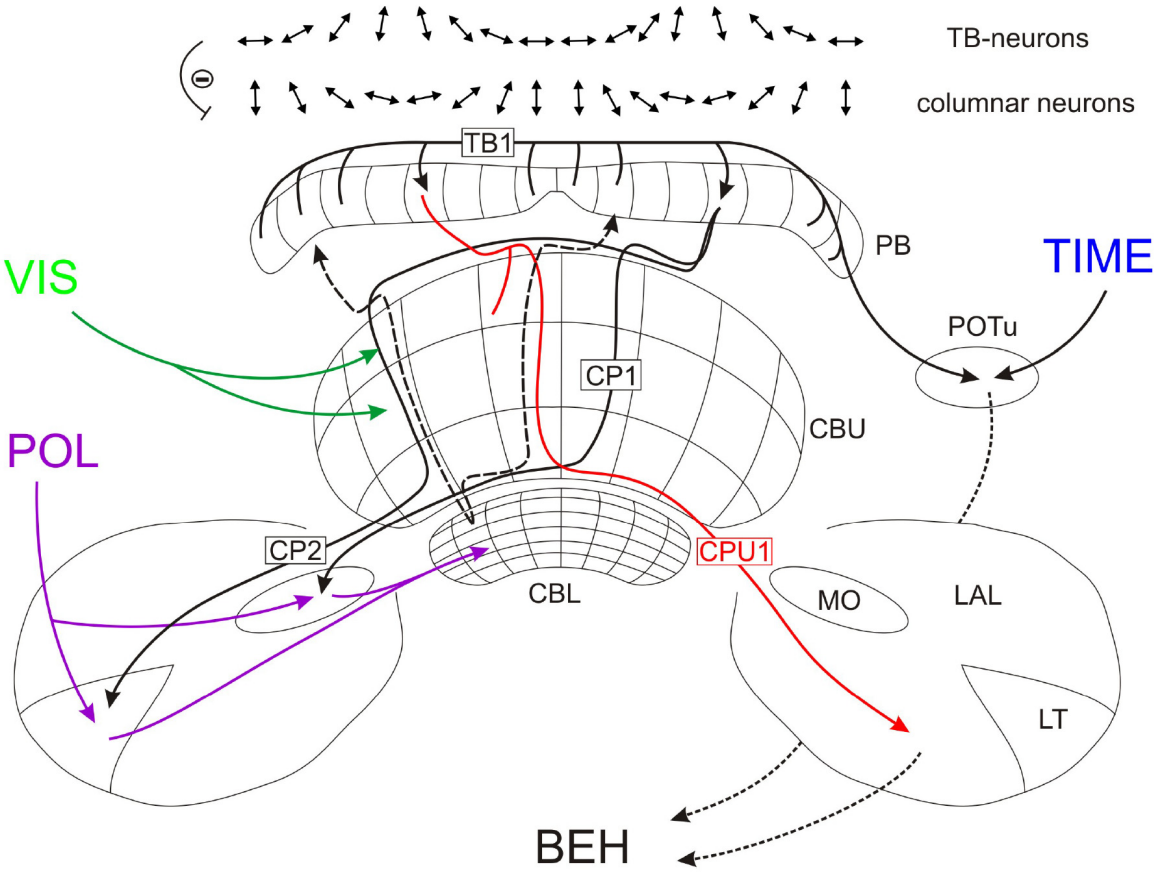

Fig. S4. Proposed network of the central complex in the locust. Two computational maps of *E*-vector orientations are present in the columns of the PB. As both maps cover the same range but are out of phase by about 90°, an inhibitory connection between TB1 and columnar neurons is most likely. When the animal is stimulated with a certain *E*-vector (e.g. the one highlighted) neurons of a single column in each hemisphere are maximally activated in each map. Although it is not clear how these maps are generated within the brain, we can put forward the general outline of a possible wiring scheme of the POL-network in the central complex. Polarized-light information enters the central complex via the medial olive (MO) and the lateral triangle (LT) (S1) and is further relayed to the lower division of the central body (CBL) (S3). It is not known how *E*-vector information enters the PB, but we postulate a connection between the CBL and the PB (dashed lines). TB1-neurons integrate *E*-vector information from several columns and transmit it further to feedback loops (CP1 and CP2-neurons) and to CPU1 neurons. CPU1 neurons (red) are suited to integrate visual information present in the layers of the CBU (VIS, green) (S7), and thus provide one of several outputs of the central complex to the LAL. Together with a possible output pathway from the posterior optic tubercle (POTu), information is finally transferred to descending neurons that guide behaviour (BEH). Inputs from the proposed circadian clock (accessory medulla, TIME) to the POTu (S8) point to a possible time compensation pathway. For simplification only neurons connected with one TB1-neuron are shown. Input neurons are shown only for the left hemisphere and proposed output connections are shown for the right hemisphere only.

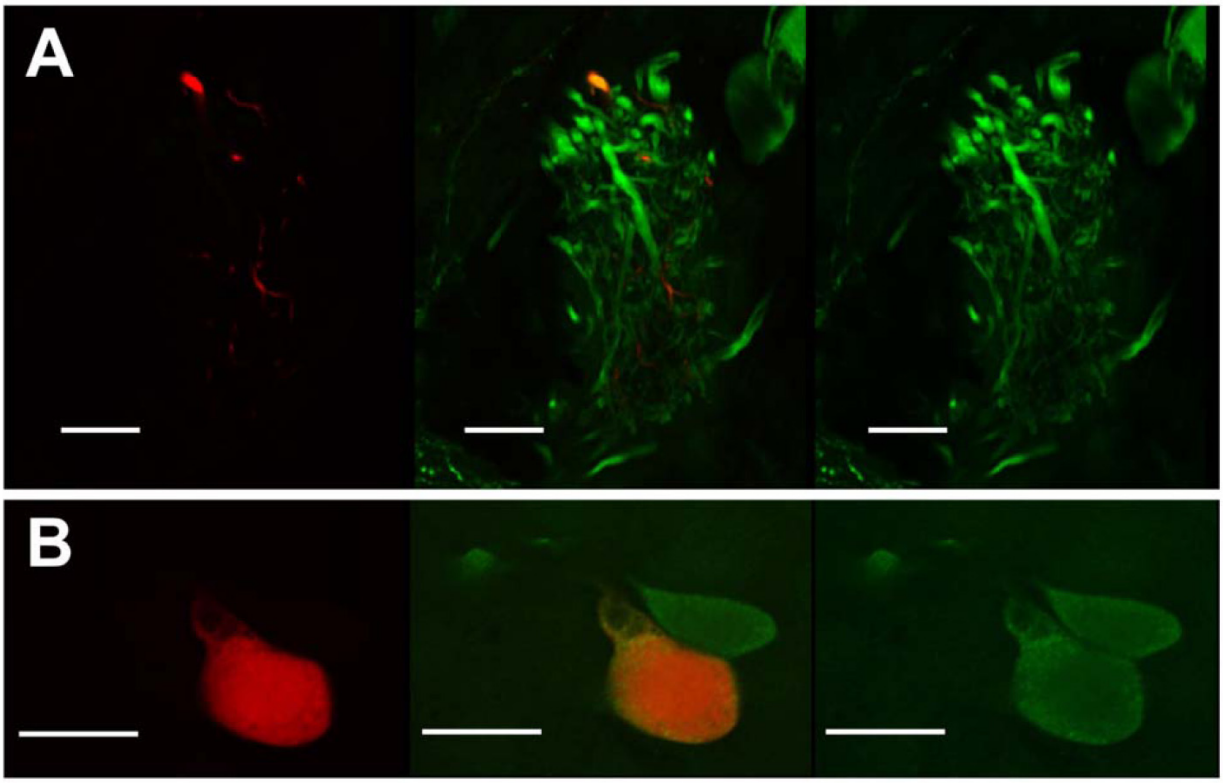

Fig. S5. Demonstration of serotonin immunostaining (green fluorescence; rabbit anti-serotonin, detected with Cy2-conjugated goat-anti-rabitt) in a TB1-neuron (red fluorescence, Neurobiotin-injected, Cy3-conjugated Streptavidin). Single frontal optical sections (0.5 µm) from confocal image stacks. **(A)** Colabelling in tangential projections within the protocerebral bridge. **(B)** Double-labelled soma of the injected neuron. Scale bars, 20µm. All serotonin-immunoreactive TB1-neurons are also Dip-allatostatin-immunoreactive (S9).

References

S1. K. Pfeiffer, M. Kinoshita, U. Homberg, *J. Neurophysiol.* **94**, 3903 (2005).

S2. A. Clements, T. May, *J. Exp. Biol.* **60**, 673 (1974).

S3. H. Vitzthum, M. Müller, U. Homberg, *J. Neurosci.* **22**, 1114 (2002).

S4. E. Batschelet, *Circular Statistics in Biology*. (Academic Press, London, 1981).

S5. W. J. Conover, *Practical Nonparametric Statistics*, (Wiley, 1999).

S6. J. Zar, *Biostatistical Analysis*. (Prentice Hall, 1999).

S7. G. Liu *et al*., *Nature* **439**, 551 (2006).

S8. U. Homberg, S. Würden, *J. Comp. Neurol.* **386**, 329 (1997).

S9. H. Vitzthum, U. Homberg, H. Agricola, *J. Comp. Neurol.* **369**, 419 (1996).

Linking the input to the output - New sets of neurons complement the polarization vision network in the locust central complex

Behavioral/Systems/Cognitive

Linking the input to the output – new sets of neurons complement the polarization vision network in the locust central complex.

Stanley Heinze[1] and Uwe Homberg[1*]

[1]Fachbereich Biologie, Tierphysiologie, Philipps-Universität Marburg, D-35032 Marburg, Germany

Polarized light is a key feature of the blue sky, used by many animals as a sensory cue for compass navigation. Like other insects, locusts perceive the *E*-vector orientation of polarized light with a specialized region of their compound eye, the dorsal rim area. Neurons in the brain relay this information through several processing stages to the central complex. The central complex consists of several subunits. It has a modular neuroarchitecture, composed of vertical columns and horizontal layers. Several types of central-complex neuron respond to dorsally presented, rotating *E*-vectors with tonic modulation of their firing frequency. These POL-neurons occur at the input stage of the central complex, as well as near the proposed output stage, where neurons are tuned to form a compass-like representation of *E*-vector orientations underlying the columnar organization of the central complex. To identify neurons suited to link input and output elements, we recorded intracellularly from 45 neurons of the central complex. We report several novel types of POL-neuron. One of these is suited to fill the gap between input and output stages of the central-complex POL-network. Three types of neuron were sensitive to polarized light in only 50% of experiments suggesting that they are recruited to the network depending on the behavioral context. Finally, we identified two types of neuron suited to transfer information toward thoracic motor circuits. The data underscore the key role of two subunits of the central complex, the lower division of the central body and the protocerebral bridge, in sky compass orientation.

Key words: neural network; insect brain; polarization vision; central complex; compass navigation; locust

Introduction

Many animals rely on a sky compass for spatial orientation during seasonal migration or homing. A major source of sky compass information is the polarization pattern of the blue sky (Labhart and Meyer, 2002; Horváth and Varjú, 2004). As a result of sunlight scattering, light from the blue sky is partially polarized with celestial *E*-vectors arranged along concentric circles around the sun. The significance of sky polarization for spatial orientation has been established for honeybees (Frisch, 1949) and desert ants (Wehner, 1984), but orientation responses to dorsally presented polarized light have been demonstrated also in flies, crickets, beetles, and locusts (Wehner and Labhart, 2006). Like other insects, locusts perceive polarized light with a specialized area of their compound eye, the dorsal rim area (Mappes and Homberg, 2004). The dorsal rim area faces the sky and is equipped with photoreceptors of high polarization sensitivity (Eggers and Gewecke, 1993). Photoreceptor axons project to dorsal areas in the lamina and medulla and to further stages of the polarization vision system, including the anterior lobe of the lobula, the anterior optic tubercle, the lateral accessory lobe (LAL), and the central complex (Homberg, 2004).

The central complex is a group of neuropils in the center of the protocerebrum. It consists of the protocerebral bridge (PB), the upper and lower divisions of the central body (CBU, CBL), and the paired noduli (Williams, 1975). The central complex has a unique modular neuroarchitecture, characterized by 16 vertical columns and several horizontal layers in the central body (Heinze and Homberg, 2008). The arrangement of layers and columns is generated by columnar and tangential neurons (Heinze and Homberg, 2008). Three types of tangential neuron connect two small areas of the LALs, the lateral triangle and the medial olive, to the CBL (Müller et al., 1997). These neurons are highly sensitive to the *E*-vector orientation of dorsally presented polarized light and respond to a rotating polarizer with tonic modulation of their firing rate (Vitzthum et al., 2002). Each cell is maximally excited when stimulated with a particular, preferred *E*-vector (Φ_{max}), and is maximally inhibited at an *E*-vector 90° different from Φ_{max} (polarization opponency). Electron microscopy showed that these tangential cells are input neurons to the CBL (Müller,

This work was supported by DFG grant HO 950/16-2.We are grateful to Dr. Keram Pfeiffer for providing Spike2-scripts for data analysis and to Dr. Keram Pfeiffer, Stephan Gebhardt, and Sascha Gotthardt for contributing to physiological data on CL1 cells. We thank Sebastian Richter and Manfred Peil for constructing the stimulation devices and control equipment and Karl Heinz Herklotz for raising desert locusts.

[*]Correspondence to: Uwe Homberg, Fachbereich Biologie, Tierphysiologie, Universität Marburg, D-35032 Marburg, Germany, Tel. +49-6421-2823402, Fax +49-6421-2828941, E-mail: homberg@staff.uni-marburg.de

1997), but their postsynaptic partners have not been identified yet.

At another level of the central complex, the PB, tangential and columnar cells form an an ordered array of *E*-vector orientation columns (Heinze and Homberg, 2007). Neurons connecting the polarization-vision pathway from the CBL to the PB have, however, not been identified. In the present study we characterize two novel types of POL-neuron in the central complex, one of which is a likely candidate for linking the CBL inputs to the PB. Three additional types of neuron were polarization-sensitive in 50% of the recordings, suggesting state dependent recruitment to the core polarization vision network. Finally, we identified candidate elements connecting the polarization vision network of the central complex to descending pathways.

Materials and Methods

Preparation of animals. Locusts (*Schistocerca gregaria*) were raised in crowded colonies at the University of Marburg in a 12L:12D photoperiod at constant temperature (28°C). Adult animals of both sexes were used 1-3 weeks after imaginal moult. They were cold anesthetized at 4°C for 15-30 minutes and were waxed onto a metal holder. In some preparations animals were fixed to the holder with tape for increased stability. Legs and wings were removed and stumps were sealed with wax or glue to prevent hemolymph leakage. The head capsule was opened frontally and the brain was freed of surrounding trachea and fat body. Most muscles in the head capsule were transected. In most preparations, antennal nerves were cut and antennae were removed. To increase stability, the oesophagus was transected and the gut was removed from the opened abdomen, which was resealed either using petroleum jelly or a tightly knotted thread. The animal was then mounted either in a horizontal or vertical orientation in the recording setup. For upright mountings, the brain was supported with a metal holder inserted ventrally. For horizontal mountings, the brain was supported with a wax/wire platform, which was inserted ventrally and waxed to the head. The latter preparation left the frontal field of view open for stimulus display. Either the metal support platform or an additional silver wire inserted into the hemolymph was used as reference electrode. To facilitate electrode penetration, the neural sheath was removed mechanically with forceps. Desiccation was prevented by submerging the brain in locust saline (Clements and May, 1974) at all times.

Electrophysiology and stimulation. Intracellular recordings were performed with sharp electrodes (resistance 60-150 MΩ), drawn from borosilicate capillaries (0.75 mm ID, 1.5 mm OD; Hilgenberg, Malsfeld, Germany) using a Flaming/Brown horizontal puller (P-97, Sutter, Novato, CA). Electrode tips were filled with 4% Neurobiotin (Vector Laboratories, Burlingame, UK) in 1M KCl and backed up with 1M KCl. Intracellular signals were amplified (10x) with a custom-made amplifier or a SEC5-LX amplifier (NPI, Tamm, Germany). After sampling at a sampling rate of at least 5 kHz (CED1401 Micro, Cambridge Electronic Design, UK; or Digidata 1322A, Molecular Devices, Sunnyvale, CA, USA), signals were stored on a PC using Spike2- (Cambridge Electronic Design) or PClamp9 software (Molecular Devices). Digital high pass filtering was applied when necessary to compensate for drifting baseline. After recording, depolarizing current was applied (1-3 nA, 1-5 min) to iontophoretically inject Neurobiotin.

For visual stimulation, two different experimental setups were used. The first setup (using vertical mounting of the animal) used a xenon-arc (XBO 150 W) as light source. It was connected via a light guide (Schölly, Denzlingen, Germany; spectral range 400-800 nm) to a perimeter placed around the animal. A polarizer (HN38S, Polaroid, Cambridge, MA) or a neutral density filter of equal transmission could be placed in the light path (irradiance at the animal's head: 94 µW/cm²; angular size: 2.7°). The second setup was equipped with a halogen bulb as light source (150 W) to present polarized light from dorsal direction (irradiance: 57µW/cm² angular size: 3.4°). Again, the polarizer could be interchanged with a neutral density filter to present unpolarized light. The horizontal mounting of the locust in this setup allowed us to present unpolarized stimuli in the frontal visual field using a CRT-screen (Mitsubishi, Diamond Pro2070SB, frame rate: 140 Hz, 38 µW/cm², angular size: 83 x 110°). The CRT-screen was controlled by a ViSaGe (Cambridge Research Systems, Cambridge, UK), programmed via MatLab. In both setups, the polarizer was rotated via custom built hard- and software by 360° counterclockwise or clockwise at speeds of 21°/s or 30°/s. An *E*-vector orientation parallel to the longitudinal axis of the animal was defined as 0°.

Data analysis. Sampled spike trains were stored on PC and evaluated using Spike2-software with implemented, custom designed scripts. Action potentials were detected with threshold based event detection. The detected events could be visualized as mean frequency using a gliding average algorithm at a bin size of 1s or as instantaneous frequency. Background frequency and maximal instantaneous spike frequency were estimated by moving horizontal cursors to the desired level in the respective channel and reading out the current values of the cursor position.

To quantify responses to polarized light, events within each 360° rotation of the polarizer were assigned a corresponding *E*-vector angle. This list of angles was exported for each rotation and the combined rotations of each neuron were tested for polarization sensitivity. A neuron was rated polarization sensitive if the distribution of angles during filter rotations was significantly different from randomness (Rayleigh-test for axial data; Oriana 2.05a; Kovach Computing Services, Anglesey, UK). The mean angle of the distribution was defined as the Φ_{max}-value of that neuron.

The distributions of Φ_{max}-values of neuronal populations were evaluated using Rao's spacing test for axial data, which allows very small sample sizes (Batschelet, 1981). To test for correlation of Φ_{max}-values with the innervated PB columns, Φ_{max}-values (ranging from 0°-180°) were plotted against the innervated columns, separately for each hemisphere or combining both hemispheres. As Φ_{max}-values are axial data with a periodicity of 180°, data points near the 0°/180° boundary were shifted by adding 180° or by subtracting 180° in the two inner- and outermost columns, respectively. The resulting datasets (ranging from -20° to 200°) were tested with linear regression analysis for correlation between the Φ_{max}-value and the innervated PB-column (t-test against a regression line with slope of 0 at significance level of 0.01; Origin 6.0; Microcal, Northampton, MA). Correlation coefficients (R) were calculated with the same datasets in Origin 6.0.

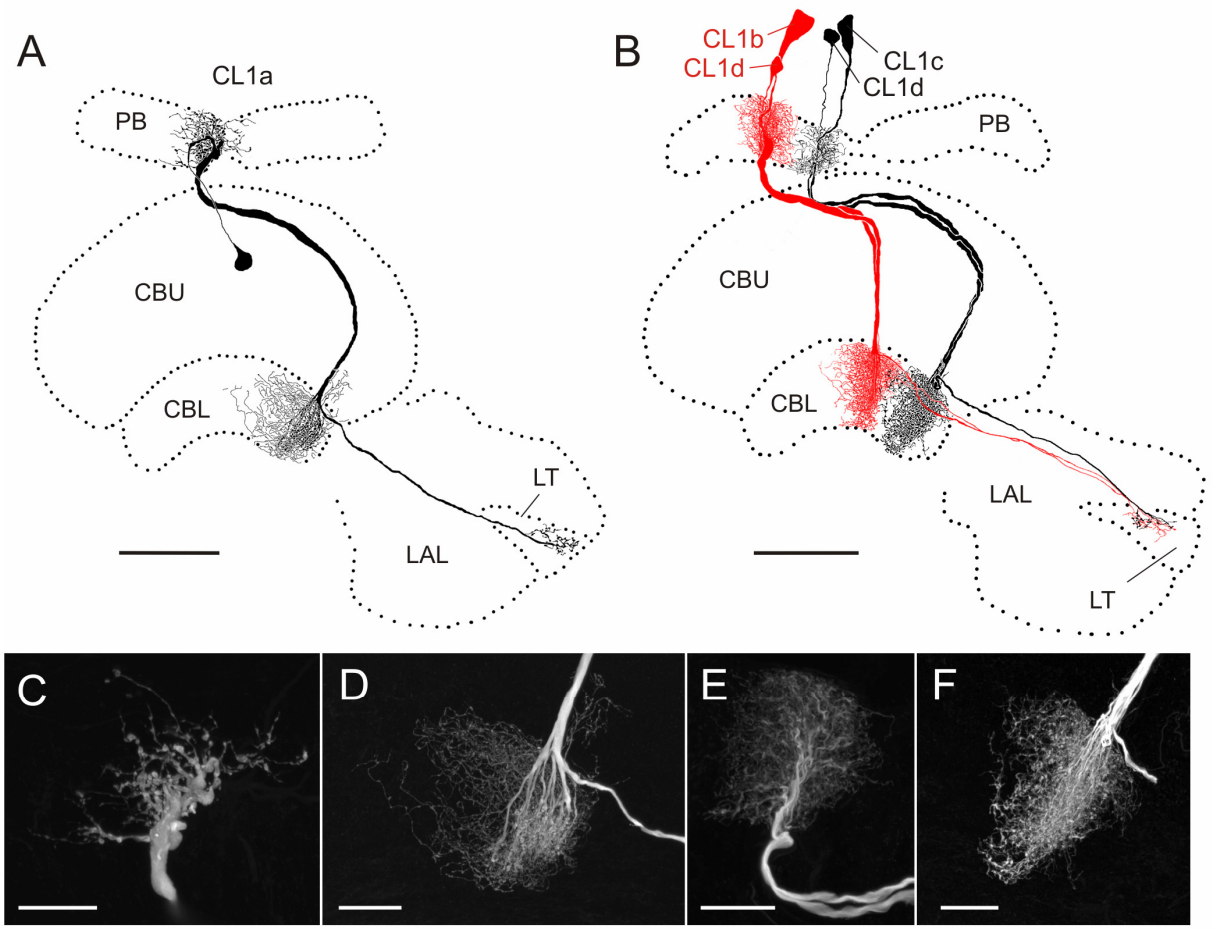

Figure 1. Morphology of CL1 neurons. ***A,*** Frontal reconstruction of a CL1a neuron. It connects the lower division of the central body (CBL) with the protocerebral bridge (PB) and the lateral triangle (LT) in the lateral accessory lobe (LAL). ***B,*** Frontal reconstruction of a CL1b (red) and a CL1c (black) neuron. Each neuron is joined by a forth type of CL1 neuron, termed CL1d, with arborizations in the same column, but much smaller soma size. CL1c cells lack the additional axonal process to the LT. ***C,D,*** Details of arborization trees from the CL1a neuron shown in ***A***. Maximal intensity projections of confocal image stacks reveal varicose endings in the PB (***C***) and a center-surround organization of the arborization tree in the CBL (***D***). CBL arborizations are of varicose appearance in the center, surrounded by smooth, fine processes in the periphery. ***E,F,*** Details of arborizations of the CL1c/d neurons shown in ***B***. Confocal images show that the polarity of these cells is reversed as compared to that of CL1a neurons. Arborizations in the PB are of smooth appearance (***E***), whereas uniformly varicose endings are present in the CBL (***F***). CBU, upper division of the central body. Scale bars, 80 µm (***A,B***), 20µm (***C-F***).

Histology. After injection of Neurobiotin, brains were dissected out of the head capsule, cleaned of fat and trachea, and fixed over night at 4°C in Neurobiotin fixative (4% paraformaldehyde, 0.25% glutaraldehyde, 2% saturated picric acid, in 0.1 M phosphate buffer). Brains were then either processed as whole mounts (see below) or embedded in albumin-gelatin (4.8% gelatin and 12% ovalbumin in demineralized water) for sectioning. Embedded brains were fixed in 8% formaldehyde (in 0.1 M phosphate buffer) over night (4°C), and hereafter sectioned with a vibrating blade microtome at 40 µm thickness (VT 1000S; Leica, Wetzlar, Germany). Sections were rinsed 3 x 15 min in 0.1 M phosphate buffer and incubated with horseradish-peroxidase-conjugated Streptavidin (1:300, Amersham Buchler, Braunschweig, Germany) in 0.1 M phosphate buffered saline (PBS)/ 0.5% Triton X-100 over night at room temperature. After rinsing in PBS (3 x 15 min) and once in 0.05 M Tris/HCl (15 min), diaminobenzidine (0.3 mg/ml 3,3´-diaminobenzidine tetrahydrochloride, 0.3% nickel ammonium sulfate in 0.05 M Tris/HCl) was added, and the reaction was started by adding 0.015% H_2O_2. The staining reaction was stopped by rinsing with 0.05 M Tris/HCl (4 x 15 min) after the desired intensity was reached. Stained sections were mounted on gelatin/chrome alum coated microscope slides, dehydrated in an increasing ethanol series (50%, 70%, 90%, 95%, 100%, 3 min each), and cleared in xylene (5 min). Finally, sections were embedded in Entellan (Merck, Darmstadt, Germany). Reconstructions from diaminobenzidine-stained preparations were performed using a camera-lucida attachment on a Leitz compound microscope equipped with a 40× objective. Drawings were scanned and optimized for contrast and brightness in Adobe Photoshop CS2 (Adobe Systems, San Jose, CA).

Wholemount preparations were rinsed 4 x 15 min in PBS after fixation, and directly incubated with Cy3-conjugated Streptavidin (Dianova, Hamburg, Germany, 1:1000) for three days at 4°C in PBT (PBS, including 0.5% Triton X-100). After rinsing with PBT (2 x 30 min) and PBS (3 x 30 min), the brains were dehydrated with an increasing ethanol series (25%, 50%, 70%, 90%, 95%, 100%; 15 min each), transferred to a fresh mixture of ethanol and methylsalicylate (1:1) for 15 min, and finally cleared in methylsalicylate for 35 min. Brains were eventually mounted in Permount (Fisher Scientific, Pittsburgh, PA) between two coverslips. To avoid compressions, reinforcement rings were used as spacers. Neurons were scanned with a confocal microscope (Leica TCS-SP2, minimal pinhole size, at 3 µm intervals) with a 10× oil immersion objective (HC PL APO

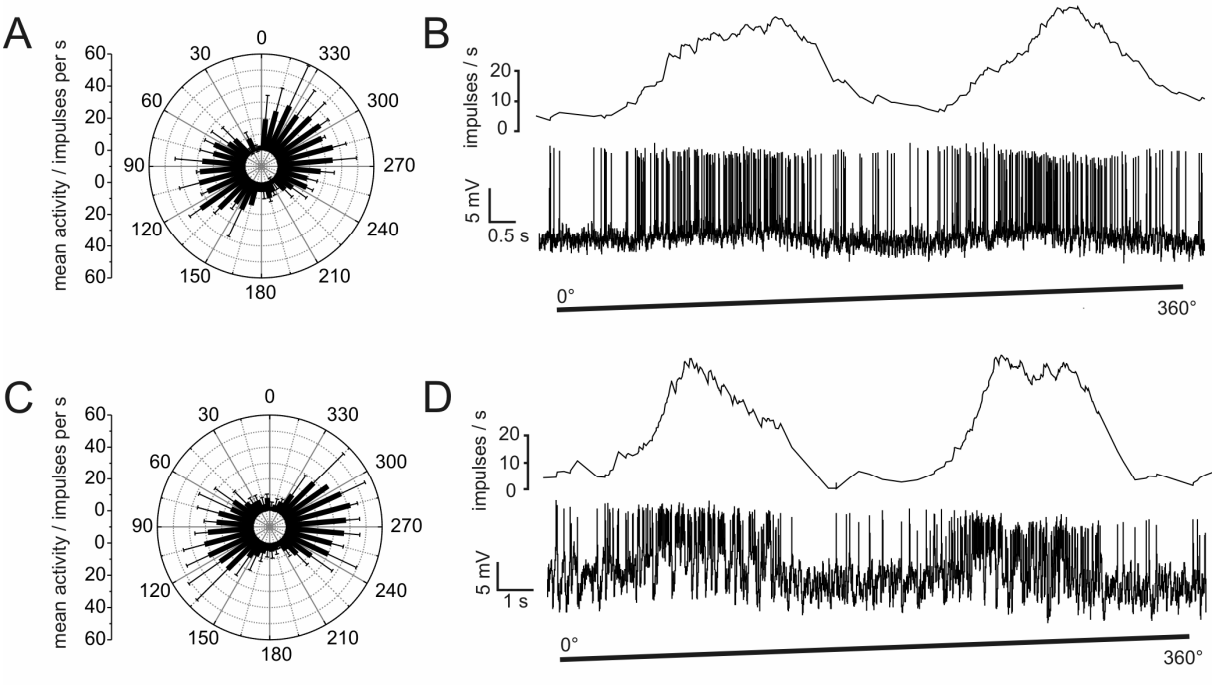

Figure 2. Responses of CL1a and CL1b/d neurons to polarized light. ***A,*** Circular diagram of mean frequencies of action potentials of a CL1a neuron plotted against *E*-vector orientation during dorsal stimulation with a rotating polarizer (n = 2, error bars = SD, bin size 10°, $p < 10^{-12}$). ***B,*** Spike train (lower trace) and mean spiking frequency (upper trace, gliding average with bin size of 1s) of the same neuron during a clockwise 360°-rotation of the polarizer. ***C,*** Mean activity of a double labelled CL1b/d neuron from four 360° rotations of the polarizer (error bars = SD, bin size 10°, $p < 10^{-12}$). ***D***, Spike train and mean spiking frequency from the same neuron as in ***C*** during a clockwise 360° rotation of the polarizer. Postsynaptic potentials are visible throughout the recording.

10×/0.4 Imm Corr CS; Leica, Bensheim, Germany). Reconstructions based on these data stacks were carried out using Adobe Photoshop CS2.

To acquire high resolution data stacks of injected neurons, whole mount preparations were rehydrated and sectioned in thick sections, containing the neuron of interest (for details see Heinze and Homberg, 2008). These preparations were scanned at high resolution (40× objective, HCX PL Apo 40×/1.25 Oil) and were reconstructed using Photoshop or shown as maximal projection views as well as single optical sections. All images were optimized for contrast and brightness.

Results

New sets of POL-neurons

Through intracellular recordings combined with dye fills we identified two sets of POL-neurons of the central complex which have not been characterized before. Both types of neuron showed tonic frequency modulations when stimulated with a dorsally rotating polarizer. One type of neuron was identified as CL1 columnar cells (Heinze and Homberg, 2008), whereas the second type was a new class of tangential neurons of the PB, termed TB2.

CL1 neurons

CL1 neurons have been subdivided into three subtypes (CL1a, CL1b, and CL1c), which differ in details of their arborizations, but share an overall common morphology (discussed in detail in Heinze and Homberg, 2008). All three cell types have somata in the *pars intercerebralis* and connect columns of the PB with columns of the CBL via large-diameter fibers (Fig. 1A,B). Each subtype consists of 16 individual neurons following a precise interhemispheric connectivity scheme (Heinze and Homberg, 2008). CL1a- and CL1b neurons have small-diameter axons projecting to the lateral triangle.

Recordings were obtained from 21 CL1a neurons. Recordings from four additional CL1 neurons revealed a CL1b and three CL1c cells which were always colabeled with a forth type of CL1 neurons, termed CL1d (Fig. 1B). The neurons were distinguished from each other based on the following characters: First, the size of the soma and primary neurite was larger in CL1b and c cells than in CL1a and d cells (Fig. 1A,B). Second, the polarity of CL1a neurons was reversed as compared to the double labeled CL1b/d and, CL1c/d neurons. CL1a cells had varicose endings in the PB (Fig. 1C) and a combination of smooth and varicose endings in the CBL (Fig. 1D). Within the CBL, varicosities were confined to single columns, but ran across all layers, whereas smooth endings were approximately three times as wide and were restricted to dorsal layers, mostly layer 2 (Fig. 1D). In contrast, the CL1b/d- and CL1c/d neurons had smooth endings in the PB (Fig. 1E) and exclusively varicose endings in the CBL (Fig. 1F). Independently of the cell type, endings in the lateral triangle were always varicose. Finally, CL1c cells were defined by the absence of an axon to the lateral triangle but were otherwise identical to CL1b neurons (Heinze and Homberg, 2008).

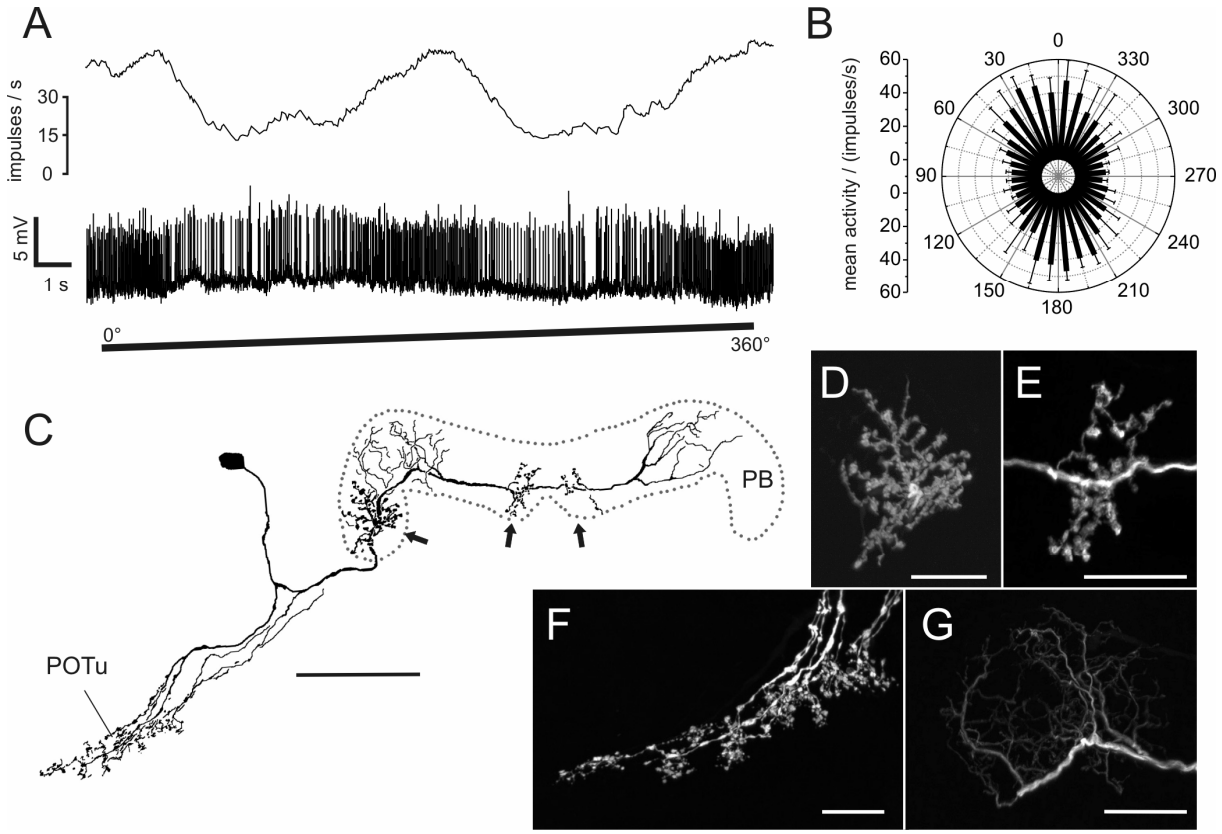

Figure 3. Physiology and morphology of a TB2 neuron. ***A,*** Mean activity and intracellular recording trace during clockwise rotation of the polarization filter. ***B,*** Mean activity of the neuron during 360° rotations of the polarizer plotted against *E*-vector orientation (n = 4, error bars = SD, bin size 10°, $p < 10^{-12}$). ***C,*** Frontal reconstruction of the neuron. Three domains of varicose arborizations (arrows) and two wider regions of smooth arborizations are present in the protocerebral bridge (PB). Ramifications in the posterior optic tubercle (POTu) are also varicose. ***D,E,*** Detailed views of varicose ramifications in the PB (***D,*** lateral arborizations; ***E,*** medial arborizations in left hemisphere; maximal intensity projections of confocal image stacks). ***F,*** Varicose endings in the POTu (maximal intensity projection). ***G,*** Smooth endings in left hemisphere of the PB (maximal intensity projection). Scale bars, 80 µm (***C***), 20 µm (***D-G***).

All CL1 neurons responded to the dorsally presented, rotating polarizer with an *E*-vector dependent modulation of spike frequency (Fig. 2). The neurons had a mean background activity of 10.2 ± 4.6 impulses per second. They were strongly activated to peak instantaneous frequencies of 57.3 ± 20.9 (mean ± SD) impulses per second at their preferred *E*-vector orientation, and were usually totally silenced at Φ_{min}. When cells were recorded from their arborizations in the PB, we observed only small postsynaptic potentials (PSPs) in most cases. The only example of strong PSPs was found for one of the three recordings from CL1b/d neurons (Fig. 2D).

TB2 neurons

The second type of POL-neuron consisted of tangential neurons of the PB, termed TB2 (Fig. 3). Their somata were located posterior-laterally from the PB in the posterior *pars intercerebralis*. The neurons had arborizations in the posterior optic tubercle and several distinct arborization domains in the PB (Fig. 3C-G). In contrast to TB1 neurons (Heinze and Homberg, 2007), TB2 neurons had three arborization domains with varicose endings in the PB. One of these was located in the lateralmost column of the ipsilateral PB hemisphere (R1 or L1), whereas the other two varicose ramifications were located on either side of the midline innervating parts of columns L8 and R8 (Fig. 3D,E). In both hemispheres of the PB, arborization domains with smooth endings (Fig. 3G) covered approximately three columns and were separated from the varicose endings by at least one column without ramifications (Fig. 3C). Endings in the posterior optic tubercle appeared strongly varicose (Fig. 3F). All recorded neurons of this type (n = 5) were of indistinguishable morphology with somata in the right hemisphere.

TB2 neurons showed marked polarization opponency with highly similar *E*-vector tuning clustered around 178° (Fig. 7B). TB2 neurons had a considerably larger tuning width than CL1 neurons and a higher mean background activity of 31 ± 3.6 impulses per second. Their peak instantaneous spiking frequency during stimulation was 112 ± 30 impulses per second (mean ± SD), and hence about twice as high as in CL1 neurons.

Conditionally polarization-sensitive neurons

In contrast to the POL-neurons described above, we encountered three types of neuron that showed polarization sensitivity in only 50% of the experiments. To account for this variability, these neurons were termed conditionally polarization-sensitive. Polarization sen-

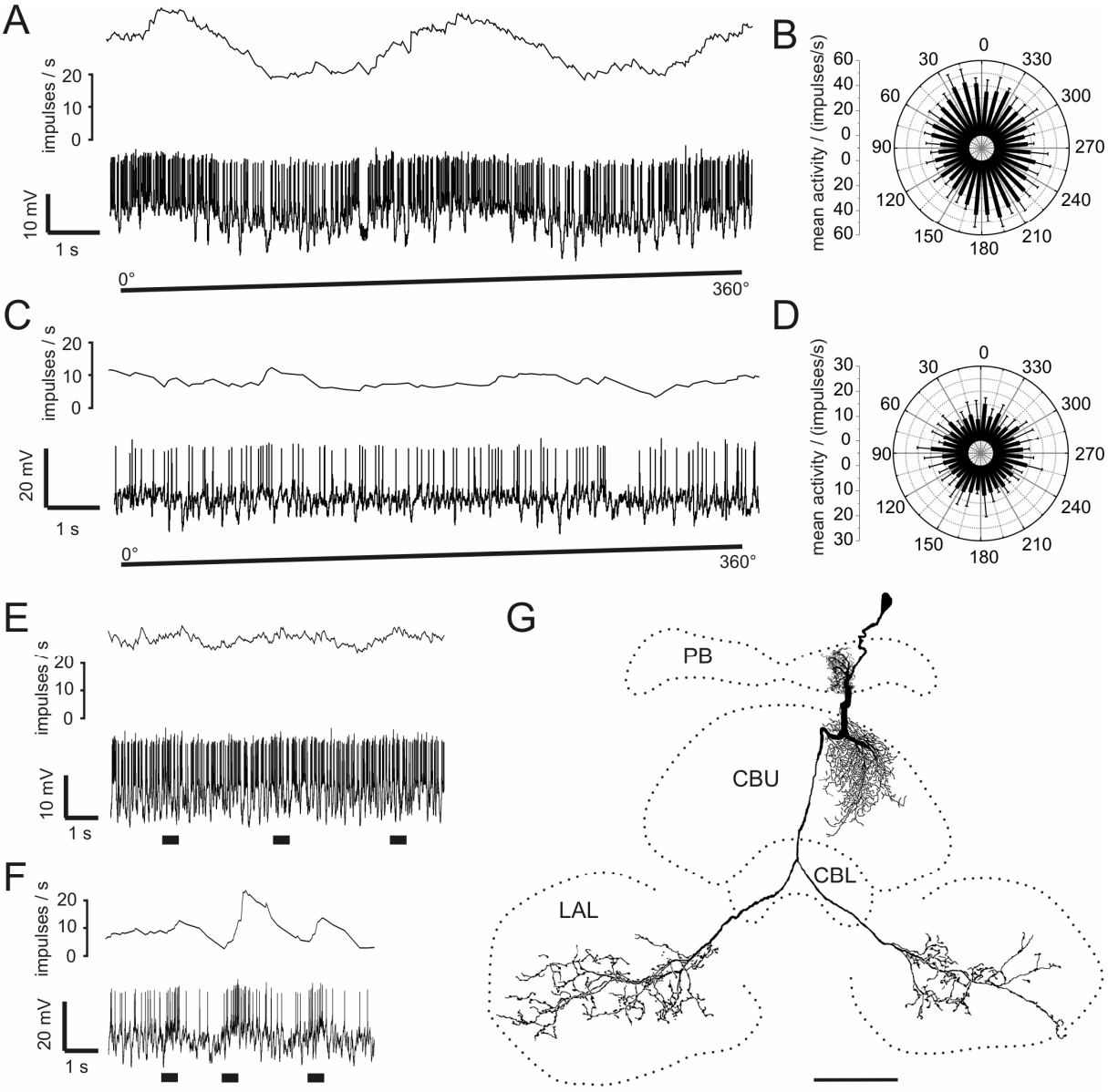

Figure 4. Response characteristics and morphology of conditionally polarization-sensitive CPU2 neurons. ***A,*** Spike train (lower trace) and mean spiking frequency (upper trace; gliding average, bin size 1s) of a polarization-sensitive CPU2 neuron during 360° rotation of the polarizer (clockwise). ***B,*** Circular diagram of mean activity during four rotations of the polarizer (same neuron as ***A***, bin size 10°, error bars = SD, $p = 2.7 \times 10^{-11}$). ***C,*** Activity of a non-polarization-sensitive CPU2 neuron during rotation of the polarizer (spike train in lower trace, mean spiking frequency in upper trace). ***D,*** Circular diagram of mean activity during four rotations of the polarizer (same neuron as ***C***, error bars = SD, bin size 10°). The mean activity of the neuron does not change significantly during rotation of the polarizer ($p = 0.68$). ***E,F,*** Neuronal activity during stimulation with large-field, frontal light flashes. ***E***, No response occurred in the polarization-sensitive neuron (same as in ***A***). ***F,*** Excitatory responses were present in the non-polarization-sensitive neuron (same as in ***C***). ***G,*** Frontal reconstruction of the CPU2 neuron recorded in ***A***. Arborizations are present in the protocerebral bridge (PB), in all layers of the upper division of the central body (CBU), and in both ventral shells of the lateral accessory lobes (LAL). CBL, lower division of the central body. Scale bar, 80 µm.

sitivity of these neurons apparently depended on an unknown factor. Differences in daytime of recording, or differences in anatomy did not correlate with the responsiveness for polarized light. All of these cells were columnar neurons and had been anatomically described as CPU2, CPU4 and CL2 neurons (Heinze and Homberg, 2008).

CPU2 neurons

CPU2 neurons had smooth arborizations in single columns of the PB and in corresponding columns of the CBU, where all layers were innervated. Large varicosities were present in the ventral shells of both LALs (Fig. 4G). From a total of six recordings, three cells were polarization-sensitive. In these three cells polarization sensitivity was pronounced and highly significant (Fig. 4A,B; Rayleigh-test against uniform distribution, $p < 10^{-10}$) with peak instantaneous spiking frequencies of 125 ± 30 impulses per second at Φ_{max}. In contrast, three CPU2 neurons were polarization-blind (Fig. 4C,D). The polarization-sensitive cells had a mean background activity of 26 ± 3.6 impulses per second, whereas the non-polarization-sensitive cells only showed a mean activity of 12 ± 7.8 impulses per

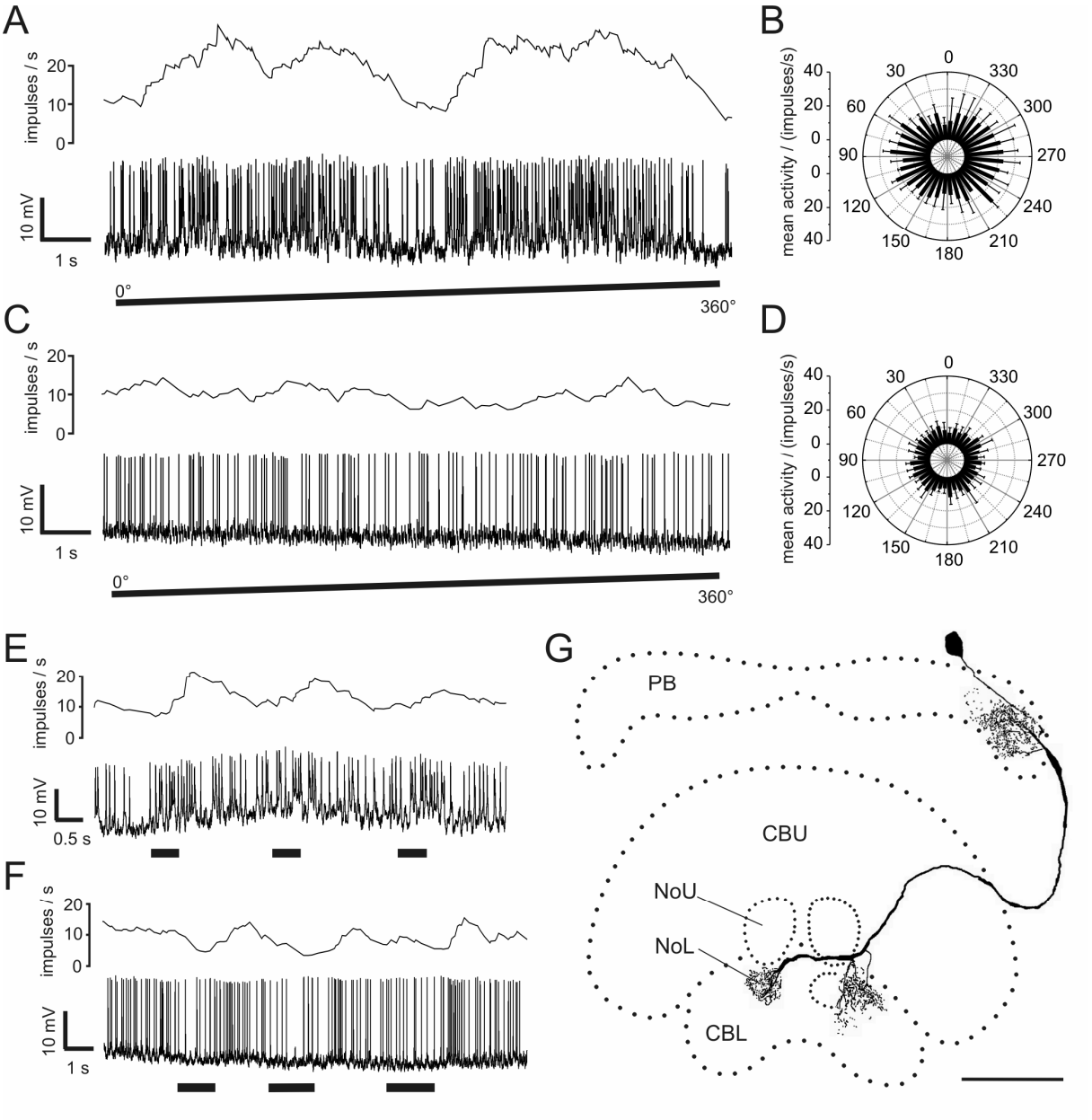

Figure 5. Conditionally polarization-sensitive CL2 neurons. ***A,*** Spike train and mean spiking frequency of a polarization-sensitive CL2 neuron during stimulation with a rotating polarizer. ***B,*** Mean response during dorsal stimulation with a rotating polarizer (n = 4, bin size 10°, error bars = SD, p = 0.009). ***C,*** Activity of a non-polarization-sensitive CL2 neuron during rotation of the polarizer. ***D,*** Mean spiking frequency from the neuron in ***C*** during four rotations of the polarizer (bin size 10°, error bars = SD, p = 0.88). ***E,F,*** Responses to unpolarized light stimuli (spike trains and mean activity). ***E,*** The polarization-sensitive neuron (shown in ***A***) shows weak excitation during large-field frontal light flashes. ***F***, The non-polarization-sensitive neuron (shown in ***C***) responds to small, dorsal flashes of unpolarized light with inhibition followed by weak rebound excitation. ***G,*** Frontal reconstruction of a CL2 neuron (same as in ***A***, ***B***, and ***E***). The neuron has arborizations in the protocerebral bridge (PB), in the lower division of the central body (CBL), and in the lower unit of the contralateral nodulus (NoL). CBU, upper division of the central body; NoU, upper unit of the nodulus. Scale bar, 80 µm.

second. All neurons were characterized by large PSPs during and in between stimulations (Fig. 4A,C).

Stimulations with unpolarized light flashes were carried out in five of the six recorded neurons, either from frontal or from dorsal directions. None of the polarization-sensitive cells showed any detectable response to these light flashes (Fig. 4E), whereas the non-polarization-sensitive cells were either inhibited in response to dorsal stimuli or were excited in response to frontal stimuli (Fig. 4F).

CL2 neurons

Four recordings were obtained from CL2 neurons. These cells connect single columns of the PB with columnar arborization domains in the CBL and with ramifications throughout the lower division of the contralateral nodulus (Fig. 5G; Heinze and Homberg, 2008).

Two of four recordings showed polarization sensitivity with a mean peak instantaneous activity of 46 ± 19 impulses per second and broad tuning curves (Fig. 5A,B). The two remaining neurons did not show frequency modulation during stimulation with a

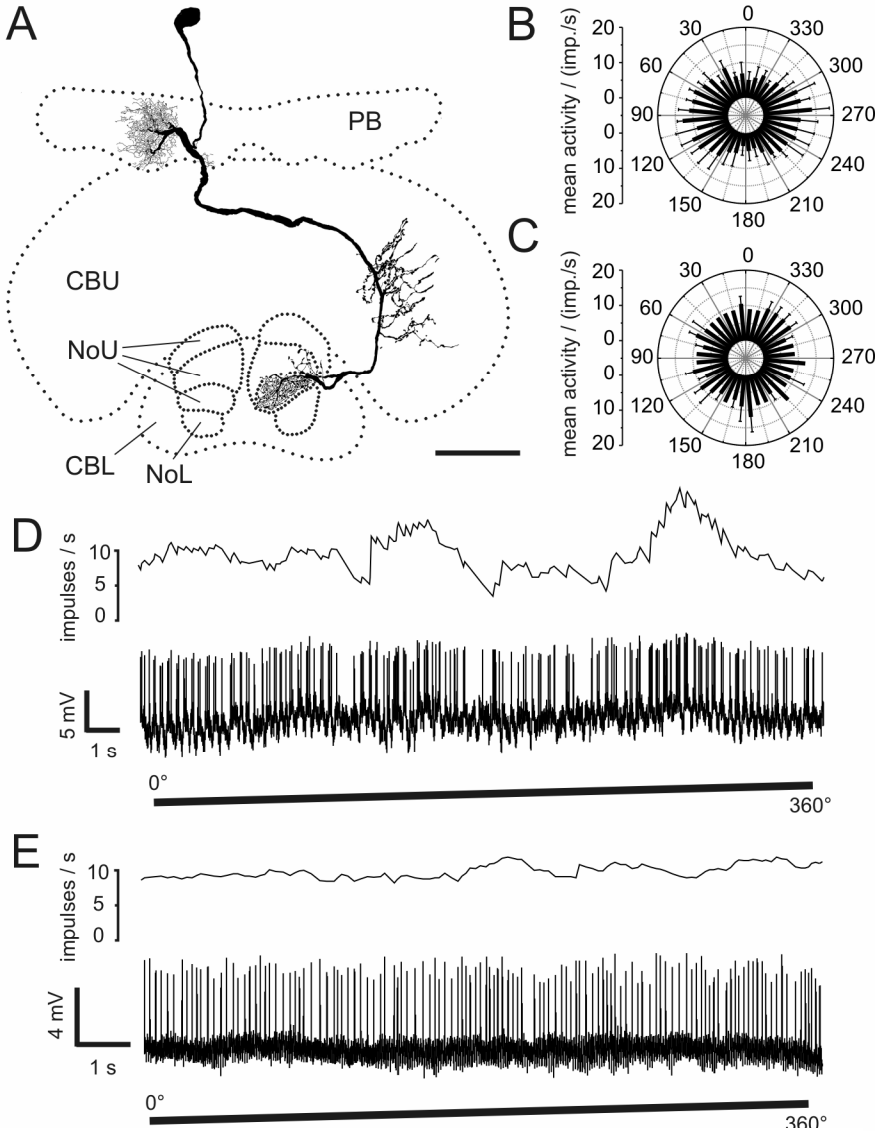

Figure 6. Conditionally polarization-sensitive CPU4 neurons. ***A,*** Reconstruction of a CPU4c neuron viewed from posterior. Smooth arborizations are present in the protocerebral bridge (PB), whereas endings in the upper division of the central body (CBU; layer III) and in layer III of the upper unit of the contralateral nodulus (NoU) are varicose. ***B,*** Mean response of the polarization-sensitive neuron in ***A*** during four rotations of the polarizer (bin size 10°, error bars = SD, $p = 4.2 \times 10^{-10}$). ***C,*** Mean spiking activity (two rotations of the polarizer) of a polarization-blind CPU4b neuron (bin size 10°, error bars = SD, $p = 0.99$). ***D,*** Spiking activity and mean frequency of the CPU4c neuron shown in ***A*** during clockwise rotation of the polarizer. ***E,*** Activity of the CPU4b neuron (same as in ***C***) during stimulation with a rotating polarizer (spike train and mean frequency). CBL, lower division of the central body; NoL, lower unit of the nodulus. Scale bar, 50 µm.

rotating polarizer (Fig. 5C,D). As in CPU2 neurons, background spiking activities of the polarization-sensitive neurons were higher (13.5 ± 3.5 impulses per second) than in the polarization-blind cells (7.5 ± 2.1 impulses per second).

Stimulation with unpolarized light stimuli either from frontal or from dorsal directions led to variable weak responses (Fig. 5E,F). One polarization-sensitive neuron was excited by frontally presented unpolarized light flashes, whereas one polarization-blind cell was inhibited by dorsally presented unpolarized light flashes, followed by rebound excitations at stimulus offset. The remaining neurons did not show any response to dorsally presented light flashes.

CPU4 neurons

Two recorded neurons could be classified as CPU4 neurons. They connect single columns of the PB with a columnar region in layer three of the CBU and a layer of the upper division of the contralateral nodulus (Fig. 6A; Heinze and Homberg, 2008). One of the two cells responded with a significant modulation of its firing rate when presented with the rotating polarizer (Fig. 6B,D), whereas the second cell did not show any response (Fig. 6C,E). Both neurons had similar background firing rates of 6 and 10 impulses per second, respectively. Unpolarized stimuli presented in the frontal visual field elicited an excitatory rebound response at stimulus offset in the non-polarization-sensitive neuron. As in CPU2 neurons, the polarization-sensitive cell did not respond to unpolarized light presented from dorsally.

The physiological differences in the two recordings from CPU4 neurons may be attributed to the fact that the two cells belonged to different subtypes of CPU4 neurons. The polarization-sensitive cell innervated layer three of the upper division of the nodulus (CPU4c neuron, Fig. 6A), while the polarization-insensitive cell innervated layer two (CPU4b neuron).

Analysis of Φ_{max}-values

Heinze and Homberg (2007) showed that *E*-vector tuning of neurons with arborizations in the PB corresponds to their columnar arborization domains in the PB in a compass-like fashion. We, therefore, asked whether this is also true for the newly presented types of POL-neurons.

Data on *E*-vector tuning and columnar arborization domains in the PB were obtained from 21 CL1a neurons. The Φ_{max}-values of these neurons covered a range of 180°. Their distribution was not significantly different from randomness, despite some apparent clustering (Fig. 7A; Rao's spacing test, $U = 133$, $p > 0.1$). The recorded neurons had arborizations in a wide range of columns in the PB. However, when plotting the Φ_{max}-values of the neurons against their

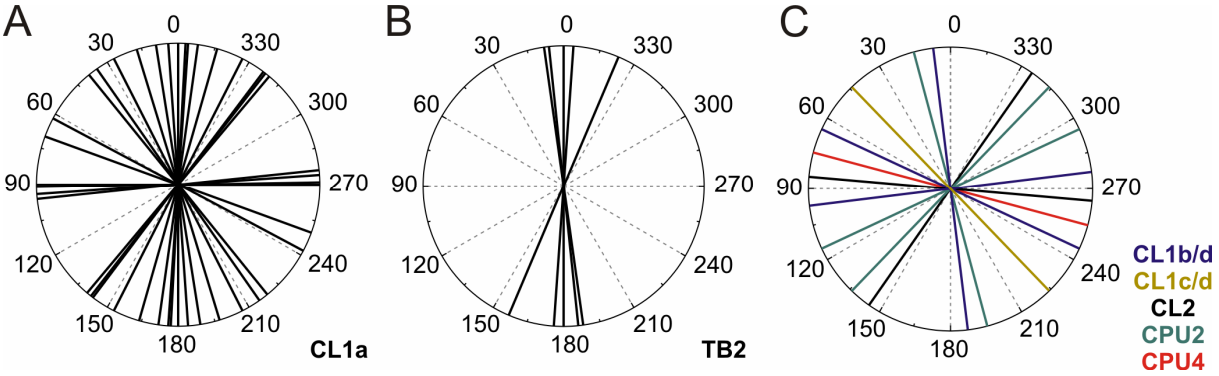

Figure 7. Distribution of Φ_{max}-values. ***A,*** Φ_{max}-values of CL1a neurons cover the complete range of 180° with a distribution not significantly different from randomness (Rao's spacing test, $p > 0.1$). ***B,*** Φ_{max}-values of TB2 neurons are clustered around 178° (Rao's spacing test, $p < 0.01$). ***C,*** Φ_{max}-values of all remaining neurons are randomly distributed over the range of 180° (Rao's spacing test, $p > 0.95$).

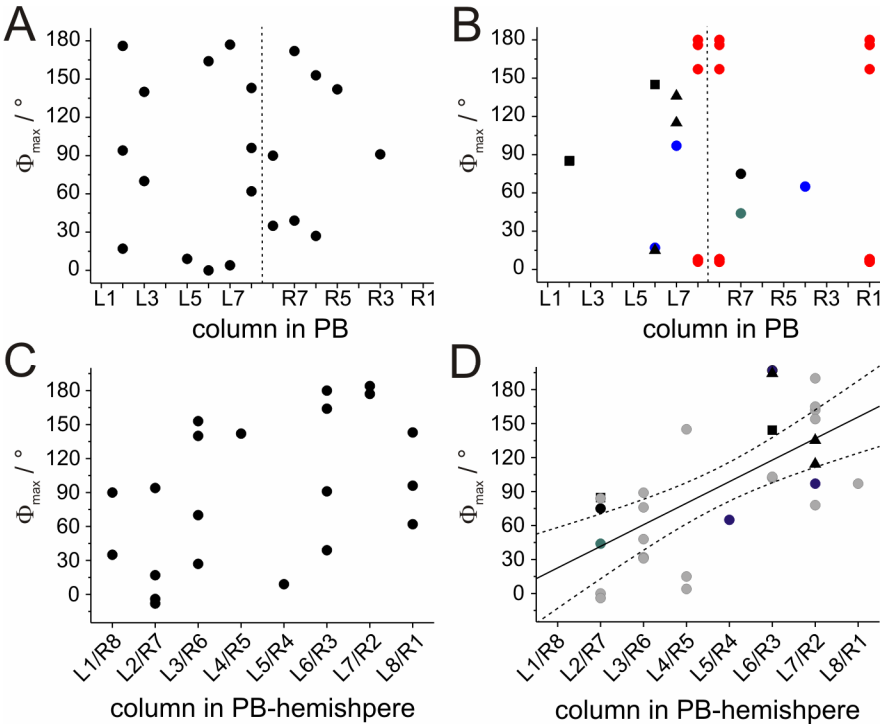

Figure 8. Relation of Φ_{max}-values to innervated column in the PB. ***A,B,*** Φ_{max}-values plotted against the innervated PB-columns. Solid vertical line indicates the midline of the brain. ***A,*** CL1a neurons. ***B,*** CL1b/d neurons (blue), CL1c/d neuron (green), CL2 neurons (black squares), CPU2 neurons (black triangles), CPU4 neurons (black circles) and TB2 neurons (red) ***C,*** For linear regression analysis, Φ_{max}-values of all CL1a neurons were combined in one hemisphere and plotted against the innervated PB column. Values near the 0°/180° boundary of *E*-vectors in medial and lateral columns were shifted by adding or subtracting 180°. Within the resulting dataset no significant correlation was observed (significance level of 0.01; t-test against slope of 0, $p = 0.03$; correlation coefficient $R = 0.47$). ***D,*** Data from CL1b/d-, CL1c/d-, CL2-, CPU2-, and CPU4 neurons (symbols as in ***B***) combined with previously published data from CPU1-, CP1-, and CP2 neurons (grey circles; Heinze and Homberg, 2007) result in a highly significant correlation (significance level: 0.01; t-test against slope of 0, $p < 0.0001$, $R = 0.67$; $y = 19x + 3.6$).

arborization domains in the PB, no obvious correlation was observed (Fig. 8A,C). Applying linear regression analysis confirmed this result for both hemispheres separately as well as for the combined data (t-test for slope = 0 with α-level = 0.01; right hemisphere: $p = 0.44$, left hemisphere: $p = 0.16$, combined: $p = 0.03$; correlation coefficients (R): 0.35, 0.40, and 0.47 respectively; Fig. 8C). As neurons with arborizations in identical columns had different Φ_{max}-values in different preparations, we wondered whether differences in daytime might be responsible for this observation. Although recording times covered a wide range from 9:45 a.m. to 6:45 p.m., no correlation was observed after plotting Φ_{max}-values against time of recording. This was true when considering all CL1a neurons, and when separating them according to columnar identity (not shown).

The remaining POL-neurons of the central complex fell into three classes: first, tangential neurons of the PB (TB2 neurons), second, CL1b/d and CL1c/d neurons, and third, conditionally polarization-sensitive columnar neurons (CPU2-, CPU4-, CL2 neurons). Corresponding to their identical morphology, the Φ_{max}-values of the 5 recorded TB2 neurons were clearly distinct from randomness and were tightly clustered around a mean vector of 178° (Fig. 7B; Rao's spacing test, $U = 226$, $p < 0.01$). The CL1b/d- and CL1c/d neurons combined with the conditionally polarization-sensitive cells covered a wide range of Φ_{max}-values (Fig. 7C; Rao's spacing test, $U = 82$, $p > 0.95$). When plotted against the innervated PB columns, Φ_{max}-values showed a tendency to cluster along the diagonals of each hemisphere (Fig. 8B), but this observation was statistically not significant. When the data from this study were combined with the data on 19 columnar neurons from Heinze and Homberg

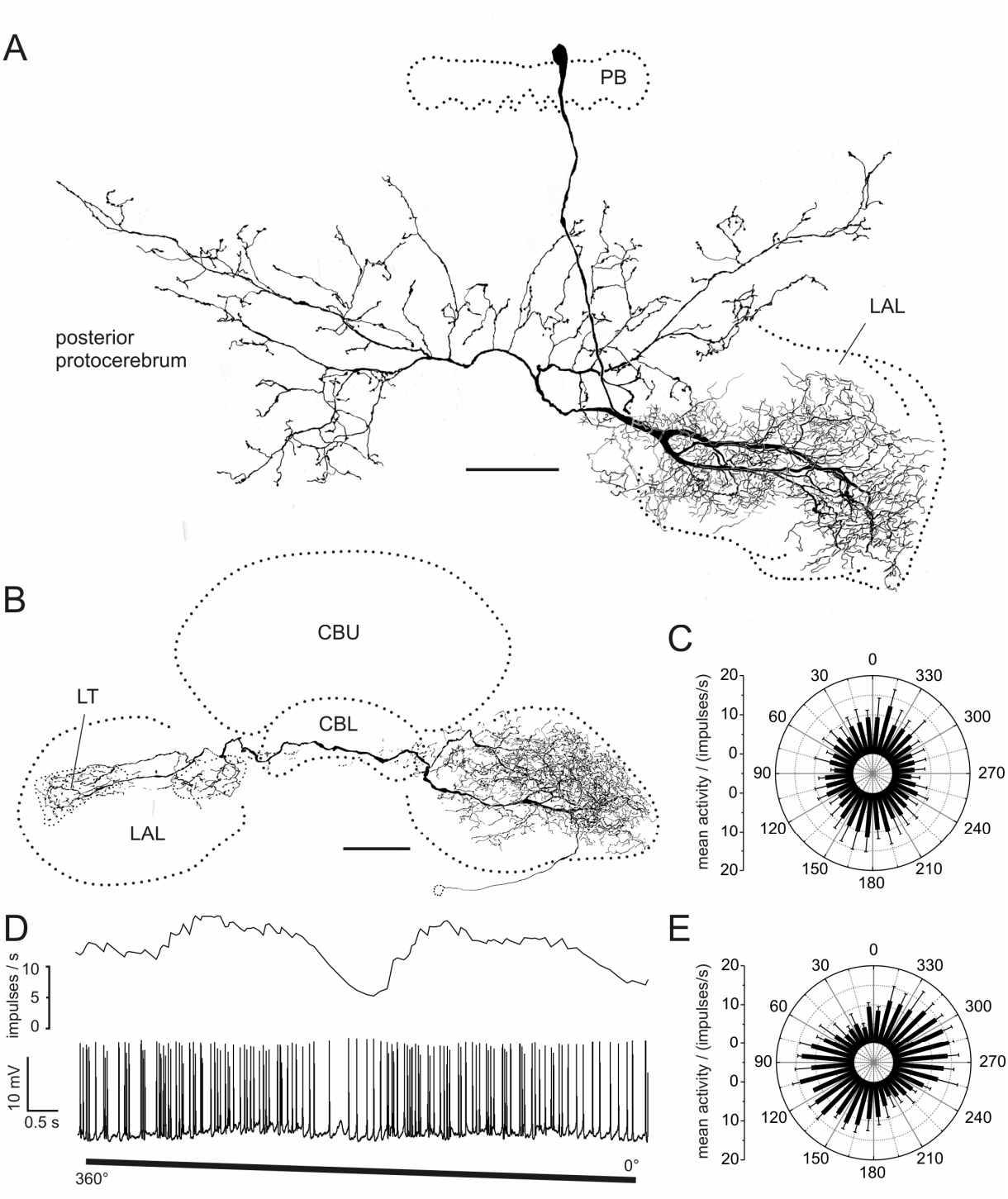

Figure 9. POL-neurons with input arborizations in the LAL. ***A,*** Frontal reconstruction of a LAL-pPC-neuron. The cell has smooth endings in the left lateral accessory lobe (LAL). Bilateral projections to the posterior protocerebrum have varicose terminals. ***B,*** Frontal reconstruction of a LAL-LT-neuron. The neuron connects the LAL of the left hemisphere with the lateral triangle (LT) in the right hemisphere. Side branches are also present in the right median olive. The location of the soma could only be inferred by the course of the faintly stained primary neurite. ***C,*** Circular plot of mean spiking frequency from the LAL-pPC neuron shown in ***A*** (means + SD, n = 6, bin size 10°, $p = 4.2 \times 10^{-8}$). ***D,*** Neuronal activity of the LAL-LT neuron presented in ***B*** during 360° rotation of the polarizer. ***E,*** Mean spiking activity of the LAL-LT neuron presented in ***B*** plotted against *E*-vector orientation during four rotations of the polarizer (error bars = SD, bin size 10°, $p < 10^{-12}$). CBU, upper division of the central body; CBL, lower division of the central body; PB, protocerebral bridge. Scale bars, 100 µm.

(2007), the new columnar cell types were not distinct from the types described already (Fig. 8D). The combined dataset exhibited a highly significant linear correlation between the Φ_{max}-values of the neurons and their innervated PB-column, despite the presence of some outliers ($p < 0.0001$, $R = 0.67$). TB2 neurons were located on the same regression line when their varicose arborization domains were plotted against the neuron's Φ_{max}-values (not shown).

Polarization-sensitive neurons with input regions in the LAL

Several types of columnar cells (types CL1, CP2, CPU1, CPU2) have varicose and, thus, presumably presynaptic terminals in areas of the LAL. We were, therefore, interested to identify potentially postsynaptic neurons in the LAL that might connect the central-complex polarization vision network to descending pathways and motor control circuits of the thorax. Two cell types were found that provide a likely substrate for processing the output signals from the central complex. Both cell types were polarization-sensitive (Fig. 9). The first cell, encountered once, had smooth input arborizations concentrated in the ventral shell of the left LAL and varicose output ramifications extending bilaterally into the posterior protocerebrum (LAL-pPC neuron; Fig. 9A). The second neuron (LAL-LT neuron, Fig. 9B) was analyzed in two recordings from the same hemisphere. It connected large parts of the ipsilateral LAL with the contralateral lateral triangle. In one preparation, additional processes were observed in the medial olive (Fig. 9B). The polarity of the neuron was unclear as all endings appeared finely beaded in one preparation and the labeling was incomplete in the second preparation.

Both cell types showed polarization opponency with broad tuning curves (Fig. 9C-E). Φ_{max}-values differed widely between the recordings (LAL-pPC: 173°; LAL-LT: 118°, 10°), whereas the background activity was similar in all cases (LAL-pPC: 10 impulses/s; LAL-LT: 9 and 6 impulses/s). During *E*-vector rotations LAL-LT neurons reached peak instantaneous frequencies of 43 and 27 impulses per second, the LAL-pPC neuron 70 impulses per second.

Discussion

In the desert locust, a variety of neurons of the central complex is sensitive to dorsally presented polarized light, suggesting a key role of this brain area in sky compass orientation (Vitzthum et al., 2002; Homberg, 2004; Heinze and Homberg, 2007). In the present study we have characterized additional elements of the polarization vision network in the central complex. Among these, CL1 neurons are likely to fill the gap between input and output elements and may be importantly involved in generating the topographic representation of *E*-vector orientations in the PB. Neurons of three other cell types were polarization-sensitive only in some recordings but not in others, suggesting their conditional recruitment to the polarization vision network. Finally, we identified neurons that are suited to relay polarization vision information to descending pathways. When these data are combined with previously described cell types (Vitzthum et al., 2002; Heinze and Homberg, 2007), a general connectivity scheme of the polarization coding network in the locust central complex emerges (Fig. 10). All major tangential cells of the CBL and the PB, and all columnar cells with ramifications in the PB are polarization-sensitive. In contrast, tangential and pontine neurons innervating the CBU have never been shown to be polarization-sensitive. These findings suggest that the CBL, together with the PB, processes compass information, whereas the CBU is involved in other types of sensory coding, which is potentially integrated with compass information via common output neurons.

Connecting the CBL with the PB

After reaching the lateral triangle and medial olive of the LAL, polarized light information is transferred to tangential neurons innervating the CBL (Pfeiffer et al., 2005; Träger et al., 2008). At a later processing stage, columnar and tangential neurons of the PB are tuned to particular *E*-vector orientations depending on the column they innervate (Heinze and Homberg, 2007). CL1a neurons, presented here, are likely to close the gap in information flow between the CBL-input and the polarotopic map in the PB. The polarity of CL1a cells is unique among columnar neurons in the locust central complex and suggests signaling from dendrites in the CBL to axonal outputs in the PB. Presumed input arborizations of CL1a neurons are concentrated in dorsal layers of the CBL, coinciding with layers served by TL2 tangential neurons, which are regarded as the dominant polarization-vision input to the CBL and have been also characterized in crickets (Sakura et al., 2008). In contrast, CL1b-d cells are likely to receive input in the PB and convey this information to the CBL. Similar cells of both polarities have been identified also in *Drosophila*, suggesting common anatomical pathways (Hanesch et al., 1989).

In contrast to the compass-like arrangement of *E*-vector tunings of all other columnar neurons in the PB, Φ_{max}-values of CL1a neurons were distributed randomly, with highly different *E*-vector tunings occurring in the same PB column. As this tuning behavior is more similar to input neurons of the central complex than to the remaining columnar cells, it supports the hypothesis that CL1a neurons represent an earlier processing stage than the polarotopic columnar neurons. Nevertheless, it raises the question why neurons within identical columns behave differently between preparations. Φ_{max}-values of CL1a neurons are either influenced by unknown parameters, or the population of these neurons consists of more than one cell per column. The latter may obscure potential column-dependencies of Φ_{max}-values, if e.g. siblings of CL1a neurons differ by 90° in their *E*-vector tuning. No evidence was found for the hypothesis that Φ_{max}-values of CL1a neurons depend on daytime.

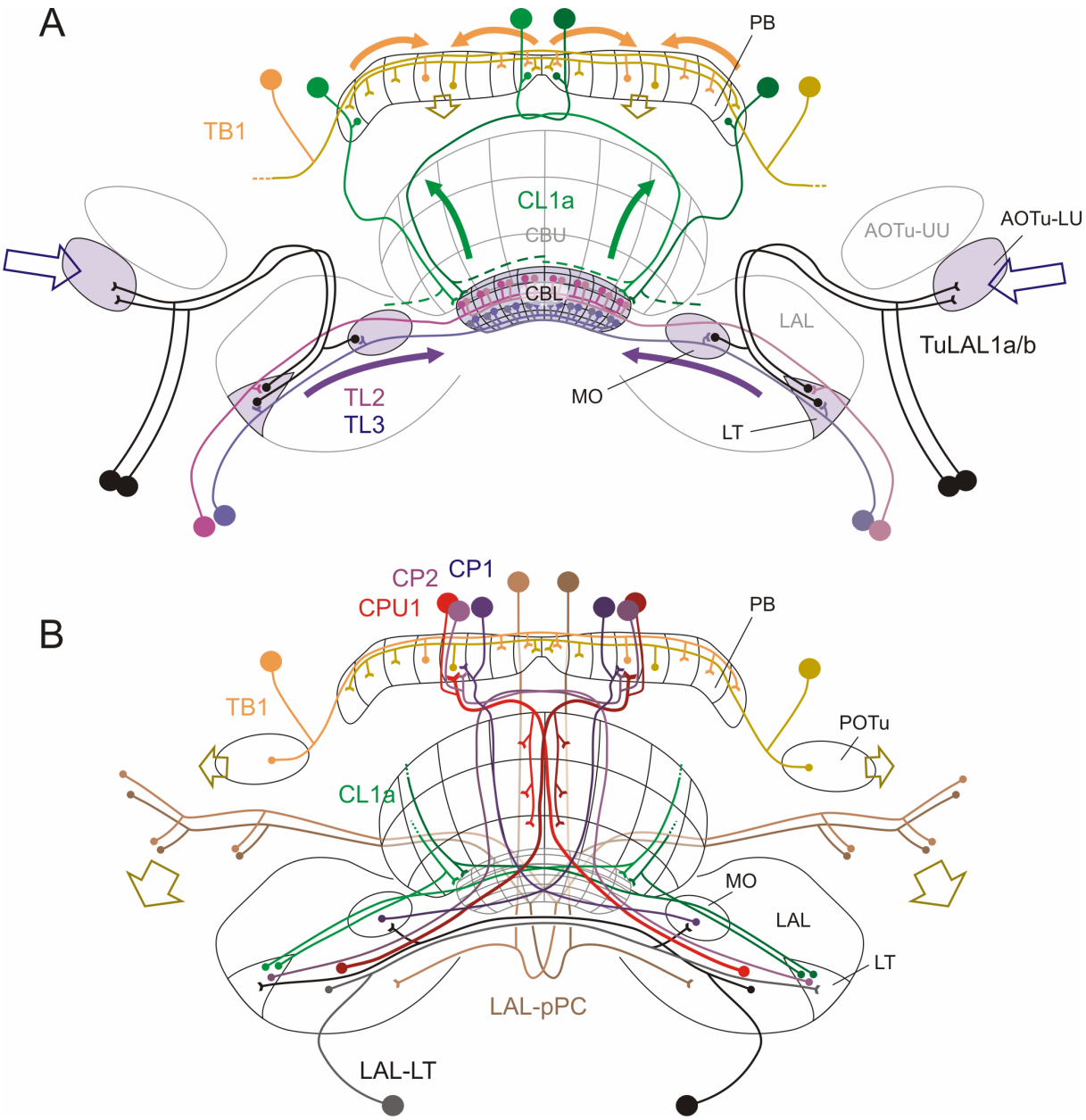

Figure 10. Proposed scheme of the polarization coding network in the central complex. ***A,*** Input pathways. Polarization vision information is transferred from the optic lobe to the lower unit of the anterior optic tubercle (AOTu-LU; open blue arrows) and reaches the lateral triangle (LT) and medial olive (MO) via TuLAL1a/b neurons (Pfeiffer et al., 2005). TL2 and TL3 tangential neurons connect the LT and MO to different layers of the lower division of the central body (CBL; Träger et al., 2008). CL1a neurons are candidates to transmit polarization vision signals from the CBL to the protocerebral bridge (PB). For clarity, this connectivity is only shown for one double-column in each hemisphere (CL1a axons to the LT have been omitted). TB1 neurons integrate the signals within the PB and are the first neurons that contribute to the topographic representation of *E*-vectors in the PB columns (shown for two TB1 cells only; Heinze and Homberg, 2007). Open, brown arrows indicate the columnar output of the two TB1 neurons. ***B,*** Output pathways. The output from TB1 neurons in the PB is likely transferred onto CPU1-, CP1-, and CP2 columnar neurons projecting to the lateral accessory lobes (LALs, red), the MO (blue), or the LT (violet; Heinze and Homberg, 2007). Of these, CPU1 neurons receive additional input in the upper division of the central body (CBU). A second pathway connects the CBL directly to the LT via small-diameter axons of CL1a/b neurons, not involving the PB. All terminals of columnar neurons within the LT and MO could potentially provide input to LAL-LT neurons (black), which connect these areas with the contralateral LAL. This neuron type, as well as CPU1 neurons might synapse onto the LAL-pPC neuron, which provides a connection to the posterior protocerebrum. TB1 neurons provide another possible output from the PB to the posterior optic tubercle (POTu). Descending neurons might receive input from either of these regions (brown, open arrows), and/or from the LAL, to provide information flow to motor control circuits in the thorax. AOTu-UU, upper unit of the anterior optic tubercle.

CL1b-d neurons have a polarity corresponding to other columnar neurons, based on structure of terminals and the occurrence of large PSPs in the PB. Their wiring scheme is identical to that of CL1a cells, which allows for complex bidirectional information flow between the CBL and the PB. Although CL1 cells constitute the potential neuronal substrate, it remains a significant challenge to explain the emergence of the ordered polarotopic *E*-vector representation from an apparently random distribution of *E*-vector tunings.

Column-specific cell types

Heinze and Homberg (2007) demonstrated a compass-like topography of *E*-vector tunings in the varicose arborization domains of TB1 tangential neurons of the PB. Their morphology is similar, but not identical to the newly described TB2 cells. Φ_{max}-values of TB2 neurons differed by 90° from the values of TB1 cells arborizing in the same columns (Heinze and Homberg, 2007). TB2 cells were only found with varicose arborizations in the inner- and outermost PB columns, suggesting that there is no isomorphic set of these cells covering the whole PB. Specific innervation of the outer- and innermost central-complex columns has also been shown for other cell types. Analysis of citrulline immunostaining revealed 16 PU1 pontine neurons (one neuron per column) plus two additional neurons, which specifically connect the inner- and outermost columns of the same hemisphere (Siegl and Homberg, in preparation). Likewise, the presumed connectivity scheme of CPU1a neurons suggests that the outermost PB-columns are connected differently from all other columns. In *Drosophila*, the exceptional projections of the outermost columns of the horizontal fiber system were interpreted to underlie a particular optomotor response. Flies turn toward objects in the frontal field of view, but turn away from objects in the rear field (Mronz and Strauss, 2008). Assuming that the width of the PB encodes azimuthal space around the animal (Strauss, 2002a; Heinze and Homberg, 2007), the outermost columns of the PB might encode the rear part of the visual field. Specialized neurons with inverted wiring and response characteristics in these columns might trigger the repulsive motor reaction in contrast to the frontally attractive stimulus. Whether similar behavioral findings also apply to the locust, remains to be shown.

Conditional polarization sensitivity

All neurons of the polarization vision system of the locust, described so far, showed robust responses to polarized light (Vitzthum et al., 2002; Pfeiffer et al., 2005; Kinoshita et al., 2007; Pfeiffer and Homberg, 2007; Heinze and Homberg, 2007). In contrast, three cell types presented here (CPU2, CL2, and likely CPU4) were polarization-sensitive or polarization-blind, depending on the individual preparation. This variability in responses was clearly not caused by varying recording quality or tissue damage, because these variations also occurred in all other recordings. In the polarization-sensitive CPU2- and CL2 neurons, background activity was higher than in the non-responding units. Furthermore, responses to unpolarized light stimuli were only present in the polarization-blind CPU2- and CPU4 units. Both findings indicate that the source of synaptic input differs between the polarization-sensitive and the polarization-blind state of the neurons. Conditionally polarization-sensitive neurons may, therefore, be recruited to the polarization vision network depending on the internal state of the animal and its behavioral context.

The central complex has a dual role as a sensory processing and a motor control center (Strausfeld, 1999; Strauss, 2002b; Homberg, 2008). Context dependent changes in network properties and neural activities are, therefore, to be expected. Only a fraction of sensory channels that continuously provide the animal with information about the outside world is relevant at any time, depending on the behavioral context (mating, feeding, migrating, escaping, etc.). In locusts, stationary flight is correlated with dramatic activity changes in neurons of the central complex and LAL (Homberg, 1994). In *Drosophila*, learning of visual objects and landmark parameters is associated with neurons of the central complex (Liu et al., 2006; Neuser et al., 2008). These findings suggest considerable learning- and behavior-dependent plasticity in the central complex. Recruitment of neuronal assemblies in motor control networks has been reported in insects (Reichert, 1993; Staudacher and Schildberger, 1998) and in vertebrates (Li et al., 2007). Obligatory POL-neurons might, therefore, be part of a core network underlying general azimuth coding, while conditional POL-neurons might be recruited only when a particular navigational task is performed. Interestingly, two of the three conditional POL-neurons innervate the noduli. Evolutionarily, the noduli are the most recent additions to the central complex and may be associated with the origin of flight (Homberg, 2008). Especially large noduli are present in flies (Strausfeld, 1999), suggesting that they provide additional computational power during complex flight maneuvers.

Beyond the central complex

The LAL-LT and LAL-pPC neurons are likely post-synaptic to the central-complex network. The LAL-LT neuron communicates between projection areas of columnar neurons across the brain midline, while the LAL-pPC neuron transfers polarization information to the posterior protocerebrum. Both the LAL and the posterior protocerebrum are regions, where many descending neurons receive their input (Williams, 1975; Strausfeld and Seyan, 1985; Staudacher and Schildberger, 1998; Okada et al., 2003). The different Φ_{max}-values of the two LAL-LT recordings implicate that several LAL-LT neurons differ in *E*-vector tuning or that *E*-vector tuning in the same neuron is dynamically adjusted corresponding to motor demands. Transforming polarization vision signals into motor commands clearly requires state-dependent gating and plasticity demonstrated at various levels of motor control (Rowell and Reichert, 1986; Reichert, 1993; Staudacher and Schildberger, 1998). These mechanisms will have to be taken into account when further analyzing the role of polarized skylight in directional steering in insects.

References

Batschelet E (1981) Circular statistics in biology. London: Academic Press.

Brunner D, Labhart T (1987) Behavioural evidence for polarization vision in crickets. Physiol Entomol 12:1-10.

Clements A, May TE (1974) Studies on locust neuromuscular physiology in relation to glutamic acid. J Exp Biol 60:673-705.

Eggers A, Gewecke M (1993) The dorsal rim area of the compound eye and polarization vision in the desert locust (*Schistocerca gregaria*). In: Sensory systems of arthropods (Wiese K, Gribakin FG, Popov AV, Renninger G, eds), pp 101-109. Basel: Birkhäuser.

Frisch K (1949) Die Polarisation des Himmelslichtes als orientierender Faktor bei den Tänzen der Bienen. Experientia 5:142-148.

Hanesch U, Fischbach KF, Heisenberg M (1989) Neuronal architecture of the central complex in *Drosophila melanogaster*. Cell Tissue Res 257:343-366.

Heinze S, Homberg U (2007) Maplike representation of celestial E-vector orientations in the brain of an insect. Science 315:995-997.

Heinze S, Homberg U (2008) Neuroarchitecture of the central complex of the desert locust: Intrinsic and columnar neurons. J Comp Neurol 511:454-478.

Homberg U (1985) Interneurons of the central complex in the bee brain *Apis mellifera*. J Insect Physiol 31:251-264.

Homberg U (1994) Flight-correlated activity changes in neurons of the lateral accessory lobes in the brain of the locust *Schistocerca gregaria*. J Comp Physiol A 175:597-610.

Homberg U (2004) In search of the sky compass in the insect brain. Naturwissenschaften 91:199-208.

Homberg U (2008) Evolution of the central complex in the arthropod brain with respect to the visual system. Arthropod Struct Dev 37:347-362.

Homberg U, Paech A (2002) Ultrastructure and orientation of ommatidia in the dorsal rim area of the locust compound eye. Arthropod Struct Dev 30:271-280.

Horváth G, Varjú D (2004) Polarized light in animal vision. Springer: Berlin.

Kinoshita M, Pfeiffer K, Homberg U (2007) Spectral properties of identified polarized-light sensitive interneurons in the brain of the desert locust *Schistocerca gregaria*. J Exp Biol 210:1350-1361.

Labhart T, Meyer EP (2002) Neural mechanisms in insect navigation: polarization compass and odometer. Curr Opin Neurobiol 12:707-714.

Li WC, Sautois B, Roberts A, Soffe SR (2007) Reconfiguration of a vertebrate motor network: specific neuron recruitment and context-dependent synaptic plasticity. J Neurosci 27:12267-12276.

Liu G, Seiler H, Wen A, Zars T, Ito K, Wolf R, Heisenberg M, Liu L (2006) Distinct memory traces for two visual features in the *Drosophila* brain. Nature 439:551-556.

Mappes M, Homberg U (2004) Behavioral analysis of polarization vision in tethered flying locusts. J Comp Physiol A 190:61-68.

Mronz M, Strauss R (2008) Visual motion integration controls attractiveness of objects in walking flies and a mobile robot. In: IEEE/RSJ International conference on intelligent robots and systems. Conference proceedings (Chatila R, Kelly A, Merlet J, eds), pp 3559-3564. New York: IEEE.

Müller M. (1997) Anatomische und funktionelle Charakterisierung der unteren Einheit des Zentralkörpers im Gehirn der Heuschrecke *Schistocerca gregaria*. PhD-Thesis, Universität Regensburg.

Müller M, Homberg U, Kühn A (1997) Neuroarchitecture of the lower division of the central body in the brain of the locust (*Schistocerca gregaria*). Cell Tissue Res 288:159-176.

Neuser K, Triphan T, Mronz M, Poeck B, Strauss R (2008) Analysis of a spatial orientation memory in *Drosophila*. Nature 453:1244-1247.

Okada R, Sakura M, Mizunami M (2003) Distribution of dendrites of descending neurons and its implications for the basic organization of the cockroach brain. J Comp Neurol 458:158-174.

Pfeiffer K, Homberg U (2007) Coding of azimuthal directions via time-compensated combination of celestial compass cues. Curr Biol 17:960-965.

Pfeiffer K, Kinoshita M, Homberg U (2005) Polarization-sensitive and light-sensitive neurons in two parallel pathways passing through the anterior optic tubercle in the locust brain. J Neurophysiol 94:3903-3915.

Reichert H (1993) Sensory inputs and flight orientation in locusts. Comp Biochem Physiol 104:647-657.

Rowell CHF, Reichert H (1986) Three descending interneurons reporting deviation from course in the locust. J Comp Physiol A 158:775-794.

Sakura M, Lambrinos D, Labhart T (2008) Polarized skylight navigation in insects: model and electrophysiology of e-vector coding by neurons in the central complex. J Neurophysiol 99:667-682.

Staudacher E, Schildberger K (1998) Gating of sensory responses of descending brain neurones during walking in crickets. J Exp Biol 201:559-572.

Strausfeld NJ (1999) A brain region in insects that supervises walking. Progr Brain Res 123:273-284.

Strausfeld NJ, Seyan HS (1985) Convergence of visual, haltere, and prosternal inputs at neck motor neurons of *Calliphora erythrocephala*. Cell Tissue Res 240:601-615.

Strauss R (2002a) Die übergeordnete Steuerung des Laufverhaltens durch das Insektengehirn, studiert mit Methoden der *Drosophila*-Neurogenetik. Habilitationsschrift, Universität Würzburg.

Strauss R (2002b) The central complex and the genetic dissection of locomotor behaviour. Curr Opin Neurobiol 12:633-638.

Träger U, Wagner R, Bausenwein B, Homberg U (2008) A novel type of microglomerular synaptic complex in the polarization vision pathway of the locust brain. J Comp Neurol 506:288-300.

Vitzthum H, Müller M, Homberg U (2002) Neurons of the central complex of the locust *Schistocerca gregaria* are sensitive to polarized light. J Neurosci 22:1114-1125.

Wegerhoff R, Breidbach O, Lobemeier M (1996) Development of locustatachykinin immunopositive neurons in the central complex of the beetle *Tenebrio molitor*. J Comp Neurol 375:157-166.

Wehner R (1984) Astronavigation in insects. Annu Rev Entomol 29:277-298.

Wehner R, Labhart T (2006) Polarization vision. In: Invertebrate vision (Warrant E, Nilsson D-E, eds), pp 291-348.Cambridge: Cambridge University Press.

Williams JLD (1975) Anatomical studies of the insect central nervous system: a ground-plan of the midbrain and an introduction to the central complex in the locust, *Schistocerca gregaria* (Orthoptera). J Zool (Lond) 176:67-86.

Transformation of polarized light information in central complex of the locust

Behavioral/Systems/Cognitive

Transformation of polarized light information in the central complex of the locust.

Stanley Heinze[1], Sascha Gotthardt[1], Stephan Gebhardt[1], and Uwe Homberg[1*]

[1]Fachbereich Biologie, Tierphysiologie, Philipps-Universität Marburg, D-35032 Marburg, Germany

Many insects perceive the E-vector orientation of polarized skylight and use it for compass navigation. In locusts, polarized light is detected by photoreceptors of the dorsal rim area of the eye. Polarized light signals from both eyes are integrated in the central complex (CC), a group of neuropils in the center of the brain. Thirteen types of CC neuron are sensitive to dorsally presented, polarized light (POL-neurons). These neurons interconnect the subdivisions of the CC, particularly the protocerebral bridge (PB), the upper and lower divisions of the central body (CBU, CBL), and the adjacent lateral accessory lobes (LALs). All POL-neurons show polarization-opponency, i.e. receive excitatory and inhibitory input at orthogonal E-vector orientations. To provide physiological evidence for the direction of information flow through the polarization vision network in the CC, we analyzed the functional properties of the different cell types through intracellular recordings. Tangential neurons of the CBL showed highest signal to noise ratio, received either ipsilateral polarized-light input only or, together with CL1 columnar neurons, had eccentric receptive fields. Bilateral polarized-light inputs with zenith-centered receptive fields were found in tangential neurons of the PB and in columnar neurons projecting to the LALs. Together with other physiological parameters these data suggest a flow of information from the CBL (input) to the PB and from here to the LALs (output). This scheme is supported by anatomical data and suggests a transformation of purely sensory E-vector coding at the CC input stage to position-invariant coding of 360°-compass directions at the output stage.

Keywords: neural network; insect brain; polarization vision; central complex; compass navigation; locust

Introduction

The central complex (CC) is a prominent group of neuropils in the center of the insect brain. It consists of the protocerebral bridge (PB), the upper and lower division of the central body (CBU, CBL), and the paired noduli. In all insect species studied, the PB, the CBL and the CBU consist of linear arrays of 16 vertical columns and the CBU and CBL, in addition, of several horizontal layers (Williams, 1975; Homberg, 1991; Müller et al., 1997; Heinze and Homberg, 2008). The major building blocks of this almost crystalline structure are columnar and tangential neurons.

Evidence for the functional role of the CC is largely provided along three lines. Analysis of structural mutants in the fruit fly *Drosophila melanogaster* promotes a role of the CC in locomotion and leg coordination (Strausfeld, 1999; Strauss, 2002a). Behavioral learning paradigms in *D. melanogaster,* furthermore, suggest that the CC is essential for the memory of specific, behaviorally relevant visual features (Liu et al., 2006; Neuser et al., 2008). Electrophysiological data from locusts and crickets finally shows that CC-neurons respond to the orientation of the electric field vector (*E*-vector) of linearly polarized light (Vitzthum et al., 2002; Heinze and Homberg, 2007; Sakura et al., 2008; Heinze and Homberg, submitted). As the pattern of *E*-vectors in the blue sky is directly correlated with the sun's position, sensitivity to polarized light points to a crucial role of the CC in sky compass navigation (Homberg, 2004). Specifically, the topographic representation of zenithal *E*-vectors underlying the columns of the PB is suited to code for global head orientation with respect to the solar azimuth (Heinze and Homberg, 2007). All lines of evidence taken together suggest a likely role of the insect CC as internal compass required for planning of goal directed behavior.

In the CC of the desert locust, at least 13 types of neurons are part of the polarization vision network (Vitzthum et al., 2002, Heinze and Homberg, 2007, Heinze and Homberg, submitted). Three additional types of neuron show polarization sensitivity in 50% of recordings and appear to be recruited to the network dependent on the behavioral context (Heinze and Homberg, submitted). Based on morphological evidence and distributions of preferred *E*-vector orientations (Φ_{max}-values) of the involved neurons, a scheme of information flow within the locust CC has

Correspondence to: Uwe Homberg, Fachbereich Biologie, Tierphysiologie, Universität Marburg, D-35032 Marburg, Germany, Tel. +49-6421-2823402, Fax +49-6421-2828941, E-mail: homberg@staff.uni-marburg.de

We are grateful to Dr. Keram Pfeiffer for providing Spike2-scripts and for contributing to physiological data on CL1, TB1, and CP2 cells. We thank Ulrike Träger for contributing reconstructions of TL2/3 neurons, Sebastian Richter and Manfred Peil for constructing the stimulation devices and control equipment, and Karl Heinz Herklotz for raising desert locusts. This work was supported by DFG grant HO 950/16-2.

been proposed, covering all stages from sensory input to potential output neurons (Heinze and Homberg, submitted). Here we provide detailed electrophysiological data on all major components of this network. We analyzed background firing properties, response amplitudes, variability, tuning precision, ocular dominance, and visual field structure of these neurons, enabling us to define distinct groups of cell types based on their physiological response characteristics. We show that polarized light information is transformed through several stages of polarization-sensitive (POL) neurons in the CC. The data strongly support a scheme of information flow from TL2/3 input neurons, via CL1 cells to TB1/2 neurons and, finally, to CPU1- and CP1/2 output cells.

Material and Methods

Animals and preparation. Adult desert locusts (*Schistocerca gregaria*) of both sexes were obtained from a crowded colony at the University of Marburg. Animals were raised in a 12L:12D photoperiod at constant temperature (28°C). Preparation for electrophysiology was performed as described by Heinze and Homberg (submitted). In short, animals were cold anesthetized, legs and wings were removed, and after fixing the locust to a metal holder in an upright position, the head capsule was opened. The brain was exposed and the gut, as well as the neural sheath near the recording area, was removed. The brain was kept submerged in locust saline (Clements and May, 1974) at all times to prevent desiccation.

Electrophysiology. Intracellular recordings were performed with sharp microelectrodes (resistance: 50-150 MΩ), drawn from borosilicate capillaries (0.75 mm ID, 1.5 mm OD; Hilgenberg, Malsfeld, Germany) using a Flaming/Brown horizontal puller (P-97, Sutter, Novato, CA). Electrode tips were filled with 4% Neurobiotin (Vector Laboratories, Burlingame, UK) in 1M KCl. The electrode shaft was backed up with 1M KCl. Intracellular signals were amplified (10x) with a custom made amplifier or a SEC5-LX amplifier (NPI, Tamm, Germany). After sampling at a sampling rate of at least 5 kHz (CED1401 micro, Cambridge Electronic Design, UK; or Digidata 1322A, Molecular Devices, Sunnyvale, CA, USA), signals were stored on a PC using Spike2- (Cambridge Electronic Design) or PClamp9 software (Molecular Devices). Digital high pass filtering was applied when necessary to compensate for drifting baseline. Depolarizing current was applied (1-3 nA, 1-5 min) to iontophoretically inject Neurobiotin immediately after recording.

Stimuli. Visual stimuli were produced with a xenon-arc (XBO 150 W), passed through light guides (Schölly, Denzlingen, Germany; spectral range 400–800 nm), to be finally presented to the animal from dorsal direction (irradiance at the animal's head: 94 μW/cm²; angular size: 2.7°). A polarizer (HN38S, Polaroid, Cambridge, MA) was inserted between the end of the light guide and the animal and could be rotated in either direction by 360° at velocities between 20 and 30°/s. Rotation velocity and direction were controlled via custom designed hard- and software. The light guide and polarizer were mounted on a perimeter and could thus be moved horizontally around the vertically mounted animal. Therefore, different elevations of stimuli could be tested. With few exceptions, the polarizer was rotated by 360° at least once in each direction (clockwise and counter clockwise) at all tested stimulus positions. To allow for monocular stimulations, a small piece of black cardboard was used to block the light path to one eye during dorsal stimulations. The piece was placed very close to the animal, either hand held or, in most cases, positioned with a micromanipulator. Stimulus presentation was always started with dorsal, binocular stimuli, followed either by stimulation from different elevations or by monocular stimulations. At the end, a binocular, dorsal control stimulus was applied in most cases.

Histology. After Neurobiotin injection, brains were dissected out of the head capsule and fixed in a mixture of 4% paraformaldehyde, 0.25% glutaraldehyde, and 2% saturated picric acid (in 0.1 M phosphate buffer) over night at 4°C. After rinsing with 0.1 M phosphate buffered saline (PBS), brains were incubated with Cy3-conjugated Streptavidin (Dianova, Hamburg, Germany, 1:1000, in PBS with 0.5% Triton X-100). Preparations were subsequently rinsed, dehydrated in an increasing ethanol series, cleared in methylsalicylate, and mounted in Permount (Fisher Scientific, Pittsburgh, PA), as described in detail in Heinze and Homberg (2008).

Labeled neurons were scanned with a confocal microscope (Leica TCS-SP2, objective: HC PL APO 10×/0.4 Imm Corr CS; Leica, Bensheim, Germany) to confirm the neuron type. For detailed analysis and reconstructions, selected preparations were rehydrated, sectioned, and stained by immunofluorescence with primary antibodies against serotonin and synapsin (Heinze and Homberg, 2008). For *camera lucida* reconstructions, rehydrated preparations were sectioned and incubated with peroxidase conjugated Streptavidin (1:200; Amersham Buchler, Braunschweig, Germany). Staining was obtained by peroxidase mediated precipitation of 3,3´-diaminobenzidine tetrahydrochloride (0.3 mg/ml), intensified with nickel ammonium sulfate (Heinze and Homberg, 2008). Neuropil reconstructions are based on anti-synapsin immunolabeling and were performed with Amira 4.2 software (Visage Imaging, Berlin, Germany).

General statistical procedures. Statistical comparison of quantitative data obtained from recorded POL-neurons (tuning width, background firing rates, response amplitudes, etc.), was performed either pair wise (e.g. for comparison of ipsilateral versus contralateral stimulations) or across all cell types. Except for linear regression, SPSS software (version 11.5; SPSS Inc., Chicago, IL) was used to perform statistical tests. For all analyses, data were tested for normality with the Kolmogorov-Smirnov-test (with significance correction after Lilliefors; significance level, 0.05) and for homogeneity of variance with the Levene test. Pair wise testing was done with Mann-Whitney`s-U-test for data not distributed normally, whereas student's t-test was applied for normally distributed data. One way ANOVA (with F-statistics, combined with Tukey-HSD *post hoc* analysis for multiple testing) was used to test for differences among multiple groups of data if data were normally distributed and variance was homogeneous. If this was not the case, ANOVA with Brown-Forsythe statistics, combined with Games-Howell *post hoc* analysis for multiple testing was applied. Significance levels of 0.05 were used in all cases. Linear regression and correlation analysis was performed in Origin6.0 software (Microcal, Northampton, MA). The correlation coefficient (R_{cor}) was calculated, and the significance of the regression was tested with student's t-test against a regression line with slope of zero (significance level, 0.05). Analysis of covariance (univariant ANCOVA, using SPSS) was used to compare the slopes of regression lines. Hereby, the interaction between the covariate (background frequency) and the fixed factor (cell type) was tested for significant influence on the independent variable (response strength; significance level: 0.05). This was done

either including all considered groups (cell types) or only including the two groups, which were compared at the time.

Standard deviations (SD) were used in graphic displays whenever the actual variability of the data was compared, whereas standard errors (SE) were used as a measure of the precision of the mean.

Analysis of general response characteristics. Sampled spike trains were stored on PC and evaluated using Spike2-software with implemented, custom designed scripts. Action potentials were detected with threshold based event detection. The detected events were visualized as mean frequency using a gliding average algorithm at a bin size of 1s. Background frequency was estimated by moving a horizontal curser to the desired level in the mean frequency channel and reading out the current values of the curser position.

To calculate the strength of a polarized-light response (response amplitude, R), each filter rotation was divided into 20°-bins. The mean frequency over all bins was calculated, as well as the frequency within each bin. The summed, absolute difference between the mean frequency and the individual frequencies was defined as the R-value of that polarized-light response and reflected the magnitude of frequency modulation during the rotation. In some cases 180° rotations of the polarizer were applied instead of 360° rotations. Then, the resulting R-value was doubled to account for the different number of bins. Due to the usage of frequencies (impulses per second) rather than spike counts per bin (Labhart, 1996; Pfeiffer, 2006), R-values derived from rotations at different rotation velocities were directly comparable.

Background variability was calculated as the R-value of a spike train, when no stimulus was presented. To reveal the magnitude of spontaneous frequency modulations relative to the amplitude of polarized-light responses, we normalized the absolute background variability to the mean response amplitude of each neuron. Variability of R was calculated by averaging R-values of all rotations from each neuron and calculating the standard deviation thereof. These values were also normalized to the mean R-value of each neuron.

Φ_{max}-values were calculated with circular statistics (Rayleigh test for axial data, significance level: 0.05) as described previously (Pfeiffer et al., 2005; Heinze and Homberg, 2007; Pfeiffer and Homberg, 2007).

Evaluation of tuning curves. *E*-vector tuning widths were calculated using custom designed scripts in MatLab (MathWorks Inc., Natick, MA). Spike frequencies during *E*-vector rotation were calculated in 5°-wide bins. The resulting data were low pass filtered, and the half maximal activation level was calculated. The width of the *E*-vector response at this level was defined as the tuning width. Mean tuning widths were calculated for each neuron.

For shape averaging of tuning curves, we selected five neurons of each category of POL-neuron, which showed the strongest response. This procedure ensured that the neurons with the best signal to noise ratio, i.e. the most reliable tuning curve shape, were analyzed. Spike frequencies were calculated in 5°-bins, and polarized-light responses were normalized to the peak activity within each 180° rotation. After aligning all responses within a window of 180° (minimal activity at 0°, maximal activity at 90°), the mean of each bin was calculated. This procedure was repeated for all five neurons and the average value (± SD) of the considered cell type was determined for each 5°-bin.

Evaluation of receptive fields. For stimuli presented at different elevation, the response amplitudes were calculated. For each neuron, these values were normalized with respect to the largest value, i.e. the center of the receptive field, and thereafter plotted against the elevation. Because different elevations were tested in different recordings, average receptive fields could not be calculated directly. After assessing the raw data, we concluded that the overall shape of receptive fields of all neuron types was not complex (with the possible exception of TL3 neurons), but response amplitudes rose and fell smoothly from background variability to maximal response amplitude in the receptive field center. This legitimized the interpolation of missing data for individual receptive fields, and eventually the calculation of mean response amplitudes at all elevations.

Results

Central-complex POL-neurons

The results are based on 114 intracellular recordings combined with dye injection for identification of the neuron type. The recordings could be assigned to twelve different types of CC neurons, all of which have been shown to respond to dorsally presented polarized light before (Fig. 1, Vitzthum et al., 2002; Heinze and Homberg, 2007; Heinze and Homberg, in preparation). In response to a rotating polarizer placed in the zenith above the animal, neurons modulated their firing rate in a sinusoidal manner (Fig. 1). Each neuron had a particular preferred orientation of the *E*-vector, corresponding to maximal spiking activity (Φ_{max}-value).

Based on morphological evidence and the distribution of Φ_{max}-values, a connectivity scheme of the CC polarization vision network has been proposed (Heinze and Homberg, in preparation). Here we examined the physiological response characteristics of all major cell types of this network, and provide independent evidence for different roles of these cells in processing polarized light information in the CC.

Background firing properties, response amplitudes and firing variability

First we compared the quantified responses of the twelve major types of CC POL-neurons to a dorsally rotating polarizer. The resulting response amplitude (R-value) measures the summed deviation from mean activity during each filter rotation. The R-value increases with increasing frequency modulation during a polarized-light response, but contains no information about the directedness of this response. Therefore, this analysis was independent from the test for significant deviation from randomness by means of circular statistics (Rayleigh-test for axial data). Mean R-values were calculated for each neuron and the distribution of these values was compared between neuron types (Fig. 2A). Due to morphological similarity and very low numbers of recordings, CL1c/d neurons (n =1) where combined with CL1b/d neurons, and CPU1c neurons (n = 2) were combined with CPU1a cells. When quailtatively examining the resulting R-value distributions, cells belonging to closely related types of neuron were indistinguishable from each other (Fig. 2A). Analysis of variance (ANOVA), likewise, did not detect significant differences between these related types of neurons (not shown). Therefore, we combined all CL1

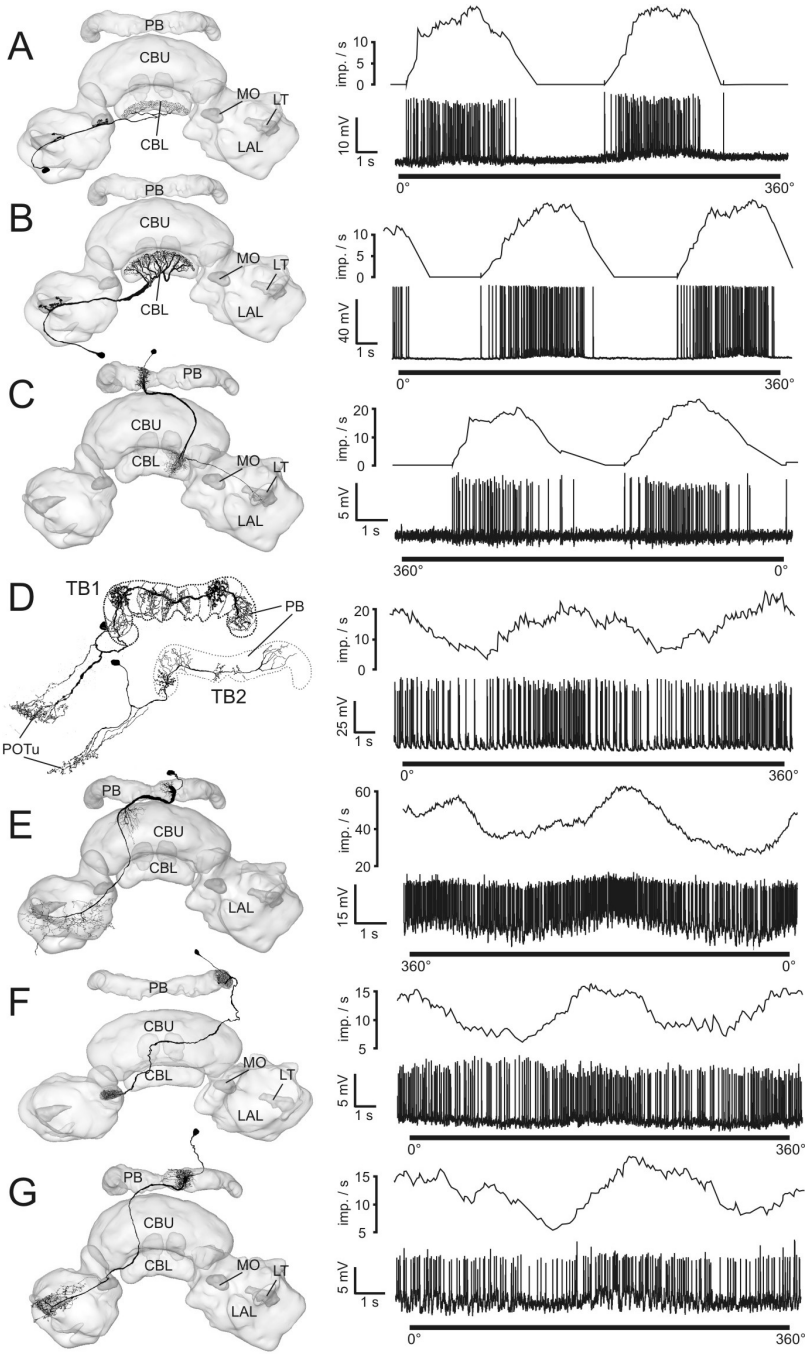

Figure 1. Morphologies of major types of POL neuron of the locust central complex and their neuronal responses to a 360° rotation of a dorsally presented polarizer. Frontal camera lucida reconstructions, projected onto three-dimensional reconstructions of the central complex, are shown on the left. Spike trains (lower lanes) and mean activities (upper lanes; gliding average, bin size: 1s) are shown on the right. Morphological and physiological data belong to neurons from the same cell type. ***A,*** TL3 neuron. ***B,*** TL2 neuron. ***C,*** CL1a neuron. ***D,*** TB1/2 neurons, physiology from a TB1 neuron. ***E,*** CPU1a neuron. ***F,*** CP1 neuron. ***G,*** CP2 neuron. CBL, CBU lower, respectively upper division of the central body; PB, protocerebral bridge; LAL, lateral accessory lobe; LT lateral triangle; MO medial olive. Neuron morphologies are modified from Träger et al., 2008 (***A,B***), Heinze and Homberg, 2008 (***C, E-G***), Heinze and Homberg, 2007 (D_{top}), and Heinze and Homberg, submitted (D_{bottom}).

cells, all CPU1 cells, both types of TB neurons, and both CP neurons for further examination of R-values. Despite their morphological similarity and lack of significant differences between R-values, TL2 and TL3 neurons were not combined, because they showed distinct reactions to more complex stimuli considered later. When performing ANOVA with grouped data, the mean R-values of all cell types were not statistically different from each other (Fig. 3A). The only exceptions were CP neurons, which showed significantly lower response amplitudes than TL3- and TB neurons.

The second feature analyzed was the background firing rate of POL-neurons. As for R-values, no apparent differences between closely related neuron types were observed (Fig. 2B). This was also confirmed by ANOVA and allowed for the same grouping of cell types as for R-values. However, considerable difference was evident between different groups of neurons. Applying ANOVA to these groups, these differences proved to be highly significant in most cases (Fig. 3B). Lowest background firing rates were present in TL neurons (TL3: 5.9 ± 0.5 impulses/s, mean ± SE; TL2: 6.5 ± 0.9 impulses/s), whereas highest rates were observed in TB neurons and CPU1 cells (TB: 24.9 ± 1.4 impulses/s; CPU1: 25.8 ± 2.7 impulses/s). Intermediate firing rates occurred in CL1 neurons (10.3 ± 1.0 impulses/s) and CP neurons (10.9 ± 2.8 impulses/s), whereas the latter ones showed large variability and were not significantly different from either of the TL neurons.

As frequency modulation during polarized-light responses is always superimposed upon background activity, the same response amplitude occurring at low or high background firing rates can be expected to have different effects on postsynaptic neurons. Therefore we next analyzed the ratio of response amplitude versus firing rate. When plotting these parameters for all neurons analyzed, each group of cells covered a certain region within this two dimensional parameter space (Fig. 2C). Analysis of each group of neurons showed, again with the exception of TL neurons, that the response amplitude and the background firing rate are linearly correlated, meaning that increased background activity was mirrored by higher R-values (Fig. 2C). Interestingly, the slope of the regression line depended partly on the type of neuron considered. Very similar values were obtained

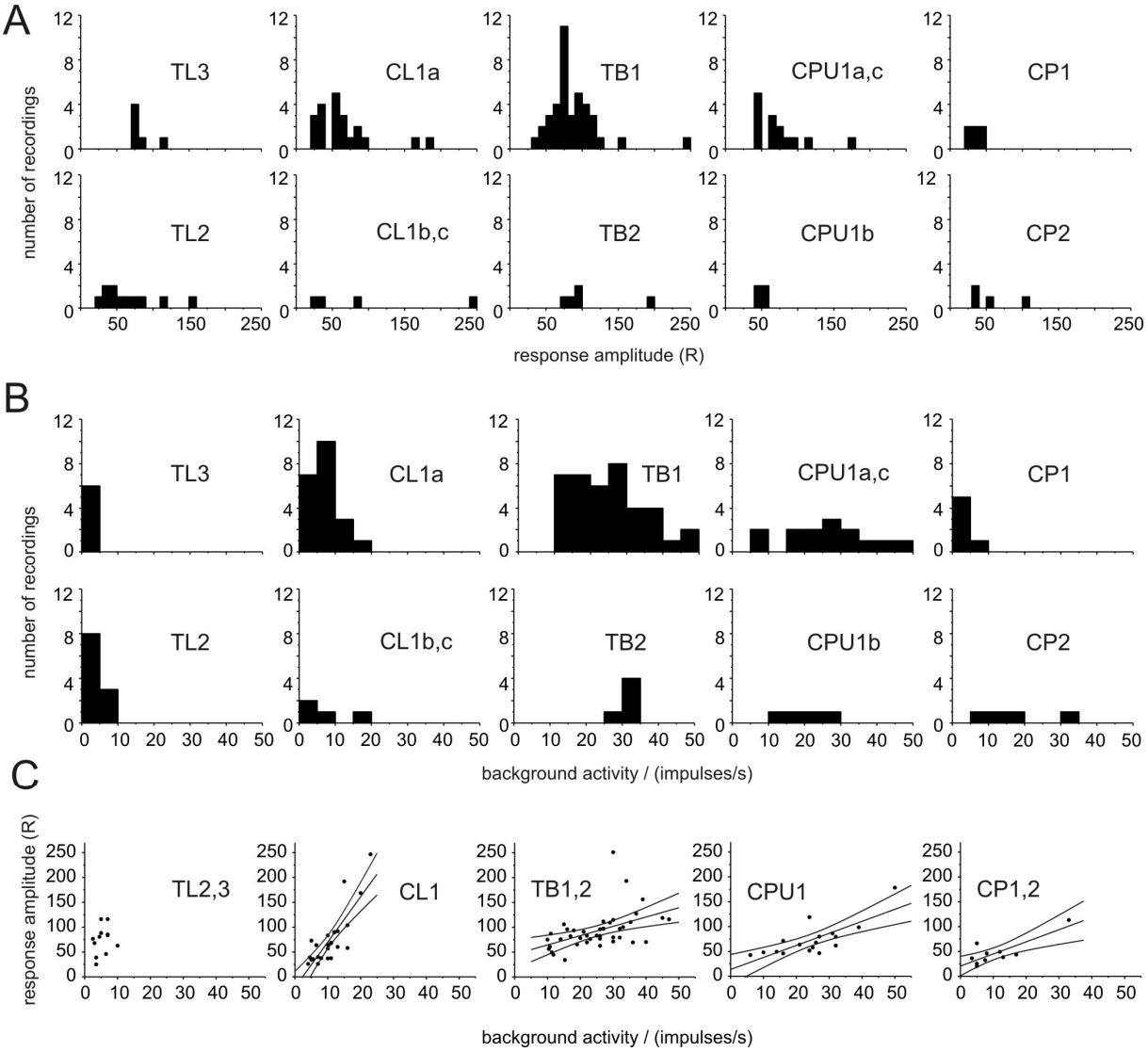

Figure 2. Response amplitudes and background firing rates of all types of POL neuron. ***A,*** Distributions of response amplitudes (R) across recordings for each type of POL neuron. The number of recordings per bin (bin size: 10) is plotted against the response amplitude. ***B,*** Distributions of background firing rates for each neuron type. The number of recordings per bin (bin size 5 impulses/s) is plotted against background activity. ***C,*** Relation between response amplitude and background activity. The graphs show all recordings grouped according to main cell type. Linear regression lines (with 95% confidence intervals) are presented for each group of neurons. There was no statistical difference between the linear regressions for TB, CPU1, and CP neurons (test for equality of slopes, using analysis of covariance; $p = 0.767$). TL neurons show no significant linear correlation, while the regression line for CL1 neurons was distinct from all remaining regressions ($p < 0.001$ for all three cell types). Data for linear regressions: TL2/3, $p = 0.47$, correlation coefficient (R_{cor}) = 0.23; CL1, $p < 0.0001$, $R_{cor} = 0.82$; TB1,2, $p = 0.0014$, $R_{cor} = 0.48$; CPU1, $p = 0.00036$, $R_{cor} = 0.76$; CP1/2, $p = 0.004$, $R_{cor} = 0.82$.

for TB, CPU1, and CP neurons (no significant difference in slope with ANCOVA, $p = 0.767$), but CL1 cells showed a much faster increase in response amplitude with increasing background activity ($p < 0.001$ in all cases), placing them between TL neurons and the remaining cell types. Statistically comparing the ratios of R-values to background activity (ANOVA) fully confirmed this observation, showing that both types of TL neuron, as well as CL1 cells, had significantly higher ratios than TB and CPU1 cells (Fig. 3C). Moreover, TL3 cells were also significantly different from CL1 cells, whereas both TL cells differed from CP neurons. Taken together, these analyses promote the separation of POL-neurons into three groups: TL cells, CL1 cells, and TB/CPU1 neurons. With some uncertainty, CP neurons may be grouped together with TB and CPU1 cells.

As the examined POL-neurons occur at different stages of information processing within the CC network, we analyzed the variability of polarized light responses in the different groups of neurons. To obtain a measure of intraneuronal variability of responses, R-values were obtained for each individual rotation of the polarizer. The standard deviation of these values was calculated and normalized against the mean R-value of that cell. The resulting values indicate the relative variability in response amplitude of each neuron. Comparison of these values between the cell types did not reveal significant differences (Fig. 4A). Variability of all types of neuron ranged between 10% and 20% of the absolute response amplitude.

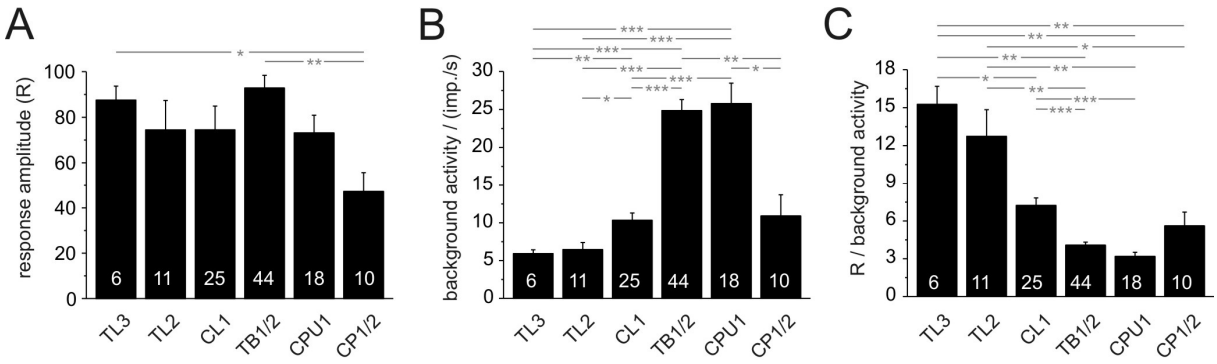

Figure 3. Response amplitudes and background firing rates of the different cell types. Numbers of recordings are indicated in each bar. Error bars represent standard error. ***A,*** Mean response amplitudes of each group of neuron. ***B,*** Background firing rates for each group of neuron. ***C,*** Ratio of response amplitude and background firing rates for each group of neuron. This ratio provides an estimate of the information content of the frequency modulations during a rotation of the polarizer. Asterisks indicate significant differences as revealed by ANOVA with Games-Howell *post hoc* test. Significance levels: *, $p < 0.05$; **, $p < 0.01$; ***, $p < 0.001$.

Finally, we analyzed the magnitude of background variability in the different groups of neuron. We reasoned that the information content of a polarized-light response depends on the magnitude of frequency fluctuations occurring without the presence of the stimulus. To quantify background variability, we calculated the R-value of a spike train during periods when no stimulus was applied, and normalized these values for the response amplitude of that neuron (Fig. 4B). The results showed that there is a general tendency of increasing background variability from lowest values in TL3 and TL2 neurons (21% and 34%), to intermediate values in CL1 and TB neurons (42% and 44%), and highest values in CPU1 and CP neurons (49% and 53%). Supporting that tendency, ANOVA revealed significantly lower background variability in TL3 cells, compared to all other cell types except TL2 cells. This implies that in CP neurons more than 50% of the frequency modulations observed during polarized-light stimulations are due to background fluctuations in spiking activity, as opposed to only 21% in TL3 neurons.

Taking together the data on response amplitude, background firing rates, relative response amplitudes, and background variability, we consistently found that certain groups of neuron behave similarly. In particular, TL2 and TL3 neurons form a group of cell types with low background activity, high relative response amplitudes and the best signal to noise ratio. On the other end, high background activities, low relative response amplitudes, and lowest signal to noise ratios were found in TB and CPU1 cells. Intermediate values were observed in CL1 neurons. CP cells tended to be most similar to CPU1 and TB1 neurons and might potentially be included in that group.

Tuning curves

To further examine differences in the considered groups of POL neurons, the shape and width of tuning curves were analyzed. The response curves of the five neurons with the highest response amplitude were selected for each cell type, binned in 5°-bins, normalized to peak activity, and aligned with respect to their Φ_{max}-values (Fig. 5A). Several distinct features were observed when comparing the different types of POL-neuron. Despite their similar morphology and firing characteristics, TL2 and TL3 neurons differed in the shape of their tuning curves. TL3 cells showed a very steep rise of activity between maximal and minimal activation, resulting in an almost rectangular, all-or-nothing like response curve, with a plateau of peak activity covering an angle of about 60°. The rising slope in activity was much gentler in TL2 cells, resulting in a more sinusoidal shape with a narrower plateau of peak activity. A distinctly triangular shape was found in CL1a cells. These neurons showed the narrowest region of peak activity, providing the most precise *E*-vector coding of all considered cell types. TB1 and CPU1 neurons were modulated only in the upper

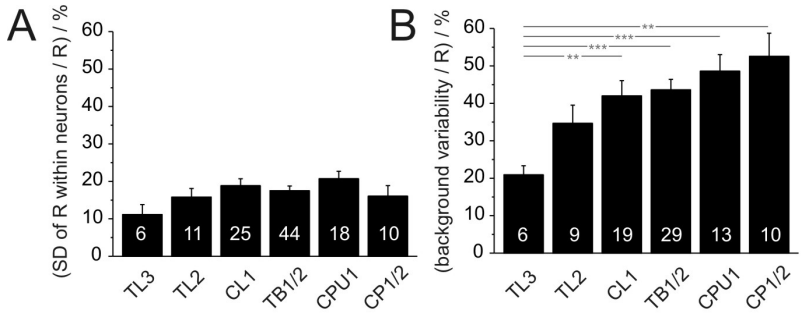

Figure 4. Variability in response amplitude and background activity in the different types of POL neuron. Numbers of recordings are indicated in each bar. ***A,*** Mean variability of R-values in each group of cells. Mean standard deviations (SD) from individual recordings are plotted. Values were normalized with respect to the absolute response amplitudes before the calculation of the mean. No differences between cell types were observed. ***B,*** Variability in background spiking activity in the different types of neuron. Means of R-values of background activity, normalized to the absolute response amplitude of each neuron are plotted. The resulting values indicate how much variability during stimulation is due to spontaneous variability. Asterisks indicate significant differences as revealed by ANOVA analysis with Games-Howell *post hoc* test. Significance levels: *, $p < 0.05$; **, $p < 0.01$; ***, $p < 0.001$. All error bars represent standard error.

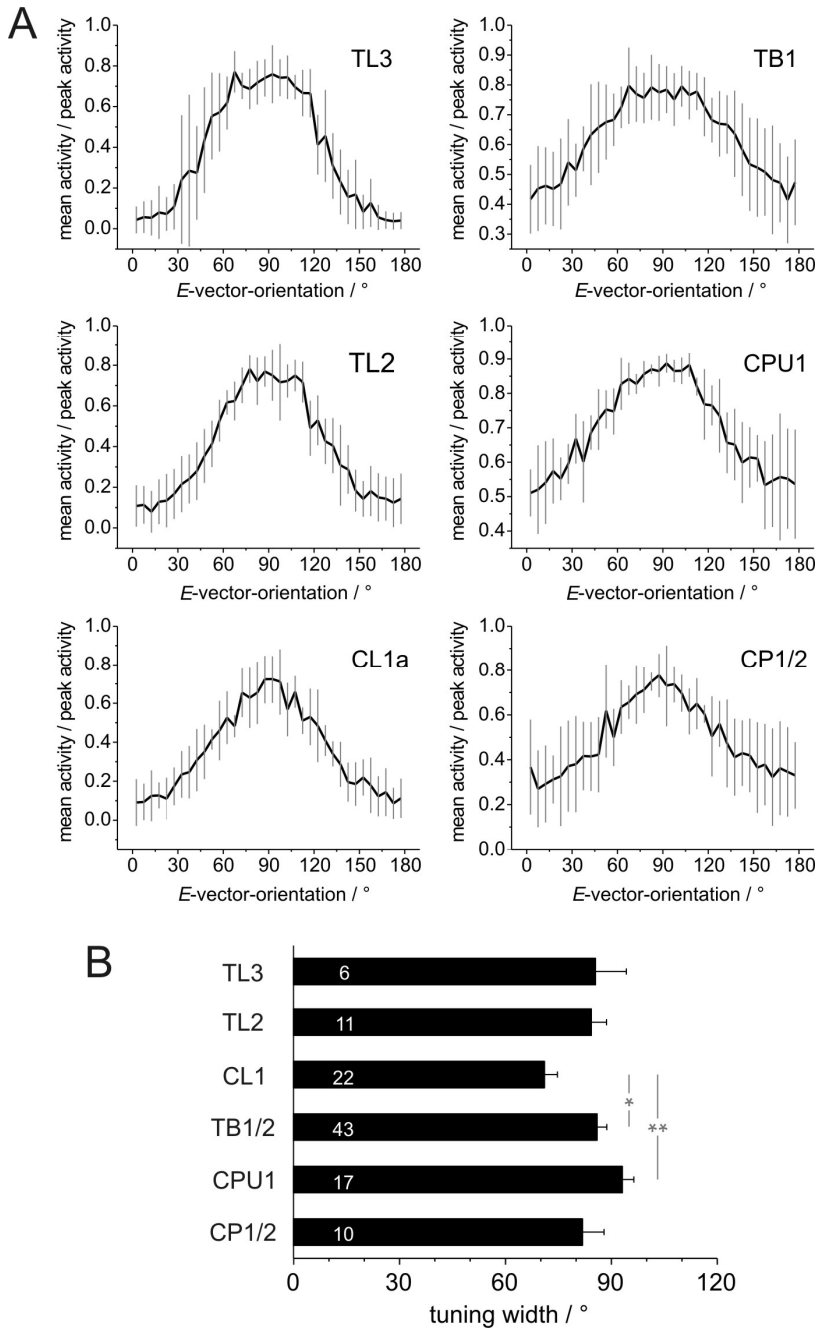

Figure 5. Characteristics of tuning curves of different types of POL neuron. ***A,*** Average shapes of tuning curves (means ± standard deviation, bin size: 5°) from the five neurons with the largest response amplitude in each category. Tuning curves were normalized to peak activity during each rotation, manually aligned, averaged within each recording, and thereafter averaged across neurons. Plots are scaled from minimal to maximal activity. ***B,*** Comparison of tuning widths at half maximal activation. Numbers of recordings are indicated in each bar. As tuning width of some recorded neurons could not be determined reliably, numbers are lower than in Fig. 3 and 4. Asterisks indicate significant differences revealed by ANOVA analysis combined with Tukey-HSD *post hoc* test. Significance levels: *, $p < 0.05$; **, $p < 0.01$. Values are means ± standard error.

half of their activity range and exhibited a broad plateau-like tuning combined with a gentle rise and fall between Φ_{max} and Φ_{min}-values. The overall shape of the tuning curve was slightly asymmetrical in about half of the included CPU1 neurons. Here, either the rising or the falling slope of the curve was convex and graded, whereas the opposite slope was more abrupt and concave. Finally, CP1/2 neurons were most variable and possessed the least distinct tuning curves, with an overall sinusoidal appearance.

These qualitative observations were supported by measurements of the tuning width at half-maximal activation (Fig. 5B). On average, largest values were found in CPU1 neurons (93° ± 3.3°), whereas the narrowest tuning was present in CL1 cells (71° ± 3.7°; significantly smaller with ANOVA analysis). The remaining types of neuron had a similar tuning width between 82° and 86°, and only TB1/2 cells had a significantly broader tuning than CL1 neurons (Fig. 5B). Therefore, for most neurons, regions of inhibition and excitation are nearly equally distributed within the 180° *E*-vector range. Only CL1 neurons exhibit consistently more inhibition, resulting in an increased coding precision within the range of activation. Taken together, the analysis of tuning curves established a distinct behavior of CL1 neurons and a clear difference between TL2 and TL3 cells. As in the previously described firing characteristics, tuning curves of TB1 and CPU1 neurons had very similar characteristics.

Ocular dominance

We next analyzed the ocular dominance of all groups of CC POL-neurons to elucidate how much information each neuron receives from either eye. Data were obtained from 29 recordings with binocular and monocular stimulation.

Most neurons showed strong responses to a rotating polarizer at monocular and binocular stimulation without obvious differences in response characteristics. The only exceptions were TL3 neurons, which responded exclusively to stimulation through the ipsilateral eye. These observations were confirmed when analyzing the response amplitudes (R-values) of each neuron during monocular and binocular stimulations. For each neuron, R-values for monocular stimulations were normalized to the binocular response amplitude and thereafter pooled within each group of neurons (Fig. 6A).

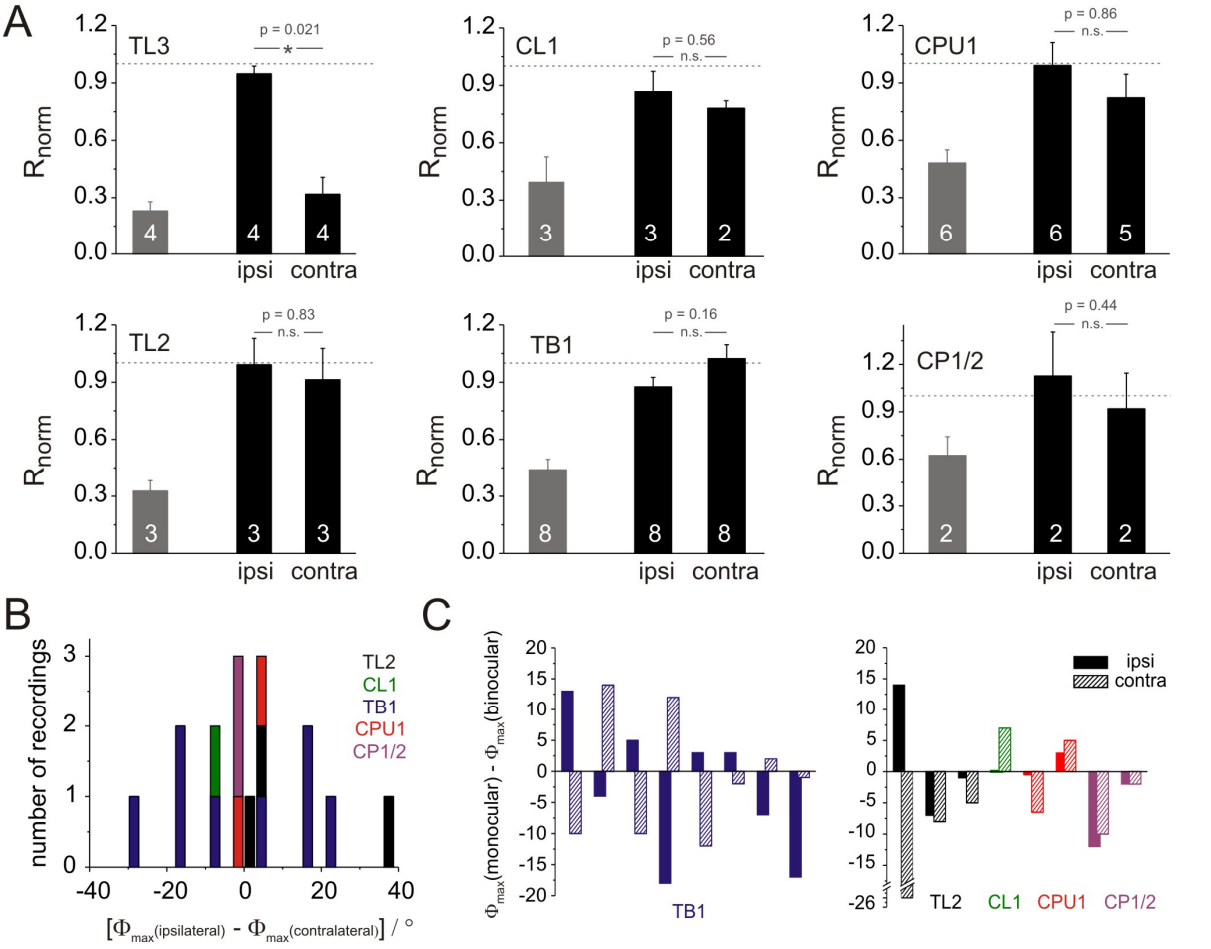

Figure 6. Ocular dominance of the different types of POL neuron. ***A,*** Response amplitudes for monocular stimulation with a dorsally rotating polarizer (ipsi, ipsilateral eye only; contra, contralateral eye only). Grey bars indicate mean background variability of the tested neurons. Response amplitudes (R) of each neuron were normalized to the binocular response amplitude (dashed line) before averaging. Numbers of recordings are indicated in each bar. Error bars represent standard error. ***B,*** Distribution of differences in Φ_{max}-values between stimulations through the ipsi- and contralateral eye. The numbers of recordings are plotted per 3° bins. Negative values indicate that the contralateral Φ_{max}-value is larger than the ipsilateral one. Values are generally distributed symmetrically around zero.TB1 neurons exhibit larger differences than the remaining cell types. ***C,*** Deviations of monocular Φ_{max}-values from binocular values. Each pair of bars (hatched and filled) represents ipsilateral (filled) and contralateral (hatched) values from one neuron. TB1 neurons are presented in the left graph, all remaining cell types in the right graph. Note that in most TB1 neurons binocular values were between the monocular stimulations, whereas this was only once the case in all remaining cell types.

Comparison of R-values for monocular and binocular stimulations (Mann-Whitney-U test, significance-level: 0.05) revealed that all neurons except TL3 cells responded equally well to ipsi- and contralateral stimuli. In three recordings from CPU1 neurons and in one recording from a CL1 cell however, the responses to the rotating polarizer were not significantly different from randomness in one of the monocular stimulus presentations (not shown).

After evaluating the response amplitudes, differences in *E*-vector tuning for monocular and binocular stimulations were analyzed. Only stimulations leading to responses that were significantly different from randomness were included. As expected, Φ_{max}-values of TL3 neurons were nearly identical for ipsilateral and binocular stimulations (maximal deviation: 6°). This was in tune with the finding that these neurons received exclusively ipsilateral input. In 16 additional recordings, significant Φ_{max}-values were obtained for all three stimulus situations. These cells could be divided into two groups; the TB1 neurons and all remaining neurons. In TB1 cells, Φ_{max}-values for binocular stimulation were between the Φ_{max}-values for ipsi- and contralateral stimulation (Fig. 6C; seven out of eight cells). For most of the remaining cells this was not the case and both monocular Φ_{max}-values were either larger (1x) or smaller (5x) than the binocular value (Fig. 6C). In six recordings, only one monocular stimulus was tested (2xCL1, 4xCPU1). In these neurons, the binocular Φ_{max}-value was always larger than the monocular one. The difference between TB1 neurons and the remaining cells was also reflected in the distribution of the differences between ipsi- and contralateral Φ_{max}-values (Fig. 6B). Here, TB1 neurons generally showed larger $\Delta\Phi_{max}$-values than all other cell types. Interestingly, values were distributed symmetrically around zero, indicating that ipsi- and contralateral Φ_{max}-values were larger in equal numbers of recordings. Quantitative analysis of the absolute $\Delta\Phi_{max}$-values resulted in a mean value of 16.4° ± 2.7° (SE) for TB1 cells and 7.6° ± 4.6° for the remainders.

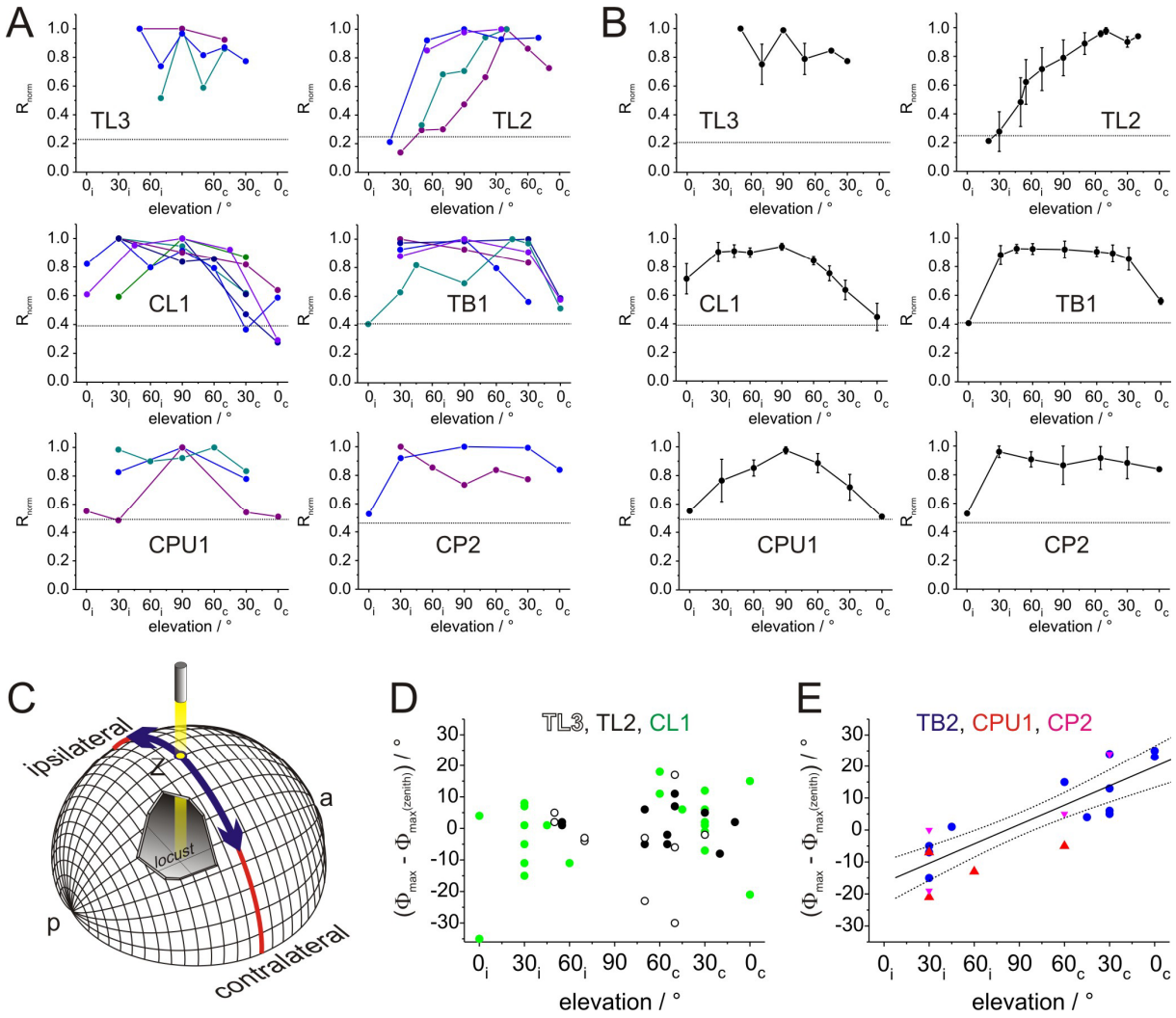

Figure 7. Receptive field properties of POL-neurons. ***A,*** Response amplitudes of different types of POL-neuron plotted against elevation of polarized-light stimulus. Elevation is plotted with respect to the location of the soma and was sampled along the meridian orthogonal to the longitudinal body axis of the locust. Values were normalized to the largest R-value of each neuron (i.e. the receptive field center). Individual recordings are distinguished by different colors. Data points are connected by lines for better visibility. Dotted lines indicate background variability for each neuron type (from Fig. 4), which have been renormalized with respect to the mean receptive field center in each cell type. ***B,*** Average receptive fields for the examined groups of POL-neuron. Dotted lines, background variability. Values are means ± standard error. Missing values in individual recordings were interpolated linearly to allow for averaging at all elevations. ***C,*** Schematic representation of stimulus display. The locust is located in the center of the sphere, facing the anterior side (a), away from posterior (p). Stimuli were moved along the meridian (blue) orthogonal to the body axis. ***D,E,*** Deviations of Φ_{max}-values at different elevations from zenithal Φ_{max}-values for TL3-, TL2-, and CL1 neurons (***D***), and for TB1-, CPU1-, and CP2 neurons (***E***). Differences in Φ_{max}-values are plotted against elevation. A significant correlation was observed for the combined values of TB1, CPU1, and CP1 (correlation coefficient (R_{cor}) = 0.84, t-test against the slope of 0, $p < 0.00001$), indicated in ***E*** by the regression line with 95% confidence intervals. No correlation was observed for neurons in ***D*** (R_{cor} = 0.19, p = 0.24).

The two distributions were significantly different from each other (Mann-Whitney-U test, p = 0.021). To test whether the responses to either ipsi- or contralateral stimuli were more similar to the binocular responses, we also examined the distributions of the differences between Φ_{max}-values of both monocular responses from the binocular response (not shown). Both resulting distributions were concentrated around zero, i.e. identical values for monocular and binocular stimulations, with a slight shift toward smaller monocular values (ipsilateral: -2.4° ± 1.8°, Fig. 6C; contralateral: -4.0° ± 2.6°). There was no significant difference between the two distributions (two-sided students-t-test, p=0.61). Because the mean Φ_{max}-values at ipsi- and contralateral stimulation deviated equally from the Φ_{max}-values during binocular stimulation, input from neither eye dominated over the other eye across the population of recorded cells.

Structure of receptive fields

As most neurons received input from both eyes, we tested whether the different types of POL- neuron could be distinguished further by the structure of their receptive fields. Therefore, rotating *E*-vectors were presented at different elevations along the right-left meridian, covering a range from 0° elevation on either side of the animal to the zenith (90°, Fig. 7C). At least three different positions (always including dorsal presentation) were tested in each of 24 recordings, including all major types of POL-neuron (3xTL3, 4xTL2, 7xCL1, 5xTB1, 3xCPU1, 2xCP2). For estimating the lateral extension and shape of receptive fields, the

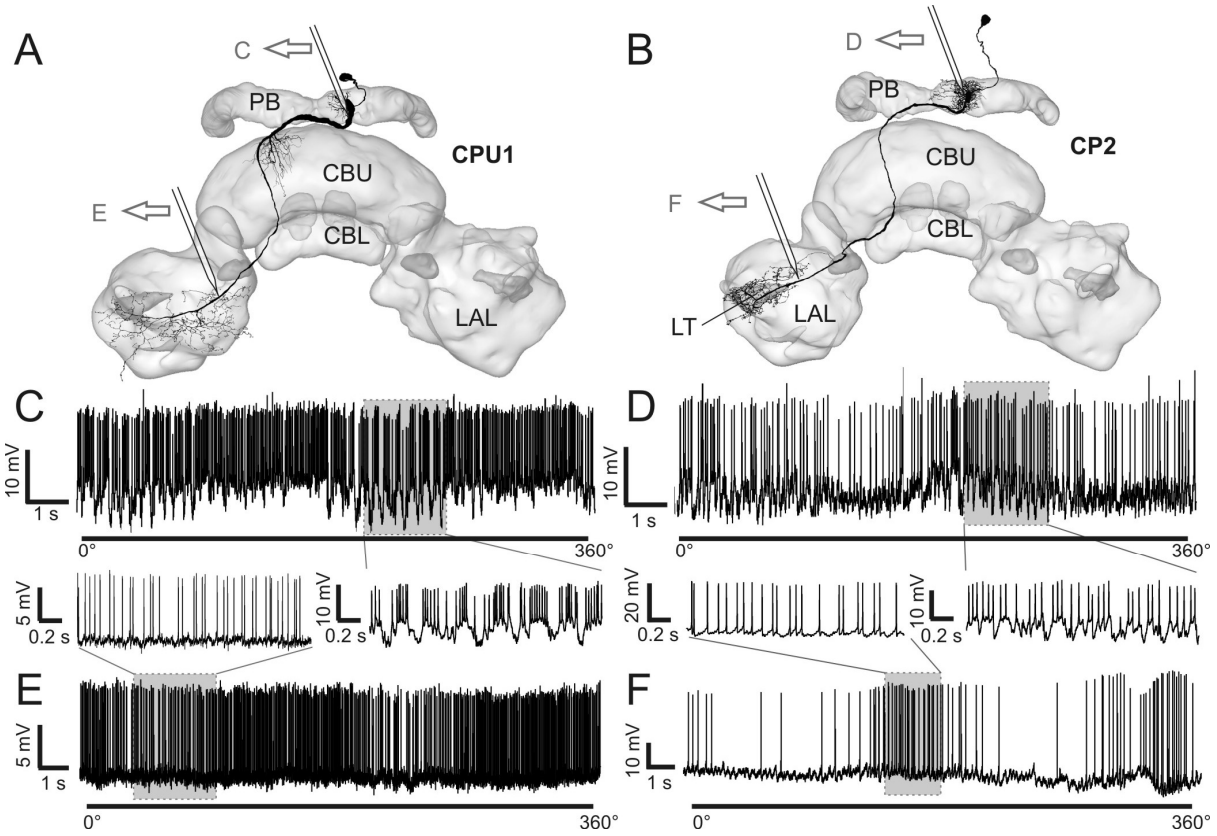

Figure 8. Indication of pre- and postsynaptic arborizations by recordings from different regions of CPU1- and CP2 neurons. ***A,B,*** Frontal reconstructions of a CPU1 (***A***) and CP2 neuron (***B***), projected onto a three-dimensional reconstruction of the CC. Approximate recording sites of the recording traces in ***C-F*** are indicated. ***C,*** Recording trace from arborizations of a CPU1 neuron in the protocerebral bridge (PB) during zenithal rotation of the polarizer. Postsynaptic, graded potentials are visible (enlargement of shaded area is shown in the inset). ***D,*** Recording trace from PB-arborizations of a CP2 neuron during a rotation of the polarizer. Postsynaptic potentials are clearly visible (enlarged in the inset). ***E,F,*** Recording traces obtained from the vicinity of the lateral accessory lobe (LAL) from a CPU1 neuron (***E***) and a CP2 neuron (***F***). Enlargements emphasize the even baseline without major graded potential changes. CBU, upper division of the central body; CBL, lower division of the central body; LT, lateral triangle.

response amplitude was calculated at each position and was normalized to the maximal value in each neuron. In all recorded cell types, receptive fields were large (Fig. 7A). The lateral size ranged from approximately 60° in a TL2 neuron to approximately 165° in a CP2 cell. With the possible exception of TL3 neurons, no complex structure, such as center-surround organization, was apparent.

As raw data for each type of neuron appeared sufficiently similar, mean receptive fields were calculated for comparison of neuron types (Fig. 7B). TL2- and CL1 neurons had eccentric fields with peak activation either in the contralateral field of view (TL2) or in the ipsilateral field of view (CL1, with one exception). TB1-, CPU1- and CP2 neurons had zenith-centered receptive fields. For TL3 neurons, no definite statement can be made due to low number of recordings and high variability. The widths of the receptive fields were calculated as the angle resulting in half-maximal response amplitude in relation to variability in background spiking activity. Thus, background variability rates (Fig. 3B) had to be re-normalized to maximum response amplitude of the receptive field center. This calculation revealed very similar background variability for TL2- and TL3 neurons, and indicated that the response strength of TL2 cells was underestimated when only considering dorsal stimulations. When comparing mean lateral extension of receptive fields, the smallest sizes were found in TL2 (100°), and very large receptive fields in CL1-, TB1-, CPU1-, and CP2 neurons (135°, 150°, 120°, and 150°). TL3 cells covered at least 90° along the tested meridian.

Surprisingly, significant activation was in some cases observed even at 0° elevation. This was most prominently found in the ipsilateral field of view of CL1 neurons. Indications of subpopulations within cell types were observed in TL2 cells, with one population of neurons responding almost exclusively to stimuli in the contralateral field of view, whereas the visual fields of the second group ranged about 30° across the midline (Fig. 7A).

In addition to response amplitudes within the receptive fields, we also analyzed the distribution of Φ_{max}-values at different elevations. When calculating the absolute deviation of Φ_{max}-values in each tested position from the Φ_{max}-value in the zenith, all POL neurons fell into one of two categories. The values for the first group (TL3, TL2, and CL1 neurons) were concentrated around zero (Fig. 7D). Variability increased toward lower elevations, as would be expected from the lower response amplitudes. Increasing deviations at lower elevations were also found in the second group. However, for TB1-, CPU1-, and CP2

neurons the deviation from zenithal Φ_{max}-values also depended on the hemispheric side of the stimulus (Fig. 7E). For stimulations in the ipsilateral field of view, Φ_{max}-values were consistently smaller than in the zenith, whereas they were consistently larger in the contralateral hemisphere (correlation coefficient (R) = 0.84, t-test against the slope of zero: $p < 0.00001$). No such hemisphere dependency was found in the first group ($R = 0.19$, $p = 0.24$).

Physiological evidence for input and output regions

To obtain information about the direction of information flow within the neurons, we compared recordings from different recording sites within the same cell types. As potential input and output areas are in close proximity in TB1/2 neurons, and also to some extend in TL2/3 neurons, this could be achieved only in columnar cells. Neurons were recorded either from the PB or from the vicinity of the LAL. Very large postsynaptic potentials (PSPs) were observed consistently in CPU1 neurons (n = 15; all subtypes), when they were recorded from the PB (Fig. 8C), whereas no PSPs were present in recordings from their axons in the LAL (n = 3). Similarly, CP2 neurons showed strong PSPs when recorded from the PB (n = 3) but none when recorded from the LAL (n = 1) (Fig. 8D). CP1 cells could not be recorded from the PB, but none of the recordings obtained from the LAL showed PSPs. For CL1 neurons, the difference was not as distinct. In only one recording of a CL1b/d neuron from the PB, strong PSPs were observed. In most other recordings from CL1 cells, no or small PSPs were present independently of the recording site.

Discussion

At least thirteen different types of neuron of the locust CC are sensitive to polarized light. While all of these cells showed polarization opponency, cell-type specific differences were found in background activity, variability in spiking, signal to noise ratio, tuning precision, ocular dominance, and receptive field structure. Together with data on neuronal morphologies, the distribution of smooth and varicose terminals, and physiological support for the association of dendritic input regions with smooth ramifications, a picture of network connectivity and information flow within the polarization vision system of the CC emerges.

Information flow through the CC

Anatomical position and physiological characteristics indicate that tangential neurons of the CBL (TL2, TL3) are at the input stage of the CC, whereas CPU1-, TB1/2-, and CP1/2 neurons are near the output. CL1 neurons show intermediate characteristics and likely link input to output elements. Neurons at the input stage (TL2, TL3) showed highest relative response amplitudes while their absolute responses ranged from total inhibition to the maximally occurring frequencies. This suggests that they are specialized for *E*-vector coding. As these neurons show very low background activity and variability, virtually all activity originates from polarization input. Neurons with similar characteristics are also present in crickets (Sakura et al., 2008) and support a common design of the input pathway to the polarization-vision network in the CC of orthopteroid insects.

Between early stage and late stage POL-neurons background variability increased while response variability remained constant. Therefore, sources of background activity not controlled by the polarization-vision network are likely. CPU1 neurons probably receive polarization-independent input through their CBU ramifications (Heinze and Homberg, 2008). This is supported by the finding that CBU tangential cells in *Drosophila* are required for memory of visual object parameters and, thus, code sensory information different from polarized light (Liu et al., 2006). As rotating *E*-vectors modulate TB1/2- and CPU1 cells only in the upper half of their activity range, i.e. they are not totally silenced during Φ_{min}, these stimuli alone are insufficient to drive these neurons optimally. In more natural stimulus situations these cells might be a converging site for multisensory information and mediate the association of head orientation with information about behaviorally relevant sensory features.

Ocular dominance analysis revealed that neurons of the anterior optic tubercle (AOTu) receive polarized light input predominantly through the ipsilateral eye (Pfeiffer et al., 2005). POL-neurons of the CC that respond to stimuli from both eyes, therefore, constitute later processing stages. This is in tune with the situation in the mammalian visual system, where binocularity emerges for the first time in the primary visual cortex, several synapses away from the sensory periphery (Horton, 2006).

The transition of receptive fields from medium-sized and eccentric to large and zenith-centered, likewise, supports a direction of information flow from TL2- and CL1 neurons to TB1-, CPU1- and CP2 neurons. The receptive fields in the latter neurons cover the complete width of the sky, implying that their responses to polarized light are independent of stimulus position. This agrees well with the concept of position invariance at higher levels of the mammalian visual cortex. Here, receptive field size increases with increasing distance from the sensory periphery, until neurons finally respond to specific aspects of the environment, independent of stimulus position (Rolls, 2007).

Two parallel input pathways to the CC

The differences in response characteristics between TL2- and TL3 neurons suggest that two separate input pathways link the LAL with the CBL. While the monocular TL3 neurons transfer information from the median olive and lateral triangle to layers 4-5 of the CBL, all TL2 neurons studied here receive their binocular input in the lateral triangle and project to layer 2 of the CBL. CL1a neurons have fine arborizations in layer 2 (Heinze and Homberg, 2008), and

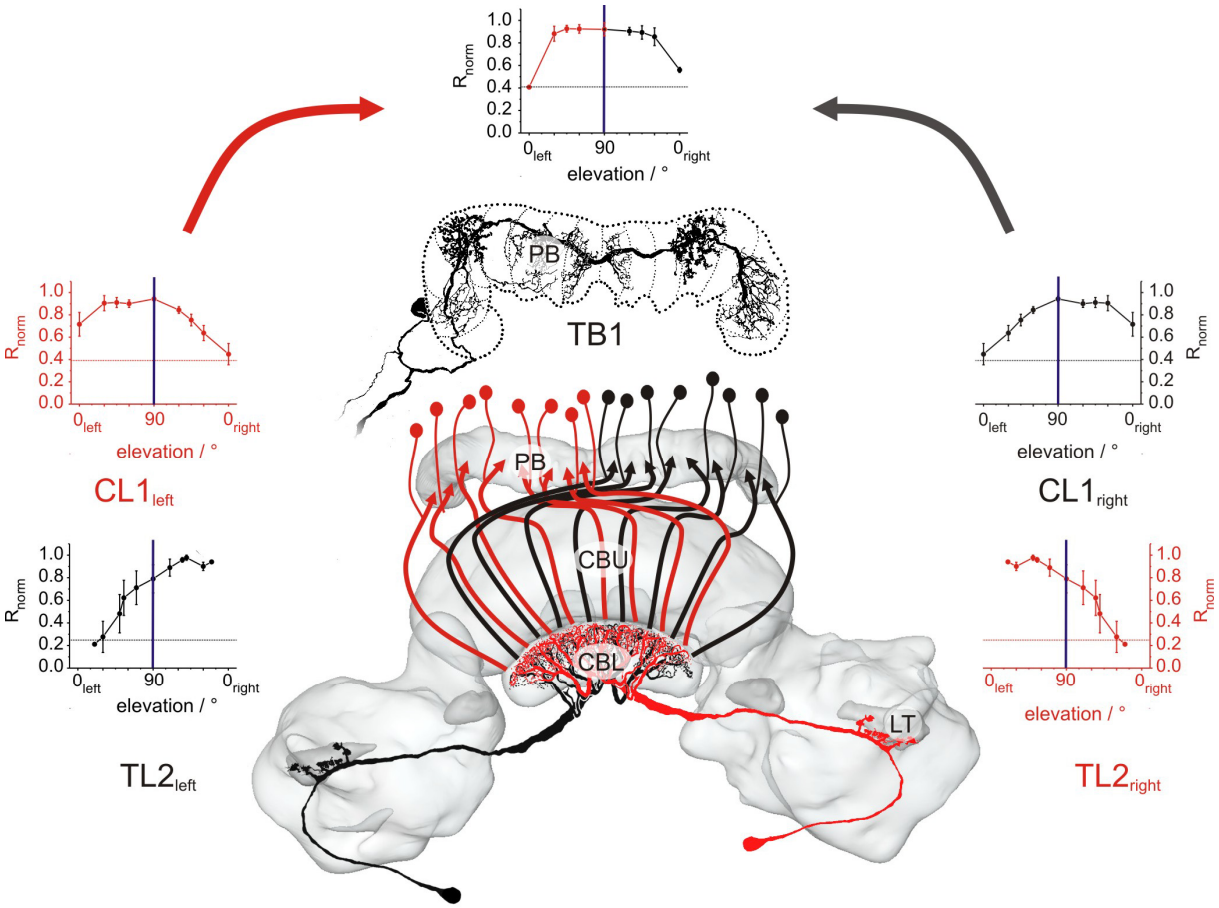

Figure 9. Model of neuronal wiring principles derived from receptive field data superimposed on a three dimensional reconstruction of the central complex. Input neurons (TL2, shown as frontal reconstructions) possess comparably small, contralaterally centered receptive fields, i.e. neurons on the left brain hemisphere possess receptive fields centered in the right sky hemisphere (black) and vice versa for the right brain hemisphere (red). CL1 neurons posses slightly larger, ipsilaterally centered receptive fields, implying midline crossing connections between TL2 and CL1 neurons (colors indicate the source of POL information). CL1 neurons are represented by arrows following the anatomical trajectories of CL1 cells. The smooth arborizations of TB1 neurons (top, shown as frontal reconstruction with projections to the posterior optic tubercle omitted) on either side of the PB-midline provide the potential targets for CL1 cells. Therefore, the bilaterally symmetrical receptive fields of TB1 neurons can be explained by integration of at least two CL1 cells from each hemisphere.

may, therefore, be the postsynaptic partners of TL2 neurons. Because neurons with smooth arborizations in CBL-layers served by TL3 cells are not known to date, parts of the varicose endings of CL1 neurons in these layers might in fact be postsynaptic. If so, both pathways would converge at the level of CL1 cells.

CL1 neurons – key players of the network

Despite their opposite polarity, CL1a- and CL1b/c/d neurons could not be distinguished physiologically. This suggests that all CL1 cells code information at the same computational level and constitute a set of cells allowing for bidirectional information exchange between the CBL and the PB. They signal *E*-vector information from one sky hemisphere with the greatest precision of all cell types and transfer it to a position-invariant population of head-orientation cells in the PB. Because CL1 neurons showed the sharpest *E*-vector tuning of all cells examined, they are promising candidates for "compass neurons", postulated by Sakura et al. (2008). Sakura et al. (2008) proposed the necessity of a gain control circuit in the polarization-vision network to insure constant response amplitudes at varying degrees of polarization. Gain control could, likewise, assess the importance of polarization vision relative to other sensory input depending on behavioral and motivational context. The dependency of response amplitudes on background activity might serve as the neuronal substrate for a gain control. Of all POL-neurons, CL1 neurons showed the steepest rise in response amplitude with increasing background activity. Neurons modulating their background activity would, therefore, dramatically change the influence of CL1 cells onto their postsynaptic partners in the PB and might also account for the switch between the polarization-sensitive and insensitive states of conditional POL-neurons (Heinze and Homberg, submitted). Polarization-insensitive TL5 neurons of the CBL (Vitzthum et al., 2002), which are probably dopaminergic (Wendt and Homberg, 1992), are promising candidates for this task.

Transformation of visual fields

At the input stage of the CC (TL2 neurons), receptive fields are centered in the contralateral hemisphere and have a size of about 60°. This corresponds well to data for POL1 neurons in the cricket optic lobe (Labhart et al., 2001). As CL1 neurons are most likely post-

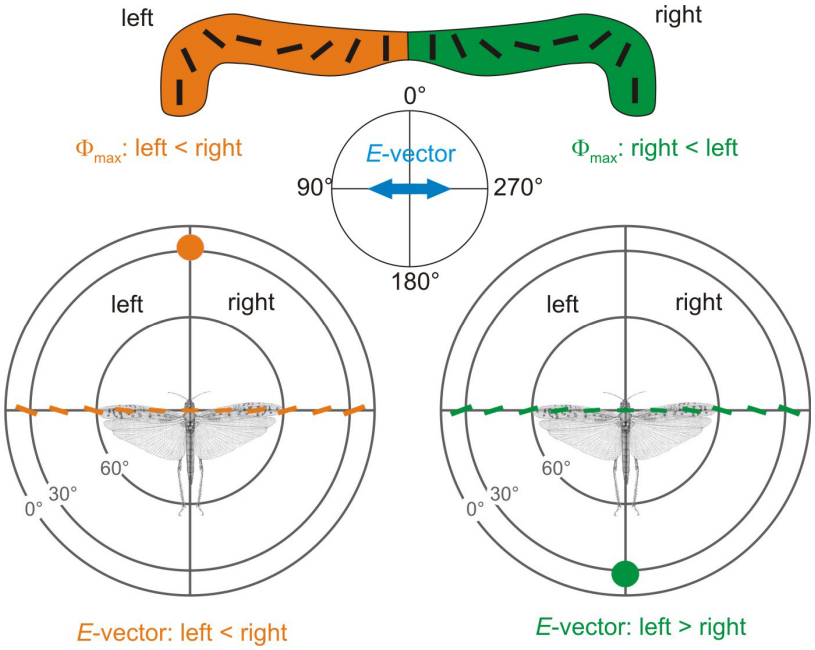

Figure 10. Schematic illustration of a potential mechanism for resolving the azimuthal ambiguity through *E*-vector signaling in columnar neurons of the PB, based on Φ_{max} distributions in the receptive fields. The top panel shows the polarotopic representation of zenithal E-vectors in the columns of the PB. As neurons comprising this representation show smaller Φ_{max}-values for stimuli presented in the ipsilateral sky hemisphere, neurons of the left brain side prefer stimulus situations with *E*-vectors in the left half of the sky to be smaller than in the right half. Accordingly, neurons of the right brain hemisphere prefer stimulus situations, in which *E*-vectors in the right half of the sky are smaller than in the left half. These two stimulus situations occur in the sky, when the sun is either behind the locust (bottom right), or in front of the locust (bottom left). Therefore, neurons in the left PB-hemisphere would be more strongly activated, when the sun is in front of the animal, whereas neurons in the right PB-hemisphere react more strongly when the sun is behind the locust. Note that the zenithal *E*-vectors are identical in both situations. *E*-vector angles in the sky at different elevations are derived from Petzold (2000).

synaptic to TL2 cells, the ipsilateral position of their receptive field centers suggests that TL2 neurons exclusively synapse onto contralateral CL1 neurons (Fig. 9). Because receptive fields were larger in CL1 cells than in TL2 cells, convergence of several TL2 neurons onto individual CL1 cells is likely. If CL1 neurons are presynaptic to late stage POL-neurons, at least one CL1 cell from each hemisphere must be sampled by a postsynaptic neuron to account for the transformation of ipsilateral receptive fields to bilaterally symmetric receptive fields. TB cells have smooth input processes in both hemispheres of the PB and are, therefore, ideally suited to achieve this integration (Fig. 9; Heinze and Homberg, 2007). Supporting evidence for multiple spike initiation zones in TB cells comes from the regular observation of action potentials with multiple sizes (Fig. 1D). Once bilateral symmetry of receptive fields is reached in TB cells, this character is transferred onto CPU1- and CP cells, which share all major receptive-field characteristics with TB neurons.

Evidence for a 360° azimuth map in the PB

Zenithal *E*-vectors are represented topographically in the columns of the PB (TB1-, CPU1-, and CP1/2 cells; Heinze and Homberg, 2007) and cover a solar azimuthal range of 180° across each PB hemisphere. As *E*-vector information only indicates the solar meridian, it is ambiguous with regard to the location of the solar versus antisolar sky hemisphere. To resolve this ambiguity, neurons of the AOTu of the locust integrate spectral cues with polarization information (Pfeiffer and Homberg, 2007). Whether and how this information is transferred to the CC remains to be shown. The distribution of Φ_{max}-values across the receptive field offers an additional possibility to solve this problem. In TB1-, CPU1-, and CP2 neurons, stimuli presented in the ipsilateral field of view elicited smaller Φ_{max}-values than stimuli from contralateral directions. Hence, neurons in the right brain hemisphere prefer *E*-vector angles in the right half of the sky to be smaller than in the left half, and vice versa for neurons in the left brain hemisphere. This matches the natural sky when the locust faces an antisolar direction (Fig. 10). For columnar neurons, stimulation with a complete sky polarization pattern would thus elicit peak activity in neurons of the right PB hemisphere when the sun is behind the animal, whereas neurons in the left PB hemisphere would respond stronger when facing the sun, even though zenithal *E*-vectors are identical in both situations (Fig. 10). Because such tuning differences were not found in CL1- and TL neurons, position-invariant *E*-vector tuning in these cells may be transformed into head orientation tuning in later-stage neurons. Thus the polarotopy in the PB would cover the whole azimuthal range of 360° around the animal, as suggested by Strauss (2002b).

If these late-stage neurons indeed match approximations of the sky polarization pattern at particular head orientations of the animal, the principle of matched filters for evaluating sky compass cues (Rossel and Wehner, 1984, Rossel and Wehner, 1987), based on behavioral data from bees, would be confirmed. We suggest that the polarotopically organized columnar and TB neurons of the locust PB are suited to act as the neuronal substrate for this matched filter.

References

Clements A, May TE (1974) Studies on locust neuromuscular physiology in relation to glutamic acid. J Exp Biol 60:673-705.

Heinze S, Homberg U (2007) Maplike representation of celestial *E*-vector orientations in the brain of an insect. Science 315:995-997.

Heinze S, Homberg U (2008) Neuroarchitecture of the central complex of the desert locust: Intrinsic and columnar neurons. J Comp Neurol 511:454-478.

Heinze S, Homberg, U. Linking the input to the output - New sets of neurons complement the polarization vision network of the locust central complex. (submitted).

Homberg U (1991) Neuroarchitecture of the central complex in the brain of the locust *Schistocerca gregaria* and *S. americana* as revealed by serotonin immunocytochemistry. J Comp Neurol 303:245-254.

Homberg U (2004) In search of the sky compass in the insect brain. Naturwissenschaften 91:199-208.

Horton JC (2006) Ocular integration in the human visual cortex. Can J Ophthal 41:584-593.

Labhart T (1996) How polarization-sensitive interneurones of crickets perform at low degrees of polarization. J Exp Biol 199:1467-1475.

Labhart T, Petzold J, Helbling H (2001) Spatial integration in polarization-sensitive interneurones of crickets: a survey of evidence, mechanisms and benefits. J Exp Biol 204:2423-2430.

Liu G, Seiler H, Wen A, Zars T, Ito K, Wolf R, Heisenberg M, Liu L (2006) Distinct memory traces for two visual features in the *Drosophila* brain. Nature 439:551-556.

Müller M, Homberg U, Kühn A (1997) Neuroarchitecture of the lower division of the central body in the brain of the locust (*Schistocerca gregaria*). Cell Tissue Res 288:159-176.

Neuser K, Triphan T, Mronz M, Poeck B, Strauss R (2008) Analysis of a spatial orientation memory in *Drosophila*. Nature 453:1244-1247.

Pfeiffer K, Homberg U (2007) Coding of azimuthal directions via time-compensated combination of celestial compass cues. Curr Biol 17:960-965.

Pfeiffer K, Kinoshita M, Homberg U (2005) Polarization-sensitive and light-sensitive neurons in two parallel pathways passing through the anterior optic tubercle in the locust brain. J Neurophysiol 94:3903-3915.

Pfeiffer K. (2006). Coding of sky-compass information in neurons of the anterior optic tubercle of the desert locust *Schistocerca gregaria*. PhD-thesis, Philipps-Universität Marburg.

Rolls ET (2007) The representation of information about faces in the temporal and frontal lobes. Neuropsychologia 45:124-143.

Rossel S, Wehner R (1984) How bees analyse the polarization patterns in the sky. J Comp Physiol 154:607-615.

Rossel S, Wehner R (1987) The bee's e-vector compass. In: Neurobiology and behaviour of honeybees (Menzel R, Mercer A, eds), pp 76-93. Berlin, Springer.

Sakura M, Lambrinos D, Labhart T (2008) Polarized skylight navigation in insects: model and electrophysiology of e-vector coding by neurons in the central complex. J Neurophysiol 99:667-682.

Strausfeld NJ (1999) A brain region in insects that supervises walking. Progr Brain Res 123:273-284.

Strauss R (2002a) The central complex and the genetic dissection of locomotor behaviour. Curr Opin Neurobiol 12:633-638.

Strauss R. (2002b) Die übergeordnete Steuerung des Laufverhaltens durch das Insektengehirn, studiert mit Methoden der *Drosophila*-Neurogenetik. Habilitationsschrift, Universität Würzburg.

Vitzthum H, Müller M, Homberg U (2002) Neurons of the central complex of the locust *Schistocerca gregaria* are sensitive to polarized light. J Neurosci 22:1114-1125.

Wendt B, Homberg U (1992) Immunocytochemistry of dopamine in the brain of the locust *Schistocerca gregaria*. J Comp Neurol 321:387-403.

Williams JLD (1975) Anatomical studies of the insect central nervous system: a ground-plan of the midbrain and an introduction to the central complex in the locust, *Schistocerca gregaria* (Orthoptera). J Zool (Lond) 176:67-86.

Integration of multiple visual stimuli in neurons of the locust central complex

Integration of multiple visual stimuli in the central complex of the desert locust.

Stanley Heinze and Uwe Homberg

Like numerous species of insects, desert locusts can perceive the polarization pattern of the blue sky and use it for oriented behavior. The planes of polarization (*E*-vectors) constituting this pattern directly depend on solar position and can thus be used as sky compass cues. Polarization-sensitive (POL) neurons in the brain of the locust respond to dorsally rotating *E*-vectors with sinusoidal changes of firing rate, resulting in maximal excitation at a preferred *E*-vector (Φ_{max}-value). Polarized light is perceived with specialized dorsal regions of the compound eyes and, via several stages, *E*-vector information is transmitted to the central complex (CC), a group of neuropils, consisting of the protocerebral bridge (PB), the upper and lower divisions of the central body (CBU, CBL) and the paired noduli. Within the CC a network of POL neurons produces a topographic representation of preferred *E*-vector orientations in the columns of the PB. How this information is used by the locust in order to guide behavior is unknown. Through intracellular recordings we present preliminary evidence that proposed output neurons of the CC polarization vision network (CPU1, CPU2 neurons) integrate edge-orientation and spectral stimuli with *E*-vector information, while neurons at an earlier stage of this network (CL1 neurons) do not respond to these stimuli. The subtle and variable nature of these responses suggests context-dependent modulation of response characteristics. In search for the source of this information, we show that unpolarized, but not polarized light information is coded in a potential input neuron to the CBU, a CC subunit not associated with the polarization vision network. When tracing these unpolarized visual information further back to the optic lobe, we found neurons strongly responding to unpolarized light, including color-opponency cells, small target detecting cells, and general motion sensitive neurons. However, the pathway of how unpolarized visual cues are transferred between the optic lobe and the CC remained unclear.

Introduction

Many animals are able to perceive linearly polarized light, a key feature of the blue sky produced by scattering of sunlight in the upper atmosphere. The electric field vectors of polarized light (*E*-vectors) are arranged in concentric circles around the sun, creating a pattern of *E*-vectors that provides information about the solar position in each patch of blue sky (Horváth and Varjú, 2004). This source of information is used by many insect species for orientation behavior, such as compass navigation or homing, even if the sun itself is not visible (Wehner and Labhart, 2006). In the context of natural behavior, the use of sky polarization for navigation has been shown for ants (Wehner, 1984), bees (von Frisch, 1949), and dung beetles (Dacke et al., 2003). Orientation responses have also been revealed for crickets (Brunner and Labhart, 1987), flies (von Philipsborn and Labhart, 1990), monarch butterflies (Reppert et al., 2004), and desert locusts (Mappes and Homberg, 2004). The latter species is particularly well characterized with regard to the neuronal mechanisms underlying polarization vision. As in other insects, the *E*-vector orientation of polarized light is detected by the dorsal rim area, a specialized region of the compound eye (Mappes and Homberg, 2004). From here, polarized light information is transferred through several processing stages to the central complex in the center of the protocerebrum (Homberg, 2004). Polarization-sensitive neurons (POL-neurons) respond to changing *E*-vector orientations with sinusoidal modulations of their activity rate at all stages of the polarization vision network, with a cell-specific preferred *E*-vector orientation eliciting maximal activation.

The central complex is a group of neuropils and consists of the protocerebral bridge (PB), the upper and lower divisions of the central body (CBU, CBL), and the posteriorly located noduli (Heinze and Homberg, submitted; Williams, 1975). Most characteristic is its highly regular neuroarchitecture comprised by a vertical array of 16 columns, which, in the central body, is intersected by horizontal layers (Homberg, 1991; Heinze and Homberg, 2008). This organization is produced by a variety of columnar and tangential cell types (Hanesch et al., 1989; Heinze and Homberg, 2008). At least 13 different types of neuron arborizing in all major components of the central complex are polarization-sensitive. De-

tailed electrophysiological analysis of these neurons revealed a topographic representation of preferred *E*-vector orientations underlying the columnar organization of the PB (Heinze and Homberg, 2007). This linear array of cells is suited to code for head direction relative to the solar azimuth. Hence it suggests that the columns of the PB represent the azimuthal space around the animal.

Although progress has been made in understanding how polarization information reaches the PB and where the key elements of the central-complex polarization vision network are (Heinze et al., submitted), virtually nothing is known about how the information represented in the PB columns is used by the locust. In order to guide behavior, the sensory information gained from polarized light has to be transformed into motor commands. That the central complex indeed plays a crucial role in motor control has been shown through mutants with structural brain deficits in *Drosophila* (Strauss, 2002). As motor command signals are unlikely to depend on only one sensory feature, polarized-light information has to be integrated with information from different modalities. Heinze and Homberg (2007) suggest that the output of the polarotopic map in the PB is used to associate a particular azimuth direction with sensory information about acutely relevant objects in the environment. In *Drosophila*, strong supporting evidence comes from the finding that memory for specific visual features (elevation and orientation of bars) depends on distinct sets of tangential neurons of the fan-shaped body (equivalent to CBU; Liu et al., 2006). Multimodal sensory input to the central complex has indeed been shown by intracellular recordings from neurons responding to mechanosensory and visual stimuli in the locust (Homberg, 1994). In cockroaches, extracellular recordings from the vicinity of the CBL revealed units responding to mechanical stimulation of the antennae, as well as to visual stimulations (Ritzmann et al., 2008). Overall, these findings point to the representation of a variety of sensory features in the central complex.

In the current work we, therefore, examined the responses of central-complex neurons, in particular the different types of POL neuron, to visual stimuli other than polarized light, such as motion, bar orientation, and spectral composition. Responses of optic lobe neurons were obtained to provide a frame of reference, allowing general comparisons of the strength of visually evoked activity in the different brain regions. Generally, it was revealed that central-complex neurons responded either in a subtle way to these stimuli or not at all. Specific responses to elevation and orientation of bars were found in individual recordings from proposed output neurons of the central-complex POL network. Optic lobe cells on the other hand showed consistently strong reactions.

Material and methods

Animals and preparation. Locusts (*Schistocerca gregaria*) were raised in crowded colonies at the University of Marburg in a 12L:12D photoperiod at constant temperature (28°C). Adult animals of both sexes were used 1-3 weeks after imaginal moult. After cold anesthetization at 4°C for 15-30 minutes they were waxed onto a metal holder. In most preparations animals were fixed to the holder with tape for increased stability. Legs and wings were removed and stumps were sealed with wax or glue to prevent hemolymph leakage. The head capsule was opened frontally and the brain was freed of surrounding trachea and fat body. Most muscles in the head capsule were transected. In some preparations, antennal nerves were cut and antennae were removed. For increased stability, the oesophagus was transected and the gut was removed from the opened abdomen, which was resealed either using petroleum jelly or a tightly knotted thread. The animal was then mounted in a horizontal orienttation (tilted upwards by ca. 20°) in the recording setup (Fig.1 A). The brain was supported with a wax/wire platform, which was inserted ventrally and waxed to the head. A silver wire was inserted into the head capsule ventrolaterally and used as reference electrode. The preparation left the frontal field of view unobscured for stimulus display. To facilitate electrode penetration, the neural sheath was removed mechanically with forceps. In some preparations this mechanical procedure was preceded by 30s exposure of the brain to pronase crystals (Boehringer Ingelheim Bioproducts, Heidelberg, Germany). Desiccation was prevented by submerging the brain in locust saline (Clements and May, 1974) at all times.

Electrophysiology. Intracellular recordings were performed with sharp electrodes (resistance 60-150 MΩ), drawn from borosilicate capillaries (0.75 mm ID, 1.5 mm OD; Hilgenberg, Malsfeld, Germany) using a Flaming/Brown horizontal puller (P-97, Sutter, Novato, CA). Electrode tips were filled with 4% Neurobiotin (Vector Laboratories, Burlingame, UK) in 1M KCl and backed up with 1M KCl. Electrodes were inserted into the brain near the midline, slightly dorsally of the exit point of the medial ocellar nerve. Hence neurons from the central complex or commissural neurons of the optic lobes could be recorded. Signals were amplified (10x) with a SEC5-LX amplifier (NPI, Tamm, Germany). After digitization at a sampling rate of 5 kHz (CED1401 Micro, Cambridge Electronic Design, UK), signals were stored on a PC using Spike2 software (Cambridge Electronic Design). Digital high pass filtering was applied when necessary to compensate for drifting baseline. After recording, de-

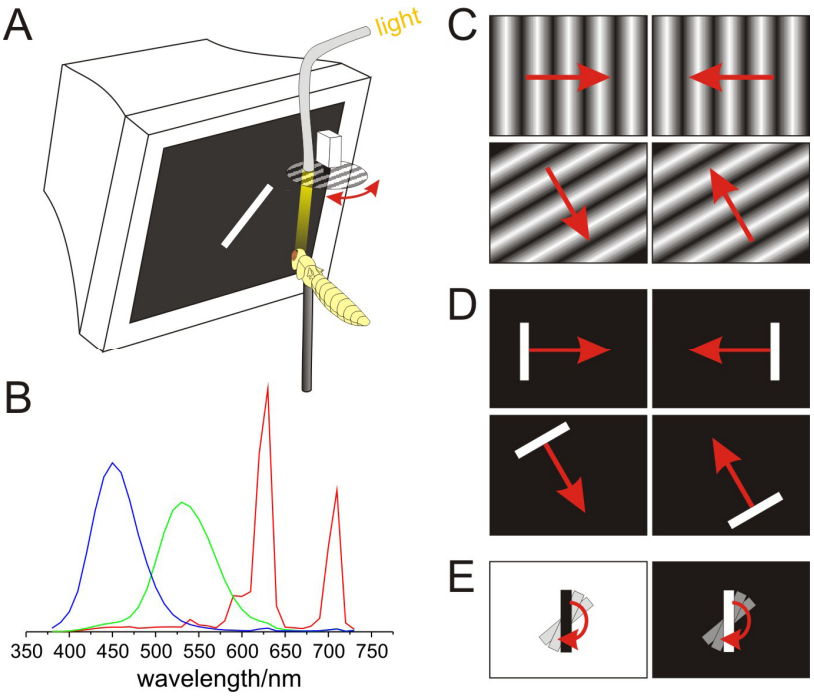

Figure 1. Schematic representation of the stimulation setup and characteristics of applied stimuli. ***A.*** Drawing of key components for stimulus presentation, including the near horizontally (20° upwards) mounted locust in the center, the CRT screen in the frontal visual field, and the rotating polarizer in the dorsal visual field. Light is provided by a 150W halogen bulb and is passed to the polarizer via a light guide. Because the stimulation devices and the locust are mounted at an angle of approximately 20° from the vertical/horizontal axis, space was left for electrode insertion from directly above the animal. ***B.*** Spectral emission curves of individual phosphors of the CRT screen. Stimualation with short-wavelength phosphors are shown in blue, with mid-range phosphors in green and long-wavelength phosphors in red (appearance on the screen to the human eye). Curves have been measured by W. Hollingworth (NEC Display Solutions service) with an identically constructed monitor. ***C.*** Schematic representation of sine-gratings presented at different orientations. Motion (indicated by red arrows) was perpendicular to orientation. ***D.*** Schematic representation of bar stimuli, moving perpendicular to their orientation. ***E.*** Rotating bar stimuli were presented either black on white background or vice versa and rotated clockwise and counterclockwise.

polarizing current was applied (1-3 nA, 1-5 min) to iontophoretically inject Neurobiotin.

Stimuli. Two types of visual stimulation were provided. First, I used a dorsally located rotating polarizer to present linearly polarized light to the animal, and secondly, a frontally mounted CRT screen was used for presentation of unpolarized stimuli (Mitsubishi, Diamond Pro 2700).

The polarizer (HN38S, Polaroid) was connected to a light source (halogen bulb, 150W) via light guides (Schölly, Denzlingen, Germany; spectral range 400–800 nm) and could be rotated through 360° in both directions with an angular velocity of 30°/s. The filter was controlled with a PC via custom designed hard- and software. The stimulus irradiance at the animal's head was 57µW/cm², at an angular size of 3.4°. Stationary *E*-vectors were applied in some recordings. Hereby, *E*-vector orientation was changed in steps of 30°, with three consecutive stimulations (duration, 2 s; pause, 2 s) for each orientation.

The CRT-screen (600 × 800 pixels, frame rate: 140Hz) covered 83° × 110° of the frontal visual field with the animal being mounted perpendicularly in front of the screen center. For white RGB stimuli irradiance at the animals head was 38 µW/cm². The screen was used to present bar-stimuli, drifting sine-gratings, small field stimuli (discs, ∅ 5.5°), and large whole-screen light flashes (duration 0.5s). Light flashes were produced either as white stimuli (R+G+B) or individual RGB-colors (long wavelengths: L-stimuli; mid-range wavelengths: M-stimuli; short wavelength: S-stimuli; spectra of phosphors shown in Fig.1B). Bars were either white on black background or inverted, at a size of 44° × 8°. They were presented in either of three ways: First, static bars centered on the screen, at 30° orientation intervals (duration: 1s, 2s pause). Secondly, bars moving perpendicular to their orientation (v = 58°/s, 30° steps, only white on black background). Each direction of movement was followed by the opposite direction without change of bar orientation (Fig.1D). Finally, rotating bars were presented at an angular velocity of 61°/s. Clockwise and counterclockwise rotations were always applied in direct sequence (Fig.1E). Bars could be exchanged for squares of variable sizes. Sine-gratings were presented similarly to moving bars at orientation intervals of 30°, and each direction of movement was directly followed by the opposite direction. The moving direction was always perpendicular to the orientation of the grating (spatial frequency, 0.05 cycles/°; drifting velocity, 50.6°/s). Small white discs (∅ 5.5°) were presented at different positions on the screen, starting from the upper left corner, proceeding to the lower right corner of the screen in five elevation levels (six steps at each elevation). All frontal stimuli were computed with a ViSaGe-visual stimulator (Cambridge Research Systems, Rochester, UK), and programmed using a MatLab-interface.

Data analysis. Digitized spike trains were stored on PC and evaluated using either Spike2-software or MatLab-software, both using implemented, custom designed scripts. For analyzing responses to rotating *E*-vectors, exclusively Spike2 was used. Hereby, action potentials were detected with threshold based event detection, and were additionally visualized as mean frequency using a gliding average algorithm (bin size of 1s). For quantification of polarized light res-

ponses, events within each 360° rotation of the polarizer were assigned their corresponding *E*-vector angle. For each rotation, this list of angles was exported to Oriana 2.05a (Kovach Computing Services, Anglesey, UK) and the combined rotations of each neuron were tested for polarization sensitivity. All neurons with distributions of these angles that were significantly different from randomness were rated polarization sensitive (Rayleigh-test for axial data). The mean angle of the distribution was defined as the preferred *E*-vector orientation (Φ_{max}-value) of that neuron.

All unpolarized stimuli as well as stationary *E*-vectors were evaluated with custom designed MatLab scripts. To prepare data for importing them into MatLab, they were exported from Spike2 and saved as text files. Depending on the displayed stimulus, different scripts were used to calculate mean responses and visualize the results. Generally, spikes were also detected using a threshold based algorithm, and thereafter automatically analyzed with respect to digitized control signals derived from the stimulus display.

For all fixed-length stimuli, scatter plots were created by vertically aligning events derived from individual presentations. These aligned stimulus responses were used to calculate a peristimulus time histogram (bin size between 5 ms and 30 ms). Orientation and direction sensitivity to either bar stimuli or gratings was determined by calculating the mean activity within each stimulation and pooling these mean frequencies for identical motion directions. The resulting values were plotted in a circular diagram against the orientation angle (motion direction - 90°). Orientation sensitivity resulted in a bimodal distribution of frequencies, whereas direction sensitivity resulted in only one preferred orientation. The preferred orientation direction was calculated by fitting the data with a sine square function (Levenberg-Marquardt chi-square minimization; wavelength fixed at 360° for unimodal or 180° for bimodal responses) using Origin6.0 (Microcal, Northampton, MA, USA). In case of unimodal data, the preferred motion direction angle was calculated as the value orthogonally to the preferred orientation.

Histology. After injection of Neurobiotin, brains were dissected out of the head capsule, cleaned of fat and trachea, and fixed over night at 4°C in Neurobiotin fixative (4% paraformaldehyde, 0.25% glutaraldehyde, 2% saturated picric acid, in 0.1 M phosphate buffer). Subsequently, brains were treated as wholemount preparations for further staining. After rinsing 4 x 15 min in PBS, they were directly incubated with Cy3-conjugated Streptavidin (Dianova, Hamburg, Germany, 1:1000) for three days at 4°C in PBT (PBS, including 0.5% Triton X-100). Brains were again rinsed with PBT (2 x 30 min) and PBS (3 x 30 min), dehydrated with an increasing ethanol series (25%, 50%, 70%, 90%, 95%, 100%; 15 min each), transferred to a fresh mixture of ethanol and methylsalicylate (1:1) for 15 min, and finally cleared in methylsalicylate for 35 min. Brains were eventually mounted in Permount (Fisher Scientific, Pittsburgh, PA) between two coverslips. To avoid compressions, reinforcement rings were used as spacers. Neurons were scanned with a confocal microscope (Leica TCS-SP2, minimal pinhole size, at 3 µm intervals) with a 10× oil immersion objective (HC PL APO 10×/0.4 Imm Corr CS; Leica, Bensheim, Germany). Reconstructions based on these data stacks were carried out using Adobe Photoshop CS2.

To acquire high resolution data stacks of injected neurons, whole mount preparations were rehydrated and sectioned in thick sections, containing the neuron of interest (for details see Heinze and Homberg, 2008). These preparations were subsequently scanned at high resolution (40× objective, HCX PL Apo 40×/1.25 Oil). Data stacks were finally reconstructed with Photoshop.

Results

This work is based on 26 intracellular recordings from neurons of the central complex (n = 14) and the optic lobes (n = 12) of the desert locust. In all recordings, polarized light was presented through a dorsally rotating polarizer, whereas a variety of unpolarized visual stimuli was presented on a frontally mounted CRT-screen. Of all 16 central-complex neurons, twelve showed polarization sensitivity (75%). In contrast, only one of the 12 optic lobe neurons was polarization sensitive (8%). Generally, responses to unpolarized stimuli were pronounced in all recordings from optic lobe cells, whereas they were subtle or absent in most central-complex neurons.

Neurons of the optic lobes

The morphology of the recorded optic lobe cells could be reconstructed at least partly in all but one case. Of these eleven neurons, seven were commissural cells, connecting the optic lobes of both brain hemispheres through a commissure located just anteriorly of the central body (n = 5), or through more posteriorly located commissures (n = 3). Two cells connected the optic lobe with the ipsilateral posterior protocerebrum, whereas the remaining two neurons projected from the posterior protocerebrum back to the optic lobe. Therefore, the recorded cells belonged to a variety of cell types, and most of them had large arborization trees tangentially innervating the lobula, the medulla, or both neuropils.

Physiologically, the majority of neurons showed phasic responses at stimulus onset and offset (n = 8). This was accompanied by motion sensitivity in five neurons (of six tested). The recorded responses to motion stimuli did not depend on stimulus orientation or motion direction in all but one case. Phasic activity without motion sensitivity was found in one of

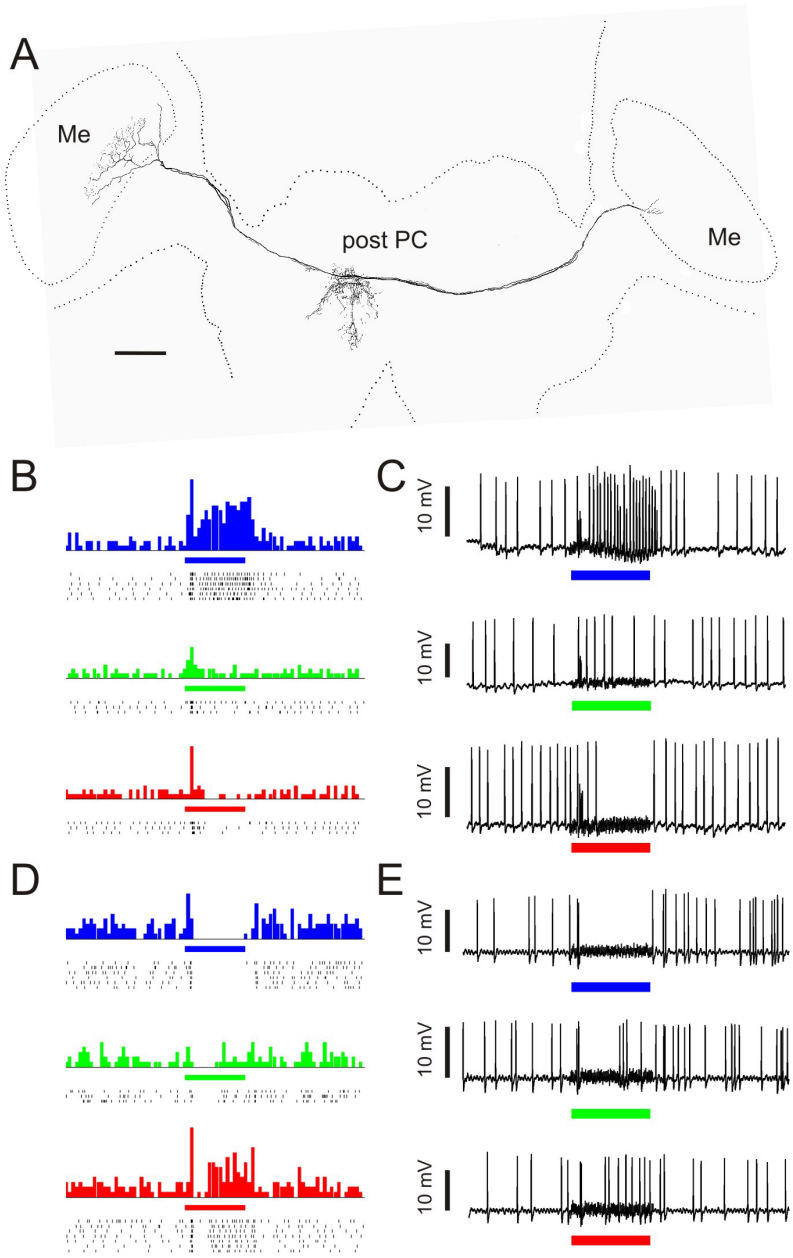

Figure 2. Physiology and morphology of color opponent cells. ***A.*** Frontal reconstruction of the recorded neuron derived from a wholemount preparation. The cell connects both medullae (Me) and has varicose arborizations in one hemisphere of the posterior protocerebrum (post PC). Due to incomplete staining the soma and full extend of arborizations in the medullae remain unresolved. ***B.*** Responses of the neuron shown in ***A*** to spectral light flashes in the frontal visual field. Scatter plots of aligned individual trials and the resulting peristimulus-time histograms (PSTH) are shown at a bin size of 30 ms. The three PSTH are drawn with identical scaling. Short wavelength stimuli are shown in blue, mid-range stimuli in green, and long wavelength stimuli in red. Duration of stimuli was 0.5 s. ***C.*** Individual examples of neuronal responses (same neuron as ***A*** and ***B***). High spike frequency during bursts lead to reduction in spike amplitude. ***D,E.*** Data as in ***B*** and ***C*** for a second neuron with unknown morphology. Note that reactions are opposite from the first neuron with regard to the spectral composition of the presented light flashes. Scale bar in ***A***, 200 µm.

the two recorded centrifugal cells (only one was tested). Strong tonic components of stimulus responses were present in four cells, including two neurons projecting to the ipsilateral posterior protocerebrum.

Of the recorded stimulus responses from optic lobe neurons, three aspects were particularly captivating and shall be addressed in more detail. These are the discovery of color opponency, the presence of neurons switching from activation to inhibition dependent on stimulus size, and the discovery of a neuron integrating motion stimuli with polarization sensitivity.

Color opponency

Most neurons tested with full-screen light flashes of different spectral composition responded equally well to S-stimuli (450 nm), M-stimuli (525 nm), and L-stimuli (625 nm) stimuli. However, two recordings revealed the existence of a color processing channel in the locust brain (Fig. 2). Both neurons showed background activity of five to ten impulses per second, and were either tonically activated, inhibited, or not affected in their spiking rate, depending on stimulus color (Fig. 2B-E). The first cell was strongly activated by short wavelength light flashes and was totally inhibited by long wavelength stimuli, whereas mid-range stimuli elicited no tonic response (Fig. 2B,C). The tonic responses were accompanied by a very short burst of activity at stimulus onset, which was largely independent of the spectral composition of the stimulus. This phasic onset burst was also present in the second recording, but was followed by a brief transient inhibition. Interestingly, the tonic responses were opposite to those of the first cell. Short wavelength stimuli totally inhibited the cell, whereas long wavelengths elicited strong excitation (Fig. 2D,E). Intermediate wavelengths produced no detectable tonic response.

The partial reconstruction of the first cell revealed a commissural neuron connecting both medullae, with additional ramifications in one hemisphere of the posterior protocerebrum

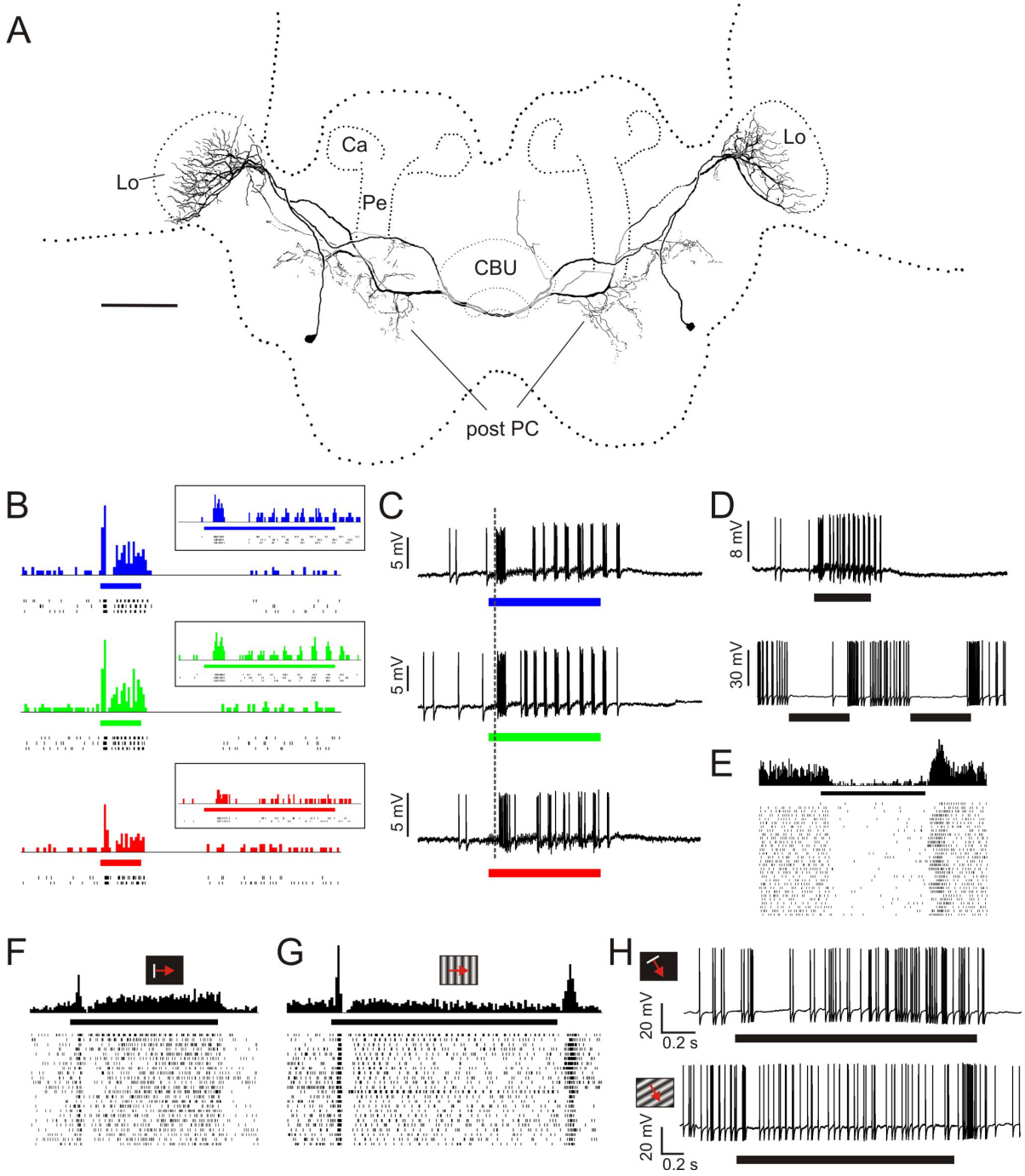

Figure 3. Morphology and response characteristics of neurons switching from activation to inhibition depending on stimulus size. ***A.*** Frontal reconstruction of a symmetrical pair of cells, connecting both lobulae (Lo) with the contralateral posterior protocerebrum (post PC). The main neurite crosses the midline just behind the central body and runs anteriorly of the pedunculus (Pe) in the ipsilateral hemisphere and posteriorly after midline crossing. ***B.*** Scatter plots and peri-stimulus-time histograms (PSTH, binsize: 30 ms) for frontally presented light flashes with different spectral composition. The insets show details of the response during the stimulus at higher resolution (binsize: 5 ms). Short wavelength stimuli are shown in blue, mid-range stimuli in green, and long wavelength stimuli in red. Duration of stimuli was 0.5 s. ***C.*** Original spike trains demonstrating strong bursting activity during the illumination. ***D.*** Distinct responses to large light flashes (upper trace) as opposed to small discs (lower trace). Stimuli were white RGB-stimuli and lasted for 0.5 s. ***E.*** Series of small dot presentations at different positions of the screen (row by row from upper left corner to lower right corner, in six columns and five rows) and the corresponding PSTH (bin size: 5 ms). Note consistently longer latencies for rebound activation for stimuli presented on the left side of the screen. ***F.*** Scatter plot and PSTH (bin size: 20 ms) for two series of moving bar stimuli (different orientations, from 0° to 150° in steps of 30°, each step was shown twice with opposite motion directions, duration: 1.45 s). ***G.*** Same as ***F***, but for oriented sine-gratings instead of bars (duration: 2 s). Tonic activation is only present during bar stimulation, while rebound activation only occurs after stimulation with the grating. ***H.*** Responses for individual presentations to stimuli shown in ***F*** and ***G***. (Orientation of stimuli: 60°, motion direction: 150°). Upper trace shows response to bar motion, lower lane the response to the moving grating. Ca, calyx; CBU, upper division of the central body. Scale bar in ***A***, 200 µm.

(Fig. 2A). The main neurite crossed the midline within the posterior optic commissure. Unfortunately, the location of the soma, and the full extent of arborizations in the medullae remained unresolved due to incomplete staining. The second recording could not be identified morphologically.

Stimulus size discrimination

In two recordings, the neuronal response strongly depended on the size of the presented stimulus. Large flashes covering the complete screen elicited strong excitatory responses, whereas small discs presented at different positions on the screen strongly inhibited the neurons.

The first neuron was stained as a symmetrical pair of cells with somata located in the ventrolateral protocerebrum, just dorsally of the antennal lobes (Fig. 3A). It connected the lobulae of both hemispheres with each other and had varicose processes in the contralateral posterior protocerebrum. The main neurite ran from the ipsilateral lobula through the superior protocerebrum, passed the pedunculus of the mushroom body anteriorly, and crossed the midline behind the central body. In the contralateral hemisphere it remained posteriorly and projected to the contralateral lobula, while giving off several ramifications throughout the posterior protocerebrum. A selective staining of this neuron type with similar response characteristics to dorsal light flashes was obtained in another preparation confirming its morphology. Responses to large light flashes were characterized by a strong burst of activity, followed by a brief inhibition and, subsequently, tonic bursting excitation (Fig. 3B,C). At long wavelength stimulation the latency of the initial burst was consistently longer (50 ms ± 1.7 ms) than for S-stimuli (37 ms ± 1.2 ms) and M-stimuli (39.5 ms ± 1.7 ms; Fig. 3C). The tonic rhythmic bursting was most pronounced when stimulating with mid-range wavelengths. After stimulus offset, the neuron was inhibited for 1.08 s ± 0.10 s at mid-range and 0.84 s ± 0.04 s at long wavelengths, but consistently longer lasting (1.50 s ± 0.08 s) for short wavelengths. Small discs presented for the same duration, resulted in an almost total inhibition, followed by rebound activation (Fig. 3E). The amplitude of this rebound excitation was much smaller and the latency of the rebound was longer for stimuli presented on the left half of the screen. This neuron also responded strongly to motion stimuli in the frontal visual field (Fig. 3F-H). These stimuli were either presented as small oriented bars, moving perpendicular to their orientation, or as full-screen sine-gratings moving perpendicular to their orientation. All motion stimuli elicited an onset burst, followed by transient inhibition, which gave way to a tonic activation. This activation was present for all motion stimuli during the first presentation of a series, but thereafter only during bar stimuli but not during gratings (Fig. 3F-H). Only gratings were followed by a strong offset excitation. Downward bar motion elicited much stronger responses than upward movements, while responses where largely restricted to the right, ventral field of view.

The second neuron connected the right optic lobe to the ipsilateral posterior protocerebrum, a region potentially overlapping with the previously described neuron (not shown). The location of the soma, as well as the arborizations in the optic lobe, could not be resolved due to incomplete staining, but were traced as far as to the medulla. The central projections showed strong similarity with cells connecting the lobula to the posterior protocerebrum (Kurylas et al., 2008). The response characteristics were similar to those of the neuron in Fig. 3. Large light flashes elicited strong onset bursts, which occurred with longer latency at long wavelengths, followed by tonic excitation and an inhibitory reaction after stimulus offset. Offset inhibition was longest at short wavelengths, and was lacking for mid-range stimuli (not shown). Small dot stimuli elicited strong inhibitory responses, followed by rebound excitation. Both of these responses were most pronounced for stimuli at the bottom right corner of the screen. Motion sensitivity could not be tested in this neuron.

Polarization-motion integration

An individual recording from a commissural neuron of the optic lobe was particularly interesting. The neuron showed strong motion sensitivity, but also responded to dorsally presented, rotating *E*-vectors (Fig. 4). The main neurite ran through an anterior commissure and connected the lobulae of both hemispheres. In one optic lobe, the arborizations also extended to the medulla (Fig. 4A). Owing to incomplete staining the morphology of the cell could only be reconstructed partly, so that the location of the soma and the extension of processes in the medulla remained unresolved. Small ramifications in the central brain were also present.

The neuron showed a significant but relatively variable reaction to the rotating polarizer with a preferred *E*-vector orientation of 127° (Fig. 4B,C). This reaction was much more

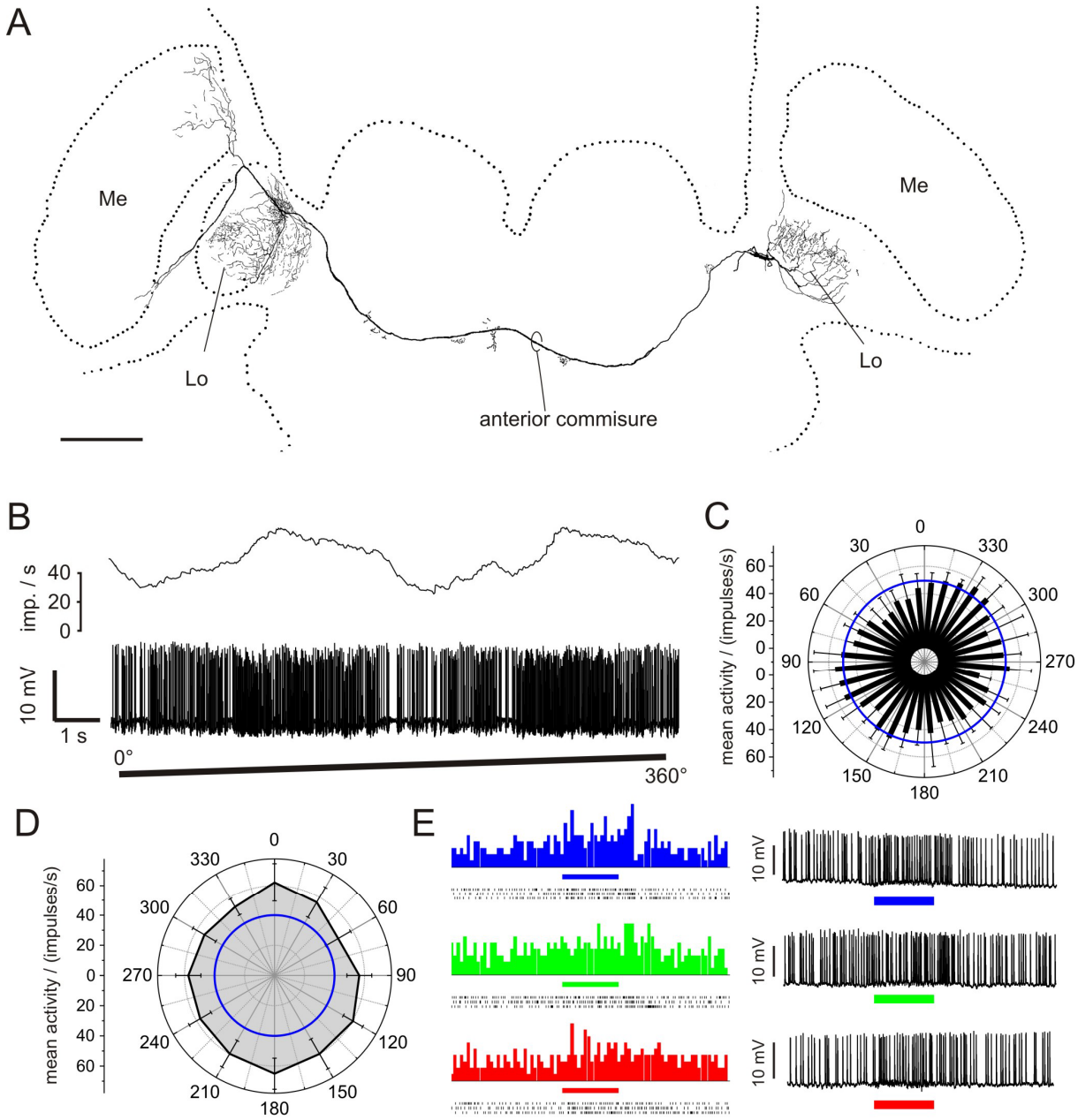

Figure 4. Polarization-sensitive and motion-sensitive neuron. ***A.*** Frontal reconstruction of the neuron. The soma and possibly some arborizations in the right medulla (Me) are missing due to incomplete staining of the neuron. The axon runs through an anterior commissure and connects both lobulae (Lo) and one medulla. Small sidebranches along the main neurite in the central brain are also shown. ***B.*** Neuronal activity during stimulation with a dorsally rotating *E*-vector (one 360° rotation). The upper trace shows mean activity (gliding average, bin size 1 s), and the lower trace depicts the original spike train. ***C.*** Circular plot of mean activity against *E*-vector orientation (n = 4; bin size: 10°; error bars are standard deviation). ***D.*** Circular diagram of mean activity during frontal motion of oriented bars plotted against bar orientation (error bars are standard deviation). Blue line represents background activity of the cell. Note that the neuron is excited by motion independently of direction or orientation. ***E.*** Left: Scatter plots and peri-stimulus-time histograms during stimulation with full-screen, frontally presented light flashes (duration: 0.5 s). Phasic activation at stimulus onset and offset is strongest at short wavelength stimuli (blue) and less pronounced at mid-range (green) and long wavelengths (red). Right: individual responses to light flashes shown by original spike trains. Scale bar in ***A***, 200 µm.

pronounced to clockwise rotations of the polarizer than to counterclockwise rotations. Strong motion sensitivity was detected as response to oriented bar stimuli in the frontal visual field (Fig. 4D), but also in the left lateral visual field in response to movements of the experimenter (not shown). Whole screen, frontal light flashes elicited weak phasic excitatory responses at stimulus onset and offset, which were most pronounced at short wavelengths (Fig. 4E,F). Frontally presented, small white discs elicited weak excitatory responses only in the left half of the screen (not shown).

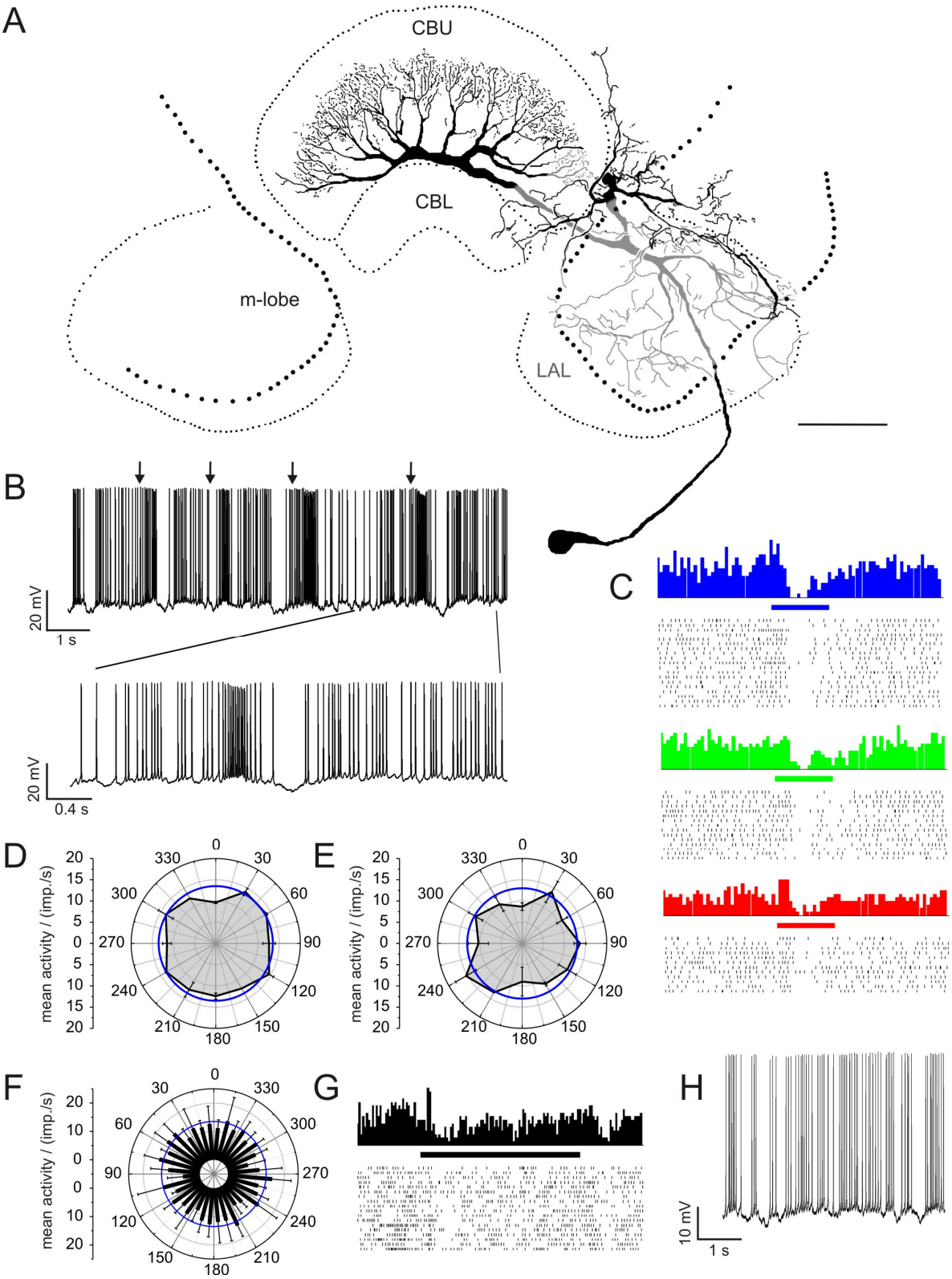

Figure 5. Characteristics of the giant fan-shaped neuron of the upper division of the central body (CBU). ***A.*** Frontal reconstruction of the neuron. Arborizations shown in grey are located posterior of black ramifications. The soma is located ventromedially of the antennal lobe. ***B.*** Movements of the experimenter's hand in the ipsilateral (left) visual field elicited strong excitatory responses (arrows). The enlargement shows one response in detail. ***C.*** Scatter plots and the corresponding peri-stimulus-time histograms showing responses to frontally presented, full-screen light flashes of different spectral composition. A slow inhibitory response is independent of the presented wavelength. ***D.*** Circular diagram of mean activity during frontal motion of oriented bars plotted against bar orientation. The blue line represents the background firing rate of the cell. ***E.*** As in ***D***, but for oriented, drifting gratings instead of bars. ***F.*** Circular plot of mean activity against *E*-vector orientation (n = 4; bin size: 10°) during dorsal rotations of the polarizer. ***G.*** Series of dorsally presented polarized light stimuli with constant *E*-vectors (from 0° to 150°, in steps of 30°, 3 presentations each, duration: 2.5 s) shows inhibition after stimulus offset and a short activity burst followed by weak inhibition at stimulus onset. ***H.*** Spike train depicting background activity with regularly occurring periods of inhibition. All error bars are standard deviations. CBU, upper division of the central body; CBL, lower division of the central body; LAL, lateral accessory lobe; m-lobe, medial lobe of the mushroom body. Scale bar in ***A***, 80 µm.

Central-complex neurons

All neurons recorded from the central complex responded to visual stimulation. Recordings could be obtained from three tangential neurons and eleven columnar cells. All columnar cells belonged to polarization-sensitive cell types (n = 7), or to conditionally polarization-sensitive types (n = 4). Of the tangential cells, one was polarization sensitive (TL2), whereas the other two were not. Responses to unpolarized visual stimuli depended strongly on the type of neuron, but were with few exceptions subtle or absent.

Non-polarization-sensitive tangential neurons

Two types of tangential neuron were not polarization sensitive and responded relatively strongly to unpolarized stimuli. One of these was identified as a giant fan-shaped neuron (GFN, Williams, 1972; Homberg, 1994). While its soma was located in the ventromedial protocerebrum, the neuron had arborizations in the dorsal and ventral shells of the LALs and in a small, band-like region surrounding the medial lobe of the mushroom body. Prominent, fan-like arborizations were present in layer IIb of the CBU (Fig. 5A). The second neuron could not be reconstructed completely due to superposition of costained neurons. However, the cell clearly possessed beaded endings emerging from a neurite running tangentially through the anterior lip, a region anterioventrally of the CBU, as well as fine processes protruding dorsally into superficial regions of layer Ia of the CBU (not shown). Other arborization areas, as well as the soma, are likely located ventrally of the calyx of the mushroom body.

The GFN was characterized by strong excitation to movement of the experimenter's hand in the left lateral visual field (Fig. 5B), superimposed on a relatively variable background firing pattern with spontaneously occurring stretches of inhibition (Fig. 5H). Due to the lack of controlled stimulus application in the lateral field of view, these responses could not be analyzed in detail. Weaker inhibitory responses were elicited by frontal stimuli covering the whole screen (Fig. 5C). These responses had a long latency (113 ms ± 29 ms) compared to responses recorded from optic-lobe neurons, and where independent of spectral composition of the stimulus. Similar responses occurred during polarized-light stimulation with stationary *E*-vectors presented from dorsal directions, but these reactions were independent of the presented *E*-vector (Fig. 5F,G). The inhibitions were transient and were preceded by a brief burst of activity. In addition, inhibitions were present after stimulus offset (Fig. 5G). Oriented bars moving across the frontal visual field did not elicit any response, whereas moving sine-gratings resulted in weak inhibition especially at the first two presentations in each stimulus series (Fig. 5D,E).

The neuron projecting to the anterior lip was also inhibited by frontal, whole-screen light flashes (not shown). These responses had a very long latency of about 300 - 350 ms and outlasted the stimulus by ca. 0.5 s at short wavelengths. For longer wavelengths, the response ended nearly 200 ms earlier, and was not accompanied by strong, graded modulations in membrane potential seen at short wavelengths. When white, moving bars were presented in the frontal visual field, the neuron was generally inhibited.

Tangential POL-neurons

One recording could be obtained from a TL2 neuron at the input stage of the polarization vision network of the central complex. The neuron was strongly polarization sensitive and, in addition, responded to frontally presented unpolarized stimuli (Fig. 6). Its soma was located in the ventromedial protocerebrum. The primary neurite passed through the LAL and the axonal fiber continued to the CBL (Fig. 6A). Input arborizations were present in the lateral triangle of the LAL, whereas output arborizations extended through dorsal layers of the CBL.

The responses to polarized light were pronounced, with high signal-to-noise ratio, as has been described earlier (Fig. 6G; Vitzthum et al., 2002; Heinze and Homberg, submitted). When oriented bars moving across the frontally mounted screen were presented, activity of the cell was strongly inhibited during the first four stimulus presentations (0°, 180°, 30°, 210°; two repetitions; Fig. 6B,C), whereas it was weakly excited during all remaining presentations (Fig. 6B,D). This suggests either strong orientation sensitivity tuned to 113°, or a general inhibitory response to frontal motion, which adapts after approximately eight seconds, and quickly recovers as soon as stimulation is paused for more than two seconds (time between trials). Frontal, full-screen light flashes elicited weak inhibitory responses most pronounced for mid-range wavelengths (Fig. 6E). Notably, for white flashes

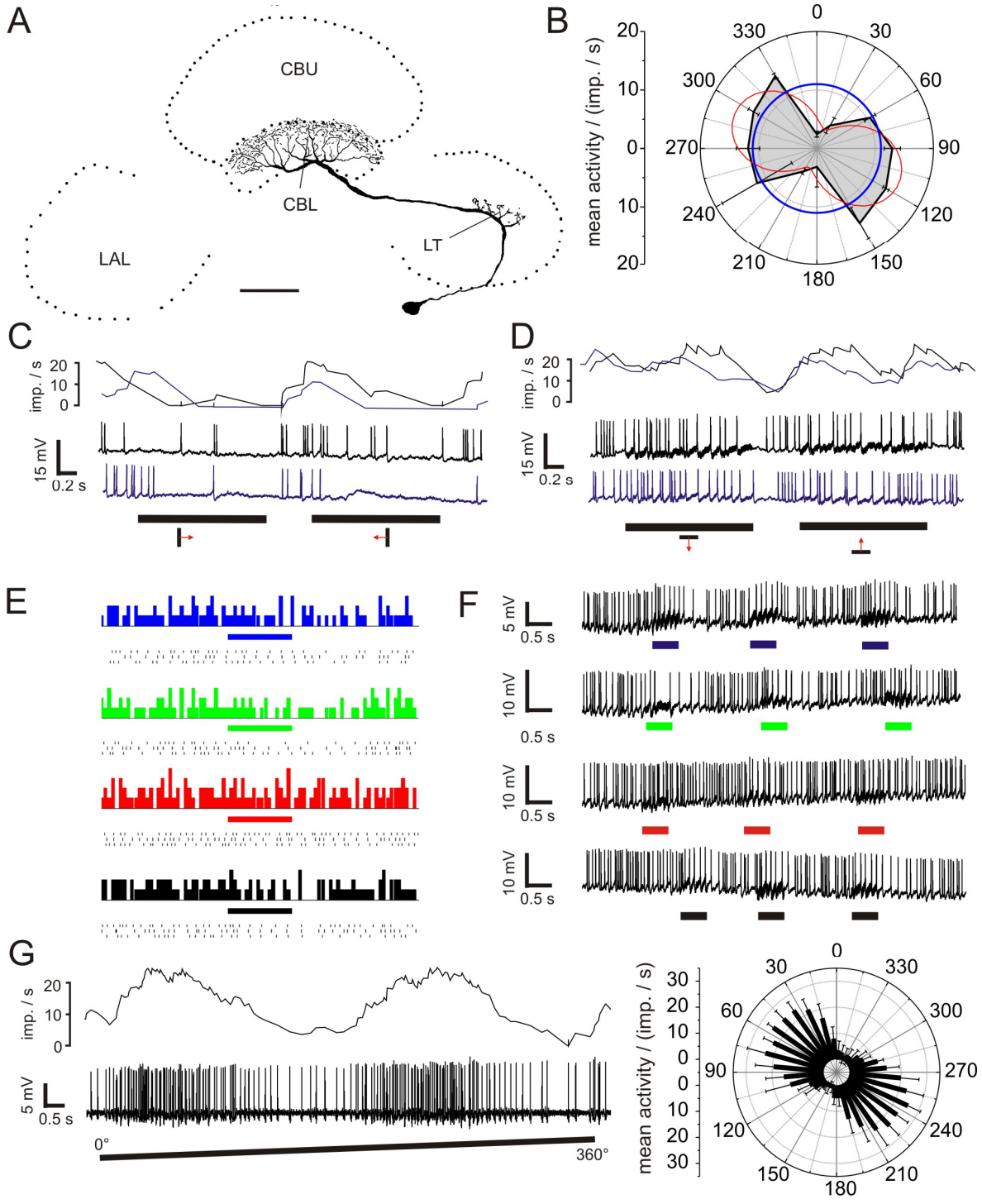

Figure 6. Morphology and response characteristics of a TL2 neuron. ***A.*** Frontal reconstruction. The neuron arborizes in the lateral triangle (LT) and in layer 2 of the lower division of the central body (CBL). ***B.*** Circular diagram of mean activity during presentation of moving bars in the frontal visual field plotted against bar orientation (black; error bars are standard deviations). The blue line indicates background activity of the neuron, the red line indicates a sine-square fit of the data (R^2-value: 0.79, preferred orientation: 113°). ***C,D.*** Spike trains and mean frequency (upper trace; gliding average, bin size: 1 s) showing responses to moving bars at 0°/180° orientation (***C***), and 90°/270° orientation (***D***). Black and blue spikes/mean frequencies are independent trials with the same stimulus. ***E.*** Scatter plots and peri-stimulus-time histograms (bin size: 30 ms) of full-screen, frontally presented light flashes with different spectral composition (blue: short wavelengths, green: mid-range wavelengths, red: long wavelengths, black: white RGB stimuli, stimulus duration: 0.5 s). Note locking of spikes to the stimulus for white stimuli. ***F.*** Data from ***E*** shown as original spike trains. ***G.*** Response of the neuron to a dorsally rotating polarizer. Left: Spike train and mean frequency during 360° rotation of the polarizer. Right: Circular plot of mean activity against *E*-vector orientation (bin size: 10°, error bars are standard deviation, Φ_{max}-value = 58°). LAL, lateral accessory lobe; CBU, upper division of the central body. Scale bar in ***A***, 80 µm.

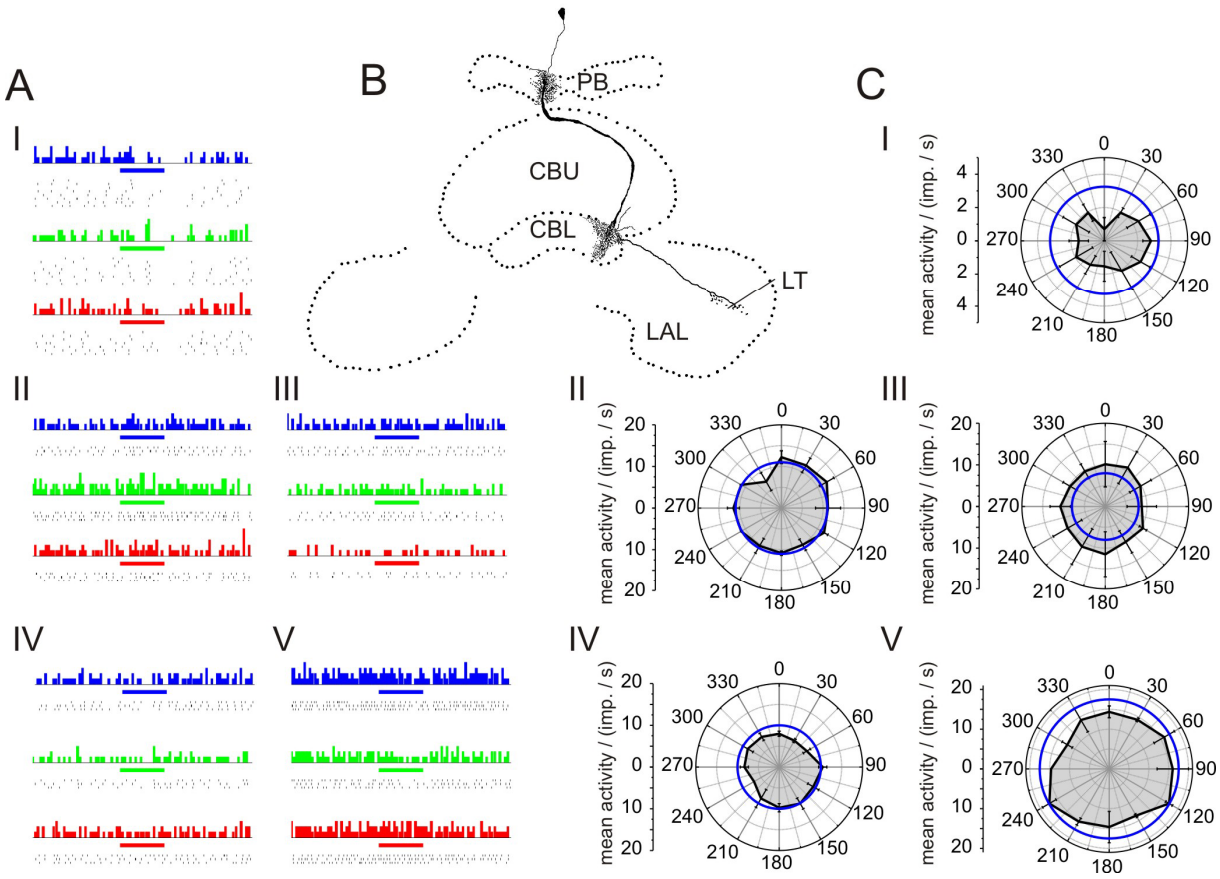

Figure 7. Morphology and responses to frontally presented, unpolarized light stimuli of CL1a neurons. ***A.*** Responses of five CL1a neurons ***(I-V)*** to full-screen light flashes of different spectral composition. Shown are scatter plots and peri-stimulus-time histograms (blue: short wavelengths, green: mid-range wavelengths, red: long wavelengths, stimulus duration: 0.5 s). Only cell I shows a clear inhibitory response. ***B.*** Frontal reconstruction of the CL1a neuron with responses shown in ***A(I)*** and ***C(I).*** The neuron connects the protocerebral bridge (PB), the lower division of the central body (CBL) and the lateral triangle (LT) of the lateral accessory lobe (LAL). ***C.*** Circular diagrams of mean activity during presentation of moving bars in the frontal visual fields plotted against the bar orientation (error bars are standard deviations). The blue lines represent the background activity of the neurons. Orientation independent, weak inhibitory responses are evident in cells ***I*** and ***V***. CBU, upper division of the central body.

and to a weaker extent for short wavelengths, spikes occurring during the response appeared to be time-locked when compared across trials.

Columnar POL- neurons

The majority of recordings from the central complex were obtained from polarization-sensitive neurons. These included five CL1a neurons, one CL1b/d neuron, and one CPU1 cell. All CL1 neurons responded strongly to dorsally rotating *E*-vectors as described by Heinze and Homberg (submitted). To frontally presented, unpolarized stimuli, however, none of the cells showed pronounced activity changes (Fig. 7). Full-screen light flashes elicited weak to moderate inhibition in two cells (Fig. 7A/I,V), whereas no reaction was observed in the remaining CL1a neurons (Fig. 7A) or in the CL1b/d neuron (not shown). Oriented bars moving across the frontal visual field produced responses consistent with light flashes, i.e. weak inhibition in two recordings, and no reaction in the remaining cells (Fig. 7C).

A CPU1 neuron showed a significant response to polarized-light stimulation (Fig. 8B) and a subtle, but consistent modulation in activity, when stimulated with oriented bars moving through the frontal visual field (Fig. 8C,D). Maximal excitation occurred at a bar angle of 125° (n = 2). A tendency to increase activity at a certain bar orientation was also found by rotating bar stimuli, either using black bars on white background or vice versa (each n = 2, not shown). The preferred orientation of 141° was similar to the preferred orientation when stimulating with moving bars, but was statistically not significantly different from random spiking (Rayleigh-test). Frontally presented, full-screen flashes elicited weak transient inhibition, followed by a weak excitation outlasting the stimulus by approximately 500 ms (Fig. 8E,F). This response was most pronounced for stimuli at mid-range wavelengths.

Conditionally POL-neurons

The last neurons considered are conditionally polarization sensitive cells. Four recordings were obtained and belonged to three cell types, CPU2 (n = 2), CPU4 (n = 1), and CL2 (n = 1). CPU2 neurons are similar to CPU1 cells. They possess smooth arborization trees in distinct columns of the PB and the CBU. Axonal projections extend to the ventral shells of both LALs, where they arborize with strongly varicose ramifications (Fig. 9A). CPU4 cells project from an individual PB-column to a columnar region of CBU-layer III and further to one layer of the upper division of the contralateral nodulus (Fig. 10D). CL2 cells connect PB-columns with columns in the CBL and with the lower unit of the contralateral nodulus (Fig. 10A). Detailed descriptions of the neuronal anatomies were provided by Heinze and Homberg (2008).

Of the two recordings of CPU2 neurons, one was polarization sensitive, whereas the other one was not. Both cells showed widely different background discharge rates and responded also differently to unpolarized light stimuli (Fig. 9). Frontal, whole screen light flashes elicited no response in the polarization-sensitive neuron (Fig. 9C), whereas the polarization blind cell was strongly excited by short wavelength and mid-range wavelength flashes (Fig. 9C'). Oriented bars moving across the frontal visual field revealed no orientation sensitivity in the polarization sensitive neuron (Fig. 9B), but it resulted in a consistent inhibition as soon as a horizontal bar reached the lower half of the screen (Fig. 9E). This reaction did not depend on the direction of motion and did not occur for other bar orientations or with moving squares at different sizes (not shown). The polarization blind neuron reacted with weak excitation to the first two presentations of bar stimuli (0° and 180° orientation; Fig. 9B', E'). Whether this represents true orientation sensitivity remains to be shown, but might appear unlikely, as all moving bar stimuli elicited an orientation independent transient inhibitory response, followed by a more or less pronounced activation (Fig. 9D').

Of the two neurons innervating the noduli, the CL2 cell was polarization-sensitive, whereas the CPU4 cell was polarization blind. Neither cell showed any response to oriented bar motion, but both were weakly activated by frontal, full-screen flashes (Fig. 10). The CL2 neuron showed an excitatory response outlasting the stimulus by several hundred milliseconds (Fig. 10B,C). This response was strongest for mid-range wavelength flashes, and did not exist for short wavelengths. White stimuli elicited a comparable reaction as mid-range stimuli. The CPU4 neuron showed different spectral response characteristics. Short wavelength flashes elicited a slow excitatory reaction, whereas neither mid-range nor long wavelength stimuli did so (Fig. 10E,F). Surprisingly, white flashes also failed to produce a response.

Discussion

In this work, responses of central-complex neurons to controlled motion stimuli, large versus small light flashes, and stimuli with distinct spectral composition were examined for the first time. However, when central-complex neurons responded to these stimuli at all, their reactions were usually very subtle. Strong responses to these stimuli in a variety of neurons from the optic lobes excluded the possibility that the stimuli used for these experiments were inadequate to be perceived by locusts. Several of these recordings proved to be highly interesting on their own account and were analyzed in more detail.

Validity of data

Before discussing the data in a broader context, some technical limitations in the generation of stimuli need to be mentioned. First, spectral stimuli applied through the CRT screen phosphors were not monochromatic and could, thus, not be adjusted for equal photon flux. As photoreceptors are not measuring light irradiance, but rather detect the number of incoming photons, effectiveness of spectral stimuli to elicit neuronal responses could not be compared quantitatively. Additionally, the spectral composition of stimuli could not be measured in the ultraviolet (UV) range, so that accidental presentation of UV light with the spectral stimuli cannot be completely excluded. Second, the presentation of series of oriented bars moving across the screen was always applied in identical sequence. This poses the problem that an unspecific light response adapting over the first few stimuli cannot be distinguished from an orientation sensitive response tuned to the orientation of these first stimuli. Consequently, in future experiments the first stimulus orientation should be added as a control to the end of each series, or the stimuli have to be shown in random sequence. Furthermore, in order to differentiate orientation sensitivity from responses due to bars moving across local receptive fields, inverted stimuli, i.e. black bars moving on white background, have to be used as control

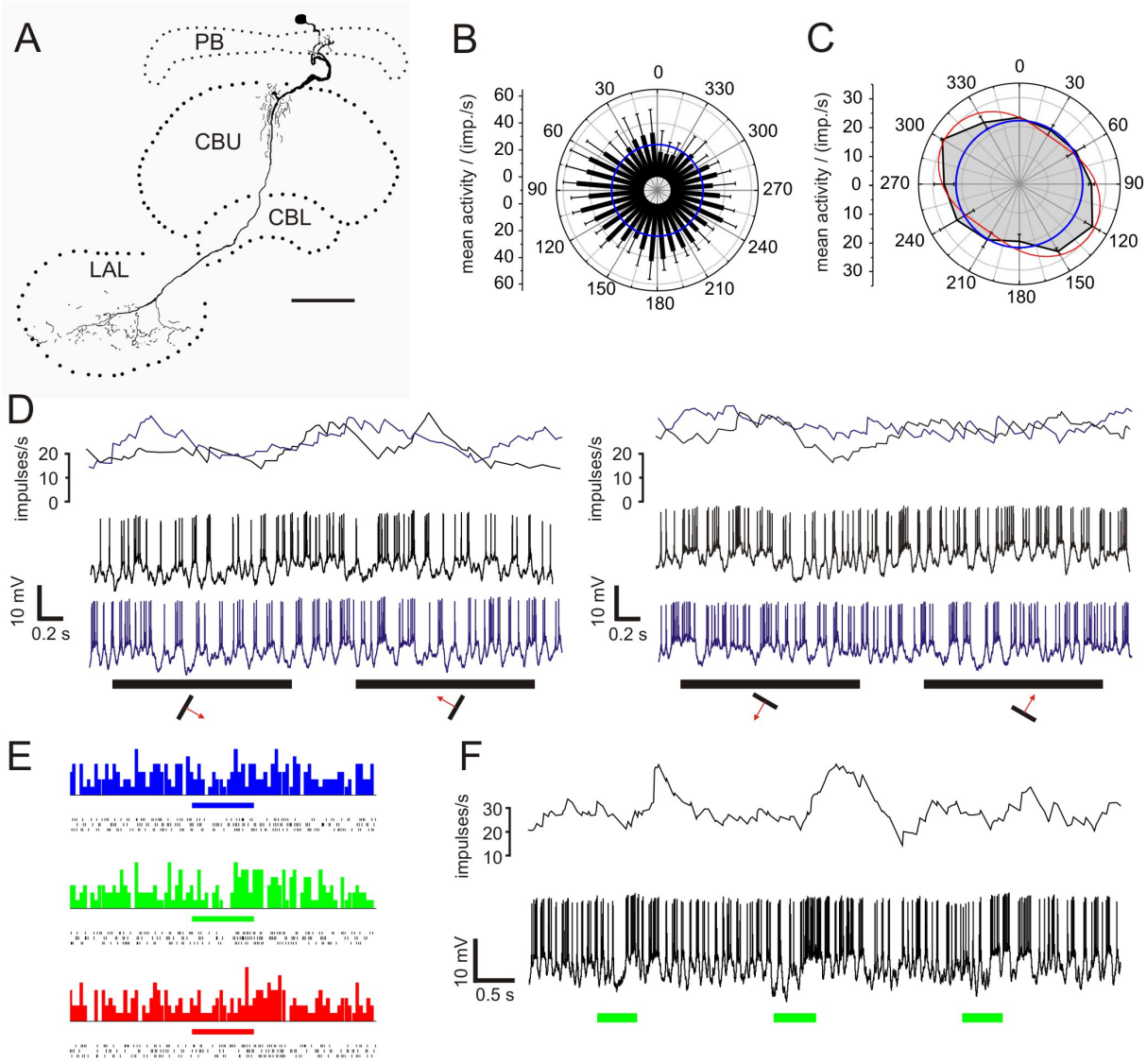

Figure 8. Physiological responses to visual stimulation and morphology of a CPU1 neuron. ***A.*** Frontal reconstruction of the neuron. The cell projects from the protocerebral bridge (PB) and the upper division of the central body (CBU) to the contralateral lateral accessory lobe (LAL). ***B.*** Circular plot of mean activity against *E*-vector orientation (n = 4; bin size: 10°, error bars are standard deviation; Φ_{max}-value = 78°).The blue line indicates background firing rate. ***C.*** Circular diagram of mean activity during presentation of moving bars in the frontal visual field plotted against the bar orientation (error bars are standard deviations). The blue line represents the background activity of the neuron, whereas the red line indicates a sine-square fit of the data, revealing orientation tuning of this neuron (R^2-value: 0.95, preferred orientation: 125°). ***D.*** Spike trains (lower traces) and mean frequencies (upper traces) for distinct bar orientations. The left side depicts 30° bar orientation (minimal activation), the right side shows 120° bar orientation (near the preferred orientation tuning). Black and blue spike trains are two independent trials with identical stimulations. ***E.*** Scatter plots and peri-stimulus-time histograms (bin size: 30 ms) of activity during presentation of full-screen, frontal light flashes with different spectral composition (blue: short wavelengths, green: mid-range wavelengths, red: long wavelengths, stimulus duration: 0.5 s). The strongest reactions occur at mid-range wavelengths. ***F.*** Spike train (lower trace) and mean activity (upper trace) during three successive stimulations with mid-range wavelength light. CBL, lower division of the central body. Scale bar in ***A***, 80 µm.

stimuli. Considering these limitations for spectral and orientation responses, some caution has to be applied when interpreting the data obtained in this work and results have to be treated as preliminary in this respect.

Motion-, size- and orientation processing in neurons of the optic lobe

Neurons recorded from the optic lobe have been found to respond to motion in many insect species. Particularly, neurons of the lobula, but also some of the medulla were characterized in detail in locusts (Stern and Gewecke, 1993; Gewecke and Hou, 1993; Osorio, 1986a; Rind, 1987, 1990; Homberg and Würden, 1997; Rind and Simmons, 1998), flies (e.g. Egelhaaf et al., 2002; Huston and Krapp, 2008; Joesch et al., 2008; Okamura and Strausfeld, 2007), dragonflies (O'Carroll, 1993), bees (Hertel and Maronde, 1987; Hertel et al., 1987; Yang and Maddess, 1997), bumblebees (Paulk et al., 2008), and hoverflies (Nordström et al., 2008). Among these, several neurons were

selective to the direction of movement, whereas others responded to motion irrespective of direction. In the current work, only one neuron was direction-sensitive. This heterolateral lobula neuron (Fig.3) with ramifications in the contralateral posterior protocerebrum will be discussed in detail with regard to its potential role as feature detection neuron (see below). All other motion sensitive neurons were activated by moving bars in the frontal visual field, and most of them innervated the lobula. Two cells projected from the optic lobe to the posterior protocerebrum, a region, which contains many motion-sensitive cells receiving input from the lobula (Osorio, 1986a; Rind, 1987, 1990). Two neurons in the current work provided input to the optic lobe from the central brain, as judged by their morphology. One of these has been described by Rind (1987) and was named G1A neuron. Responses have been described as motion sensitive, but not direction selective. Additionally, it responded to other modalities, such as touch of the abdomen, or auditory stimuli. Although the neuron could not be tested for motion stimuli in the current work, the quickly adapting ON and OFF responses together with its morphology proved sufficiently similar to identify the recorded cell as G1A neuron.

Considering all species studied, motion sensitive neurons appear to project either to the posterior protocerebrum or to the lateral protocerebrum, regions, which are both innervated by descending neurons (Strausfeld and Okamura, 2007). This suggests that the major motion processing pathways bypass the central complex. This is reasonable, given that moving objects require fast behavioral responses with as few synapses as possible from the sensory periphery to motor output.

The next class of neuron known from the insect optic lobe are orientation sensitive cells, described in flies (Okamura and Strausfeld, 2007), bees (Yang and Maddess, 1997), bumblebees (Paulk et al., 2008), and dragonflies (O'Carroll, 1993). These neurons also respond to moving objects, but only if they are presented in a particular orientation. Orientation-sensitive neurons can be expected in the central complex, as CBU-tangential neurons in *Drosophila* are required for memory of oriented bars. To understand where these cells receive their input from, orientation sensitive optic-lobe neurons would have to be characterized. However, none of the recorded cells from the optic lobe responded to this stimulus feature.

At last, neurons tuned specifically to small targets have been described in predatory insects, particularly in dragonflies (O'Carroll, 1993), but also in non predatory species such as hoverflies (Nordström and O'Carroll, 2006; Geurten et al., 2007) and flies (Egelhaaf, 1985). These neurons respond to small moving targets and are thus termed small moving target detectors (SMTDs). Their strong responses to small stimuli become continuously less pronounced for larger objects and finally vanish altogether above a certain size. Large gratings do not elicit any response during presentation. For the hoverfly, two described SMTDs innervate the lobula and project either to the contralateral lobula or to the ipsilateral subesophageal ganglion (Nordström et al., 2006), whereas one neuron connecting two regions in the protocerebrum to one lobula has been described in a dragonfly (Geurten et al., 2007). Two recordings of the current work show intriguing similarities with SMTDs. One of these was the heterolateral lobula neuron (Fig. 3) with additional ramifications in the contralateral posterior protocerebrum, whereas the other one connected an unresolved area (due to incomplete staining) in the optic lobe with the ipsilateral posterior protocerebrum. The first neuron was tested with stationary and moving objects, whereas the second neuron was only tested for responses to stationary objects. The first neuron showed remarkably similar responses to motion of bars across the frontal visual field with SMTDs of the hoverfly (Nordström and O'Carroll, 2006, Nordström et al., 2006). The visual fields of the hoverfly neurons were restricted to one half of the frontal visual field, where most cells showed optimal tuning to small objects of 0.8° x 3°. Some neurons also responded to larger bars of 0.8° x 75°, a size roughly comparable to bars used in the current experiments on the locust (8° x 44°). The recorded locust neuron responded considerably stronger to downward motion than compared to upward motion. Some of the SMTD neurons from the hoverfly also preferred either upward or downward motion (Nordström et al., 2006). A possible role of the described locust neurons in object detection or size discrimination is also suggested by the antagonistic responses to large and small static stimuli. However, due to different intervals between stimuli and the exceptionally strong first response after long periods without stimulation, some caution must be applied when interpreting these results. The exceptionally strong bursting responses are highly similar to light-driven, 20 Hz oscillations found in medulla-neurons of the cockroach, but could be elicited at much lower light intensity (Loesel and Homberg, 1998). Both neurons with size-discriminatory responses in this

work had very similar characteristics and projected either to the ipsilateral or to the contralateral posterior protocerebrum, suggesting a role of this brain region for object recognition during fast behaviors, possibly in the context of predator avoidance or detection of conspecifics (Nordström and O'Carroll, 2006).

Whether any of the described stimulus responses is passed on to neurons of the central complex is unknown. If connections exist, they are likely indirect via intercalated interneurons, and thus would probably be rather involved in long term behavioral planning or memory, than in acute, fast responses.

Color processing

Insects generally possess color vision (Briscoe and Chittka, 2001), which is trichromatic in most cases (UV-, blue-, green-receptors), but can also be based on receptors sensitive to as many as five different spectral ranges (*Papilio* butterflies). Red receptors have evolved in several species of Odonata, Hymenoptera, Lepidoptera, and Coleoptera (Briscoe and Chittka, 2001). For the migratory locust (*Locusta migratoria*) photoreceptors of the main compound eye have been shown to belong to UV-, blue-, or green receptors (360 nm, 430 nm, and 530 nm; Vishnevskaya and Shura-Bura, 1990). In the DRA of the desert locust (*Schistocerca gregaria*), two types of photoreceptors have been described, a blue receptor with high polarization sensitivity (450 nm) and a weakly polarization-sensitive UV receptor (320 nm; Eggers and Gewecke, 1993).

Responses in the current work were found for all spectral ranges presented to the locust (range from 400 nm to 725 nm). Surprisingly, stimuli peaking at 600 nm (L-stimuli) elicited strong responses in some neurons. However, these red light flashes include a spectral range down to approximately 575 nm and are thus likely to activate green receptors. S-stimuli (peaking at 450 nm) optimally activate blue receptors, but also show considerable overlap with the estimated sensitivity range of green receptors and potentially also weakly excite UV receptors. Finally, M-stimuli (peaking at 550 nm) will most strongly activate green-receptors and, to a lesser extent, blue receptors. Overall, a variety of chromatic responses was found. Of the 17 neurons responding to frontal light flashes eight neurons responded to all wavelengths (three in the CC, five in the optic lobe), whereas three neurons showed no responses to L-stimuli, implying that they do not receive input from green receptors. One cell only responded to S-stimuli, suggesting UV, but neither blue nor green input (as M-stimuli also overlap with blue-receptors). In five neurons specific components of the response (e.g. inhibitory aftereffects) depended on the spectral composition of the stimulus, whereas others did not. Similar effects have been described for bumble bees (Paulk et al., 2008).

Two color opponent cells were particularly interesting. They are best described as S+/L- and S-/L+, while M-stimuli did not elicit a distinct response in these cells. This behavior can be interpreted either as blue-green opponency, UV-green opponency, or a combination thereof. Without precisely knowing the spectral sensitivity ranges of *S. gregaria* photoreceptors, these possibilities cannot be distinguished. UV-green opponency has been found in local medulla neurons of *L. migratoria* (Osorio, 1986b) and in polarization sensitive neurons of the anterior optic tubercle of *S. gregaria* (Kinoshita et al., 2007). In the latter neurons, the spectral responses depend on the azimuth in which they are presented and are thus likely involved in coding spectral gradients at the sky Pfeiffer and Homberg, 2007). Color opponent neurons have been shown in the lobula and the medulla of honey bees (Kien and Menzel, 1977; Yang et al., 2004) and in the lobula of bumble bees (Paulk et al., 2008).

All color opponent neurons described in

Figure 9. Characteristics of CPU2 neurons. Data from two individual recordings are shown, one of which was polarization sensitive (***A-E***), whereas the second one was polarization blind (***B'-E'***). ***A.*** Frontal reconstruction of the morphology of the polarization-sensitive CPU2 neuron (modified from Heinze and Homberg, submitted). The cell connects the protocerebral bridge (PB) and the upper division of the central body (CBU) with both lateral accessory lobes (LAL). ***B/B'.*** Circular diagrams of mean activity during presentation of moving bars in the frontal visual field plotted against the bar orientation (error bars are standard deviations). The blue lines represent the neurons' background activity. The polarization-blind neuron is weakly activated at 0°/180°. ***C/C'.*** Responses to frontally presented, full-screen light flashes of different spectral composition. Shown are scatter plots and the corresponding peri-stimulus-time histograms (PSTH; blue: short wavelengths, green: mid-range wavelengths, red: long wavelengths, stimulus duration: 0.5 s, bin size: 30 ms). The polarization-sensitive neuron shows no response, while the polarization blind neuron is strongly excited at short and mid-range wavelengths. ***D/D'.*** Scatter plots and PSTH (bin size: 30 ms) for two series of moving bar stimuli (different orientations, from 0° to 150° in steps of 30°, each step is shown twice with opposite motion directions, duration: 1.45 s). A transient inhibition followed by a weak excitation can be observed for all orientations in the polarization blind neuron (***D'***). ***E/E'.*** Spike trains (lower traces) and mean frequencies (upper traces) during stimulation with moving bars at distinct bar orientations. The upper graphs show 90° bar orientation, the lower graphs 0° orientation. Black and blue spike trains are two independent trials with identical stimulations. The polarization-sensitive neuron (***E***) is inhibited when a horizontal bar moves through the lower region of the screen (asterisks), but shows no response to vertical bars. The polarization- blind cell (***E'***) shows no response to horizontal bars, but an excitatory reaction to vertical bars. CBL, lower division of the central body. Scale bar in ***A***, 80 µm.

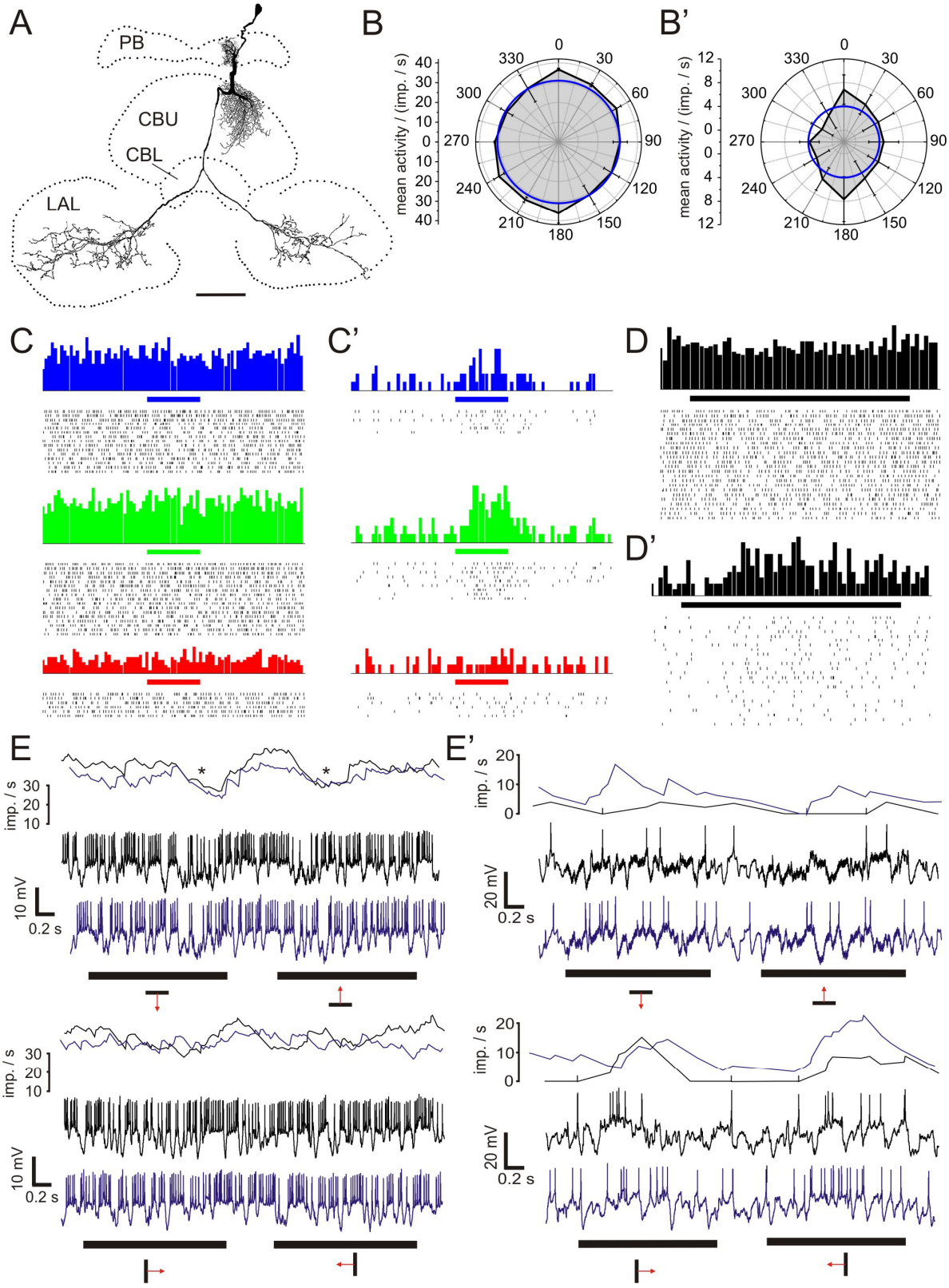
A
PB
CBU
CBL
LAL
B
mean activity / (imp. / s)
0
30
60
90
120
150
180
210
240
270
300
330
B'
C
C'
D
D'
E
E'
imp. / s
10 mV
0.2 s
20 mV

various insects are either intrinsic to the optic lobe, project from the lobula to the posterior, dorsal and lateral protocerebrum, or to the mushroom bodies (in bumble bees). The heterolateral medulla neuron shown here had central arborizations in the posterior protocerebrum, and thus suggests that this area serves as processing region for color vision also in the locust.

Integration of Motion and *E*-vector information

A single neuron responded to polarized-light as well as to motion stimuli (Fig. 4). A morphologically similar neuron has been described by Stern and Gewecke, (1993). It responded to a locally moving black spot on white background with excitations, which were restrictted to the contralateral half of the frontal visual field (side with medulla arborizations). In the neuron shown here, small white, stationary discs on black background resulted in excitations also restricted to the half of the frontal visual field ipsilateral to the medulla arborizations. Heterolateral neurons of the optic lobe have been found to respond to polarized light in crickets and locusts (Labhart and Meyer, 2002; Homberg and Würden, 1997). In the cricket, POL1 neurons connect the medullae of both hemispheres and have been described in great detail with regard to their response characteristics. Importantly, they do not respond to unpolarized light (Labhart, 1988), which differs clearly from the neuron recorded here. Neurons of the locust optic lobe received input in one medulla and projected contralaterally, where arborizations could not be resolved (Homberg and Würden, 1997). They responded with phasic or tonic inhibitions to unpolarized light flashes, but were insensitive to motion stimuli. Additionally, polarization-sensitive cells innervating the medulla and projecting to the lamina have been described (Homberg and Würden, 1997). None of these types of neuron had direct connections to the dorsal rim areas of the medulla or lamina, which is most likely also the case for the cell type reported here. As photoreceptors in the main compound eye also show some polarization sensitivity, this capacity could be used for polarization-dependent color vision, as suggested for *Papilio* butterflies (Kelber et al., 2001). Hence, the polarization-sensitive neurons reported in the locust medulla might participate in roles distinct from sky compass navigation. This is in tune with the finding that none of these neurons arborize in regions innervated by neurons of the polarization-vision pathway originating in the dorsal rim area of the compound eye.

Recent recordings from descending neurons of the locust (U. Träger, personal communication) as well as from lobula neurons projecting to the posterior protocerebrum (B. el Jundi, personal communication) also revealed units responding to motion and polarized light stimuli. These data together suggest the existence of a second polarization-sensitive pathway in the brain of the locust, which bypasses the central complex.

Processing of unpolarized light in neurons of the CC polarization-vision network

In the central complex several types of neuron responded to unpolarized light stimuli as well as to polarized light. Of the seven major types of neuron constituting the core polarization-vision-network (TL2, TL3, CL1, TB1, CPU1, CP1, CP2), three could be tested for responses to unpolarized visual stimuli. Among these were one TL2 neuron, six CL1 neurons, and one CPU1 cell. TL2 cells are at the input stage of the network, CL1 neurons are likely responsible for transferring polarized-light information from the CBL to the PB, and finally, CPU1 neurons are the proposed major output elements of the central-complex polarization vision network (Heinze and Homberg, 2007; Heinze and Homberg, submitted; Heinze et al., submitted).

In CL1 neurons, no reaction (n = 5) or weak inhibitory responses (n = 1) resulted from frontal stimulation with unpolarized light flashes or moving bars, while polarization responses were consistently pronounced. These findings are in tune with the proposed role for CL1 neurons. They are key elements of the polarization-vision network, have precise *E*-vector tuning and low background activity suggesting that these cells are reserved for *E*-vector coding (Heinze et al., submitted). The inhibitory response to frontal light flashes observed in one recording might be a hint that these cells receive azimuth-dependent spectral information from neurons of the AOTu. CPU1 neurons possess a large input arborization tree extending through all layers of the CBU, in addition to their input regions in the PB (Heinze and Homberg, 2008). As these ramifications are suited to receive information from tangential neurons of the CBU which have never been shown to be polarization-sensitive, CPU1 neurons might be expected to respond to unpolarized stimuli. Their proposed role as major output elements of the central complex, their high background activity, and their only moderate *E*-vector responses also suggest that they are not solely reserved for *E*-vector coding (Heinze et al.,

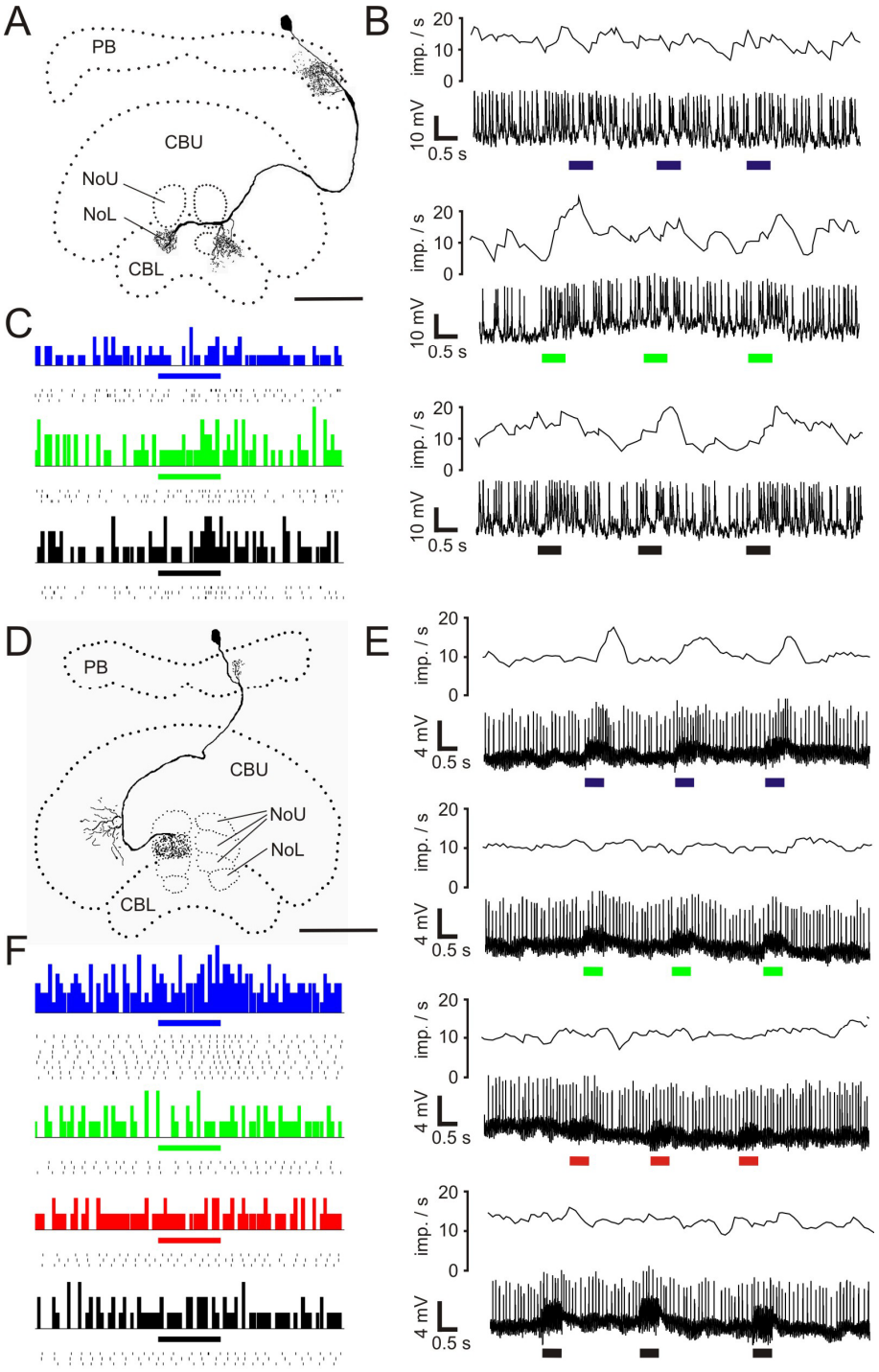

Figure 10. Morphologies and response characteristics of neurons innervating the noduli. ***A.*** Frontal reconstruction of a polarization-sensitive CL2 neuron, connecting the protocerebral bridge (PB) with the lower division of the central body (CBL), and the lower unit of the contralateral nodulus (NoL) (modified from Heinze and Homberg, submitted). ***B.*** Responses of the CL2 neuron in ***A*** to frontally presented, full-screen light flashes of different spectral composition (blue: short wavelengths, green: mid-range wavelengths, black: white RGB stimuli; stimulus duration: 0.5 s). Shown are spike trains and mean activity (gliding average, bin size 1 s). Slow, excitatory responses occurred at mid-range wavelength stimuli and white stimuli. ***C.*** Scatter plots and corresponding peri-stimulus-time histograms (bin size: 30 ms) of data presented in ***B***. ***D.*** Frontal reconstruction of a polarization-blind CPU4 neuron. It connects the PB with layer III of the upper division of the central body (CBU) and layer II of the upper unit of the contralateral nodulus (NoU). ***E.*** Stimulation of the CPU4 neuron as in ***B***. In addition, long wavelength stimuli were presented (red). Only short wavelength stimuli elicit slow, excitatory responses. ***F.*** Scatter plots and corresponding peri-stimulus-time histograms (bin size: 30 ms) for data presented in ***E***. Scalebars, 80 µm.

submitted). Indeed, the CPU1 neuron recorded here responded to frontal light flashes and showed moderately strong orientation sensitivity to frontally presented moving bars. This is well in tune with data from *Drosophila*, where oriented bars were one stimulus parameter, which depended on CBU tangential cells for memory formation in an aversive conditioning regime (Liu et al., 2006). For light flashes, an inhibitory component was observed for S- and M-stimuli, whereas rebound activation after stimulus offset was found for M- and L-stimuli. This suggests that two pathways converge on these cells, one driven by blue receptors (the inhibitory component) and the second one by green receptors (rebound activation). Nevertheless, all observed responses were subtle, indicating that stimuli were either not optimally designed or that they only result in strong responses if they are behaviorally relevant to the animal (e.g. due to pairing with punishment as in Liu et al., 2006).

The rather strong response of the recorded TL2 neuron to unpolarized frontal stimuli was surprising, as lateral and frontal light flashes

were described as largely ineffective to drive these neurons, whereas dorsal presentation of unpolarized white light elicited tonic inhibition in around 60% of these cells (Vitzthum et al., 2002). In the current work, light flashes were ineffective at long wavelengths, as opposed to short and mid-range wavelengths. Thus it can be concluded that the response is most likely not mediated by green receptors but relies on blue receptors. As white flashes resulted in precisely timed spikes, a role of the highly specialized input synapses of these neurons in the control of spike timing is supported (Träger et al., 2008). Frontally presented, moving bars elicited strong tonic inhibitions during the first four presentations, i.e. orientations of 0°/180° and 30°/210°. Whether this represents true orientation sensitivity or an adapting response to frontal motion remains to be shown. Both possibilities, however, suggest strong, polarization independent input at this early stage of the central-complex polarization vision network; a puzzling, but challenging finding.

Context dependency of responses?

In contrast to neurons that always respond to polarized light, conditionally POL-cells respond to polarized light only in approximately 50% of recordings (Heinze and Homberg, submitted). All three known types of conditionally POL-neurons were tested with unpolarized stimuli presented in the frontal field of view. Among these were two CPU2 neurons, which are morphologically similar to CPU1 neurons and constitute another major proposed central-complex output element (Heinze and Homberg, 2008). The remaining two neurons innervated the noduli and belonged to CPU4 and CL2 type neurons (Heinze and Homberg, 2008; Heinze and Homberg, submitted).

Like CPU1 neurons, CPU2 cells receive input from the PB as well as from all layers of the CBU and could thus be expected to respond to unpolarized light stimuli for the same reasons as CPU1 cells. Interestingly, one recorded cell was polarization sensitive, whereas the second one was polarization blind. Although both neurons showed weak to moderate responses to oriented bar motion, frontal light flashes only elicited activity changes in the polarization blind neuron. This cell was strongly activated by S- and M-stimuli, but not by L-stimuli, suggesting that green receptors might not contribute to the response. The observed inhibition in response to a horizontal bar in the ventral part of the frontal field of view in the polarization-sensitive CPU2 neuron can be interpreted as an elevation specific response. This is supported by the finding that elevation was the second feature, which could only be memorized when specific CBU tangential cells were intact in *Drosophila* (Liu et al., 2006). Additionally, the different response to oriented bar motion in the second neuron points to context dependent gating of input to these neurons, as has already been suggested by Heinze and Homberg (submitted). The two neurons innervating the noduli behaved differently with respect to the spectral sensitivity of their responses, suggesting a distinct source of visual information for each of the cells, at least for the frontal field of view.

Data from *Drosophila* suggest that tangential neurons of the CBU are input channels for unpolarized visual information into the central complex. The recording from the giant fan-shaped neuron of the CBU supports this view, as it strongly responded to movements of the experimenter in the lateral field of view of the animal. Its broad spectral tuning substantiates the view that this neuron represents an achromatic motion/object channel. Homberg (1994) reported flight-correlated rise in activity in the giant fan-shaped neurons as well as an inhibitory light response, indicating that this neuron also receives proprioreceptive input.

Altogether, these data raise several questions: What information is gated toward central-complex output dependent on which behavioral or motivational context? How is contextual information represented in the central complex? Also, it appears not trivial to distinguish context information from the actual object of interest for a behavioral response. Nevertheless, both types of information might be present in the central complex, in order to be integrated with directional compass information derived from the polarization vision system. Each type of tangential neuron may carry a specific piece of information that is potentially behaviorally relevant (e.g. presence of a large vertical object). Depending on the behavioral context, e.g. sitting versus flying, this information is more or less important. Different background activity in tune with the behavioral context could flag each neuron as important or not in a particular situation. For example, the giant fan-shaped neuron might code information, which is more relevant during flight, as flight activity raises its background firing rate and thus the potential to influence postsynaptic neurons. A similar mechanism has been suggested to serve as gain control for POL-neurons (Heinze and Homberg, submitted). Visual information itself can also serve as contextual information, such as optic flow (indicating flight), or general levels of illumination (indicating daytime or an exposed

situation in open space). Altogether, interaction between contextual and specific information (both potentially multimodal) in central-complex input pathways (in particular in CBU tangential neurons) might lead to the segregation of relevant versus irrelevant information for each behavioral situation, based on the suppression or enhancement of neuronal activity. Neuronal activity does obviously not only comprise changes in spike frequency, but also spike precision and temporal structure of spike trains. Ultimately, only relevant stimuli would be transformed into motor command signals along the output pathways of the central complex. Although largely speculative, the multitude of neuromodulatory substances in the central complex (for review see Homberg, 2002; Nässel and Homberg, 2006) as well as the often subtle and variable responses of neurons in this brain area supports the proposed hypothesis.

Future experiments

The subtle, variable, and potentially context-dependent responses to unpolarized visual stimuli of neurons in the central complex post significant challenges for future experiments. Ultimately, the behavioral situation of the locust should be controlled during the recordings. As a starting point, visual context information should be provided. To simulate flight, optic flow in the frontal field is simple to generate and can be easily combined with polarized light stimuli as well as object presentation in the frontal or lateral field of view. Also, different levels of background illumination can be easily provided. Comparison of responses to identical stimuli presented during different contextual situations should allow identifying crucial elements of the central-complex network. Providing motivational or actual behavioral context can be achieved by starving or isolating animals before recordings, and by recording during flight or walking activity.

Besides these experiments, the data in the current work clearly need substantiation by more recordings, especially for neurons of the polarization vision network in the central complex. Responses for spectral stimuli should be verified with monochromatic stimuli, which would additionally allow for quantitative analysis.

To characterize input regions of tangential neurons of the central complex in more detail, additional recordings from optic lobe neurons with central projections will be rewarding. Especially neurons involved in higher order processing, such as feature detection and orientation sensitivity should provide insight into which sensory aspects might be transferred to the central complex, and which aspects are directly relayed to motor circuits without passing through the central complex.

Acknowledgments

We kindly thank Dr. Keram Pfeiffer for providing Spike2 scripts for evaluating polarized light responses, Manfred Peil, Sebastian Richter, and Karl Ploch for constructing the recording setup and control devices for polarized light stimuli, and Karl-Heinz Herklotz for raising desert locusts. This work was supported by DFG-grant HO 950/16-2.

References

Briscoe AD, Chittka L (2001) The evolution of color vision in insects. Annu Rev Entomol 46:471-510.

Brunner D, Labhart T (1987) Behavioural evidence for polarization vision in crickets. Physiol Entomol 12:1-10.

Clements A, May TE (1974) Studies on Locust Neuromuscular Physiology in Relation to Glutamic Acid. J Exp Biol 60:673-705.

Dacke M, Nilsson D, Scholtz CH, Byrne M, Warrant EJ (2003) Animal behaviour: insect orientation to polarized moonlight. Nature 424:33.

Egelhaaf M (1985) On the neuronal basis of figure–ground discrimination by relative motion in the visual system of the fly. II. Figure detection cells, a new class of visual interneurones. Biol Cybern 52:195–209.

Egelhaaf M, Kern R, Krapp HG, Kretzberg J, Kurtz R, Warzecha AK (2002) Neural encoding of behaviourally relevant visual-motion information in the fly. Trends Neurosci 25:96-102.

Eggers A, Gewecke M. 1993. The dorsal rim area of the compound eye and polarization vision in the desert locust (*Schistocerca gregaria*). In: Wiese K; Gribakin FG; Popov AV; Renninger G, editors. Sensory systems of arthropods. Basel: Birkhäuser. p 101-109.

Geurten BRH, Nordström K, Sprayberry JDH, Bolzon DM, O'Carroll DC (2007) Neural mechanisms underlying target detection in a dragonfly centrifugal neuron. J Exp Biol 210:3277-3284.

Gewecke M, Hou T. 1993. Visual brain neurons in *Locusta migratoria*. In: Wiese K, Gribakin F, Popov A, Renninger G, editors. Sensory systems of arthropods. Basel: Birkhäuser. p 119-144.

Hanesch U, Fischbach KF, Heisenberg M (1989) Neuronal architecture of the central complex in *Drosophila melanogaster*. Cell Tissue Res 257:343-366.

Heinze S, Homberg U (2007) Maplike representation of celestial *E*-vector orientations in the brain of an insect. Science 315:995-997.

Heinze S, Homberg U (2008) Neuroarchitecture of the central complex of the desert locust: Intrinsic and columnar neurons. J Comp Neurol 511:454-478.

Heinze S, Homberg U. Linking the input to the output – New sets of neurons complement the polarization vision network in the locust central complex. (submitted).

Heinze S, Gotthardt S, Gebhardt S, Homberg U. Transformation of polarized light information in the central complex of the locust. (submitted).

Hertel H, Maronde U (1987) The physiology and morphology of centrally projecting visual interneurones in the honeybee brain. J Exp Biol 133:301-315.

Hertel H, Schäfer S, Maronde U (1987) The physiology and morphology of visual commissures in the honeybee brain. J Exp Biol 133:283-300.

Homberg U (1991) Neuroarchitecture of the central complex in the brain of the locust *Schistocerca gregaria* and *S. americana* as revealed by serotonin immunocytochemistry. J Comp Neurol 303:245-254.

Homberg U (1994) Flight-correlated activity changes in neurons of the lateral accessory lobes in the brain of the locust *Schistocerca gregaria*. J Comp Physiol A 175:597-610.

Homberg U (2002) Neurotransmitters and neuropeptides in the brain of the locust. Micros Res Tech 56:189-209.

Homberg U (2004) In search of the sky compass in the insect brain. Naturwiss 91:199-208.

Homberg U, Würden S (1997) Movement-sensitive, polarization-sensitive, and light-sensitive neurons of the medulla and accessory medulla of the locust, *Schistocerca gregaria*. J Comp Neurol 386:329-346.

Horváth G, Varjú D (2004) Polarized light in animal vision. Springer, Berlin.

Huston SJ, Krapp HG (2008) Visuomotor transformation in the fly gaze stabilization system. PLoS Biol 6:e173.

Joesch M, Plett J, Borst A, Reiff DF (2008) Response properties of motion-sensitive visual interneurons in the lobula plate of *Drosophila melanogaster*. Curr Biol 18:368-374.

Kelber A, Thunell C, Arikawa K (2001) Polarisation-dependent colour vision in *Papilio* butterflies. J Exp Biol 204:2469-2480.

Kien J, Menzel R (1977) Chromatic properties of interneurons in the optic lobes of the bee. J Comp Physiol A 113:17-34.

Kinoshita M, Pfeiffer K, Homberg U (2007) Spectral properties of identified polarized-light sensitive interneurons in the brain of the desert locust *Schistocerca gregaria*. J Exp Biol 210:1350-1361.

Kurylas AE, Rohlfing T, Krofczik S, Jenett A, Homberg U (2008) Standardized atlas of the brain of the desert locust, *Schistocerca gregaria*. Cell Tissue Res 333:125-145.

Labhart T (1988) Polarization-opponent interneurons in the insect visual system. Nature 331:435-437.

Labhart T, Meyer EP (2002) Neural mechanisms in insect navigation: polarization compass and odometer. Curr Opin Neurobiol 12:707-714.

Liu G, Seiler H, Wen A, Zars T, Ito K, Wolf R, Heisenberg M, Liu L (2006) Distinct memory traces for two visual features in the *Drosophila* brain. Nature 439:551-556.

Loesel R., Homberg U. (1998) Sustained oscillations in an insect visual system. Naturwissenschaften 85:238-240.

Mappes M, Homberg U (2004) Behavioral analysis of polarization vision in tethered flying locusts. J Comp Physiol A 190:61-68.

Nässel DR, Homberg U (2006) Neuropeptides in interneurons of the insect brain. Cell Tissue Res 326:1-24.

Nordström K, Barnett PD, Moyer de Miguel IM, Brinkworth RSA, O'Carroll DC (2008) Sexual dimorphism in the hoverfly motion vision pathway. Curr Biol 18:661-7.

Nordström K, Barnett PD, O'Carroll DC (2006) Insect detection of small targets moving in visual clutter. PLoS Biol 4:e54.

Nordström K, O'Carroll DC (2006) Small object detection neurons in female hoverflies. Proceedings of the Royal Society B: Biological Sciences 273:1211-1216.

O'Carroll D (1993) Feature-detecting neurons in dragonflies. Nature 362:541-541.

Okamura J, Strausfeld NJ (2007) Visual system of calliphorid flies: motion- and orientation-sensitive visual interneurons supplying dorsal optic glomeruli. J Comp Neurol 500:189-208.

Osorio D (1986a) Directionally selective cells in the locust medulla. J Comp Physiol A 159:841-847.

Osorio D (1986b) Ultraviolet sensitivity and spectral opponency in the locust. J Exp Biol 122:193-208.

Paulk AC, Phillips-Portillo J, Dacks AM, Fellous J, Gronenberg W (2008) The processing of color, motion, and stimulus timing are anatomically segregated in the bumblebee brain. J Neurosci 28:6319-6332.

Pfeiffer K, Homberg U (2007) Coding of azimuthal directions via time-compensated combination of celestial compass cues. Curr Biol 17:960-965.

Reppert SM, Zhu H, White RH (2004) Polarized light helps monarch butterflies navigate. Curr Biol 14:155-158.

Rind FC (1987) Non-directional, movement sensitive neurones of the locust optic lobe. J Comp Physiol A 161:477-494.

Rind FC (1990) Identification of directionally selective motion-detecting neurons in the locust lobula and their synaptic connections with an identified descending neurone. J Exp Biol 149:21-43.

Rind FC, Simmons PJ (1998) Local circuit for the computation of object approach by an identified visual neuron in the locust. J Comp Neurol 395:405-415.

Ritzmann RE, Ridgel AL, Pollack AJ (2008) Multi-unit recording of antennal mechano-sensitive units in the central complex of the cockroach, Blaberus discoidalis. J Comp Physiol A 194:341-360.

Stern M, Gewecke M. 1993. Spatial sensitivity profiles of motion sensitive neurons in the locust brain. In: Weise K, Gribakin F, Popov A, Renninger G, editors. Sensory Systems in Arthropods. Basel: Birkhäuser. p 184-192.

Strausfeld NJ, Okamura J (2007) Visual system of calliphorid flies: organization of optic glomeruli and their lobula complex efferents. J Comp Neurol 500:166-188.

Strauss R (2002) The central complex and the genetic dissection of locomotor behaviour. Curr Opin Neurobiol 12:633-638.

Träger U, Wagner R, Bausenwein B, Homberg U (2008) A novel type of microglomerular synaptic complex in the polarization vision pathway of the locust brain. J Comp Neurol 506:288-300.

Vishnevskaya TM, Shura-Bura TM. 1990. Spectral sensitivity of photoreceptors and spectral inputs to the neurons of the first optic ganglion in the locust (*Locusta migratoria*). In: Wiese K, Gribakin F, Popov A, Renninger G, editors. Sensory Systems in Arthropods. Basel: Birkhauser.

Vitzthum H, Müller M, Homberg U (2002) Neurons of the central complex of the locust *Schistocerca gregaria* are sensitive to polarized light. J Neurosci 22:1114-1125.

von Frisch K (1949) Die Polarisation des Himmelslichtes als orientierender Faktor bei den Tänzen der Bienen. Experientia 5:142-148.

von Philipsborn A, Labhart T (1990) A behavioral study of polarization vision in the fly. *Musca domestica*. J. Comp. Physiol. A 167:737-743.

Wehner R (1984) Astronavigation in Insects. Ann Rev Entomol 29:277-298.

Wehner R, Labhart T. 2006. Polarization vision. In: Warrant E.; Nilsson D.-E., editors. Invertebrate Vison. Cambridge, UK: Cambridge Univ. Press. p 291-348.

Williams J. (1972) Some observations on the neuronal organization of the supra-oesophageal ganglion in *Schistocerca gregaria Forskål* with particular reference to the central complex PhD-Thesis, University of Wales.

Williams JLD (1975) Anatomical studies of the insect central nervous system: a ground-plan of the midbrain and an introduction to the central complex in the locust, *Schistocerca gregaria* (Orthoptera). J Zool (Lond) 176:67-86.

Yang E, Lin H, Hung Y (2004) Patterns of chromatic information processing in the lobula of the honeybee, *Apis mellifera L.* J Insect Physiol 50:913-925.

Yang EC, Maddess T (1997) Orientation-sensitive neurons in the brain of the honey bee (*Apis mellifera*). J Insect Physiol 43:329-336.

Danksagung

Mein ganz besonderer Dank gilt Prof. Dr. Uwe Homberg für die Bereitstellung des spannenden Themas, das Wecken meine Begeisterung für die faszinierendste Region des Insektengehirns, die großen Freiheiten und Möglichkeiten zum selbständigen Arbeiten, stete Unterstützung und zahlreiche motivierende Gespräche, unermüdliches Korrigieren von Manuskripten, ein ausgesprochen kollegiales und unkompliziertes Arbeitsverhältnis, die Anleitung zum wissenschaftlichen Arbeiten und kritischem Umgang mit Ergebnissen, und nicht zuletzt für die Chance zur Erkundung der Welt der Insektenneurobiologie auf zahlreichen Tagungen.

Weiterhin möchte ich Prof. Dr. Monika Stengl für die Zweitkorrektur dieser Arbeit, sowie für ein motivierendes und richtungweisendes Gespräch am Beginn meiner Zeit in der AG Homberg danken. Dafür, dass sich Prof. Dr. Hassel und Prof Dr. Renkawitz-Pohl als Mitglieder meiner Prüfungskommission zur Verfügung stellen, möchte ich ihnen ebenfalls herzlich danken.

Ohne die gute und inspirierende, meist lustige und stets unkomplizierte Atmosphäre in den AGs HoSchaWeSte wäre die Zeit meiner Promotion weit weniger angenehm gewesen, wofür ich mich bei allen Mitgliedern dieser AGs bedanken möchte.

In höchstem Maße essentiell war die Hilfe meines ‚Mentors' in Sachen Elektrophysiologie, Dr. Keram Pfeiffer, der mich mit viel Geduld und Gelassenheit in die Geheimnisse von Verstärkern, Elektroden sowie links- und rechtsdrehenden Polarisationsfiltern eingewiesen hat. Außerdem wäre die Auswertung meiner Daten ohne die von ihm verfassten Spike2-Skripte nicht innerhalb dieser Dekade durchzuführen gewesen.

Basil el Jundi möchte ich danken für stets humorvolle Zwischentöne, insbesondere als Mitglied der ‚AG' BaDa (Moschusochsen und Phycomyces), sowie seine höchst effektive Einführung in die 3D-Software Amira.

Weiterhin zu Dank verpflichtet bin ich Bianca Backasch für wertvolle Diskussionen und Tipps zu Statistik, Dr. Wolf Hütteroth für Hilfe mit KLSM und Immuncytochemie, sowie Ulrike Träger für viele nette Diskussionen zum Polarisationssehen.

Mein dreiwöchiger Aufenthalt am Janelia Farm Research Campus führte zur Optimierung der Präparationsmethode für meine Ableitungen an Heuschrecken, einigen ersten Erfahrungen mit Patch-Clamp Ableitungen von POL-Zellen, und unzähligen aufbauenden, ja wegweisenden Gesprächen. Dafür möchte ich dem unerschöpflichen Engagement von Dr. Vivek Jayaraman ganz besonders danken.

Der arbeitsame Aufenthalt im ‚Science Boot Camp' am MBL in Woods Hole war ein wahrer Quantensprung in Sachen elektrophysiologisches Verständnis und ein hoch inspirierender und motivierender Einblick in die Welt der Wissenschaft. Allen, die an dieser Zeit beteiligt waren, insbesondere auch den finanziellen Unterstützern (MBL und Boehringer Ingelheim Fonds) drücke ich hiermit nochmals meinen tiefen Dank aus.

Für die stete Unterstützung über die letzten Jahre hinweg sowie den immer verlässlichen Rückhalt in schwierigen Zeiten möchte ich mich ganz besonders herzlich bei meiner Familie bedanken, ohne die weder diese Doktorarbeit noch das zugrunde liegende Studium möglich gewesen wäre.

Zum Abschluss fehlen mir die Worte auszudrücken wie unendlich dankbar ich bin für die Liebe, die Inspiration, die Motivation, die stets neue Kraft und nicht zuletzt die Aussicht auf eine wundervolle Zukunft, die mir meine Freundin Tini jeden Tag gegeben hat, den wir bisher gemeinsam verbringen durften.

Appendix

A Documentation of MatLab-scripts

During the course of my this dissertation, in particular during the experiments in chapter 5, several MatLab-scripts have been developed in order to be able to generate stimuli with the used ViSaGe-stimulation device (Cambridge Research Systems), and to analyze the data obtained during these stimulations. Additionally, scripts for analysis of polarized-light stimuli have been developed.

In this appendix to my dissertation, a short overview will be given about these scripts, in order to provide some practical instructions for further useage. The source code for all scripts is available on request from me via email (stanley.heinze@gmx.de)

A1. Generation of visual stimuli with ViSaGe

The most important script allows to present stimuli via a ViSaGe-stimulator connected to a CRT screen. The script uses a MatLab toolbox provided by Cambridge Research Systems together with the stimulator.

Instructions for usage

After startup of MatLab on the PC connected with the ViSaGe, the ViSaGe is automatically initialized (if not, then this has to be accomplished manually). Then run the script ‘stimuli’. It requires a second script in the same directory (called ‘oriented_bars’). It creates a graphical user interface with many buttons to choose from (Fig.A1)

The axis: Shows the center of the current stimulus position for stationary bars.

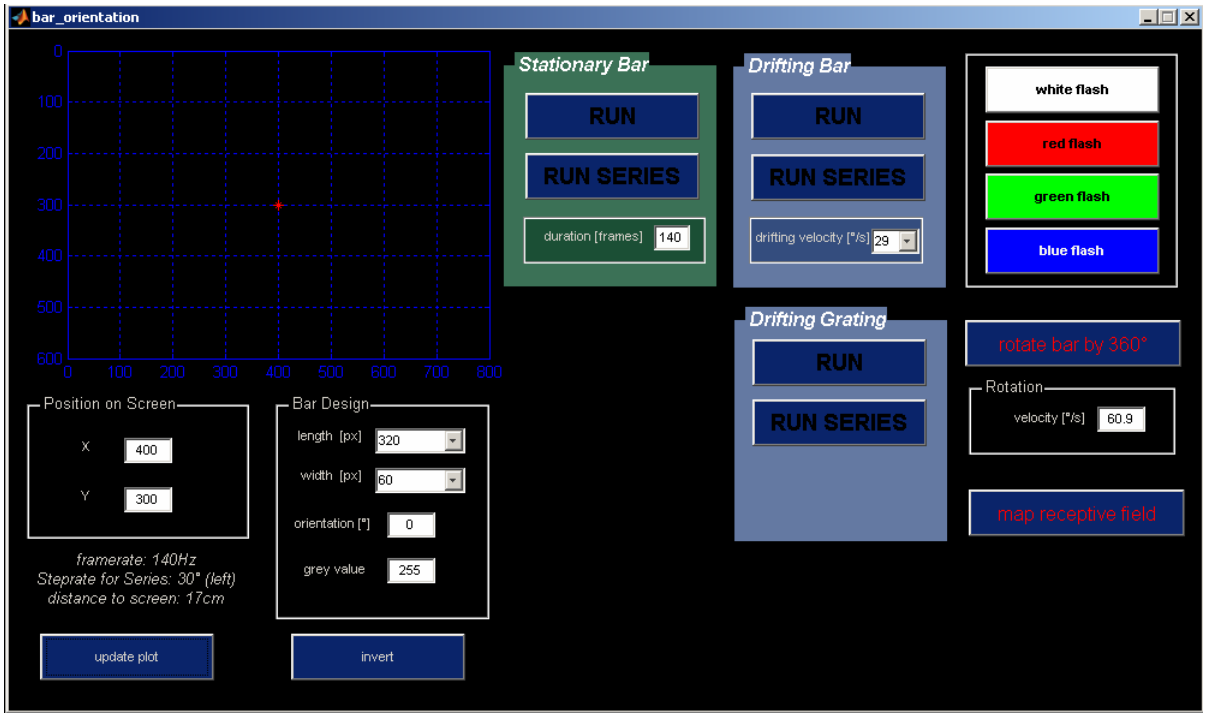

Fig.A1 Graphical user interface of the script to create the stimuli for presentation on a CRT-screen during intracellular recordings.

Position on screen: Coordinates for the center of stationary bars (numbers as shown in the axis window).

Bar design: Here the length, width, orientation and grey value of presented bars can be defined. Orientation only applies for single runs, not for series.

Update plot: updates the axis window to show coordinates currently defined by 'bar position'.

Invert: Inverts the stimuli (black on white background instead of white on black background); applies to stationary and rotating bars.

All **remaining buttons** are designed for stimulus display. They produce either single runs of stationary bars, moving bars and moving gratings, or complete series of stimuli. The 'flash'-buttons produce full-screen flashes in the color indicated (duration 0.5 s). Rotating bars can be presented by using the 'rotate bar by 360°'-button. At last, a series of small white disks in black background is presented on different positions on the screen by the 'map receptive field'-button.

Known bugs

The script only works after starting it twice. After first start, it is required to close the user interface and rerun the script. Otherwise, only the first stimulus display will work, whereas all successive presentations will return an error. Rotation velocity of rotating bars cannot be changed.

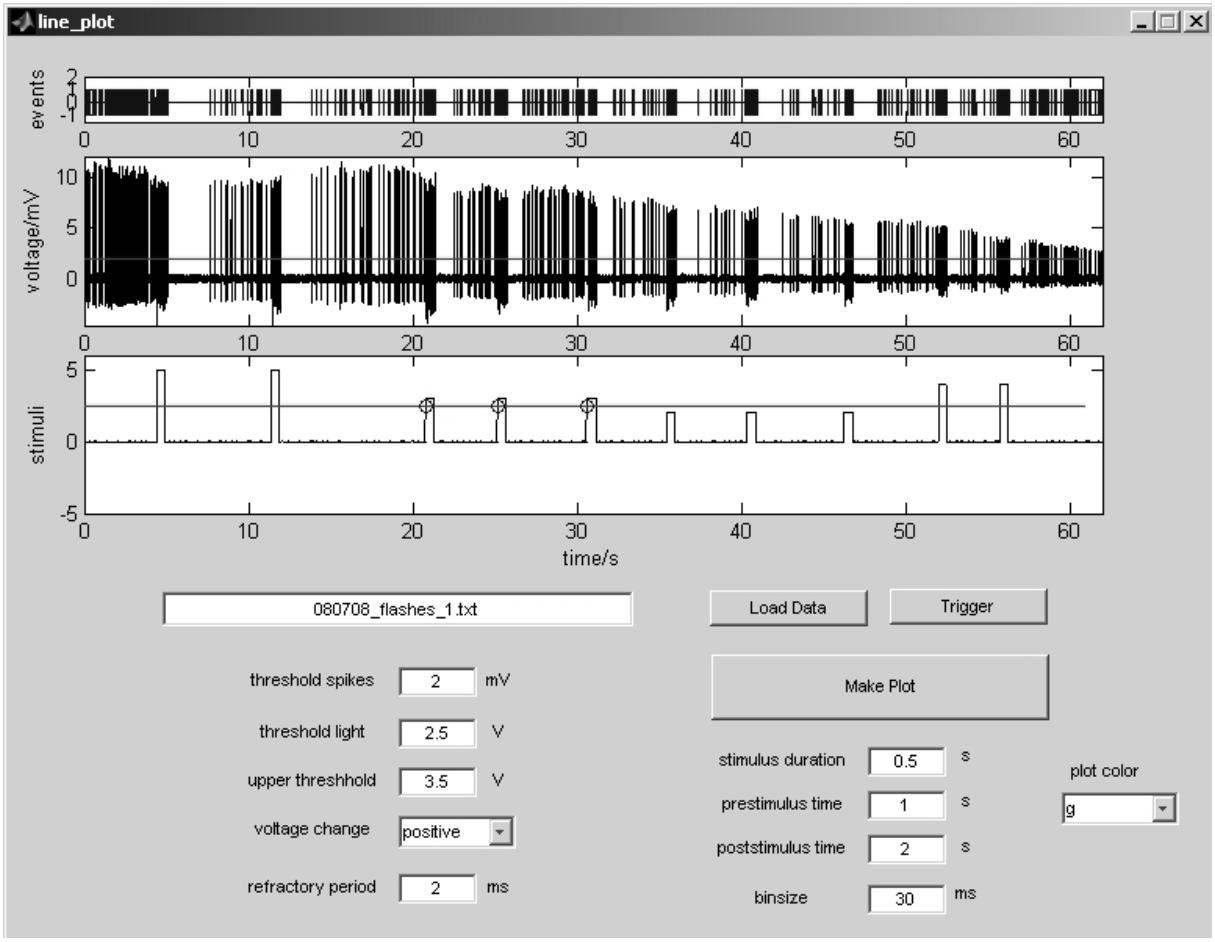

Fig.A2 Graphical user interface for Script: Rasta-Plot and PSTH

A2. Rasterplot and PSTH

This script, along with the following ones, uses recorded spike trains together with recorded stimulus control signals, on order to perform evaluation procedures on these data. This script creates a rastaplot of multiple fixed length stimulations (no limit), and calculated the corresponding peri-stimulus-time histogram. A compound figure is created and copied to the clipboard. A subscript ('spike_detection') is required in the MatLab-path.

Instructions for usage

Data have to be prepared as txt-files before they can be loaded by the script! From Spike2-Files this can be achieved by using the Spike2-function 'copy for spreadsheet'. This function writes all visible channels into the clipboard. It uses one column per channel in the order the channels are arranged in Spike2 (top to bottom). The sampling rate can be set manually to any desired value (I recommend 3000Hz). These data have to be pasted into an empty txt-file. After deleting the first line of this file (no data, but the Spike2-header), the data are ready to be used in MatLab. For pClamp users, data can be exported via the 'Save as' function in ClampFit (setting 'atf' instead of 'abf', i.e. axon text file). Also, the header has to be deleted from the resulting file, which should be renamed from atf to txt.

Data have to consist of two columns, the first one must contain the voltage values of the spiketrain (without baseline drift to allow threshold base event detection), and the second one must contain the voltage values of the stimulus control signals as rectangular voltage changes. After adding the location of the file of interest to the MatLab-path ('Set Path'-function in MatLab), the script can be run. It creates a user interface with many buttons (Fig.A2)

Top-axis: Display of triggered events (detected spikes). A value of 1 is assigned to all events used for analysis, while a value of 2 are assigned to all events deleted because they fall into the refractory period.

Middle-axis: Analyzed voltage signal (spike train)

Bottom-axis: Stimulus control signals

Refractory period: Sets the minimal interval for two successive spikes.

Load Data: Loads the text-file specified in the text-field on the left.

Trigger: Applies threshold based event detection to the spike train. Values can be specified on the left (threshold spikes: voltage level above which spikes are detected; threshold light: trigger level for detection of stimulation events; upper threshold: stimulation events detected by this threshold are not used for evaluation; voltage change: specifies whether stimulations are positive or negative changes in voltage)

Make Plot: Creates rasta-plot and PSTH with the following display specifications: stimulus duration, prestimulus time, poststimulus time, binsize (for PSTH), and plot color (one of red, green, blue, or black).

Known bugs

Sometimes the trigger function for spikes creates an error message, if the standard value (5 mV) is used. After typing in another value for each of the trigger levels, this is not a problem anymore. The axis of the PSTH has to be set manually to a value specified in script line number 315, or can be scaled to the maximum by activating line number 316.

A3. Evaluation of stationary polarized light stimuli

This script analyzes a series of polarized light stimulations with stationary *E*-vectors. It requires two columns of voltage signals in a txt-file (see A2 for export procedures from Spike2 and Clampfit). Stimuli are expected to be structured in a series of stimulations starting from 0° *E*-vector orientation to

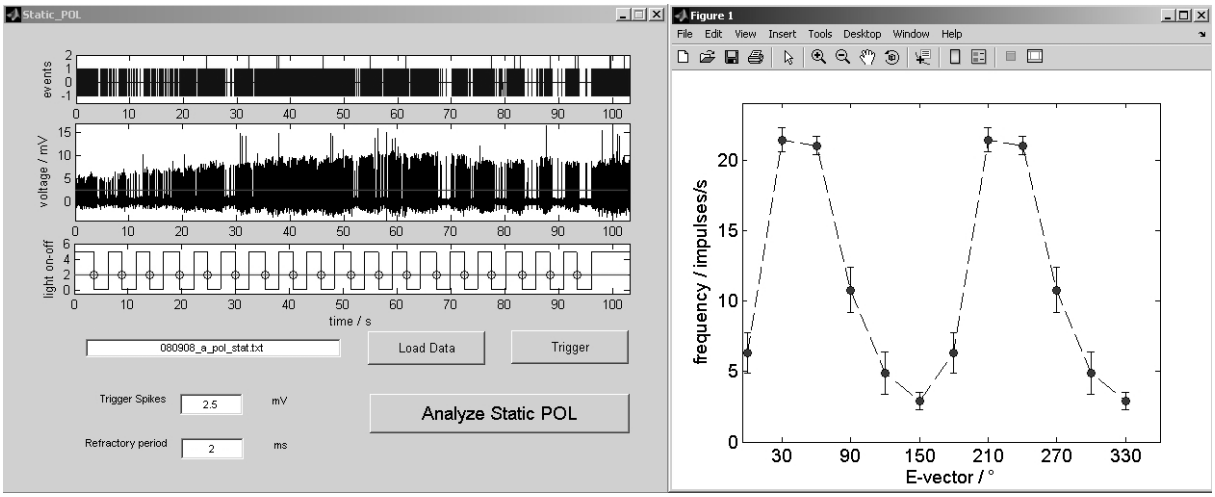

Fig.A3 Graphical user interface for evaluation of stationary *E*-vector stimulations on the left, and resulting graph on the right.

150° in steps of 30°, each *E*-vector angle must be presented three times. Stimulus control signals must be negative drops in voltage crossing a threshold at 2 V. A subscript ('spike_detection') is required in the MatLab-path.

Instructions for usage

The script creates a user interface with the following buttons (Fig.A3):

Top-axis: Display of triggered events (detected spikes). A value of 1 is assigned to all events used for analysis, while a value of 2 are assigned to all events deleted because they fall into the refractory period.

Middle-axis: Analyzed voltage signal (spike train)

Bottom-axis: Stimulus control signals

Refractory period: Sets the minimal interval for two successive spikes.

Load Data: Loads the text-file specified in the text-field on the left.

Trigger: Applies threshold based event detection to the spike train at the voltage level specified on the left ('Trigger Spikes'). A value of 1 is assigned to all events used for analysis, while a value of 2 are assigned to all events deleted because they fall into the refractory period.

Analyze Static POL: Creates the graph shown in Fig.A3.

A4. Evaluation of moving bars and sine-gratings

This script analyzes a series of moving bar stimuli. It requires two columns of voltage signals in a txt-file (see A2 for export procedures from Spike2 and Clampfit). Stimuli are expected to be structured in a series of stimulations each consisting in successive stimulations starting with a bar/sine orientation of 0° (moving at 90° to the right) and finishing with 150° orientation, in steps of 30°. Each orientation has to be directly followed by the opposite motion direction. At least two series of stimulations are required. A subscript ('spike_detection') is required in the MatLab-path.

Instructions for usage

The script creates a user interface with the following buttons (Fig.A5):

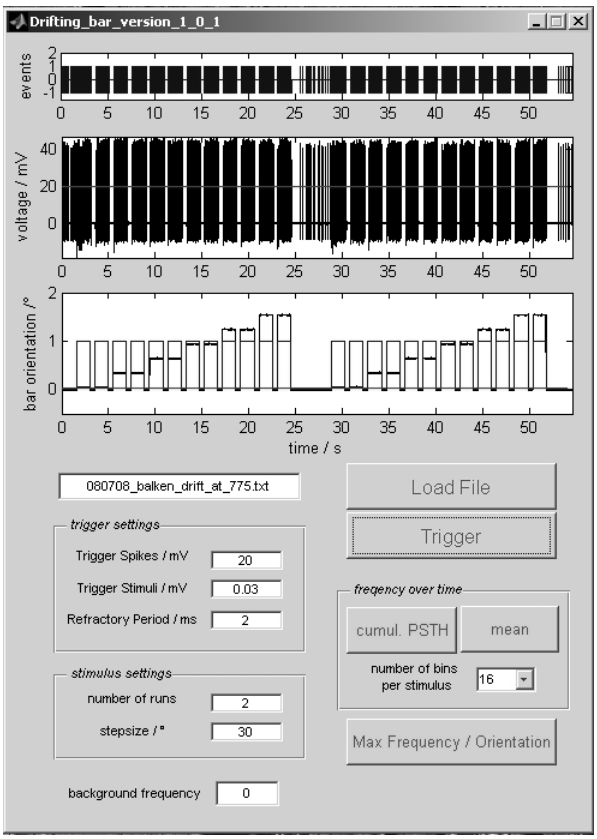

Fig.A5 Graphical user interface of the script for analysis of moving bars/sine-gratings.

Top-axis: Display of triggered events (detected spikes). A value of 1 is assigned to all events used for analysis, while a value of 2 are assigned to all events deleted because they fall into the refractory period.

Middle-axis: Analyzed voltage signal (spike train)

Bottom-axis: Stimulus control signals

Refractory period: Sets the minimal interval for two successive spikes.

Load Data: Loads the text-file specified in the text-field on the left.

Trigger: Applies threshold based event detection to the spike train at the voltage level specified on the left ('Trigger Spikes'). Stimuli are detected by the same algorithm using the value from the field 'trigger stimuli'.

Number of runs: defined the number of presented stimulus series.

Stepsize: defines the step size between two successive orientations (only working for 30° up to now).

Cumul. PSTH: creates a PSTH of each orientation with the bin size specified in the field below.

Mean: creates a series of graphs with the mean spike frequency with standard deviations during each bar orientation, using the bin size specified in the field below.

Max Frequency / Orientation: Creates two graphs. The first plots the mean frequency of all stimulations against their respective orientation (three lines: upwards motion, downwards motion, mean of both). The second plots all individual series against the orientation to reveal variability in responses (two lines for each series, one depicting upward motion, and the other downward motion). All mean values with their standard deviation are also prompted in the MatLab main window.

A5. Evaluation of receptive field probing

This script analyzes a series of presentations of small white discs on black background in different positions on the screen. It requires two columns of voltage signals in a txt-file (see A2 for export procedures from Spike2 and Clampfit). Stimuli are expected to be structured in a series of stimulations each consisting of 30 stimulations starting at the top left position on the screen, stepwise changing positions to reach the bottom right corner of the screen (in five rows, consisting of six presentations each). At least two series of stimulations are required. A subscript ('spike_detection') is required in the MatLab-path.

Instructions for usage

The script creates a user interface with the following buttons (Fig.A6):

Top-axis: Display of triggered events (detected spikes). A value of 1 is assigned to all events used for analysis, while a value of 2 are assigned to all events deleted because they fall into the refractory period.

Middle-axis: Analyzed voltage signal (spike train)

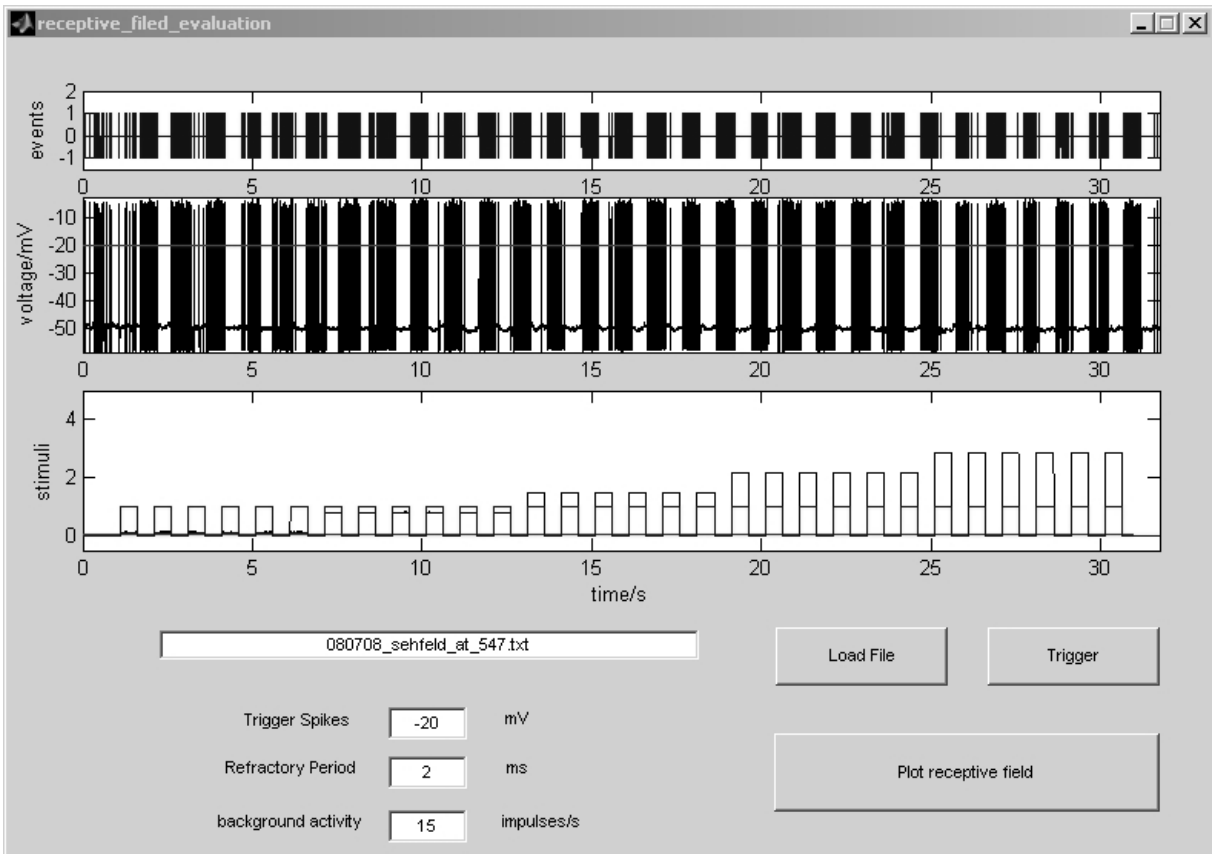

Fig.A6 Graphical user interface of the script for receptive field evaluation.

Bottom-axis: Stimulus control signals

Refractory period: Sets the minimal interval for two successive spikes.

Background activity: The background activity of the analyzed cell has to be typed in. (This is basically a reminder to adjust the resulting colormap to the background activity. Not inserting a value here has no actual consequences).

Load Data: Loads the text-file specified in the text-field on the left.

Trigger: Applies threshold based event detection to the spike train at the voltage level specified on the left ('Trigger Spikes').

Plot receptive field: This button creates a series of graphs. For each individual stimulus series a composite graph is produced consisting of three two-dimensional color-coded representations of the screen, showing activation and inhibition during each disk presentation with respect to its location. The first graph shows tonic activity during the stimulus, the second one phasic onset activity (0.2 s bin), and the last one phasic offset activity (0.2 s bin). Additionally, the same graphs are produced as average over all stimulations series. *Important note: the resulting graphs code activation (red) and inhibition (blue) relative to background frequency (white). The white-point of the color map has to be adjusted manually in the automatically opened color map editor!*

A6. Evaluation of stationary bars

This script analyzes a series of presentations of stationary bars. It requires two columns of voltage signals in a txt-file (see A2 for export procedures from Spike2 and Clampfit). Stimuli are expected to be structured in a series of stimulations starting at an orientation of 180° and finishing at 0°, in steps of 30° with at least 1 second pause between individual stimulations. A subscript ('spike_detection') is required in the MatLab-path.

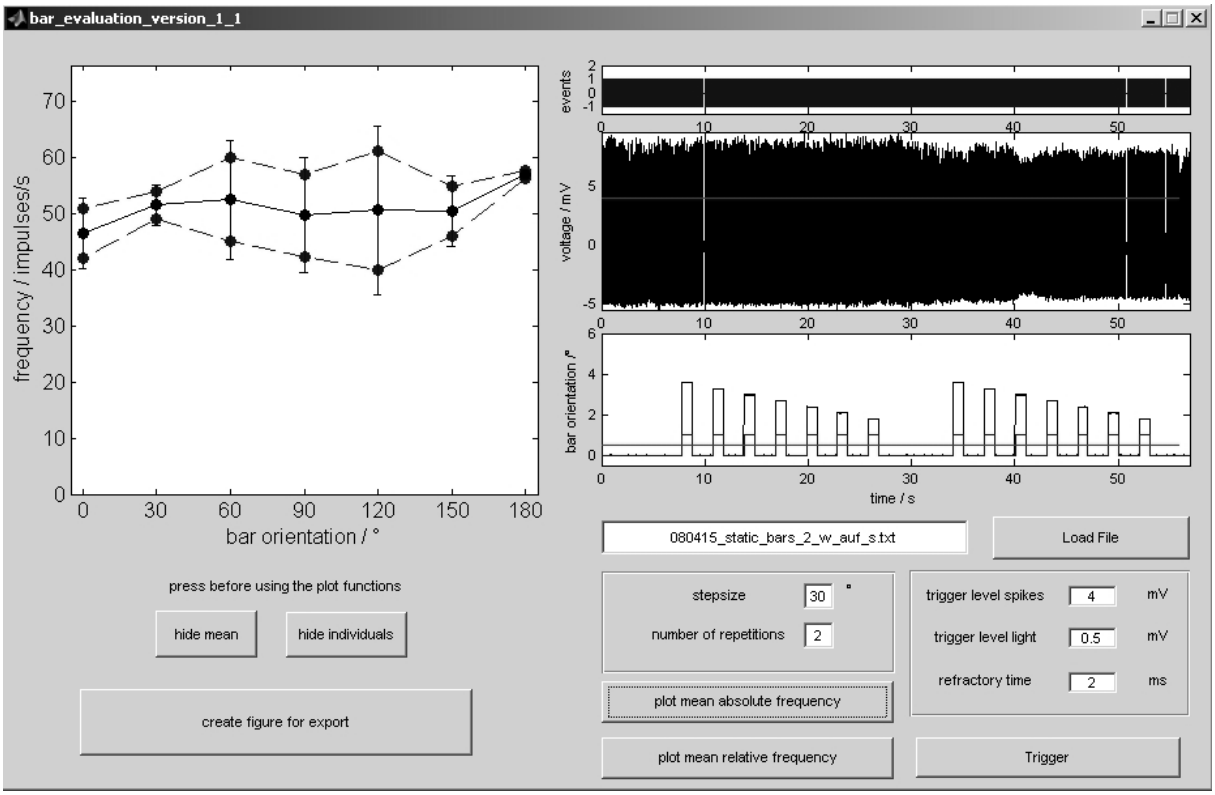

Fig.A7 Graphical user interface of the script for evaluating static oriented bars.

Instructions for usage

The script creates a user interface with the following buttons (Fig.A7):

Top-axis: Display of triggered events (detected spikes). A value of 1 is assigned to all events used for analysis, while a value of 2 are assigned to all events deleted because they fall into the refractory period.

Middle-axis: Analyzed voltage signal (spike train)

Bottom-axis: Stimulus control signals

Refractory time: Sets the minimal interval for two successive spikes.

Load File: Loads the text-file specified in the text-field on the left.

Trigger: Applies threshold based event detection to the spike train at the voltage level specified on the left (‘Trigger level spikes’).

Stepsize: Defines the step size between two successive orientations

Number of repetitions: Defined the number of presented stimulus series.

Plot mean absolute frequency: Plots the mean absolute frequency together with the individual absolute frequencies of each stimulus series into the graph-field in the left side.

Plot mean relative frequency: Plots the mean relative frequency together with the individual relative frequencies of each stimulus series into the graph-field in the left side.

Hide mean / hide individuals: Two buttons that, if pressed before the plotting functions, result in display of either only the mean curve or the curved of the individual stimulations.

Create figure for export: Creates a separate figure, displaying the graph shown in the script user interface.

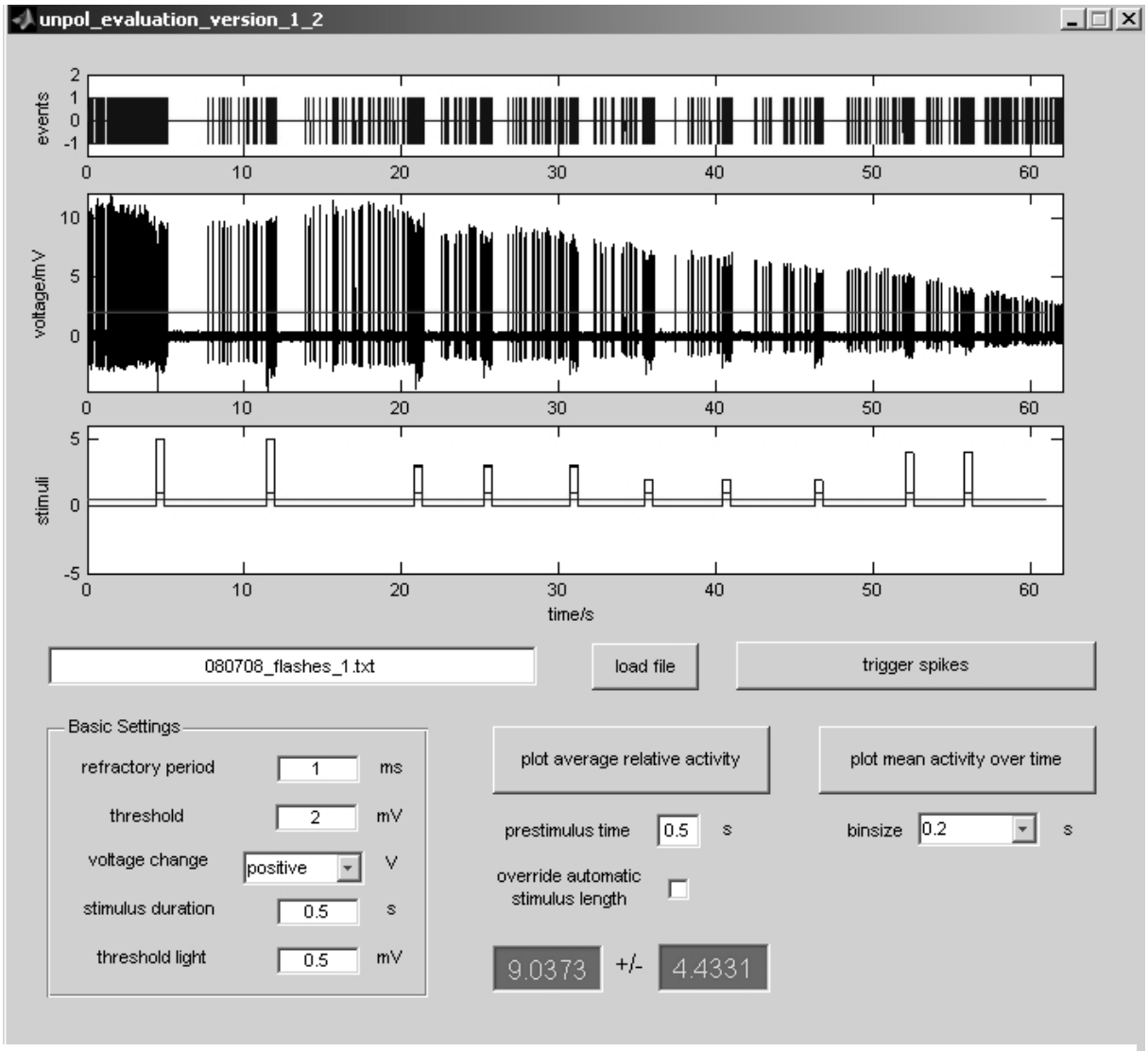

Fig.A8 Graphical user interface of the script for evaluation of light flashes.

A7. Mean frequency and relative frequency

This script analyzes a series of presentations of light flashes of equal length. It requires two columns of voltage signals in a txt-file (see A2 for export procedures from Spike2 and Clampfit). Between stimuli, and at the beginning of each analyzed spike train, there has to be a period without stimulation at least as long as specified in the 'prestimulus' field. After the last stimulation a period of at least 2 seconds has to be present. A subscript ('spike_detection') is required in the MatLab-path.

Instructions for usage

The script creates a user interface with the following buttons (Fig.A8):

Top-axis: Display of triggered events (detected spikes). A value of 1 is assigned to all events used for analysis, while a value of 2 are assigned to all events deleted because they fall into the refractory period.

Middle-axis: Analyzed voltage signal (spike train)

Bottom-axis: Stimulus control signals

Refractory period: Sets the minimal interval for two successive spikes.

Load File: Loads the text-file specified in the text-field on the left.

Trigger spikes: Applies threshold based event detection to the spike train at the voltage level specified on the left ('threshold'). Stimuli are detected by the same algorithm using the value from the field 'threshold light'.

Stimulus duration: specifies the stimulus length in case the 'override automatic stimulus length'-function is activiated. It is also used for display of the stimulus and plot specifications in the 'plot mean activity over time'-function.

Voltage change: specifies whether stimulations are positive or negative changes in voltage.

Plot average relative activity: Plots the mean activity during the stimuli divided by the mean frequency before each stimulation (length defined by the 'prestimulus time' field). It also posts the resulting values into the green fields underneath.

Plot mean activity over time: This function plots the average activity during the stimulation in bins of either 0.2 s or 0.4 s (specified below the function button).

A8. Tuning width

This script analyzes the tuning width of one rotation of the polarizer. It requires only one column of voltage signals in a txt-file (see A2 for export procedures from Spike2 and Clampfit), which contains the spike train during the rotation of the polarizer (precisely!). Either 360°-rotations or 180° rotations can be analyzed. A subscript ('spike_detection') is required in the MatLab-path.

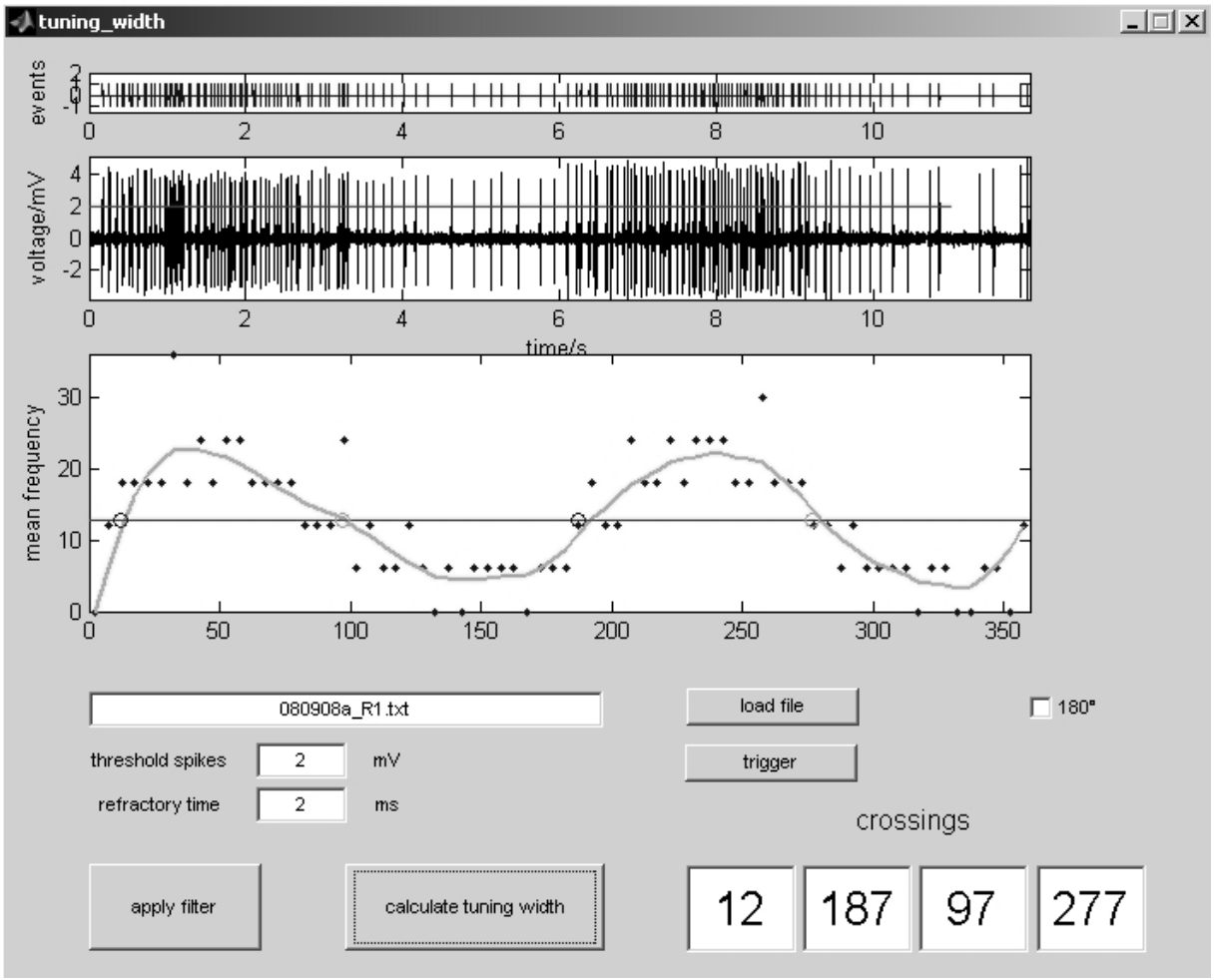

Fig.A9 graphical user interface of the script for evaluation of the E-vector tuning width.

Instructions for usage

The script creates a user interface with the following buttons (Fig.A9):

Top-axis: Display of triggered events (detected spikes). A value of 1 is assigned to all events used for analysis, while a value of 2 are assigned to all events deleted because they fall into the refractory period.

Middle-axis: Analyzed voltage signal (spike train)

Bottom-axis: Stimulus control signals

Refractory time: Sets the minimal interval for two successive spikes.

Load File: Loads the text-file specified in the text-field on the left.

Trigger: Applies threshold based event detection to the spike train at the voltage level specified on the left ('threshold spikes'). After triggering, the whole spike train is divided into 5° wide bins. Within these bins the mean frequency is calculated and plotted (values are also prompted in the MatLab main window).

Apply filter: A lowpass filter is applied to the binned frequency data and the resulting curve is displayed.

Calculate tuning width: The half maximal activity rate of the spike train is calculated by using the filtered data (ignoring the first and last two values, as filtering does not work for them). The intersection points of this half maximal frequency with the filtered line are calculated and displayed in the fields below ('crossings'). *Note: if there are more than four crossings, values are not correctly displayed in the user interface. Then, values prompted in the MatLab main window have to be used!*

Curriculum Vitae

Stanley Heinze
Marbacher Weg 32
35037 Marburg
Telephone: 06421/63383 (private), 06421/2823475 (work)
Email: stanley.heinze@gmx.de / heinzest@staff.uni-marburg.de

Personal details:

Date of birth:	15/11/1979
Place of birth:	Großröhrsdorf
Nationality:	German

Academic education

05/2008-06/2008	Invited guest researcher at Janelia Farm Research Campus (HHMI). Development of a patch-clamp approach for double recordings from polarization sensitive neurons (in the desert locust) in collaboration with HHMI-fellow Vivek Jayaraman.
01/2008	Participation in the PENS-Hertie winter school in Obergurgl, Austria, on the topic: 'The design of neural networks: contributions from invertebrates'.
06/2006 – 07/2006	Participation in the summer course 'Neural systems and Behavior' at the MBL in Woods Hole, MA, USA.
Since 10/2005	PhD-thesis in the research group of Prof. Dr. Homberg, department neurobiology/ethology at the Philipps-University of Marburg (working title: 'Characterization of the polarization vision system in the brain of the desert locust (*Schistocerca gregaria*)').
09/2005	Diploma at the Philipps-University of Marburg, mark: 'Ausgezeichnet' (exceptional). Final examinations in the subjects: animal physiology, developmental biology, and genetics. Diploma thesis (11/2004 – 09/2005) in the laboratory of Prof. Dr. Homberg, department of Biology, Neurobiology/Ethology.
03/2002 – 11/2002	Study-abroad year at the *Northern Territory University*, Darwin, Australia.
10/2001	Prediploma at the Philipps-University of Marburg , mark: 1.1.
10/1999 – 09/2005	Studies of Biology at the Philipps-University of Marburg.
10/1990 – 07/1998	Attendance of grammar schools in Treuchtlingen (Senefelder Schule, 1990-1996) and Wilthen (Städt. Gymnasium Wilthen, 1996-1998), final examination 1998: Abitur (mark: 1.0).

Vocational Experience

Since 10/2007	Research/teaching assistant in the research group of Prof. Dr. Homberg, University of Marburg, Germany.
04/2003 – 05/2006	Weekly supervision of undergraduate courses in animal physiology (April – July 2003- 2005, April /May 2006)
08/2003	Student assistant in the laboratory of Prof. Dr. R. Renkawitz-Pohl, department of Developmental Biology at the Philipps-University of Marburg (August 2003). Participation in the research project for characterization of the *Drosophila*-protein *Rolling Pebbles*.
08/1998 – 08/1999	*Alternative service* in the district office of Bautzen (environmental department)

Academic Honors

04/2002 – 08/2005	Scholarship by the 'Studienstiftung des Deutschen Volkes' (German National Academic Foundation).
05/2006	Travel Allowances by Boehringer Ingelheim Fonds for attendance of the Neural Systems and Behavior Course at the MBL in Woods Hole, USA.
08/2007	Heiligenberg Travel Award by the International Society for Neuroethology for attendance of the 8th ISN conference in Vancouver.
01/2009	Neuroethology Prize by the Capranica Foundation, Tuscon Arizona.

Publications

Heinze S., Homberg U. (2008) Neuroarchitecture of the central complex of the desert locust: Intrinsic and columnar neurons. *J. Comp. Neurol.* **511**:454–478.

Heinze, S., Homberg, U. (2007) Map-like Representation of Celestial E-vector Orientations in the Brain of an Insect. *Science* **315**:995-997.

Heinze, S., Homberg, U. (2007) Mapping of celestial *E*-vector orientations in the columns of the locust central complex. 8th ISN conference, Vancouver.

Heinze S., Homberg U. (2007) Topographic organization of *E*-vector orientation columns in the central complex of the locust brain. 7th NWG meeting, Göttingen T14-5B.

Heinze S., Homberg U. (2006) A computational map of *E*-vector orientations in the central complex of the desert locust (*Schistocerca gregaria*). FENS Forum Abstracts Vol. 3, Abstract A129.9.

Heinze, S. (2005) Charakterisierung von polarisationssensitiven Interneuronen aus dem Zentralkomplex der Wüstenheuschrecke *Schistocerca gregaria* [Characterization of polarization-sensitive interneurons from the central complex of the desert locust *Schistocerca gregaria*]. Diploma thesis, University of Marburg, Germany.

Heinze, S., Homberg, U. (2005) A new set of tangential neurons of the protocerebral bridge in the desert locust *Schistocerca gregaria* is sensitive to polarized light. 98. DZG meeting Bayreuth. [conference talk].

Erklärung

Hiermit versichere ich, dass ich meine Dissertation

„Characterization of polarization sensitive neurons of the central complex in the brain of the desert locust (*Schistocerca gregaria*)“

(Charakterisierung von polarisationssensitiven Neuronen des Zentralkomplexes im Gehirn der Wüstenheuschrecke (*Schistocerca gregaria*))

selbständig, ohne unerlaubte Hilfe angefertigt und mich dabei keiner anderen als der von mir ausdrücklich bezeichneten Quellen und Hilfen bedient habe.

Die Dissertation wurde in der jetzigen oder einer ähnlichen Form noch bei keiner anderen Hochschule und hat noch keinen sonstigen Prüfungszwecken gedient.

Marburg, den 08.02.2009

_____

(Stanley Heinze)